CVEN6511: Nonlinear Finite Element Analysis of Solids and Porous Media

by

Richard A. Regueiro
Professor
Department of Civil, Environmental, and Architectural Engineering
University of Colorado Boulder
1111 Engineering Dr.
428 UCB, ECOT 441
Boulder, CO 80309-0428

University of Colorado Boulder
Spring 2024

©Richard A. Regueiro, January 2024

Contents

List of Figures

This page intentionally left blank.

Chapter 1

Introduction

1.1 Importance of Nonlinear Finite Element Analysis of Solids and Porous Media

Why do we need nonlinear finite element analysis (FEA) for solids and porous media? Because all "real" problems are nonlinear. They are difficult to solve numerically and nearly impossible to solve analytically. Hence, we opt for the more tractable of the two: the numerical solution. With that said, it is still useful to "verify" nonlinear solution methods against analytical solutions of linear partial differential equations, which we will take advantage of in this course.

The source of nonlinearity in FEA takes the following forms:

- **Material:** plasticity, nonlinear elasticity, failure (damage, fracture, shear banding, ...).
- **Geometric:** large deformations (including large strains *and* large rotations).
- **Constraints:** (1) kinematic (contact): impenetrability and traction equilibrium along

contacting free surfaces; (2) boundary conditions: displacement-dependent force, nonlinear pressure loading.

1.2 How This Course is Taught

We will cover the theory and numerical implementation of nonlinear solution methods, the nonlinear finite element method (FEM), biphasic (solid-fluid) mixture poromechanics in the small strain regime (notes provided, but time-permitting during the semester), and constitutive modeling (elastoplasticity, viscoplasticity, viscoelasticity, elastodamage, and variants thereof) at small strain. Full geometrically nonlinear constitutive modeling is covered in a follow-on course, CVEN 7511, *Computational Finite Inelasticity and Multiphase Mechanics.*

We will learn how to *verify* nonlinear solution implementations in `Python` (or other programming language of your choosing), and compare to similar continuum constitutive models built-in to the general purpose nonlinear continuum mechanics FEA software package ABAQUS (refer to `www.simulia.com`). We will learn to use existing nonlinear constitutive models built-in to ABAQUS to solve nonlinear engineering problems, and also how to implement new ones via the `UMAT`.

For a limited discussion of the procedure of **verification and validation (V&V)**, refer to Oberkampf et al. [2004], Babuska and Oden [2004], Schwer [2007], TMS [2019]:

- **verification:** we check if the nonlinear governing equations are implemented correctly in our finite element (FE) code. This typically involves a combination of comparison to an analytical solution (if one exists, even if analyzing a linear problem with known analytical solution, with a nonlinear code) and/or to a separate numerical implementation (such as in Python); we also consider time step and mesh size refinement (convergence). In CVEN6511, we will do verification to some degree.

- **validation:** we check that the nonlinear governing equations are the correct ones to solve; i.e., are the physics of the problem being represented correctly in the model? This involves *prediction* of experimental data with quantified uncertainty. Validation could be partly accomplished through your project, but for true validation, this is beyond the scope of the course. **Calibration** is parameter-fitting, which is a step toward validation, but is not validation itself. If you have experimental data, you will likely conduct a calibration-exercise for your course project.

This page intentionally left blank.

Chapter 2

Numerical Solution of 1D Nonlinear Axially-loaded Bar using the Finite Element Method and Newton-like Methods

2.1 Nonlinear Solution by Newton-like Methods

In this section, we introduce the Newton-Raphson method for solution of nonlinear equations, and its modifications and extensions. In Section 2.2, we formulate the nonlinear vector equations using the finite element method (FEM).

2.1.1 Newton-Raphson Method

We start with a one degree-of-freedom (dof) example, as shown in Fig.2.1.

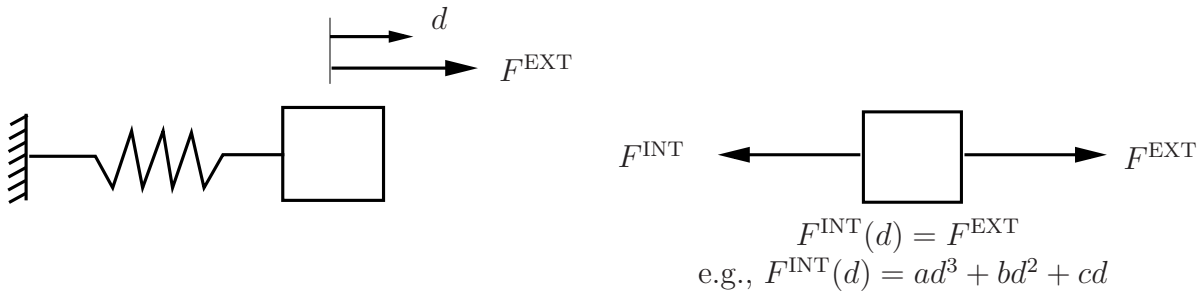

Figure 2.1. One dof example for demonstrating the Newton-Raphson (NR) solution method, and its modifications and extensions. Nonlinear internal force $F^{\mathrm{INT}}(d)$ as a function of displacement d represents the nonlinear spring, such as a nonlinear constitutive model (e.g., elastoplasticity).

The steps for solving for the unknown dof d given an applied external force F^{EXT} and an internal force $F^{\mathrm{INT}}(d)$ representing a nonlinear spring, are as follows:

1. define residual r as a function of displacement d for static force equilibrium:

$$r(d) = F^{\mathrm{EXT}} - F^{\mathrm{INT}}(d) = 0 \tag{2.1}$$

2. Consider the 'exact' solution d^* (usually unknown, hence the need for Newton-Raphson nonlinear solution) such that $r(d^*) = 0$ given the applied external force F^{EXT}. Consider the Taylor-series expansion about the past iteration value d^k (where $k+1$ denotes the current iteration):

$$d^* = d^k + \delta d^k \tag{2.2}$$

$$r(d^*) = r(d^k) + \frac{\partial r(d^k)}{\partial d}\delta d^k + \frac{1}{2}\frac{\partial^2 r(d^k)}{\partial d^2}(\delta d^k)^2 + \text{h.o.t.} = 0 \tag{2.3}$$

3. "linearization:" We call $\partial r(d^k)/\partial d$ the consistent tangent at iteration k, and drop the

quadratic and higher order terms (h.o.t.s), and thus $d^* \approx d^{k+1}$.

$$r(d^k) + \frac{\partial r(d^k)}{\partial d}\delta d^k \approx 0 \quad ; \qquad d^* \approx d^{k+1} = d^k + \delta d^k$$

4. solution method to update current iteration value d^{k+1} (see Fig.2.2 for illustration):

$$r(d^k) = F^{\text{EXT}} - F^{\text{INT}}(d^k) \tag{2.4}$$

$$\delta d^k \;=\; \left(\frac{\partial r(d^k)}{\partial d}\right)^{-1} [-r(d^k)] \;=\; \left(\frac{\partial F^{\text{INT}}(d^k)}{\partial d}\right)^{-1} r(d^k) \tag{2.5}$$

update d^{k+1}

$$d^{k+1} = d^k + \delta d^k \tag{2.6}$$

update $r(d^{k+1})$

5. check for convergence:

`IF` $\frac{|r(d^{k+1})|}{|r(d^0)|} <$ `tol THEN` $d^* = d^{k+1}$

`ELSE iterate`

where `tol` $\approx 1 \times 10^{-10}$ (or `1e-10` in computer code) is a relative residual tolerance (relative to the initial residual $r(d^0)$), a value chosen based on user experience. Relative convergence checks are usually programmed in order to avoid tolerances dependent upon units (such as Newtons, Mega-Newtons, etc). *Note, we do not see this choice in Abaqus, which can be frustrating because we do not see how Abaqus is converging or not.* More later on *convergence* with respect to a nonlinear iterative solution method.

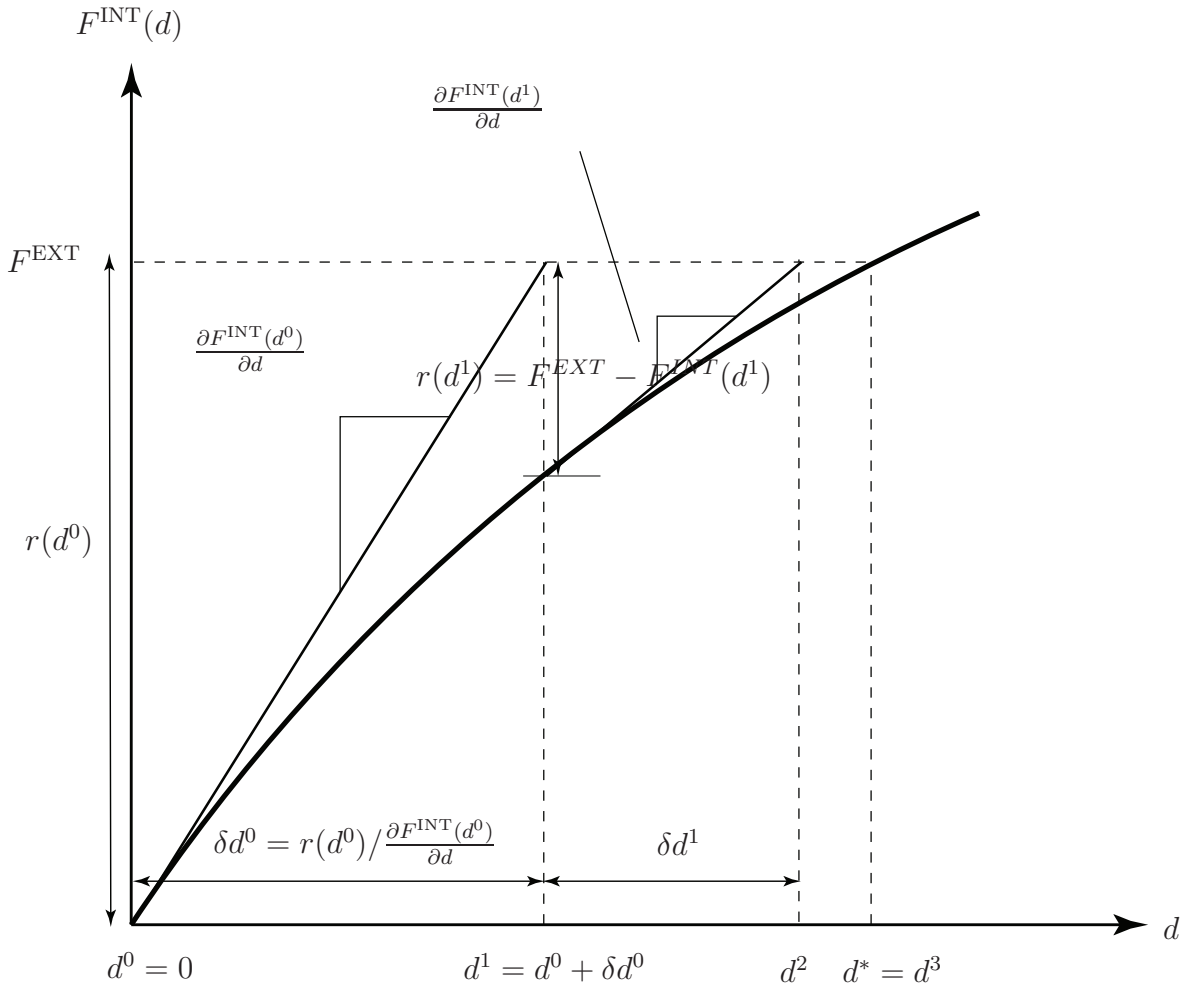

Figure 2.2. Illustration of Newton-Raphson (NR) method for solution of d, where we show iteration $k = 0, 1, 2$, and convergence likely at iteration $k = 3$. Black curve is plot of $F^{\mathrm{INT}}(d)$. d^* denotes converged value.

6. Consider incremental loading, where n_{inc} are the number of increments assuming equal increments*: $\Delta F^{\text{EXT}} = F^{\text{EXT}}/n_{\text{inc}}$ is applied over one time increment $\Delta t = t_{n+1} - t_n$. This is done because oftentimes the nonlinear equations cannot be solved for d^* with full application of F^{EXT} in one step, or you require more resolution of the solution d as the external force F^{EXT} is applied. Refer to Fig.2.3 for an illustration of applying the Newton-Raphson solution method over a force increment ΔF^{EXT}. Note that ΔF^{EXT} could be variable with adaptive time stepping techniques.

   Write the residual at current time t_{n+1}, to solve for d^*_{n+1}:

$$r(d^k_{n+1}) = F^{\text{EXT}}_{n+1} - F^{\text{INT}}(d^k_{n+1}) \tag{2.7}$$

$$\delta d^k = \left(\frac{\partial F^{\text{INT}}(d^k_{n+1})}{\partial d} \right)^{-1} r(d^k_{n+1}) \; ; \quad d^{k+1}_{n+1} = d^k_{n+1} + \delta d^k \tag{2.8}$$

   Then check for convergence:

   IF $\frac{|r(d^{k+1}_{n+1})|}{|r(d^0_{n+1})|} <$ tol THEN

   $d^*_{n+1} = d^{k+1}_{n+1}$, $n = n + 1$

   ELSE $k = k + 1$, iterate

   We do not apply the load in one step because typically the nonlinear equations are not smooth enough to accommodate such loading. Also, for dynamic or transient problems, the numerical integration (finite differencing in time) will provide a natural time step. Thus, we typically *increment* the load: $\Delta F^{\text{EXT}} = F^{\text{EXT}}/n_{\text{inc}}$.

*Most commercial finite element software packages employ some form of adaptive time stepping leading to unequal loading increments.

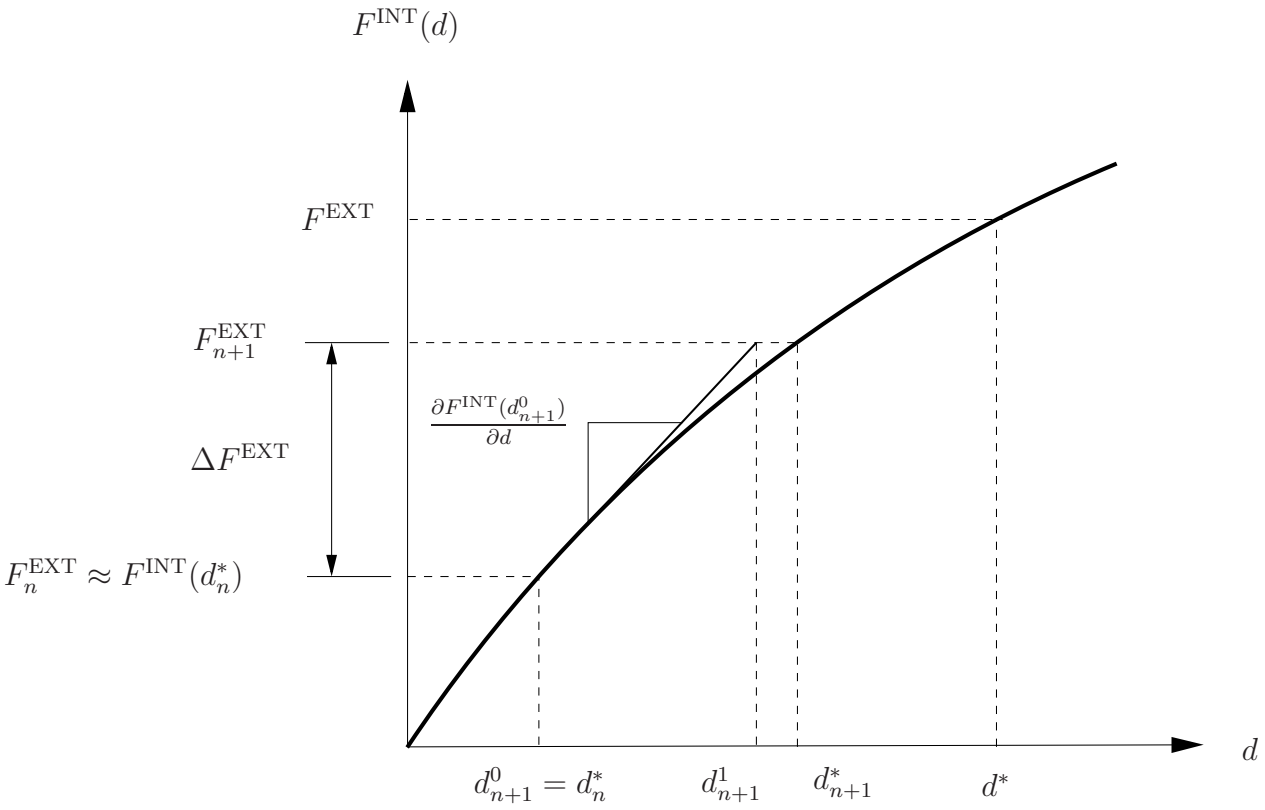

Figure 2.3. Incremental solution using Newton-Raphson (NR) method for solving d^*_{n+1} at current time t_{n+1}.

The Newton-Raphson solution method just illustrated for a single dof problem can be extended to **multiple dof systems**. In this case, the unknown variable is a vector $\boldsymbol{d}$ with components d_M, where $M = 1, ..., n_{\text{dof}}$ and n_{dof} are the number of dofs in the system of equations ($N = 1, ..., n_{\text{dof}}$) to solve numerically. We will show in Sect.2.2 how $\boldsymbol{d}$ can be the vector of unknown nodal displacements for a finite element solution. We summarize the solution method as follows. We write the residual for the system of equations $R_N(\boldsymbol{d})$ as

$$R_N(\boldsymbol{d}) = F_N^{\text{EXT}} - F_N^{\text{INT}}(\boldsymbol{d}) \tag{2.9}$$

where upon linearization by Taylor series expansion, we can update the current iterate d_N^{k+1} by solving the linear system of equations,

$$\frac{\partial R_N(\boldsymbol{d}^k)}{\partial d_M}\delta d_M^k = -R_N(\boldsymbol{d}^k) \quad ; \qquad d_N^{k+1} = d_N^k + \delta d_N^k \tag{2.10}$$

where $\frac{\partial R_N(\boldsymbol{d}^k)}{\partial d_M}$ is the consistent tangent. We check for convergence

`IF` $\frac{\|\boldsymbol{R}(\boldsymbol{d}^{k+1})\|}{\|\boldsymbol{R}(\boldsymbol{d}^0)\|} <$ `tol THEN` $\boldsymbol{d}^* = \boldsymbol{d}^{k+1}$,
`ELSE iterate`

where recall the Euclidean norm $\|\boldsymbol{R}\| = \sqrt{R_N R_N}$ (sum over repeated indices N).

It should be noted that the Newton-Raphson method converges quadratically if linearized properly (and if your initial guess is already close to the solution), meaning the relative residual norm $\frac{\|\boldsymbol{R}(\boldsymbol{d}^{k+1})\|}{\|\boldsymbol{R}(\boldsymbol{d}^0)\|}$ should decrease quadratically, e.g., 1e0, 1e-1, 1e-2, 1e-4, 1e-8, 1e-16. This is extremely attractive but comes with an associated cost: at each iteration a tangent is calculated and a linear system of equations is solved (for this reason, the method is called a 'direct' iterative solver). This can become prohibitively expensive for large problems. We normally set the relative tolerance to a value, such as `tol=1e-8`, to provide a strict convergence criterion, but not so strict that the algorithm does not converge. There is no

guarantee for convergence of nonlinear solution methods. The initial conditions will play a critical role in determining whether convergence is obtained or not.

There are a number of references that explain in more detail the Newton-Raphson method, and its modifications which we will discuss next [Ortega and Rheinboldt, 1970, Dennis and Moré, 1977, Matthies and Strang, 1979, Hughes and Ferencz, 1990, Crisfield, 1991, Ferencz and Hughes, 1998, Belytschko et al., 2000, Anandarajah, 2010].

2.1.2 Modified Newton Method

The Modified Newton method is similar to the Newton-Raphson method, except that the initial consistent tangent is used for each iteration rather than updated at each iteration, which can be costly if solving multiple dof systems. The Modified Newton method will typically converge linearly (e.g., relative residual norm is 1e0, 1e-1, 1e-2, 1e-3, 1e-4, 1e-5, ...). Modified Newton is more efficient in terms of not updating a tangent at each iteration (especially for large systems), but requires more iterations to converge. Also, for difficult-to-converge problems such as failure mechanics with post-peak softening and/or buckling, not updating the consistent tangent at each iteration may mean not converging to a solution. Thus, there is a trade off.

The Modified Newton solution method can be summarized by the following equations, and is illustrated in Fig.2.4. The residual for a one dof system is written the same as Newton-Raphson,

$$r(d^k) = F^{\text{EXT}} - F^{\text{INT}}(d^k) \tag{2.11}$$

whereas now the consistent tangent is held constant during the iteration process as

$$\delta d^k \;=\; \left(\frac{\partial r(d^0)}{\partial d}\right)^{-1} [-r(d^k)] \;=\; \left(\frac{\partial F^{\text{INT}}(d^0)}{\partial d}\right)^{-1} r(d^k) \tag{2.12}$$

$$d^{k+1} = d^k + \delta d^k \tag{2.13}$$

We check for convergence as before:

IF $\frac{|r(d^{k+1})|}{|r(d^0)|} < \texttt{tol}$ THEN $d^* = d^{k+1}$

ELSE iterate

This will lead to more iterations to converge to the solution d^*, as illustrated in Fig.2.4, because the tangent is not updated at each iteration.

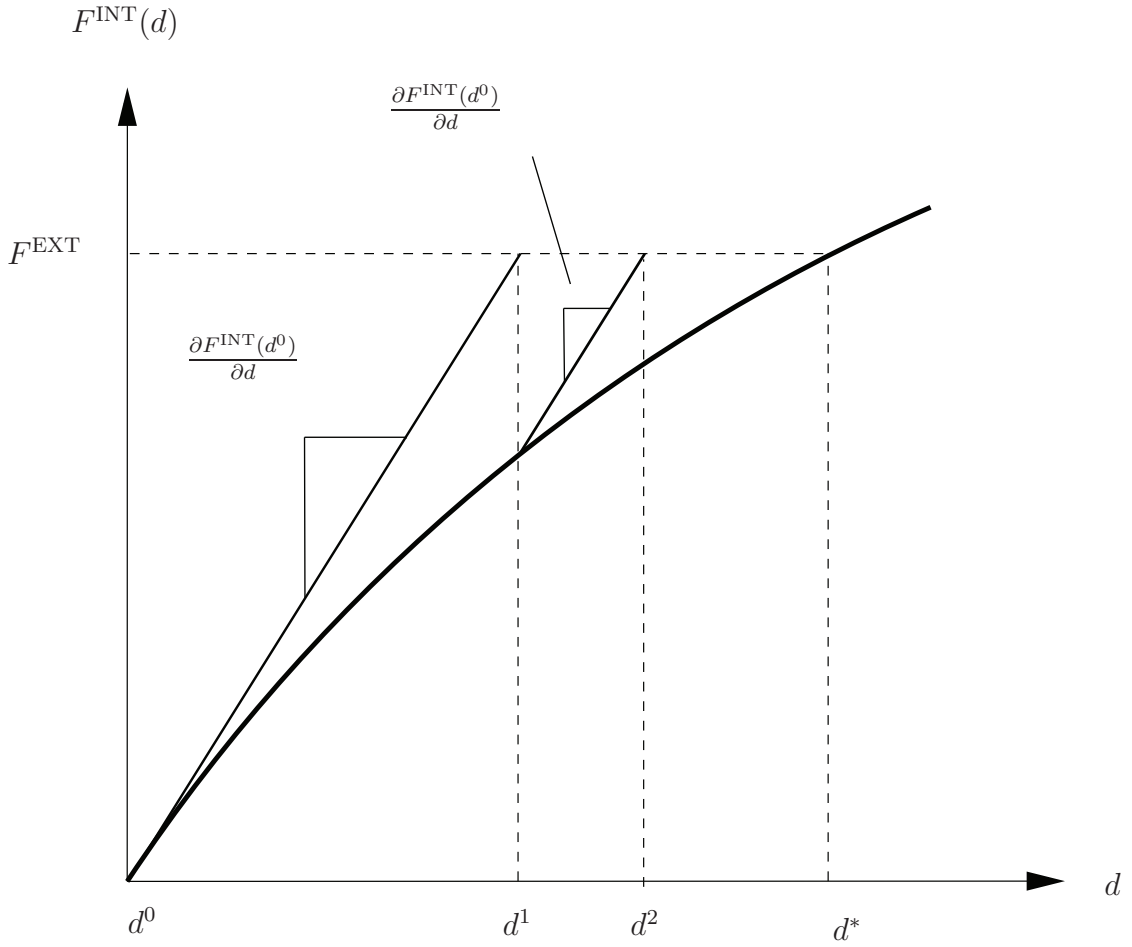

Figure 2.4. Modified Newton solution method.

2.1.3 Quasi-Newton Methods

If the consistent tangent is intractable to find in a closed form manner that can in turn be programmed and updated either at each iteration of a time step (Newton-Raphson, $(\partial r/\partial d)_{n+1}^{k+1}$) or held constant for the time step (Modified Newton, $(\partial r/\partial d)_{n+1}^{0}$), then there are further variants on the Newton-Raphson method, called *Quasi-Newton methods*. Quasi-Newton methods approximate the consistent tangent numerically, such as one well-known method called a 'secant'-type method. We consider the one dof problem again as motivation, where upon linearization we have,

$$\bar{K}^k \delta d^k = -\delta r^k \implies \bar{K}^k = \frac{-\delta r^k}{\delta d^k} = \frac{F^{INT}(d^{k+1}) - F^{INT}(d^k)}{(d^{k+1} - d^k)} \tag{2.14}$$

$$\delta d^{k+1} = (\bar{K}^k)^{-1} r(d^{k+1}) \tag{2.15}$$

where $\bar{K}^k$ is the secant tangent approximated from the current and previous iterations in order to update the next iteration d^{k+2} as

$$d^{k+2} = d^{k+1} + \delta d^{k+1} \tag{2.16}$$

The solution method is illustrated in Fig.2.5.

For multi-dof problems, we generalize the one dof case to multiple dofs in the form of the Quasi-Newton equation:

$$\bar{K}^k_{NM} \delta d^k_M = -\delta R^k_N \tag{2.17}$$

We then attempt to find $\bar{\boldsymbol{K}}^k$ via a 'secant'-type method. Note that this equation is a constraint on $\bar{\boldsymbol{K}}^k$ and does not uniquely define it. The Quasi-Newton update $\delta \boldsymbol{d}^{k+1}$ can be solved as,

$$\delta d^{k+1}_M = (\bar{K}^k_{NM})^{-1} \delta R^{k+1}_N \quad ; \qquad d^{k+2}_N = d^{k+1}_N + \delta d^{k+1}_N \tag{2.18}$$

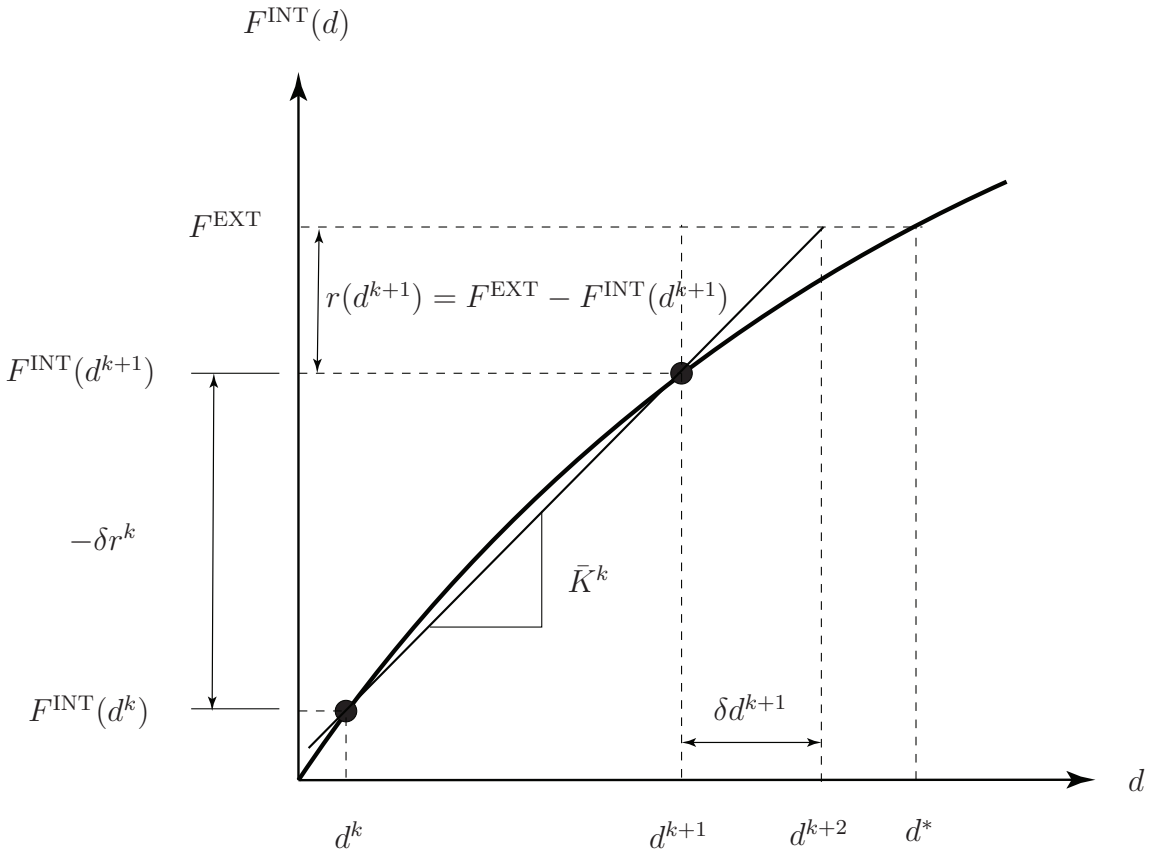

Figure 2.5. A Quasi-Newton solution method: 'secant'-type.

We check for convergence as before. There are many Quasi-Newton updates, with BFGS (Broyden, Fletcher, Goldfarb, Shanno) being one [Dennis and Moré, 1977]. *Since we are approximating the tangent*, if a problem is highly nonlinear, the algorithm could have trouble converging (e.g., generating noise and oscillations in the relative residual norm). For more details, refer to Dennis and Moré [1977], Matthies and Strang [1979], Crisfield [1991].

2.1.4 Line-Search Methods

If there is difficulty in converging within a time step, there are methods to try to fix this "lack of convergence," also known as "divergence." One such method is Line Search. It can

be motivated for the linear case, minimizing the potential energy as,

$$\Pi(\boldsymbol{d}) = \frac{1}{2} d_N K_{NM} d_M - d_N F_N^{\text{EXT}} \quad ; \qquad \frac{\partial \Pi(\boldsymbol{d})}{\partial d_N} = 0 \implies K_{NM} d_M = F_N^{\text{EXT}} \tag{2.19}$$

We introduce a line search parameter s in the update equation for an iterative solution as,

$$d_N^{k+1} = d_N^k + s^k \delta d_N^k \tag{2.20}$$

Then minimize the potential energy with respect to s as,

$$\Pi(\boldsymbol{d}^{k+1}) = \Pi(s^k) = \frac{1}{2}(d_N^k + s^k \delta d_N^k) K_{NM} (d_M^k + s^k \delta d_M^k) - (d_N^k + s^k \delta d_N^k) F_N^{\text{EXT}} \tag{2.21}$$

$$\frac{\partial \Pi(s^k)}{\partial s} = 0 \Longrightarrow \delta d_N^k [K_{NM}(d_M^k + s^k \delta d_M^k) - F_N^{\text{EXT}}] = 0 \tag{2.22}$$

where we assumed symmetric stiffness matrix $K_{NM} = K_{MN}$ (not necessary for nonlinear solution below). Solving, we obtain the line search parameter at iteration k as,

$$s^k = \frac{\delta d_N^k R_N^k}{\delta d_N^k K_{NM} \delta d_M^k} \quad ; \qquad R_N^k = F_N^{\text{EXT}} - \underbrace{K_{NM} d_M^k}_{F_N^{INT}(\boldsymbol{d}^k)} \tag{2.23}$$

Now consider the nonlinear case. Find s^k such that

$$\delta d_N^k R_N(\boldsymbol{d}^k + s^k \delta \boldsymbol{d}^k) = 0 \tag{2.24}$$

$$R_N(\boldsymbol{d}^{k+1}) = F_N^{\text{EXT}} - F_N^{\text{INT}}(\boldsymbol{d}^k + s^k \delta \boldsymbol{d}^k) \tag{2.25}$$

The root is not found exactly, but $s^k \in (0, 1]$ is determined such that

$$\frac{|G(s^k)|}{|G(0)|} < \text{tol} \quad , \qquad G(s^k) = \delta d_N^k R_N(\boldsymbol{d}^k + s^k \delta \boldsymbol{d}^k) \tag{2.26}$$

where tol = 0.5 is recommended. If tol is not satisfied, set $s^k = 1$, which means no influence of line search parameter during the iteration k.

Newton-Raphson will converge if 'close' to the solution (i.e., good initial guess) and if the nonlinear equations are sufficiently smooth (i.e., well-conditioned tangent). Nonlinear problems, however, do not always have these qualities and thus are prone to 'diverge' from the actual solution (i.e., residual grows). Thus, a line search algorithm is meant to help prevent 'divergence'. A note on terminology: purests prefer to avoid the use of the word *divergence* and instead use *lack of convergence* when a Newton-like nonlinear iteration procedure does not converge.

2.1.5 Arc-Length Methods

A powerful modification to the Newton-Raphson method is a class of methods called "arc-length" methods because the "arc" of the nonlinear solution curve is followed by the nonlinear solution algorithm (see Fig.2.6). This is particularly useful for "load-driven" problems for which there may be an instability (e.g., column buckling), or failure (e.g., soil slope failure under gravity loading, or concrete dam failure under reservoir water loading). For more details, refer to Crisfield [1991]. We will illustrate the method here, by motivating with a one dof example from Hughes and Ferencz [1990].

First, introduce a dimensionless load control parameter $\lambda(t)$, scalar arc-length function f (which must be a norm) constrained by dimensionless arc-length increment Δa (user-defined), scaling parameter b (user-defined), and an auxiliary displacement solution $\tilde{d}_0$ (to nondimensionalize the displacement increment), where displacement increment $\Delta d = d_{n+1} - d_n$, load control parameter increment $\Delta\lambda = \lambda_{n+1} - \lambda_n$, and time increment $\Delta t = t_{n+1} - t_n$,

such that,

$$\text{at } t_{n+1}: \quad r(d_{n+1}, \lambda_{n+1}) = F^{\text{INT}}(d_{n+1}) - \underbrace{\lambda_{n+1} F^{\text{EXT}}}_{F^{\text{EXT}}_{n+1}} = 0 \tag{2.27}$$

$$f(\Delta d, \Delta\lambda) - \Delta a = 0 \tag{2.28}$$

$$f(\Delta d, \Delta\lambda) := \sqrt{(1-b)\left(\frac{\Delta d}{\tilde{d}_0}\right)^2 + b(\Delta\lambda)^2} \tag{2.29}$$

$$\tilde{d}_0 := \tilde{K}_0^{-1} F^{\text{EXT}} \tag{2.30}$$

$$b \in [0, 1] \tag{2.31}$$

where b and Δa are prescribed by the user, and F^{EXT} is the *total* applied force. The increments Δd and Δa are illustrated in Fig.2.6.

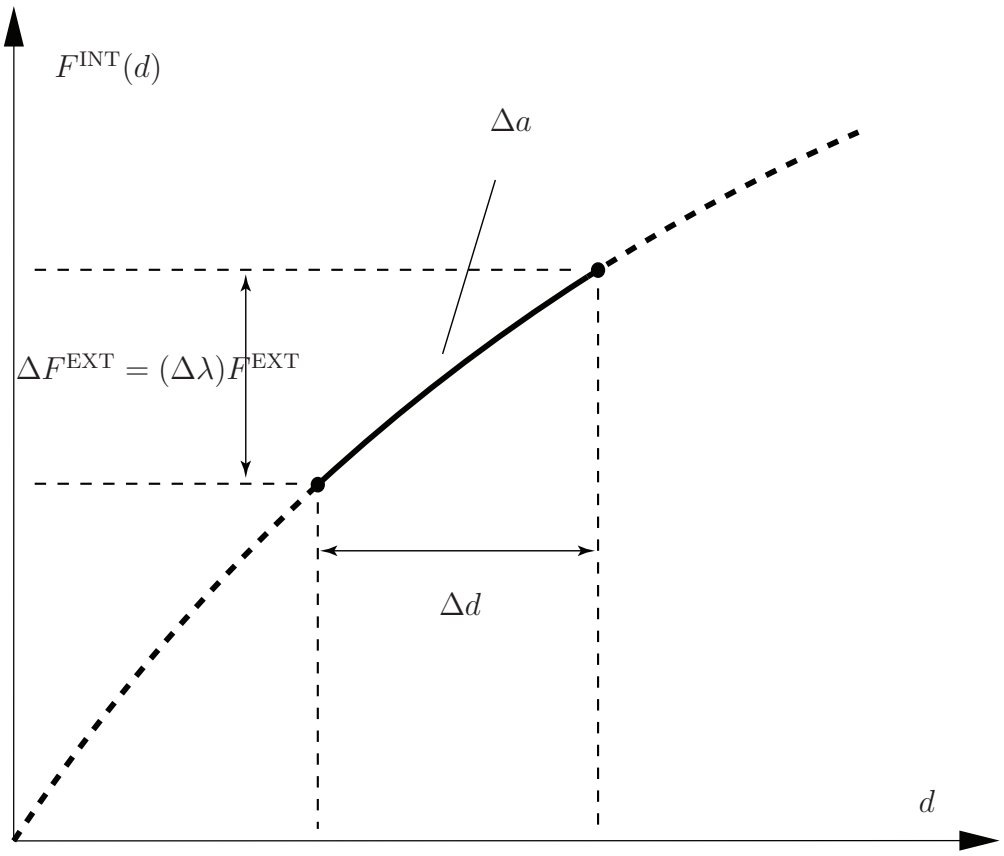

Figure 2.6. Illustration of arc-length method with load control.

We can visualize the arc-length constraint in Fig.2.7. Here, $f = \Delta a$, and the ellipse plotted for $1/2 < b < 1$ indicates *more load control*. Recall the equation of an ellipse as,

$$\frac{x^2}{A^2} + \frac{y^2}{B^2} = 1 \tag{2.32}$$

We can express Eq.(2.29) for $f = \Delta a$ in the form of an equation of an ellipse as,

$$\frac{f^2}{(\Delta a)^2} = 1 \Longrightarrow \frac{(\Delta d/\tilde{d}_0)^2}{(\Delta a/\sqrt{1-b})^2} + \frac{(\Delta\lambda)^2}{(\Delta a/\sqrt{b})^2} = 1 \tag{2.33}$$

where $x = \Delta d/\tilde{d}_0$, $y = \Delta\lambda$, $A = \Delta a/\sqrt{1-b}$, $B = \Delta a/\sqrt{b}$, and thus Fig.2.7 results.

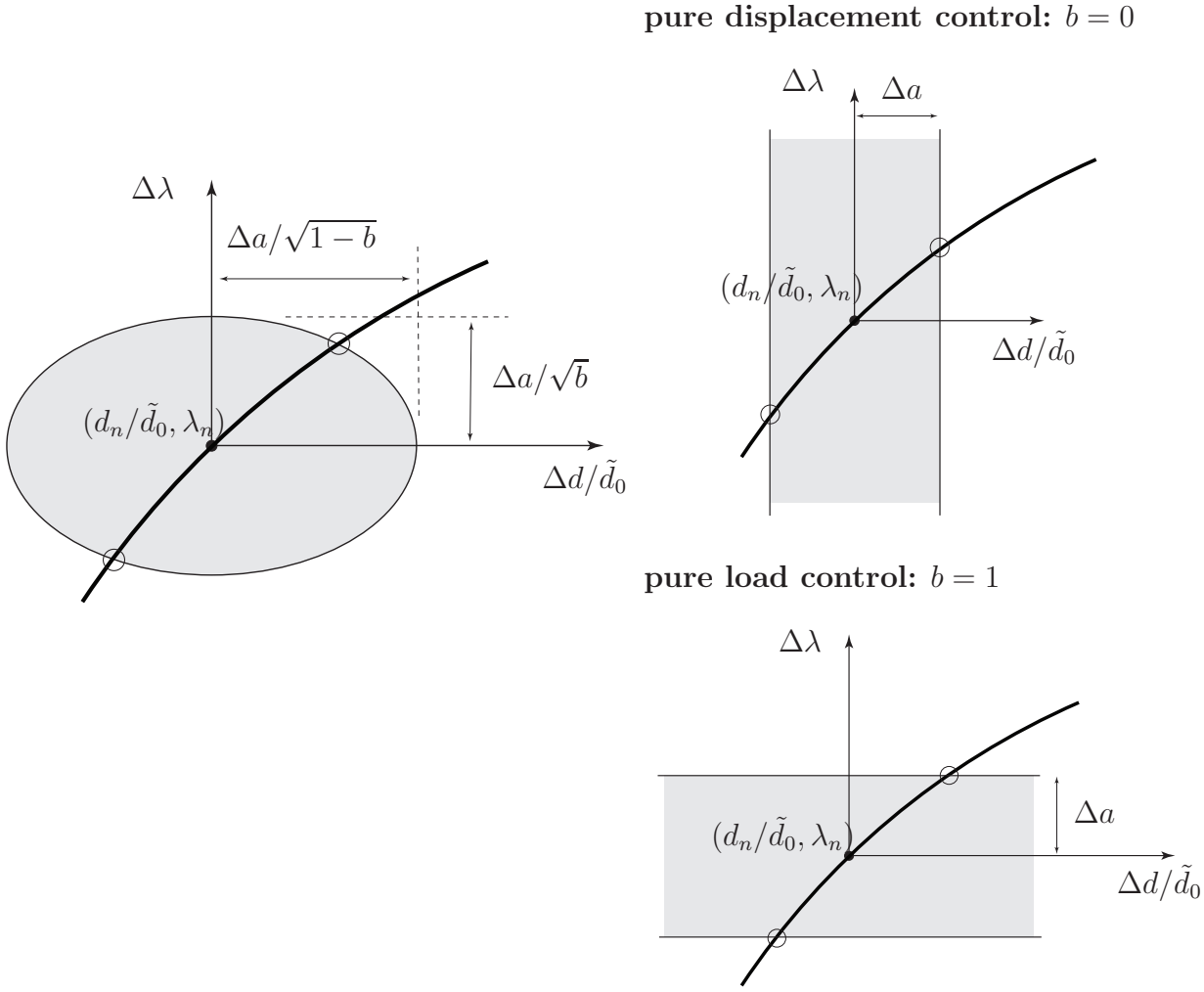

Figure 2.7. Illustration of arc-length method with load control at converged time t_{n+1}.

We solve the nonlinear equations using Newton-Raphson (or modifications thereof) as before, but with additional load-control parameter λ and constraint equation as,

$$\begin{aligned} r(d_{n+1}^{k+1}, \lambda_{n+1}^{k+1}) = F^{\text{INT}}(d_{n+1}^{k+1}) - \lambda_{n+1}^{k+1} F^{\text{EXT}} &= 0 \\ f(\Delta d^{k+1}, \Delta\lambda^{k+1}) - \Delta a &= 0 \end{aligned} \tag{2.34}$$

These coupled equations are usually solved in a staggered manner, rather than monolithically. The dimensionless arc-length increment Δa is usually varied each time step depending on whether convergence is slow (make smaller) or fast (make larger). There are various initialization strategies for the algorithm, which we will discuss shortly, with further reading in Hughes and Ferencz [1990], Crisfield [1991]. Later, we will continue this line of thought by generalizing to multi-DOF systems. We typically apply separate convergence criteria: $\|\boldsymbol{R}(\boldsymbol{d}_{n+1}^{k+1}, \lambda_{n+1}^{k+1})\| / \|\boldsymbol{R}(\boldsymbol{d}_{n+1}^{0}, \lambda_{n+1}^{0})\| < \text{tol}_R$, $(f_{n+1}^{k+1} - \Delta a)/\Delta a < \text{tol}_f$. We note that in `ABAQUS`, the arc-length method is called `Static Riks` procedure, after Riks, who was one of the first to come up with the idea [Riks, 1979].

Here, we review the nonlinear solution method applied to Eqs.(2.34). We can apply Newton-Raphson, or modification thereof. For illustration purposes, we will apply Newton-Raphson to solve the equations. We note that $\Delta d^{k+1} = d_{n+1}^{k+1} - d_n = d_{n+1}^{k} + \delta d^k - d_n = \Delta d^k + \delta d^k$ and $\Delta\lambda^{k+1} = \Delta\lambda^k + \delta\lambda^k$. Linearizing Eqs.(2.34) about state $(\bullet)^k$, we have,

$$\begin{aligned} r(d_{n+1}^{k+1}, \lambda_{n+1}^{k+1}) \approx r(d_{n+1}^{k}, \lambda_{n+1}^{k}) + \left[\begin{array}{cc} \frac{\partial F^{INT}}{\partial d} & -F^{EXT} \end{array}\right]^k \cdot \left[\begin{array}{c} \delta d^k \\ \delta\lambda^k \end{array}\right] &= 0 \\ f(\Delta d^{k+1}, \Delta\lambda^{k+1}) - \Delta a \approx \big(f(\Delta d^k, \Delta\lambda^k) - \Delta a\big) + \left[\begin{array}{cc} \frac{\partial f}{\partial(\Delta d)} & \frac{\partial f}{\partial(\Delta\lambda)} \end{array}\right]^k \cdot \left[\begin{array}{c} \delta d^k \\ \delta\lambda^k \end{array}\right] &= 0 \end{aligned} \tag{2.35}$$

which leads to the coupled system of equations to solve for the iteration increments,

$$\begin{bmatrix} \frac{\partial F^{INT}}{\partial d} & -F^{EXT} \\ \frac{\partial f}{\partial(\Delta d)} & \frac{\partial f}{\partial(\Delta\lambda)} \end{bmatrix}^k \cdot \begin{bmatrix} \delta d^k \\ \delta\lambda^k \end{bmatrix} = \begin{bmatrix} -r^k_{n+1} \\ \Delta a - f^k \end{bmatrix} \tag{2.36}$$

The values at $k+1$ are then updated as follows,

$$d^{k+1}_{n+1} = d^k_{n+1} + \delta d^k \ , \ \lambda^{k+1}_{n+1} = \lambda^k_{n+1} + \delta\lambda^k \tag{2.37}$$

$$\Delta d^{k+1} = \Delta d^k + \delta d^k \ , \ \Delta\lambda^{k+1} = \Delta\lambda^k + \delta\lambda^k \tag{2.38}$$

Initialization of Δd^0 and $\Delta\lambda^0$ at the start of the iteration procedure: We will describe two procedures used to initialize the increments of d and λ at $k = 0$ [Hughes and Ferencz, 1990].

Procedure 1: (used also to initialize Procedure 2)

1.(a) Let $\tilde{d}_n = \tilde{K}_n^{-1} F^{EXT}$, where, for example, $\tilde{K}_n = \partial F^{INT}(d_n)/\partial d$

1.(b) Let $\Delta d^0 = \underbrace{\Delta\lambda^0}_{\text{solve for}} \tilde{d}_n$

1.(c) Solve for magnitude of $\Delta\lambda^0$ as follows:

$$f(\Delta d^0, \Delta\lambda^0) = \Delta a \tag{2.39}$$

$$f(\Delta\lambda^0 \tilde{d}_n, \Delta\lambda^0) = \Delta a \tag{2.40}$$

$$\Longrightarrow |\Delta\lambda^0| = \frac{\Delta a}{f(\tilde{d}_n, 1)} \tag{2.41}$$

1.(d) Determine sign of $\Delta\lambda^0$ with these conditions: (i) if $\text{sign}[\tilde{K}_n] = -\text{ sign}[\tilde{K}_{n-1}]$, and (ii) if $\tilde{K}_{n-1}$ to $\tilde{K}_n$ passes through 0 or ∞, then $\text{sign}(\Delta\lambda^0_{n+1}) = -\text{ sign}(\Delta\lambda^0_n)$, else $\text{sign}(\Delta\lambda^0_{n+1}) =$

$\text{sign}(\Delta\lambda_n^0)$. Then, $\Delta\lambda_{n+1}^0 = \text{sign}(\Delta\lambda_{n+1}^0)|\Delta\lambda^0|$, and $\Delta d_{n+1}^0 = \Delta\lambda_{n+1}^0 \tilde{d}_n$.

Procedure 2: extrapolate using Lagrange polynomials

*consider quadratic interpolation, followed by extrapolation to time t_{n+1} given a_{n+1} and previous values of arc-length a (insert figure)

Lagrange polynomials for quadratic interpolation (let $a_{n+1} = a$) between states $n-2$, $n-1$, and n, and then extrapolate to a_{n+1} such that,

$$\ell_1^2(a_{n+1}) = \frac{(a_{n+1} - a_{n-1})(a_{n+1} - a_n)}{(a_{n-2} - a_{n-1})(a_{n-2} - a_n)} \tag{2.42}$$

$$\ell_2^2(a_{n+1}) = \frac{(a_{n+1} - a_{n-2})(a_{n+1} - a_n)}{(a_{n-1} - a_{n-2})(a_{n-1} - a_n)} \tag{2.43}$$

$$\ell_3^2(a_{n+1}) = \frac{(a_{n+1} - a_{n-1})(a_{n+1} - a_{n-2})}{(a_n - a_{n-1})(a_n - a_{n-2})} \tag{2.44}$$

Using these Lagrange polynomials, extrapolate to time t_{n+1} to initialize λ and d, such that,

$$\lambda_{n+1}^0 = \ell_1^2(a_{n+1})\lambda_{n-2} + \ell_2^2(a_{n+1})\lambda_{n-1} + \ell_3^2(a_{n+1})\lambda_n \tag{2.45}$$

$$d_{n+1}^0 = \ell_1^2(a_{n+1})d_{n-2} + \ell_2^2(a_{n+1})d_{n-1} + \ell_3^2(a_{n+1})d_n \tag{2.46}$$

Note that if the increments of arc-length a are constant, such that $\Delta a = a_{n+1} - a_n = a_n - a_{n-1}$ and so forth, then the Lagrange polynomial coefficients are $\ell_1^2(a_{n+1}) = 1$, $\ell_2^2(a_{n+1}) = -3$, and $\ell_3^2(a_{n+1}) = 3$. Now initialize $\Delta\lambda_{n+1}^0 = \lambda_{n+1}^0 - \lambda_n$ and $\Delta d_{n+1}^0 = d_{n+1}^0 - d_n$.

The advantage of Procedure 2 is that we do not need to determine the magnitude and sign of $\Delta\lambda_{n+1}^0$ separately, but we still need to use Procedure 1 for the first few time steps because Procedure 2 requires three previous states to initialize.

Convergence Check: We have separate tolerances tol_r and tol_f for the balance equation

residual and arc-length function, respectively, such that,

$$\begin{aligned} \text{if } \frac{|r(d_{n+1}^{k+1}, \lambda_{n+1}^{k+1})|}{|r(d_{n+1}^{0}, \lambda_{n+1}^{0})|} &< tol_r \\ \text{and } \frac{f_{n+1}^{k+1} - \Delta a}{\Delta a} &< tol_f \end{aligned} \tag{2.47}$$

then converged, else iterate.

Multi-DOF Systems: Let us now generalize the previous discussion to multi-dof systems, such as for nonlinear FE analysis. We write the balance equation residual and arc-length function, respectively, as,

$$\begin{aligned} \boldsymbol{R}(\boldsymbol{d}_{n+1}^{k+1}, \lambda_{n+1}^{k+1}) = \boldsymbol{F}^{\text{INT}}(\boldsymbol{d}_{n+1}^{k+1}) - \underbrace{\lambda_{n+1}^{k+1}\boldsymbol{F}^{\text{EXT}}}_{(\boldsymbol{F}^{\text{EXT}})_{n+1}^{k+1}} &= \boldsymbol{0} \\ f(\Delta\boldsymbol{d}^{k+1}, \Delta\lambda^{k+1}) - \Delta a &= 0 \end{aligned} \tag{2.48}$$

where the arc-length function is now,

$$f(\Delta\boldsymbol{d}^{k+1}, \Delta\lambda^{k+1}) = \left[(1-b)\frac{(\Delta\boldsymbol{d}^{k+1})^T \cdot diag(\tilde{\boldsymbol{K}}_0) \cdot \Delta\boldsymbol{d}^{k+1}}{(\tilde{\boldsymbol{d}}_0)^T \cdot diag(\tilde{\boldsymbol{K}}_0) \cdot \tilde{\boldsymbol{d}}_0} + b(\Delta\lambda^{k+1})^2 \right]^{\frac{1}{2}} \tag{2.49}$$

where the auxiliary solution is $\tilde{\boldsymbol{d}}_0 = \tilde{\boldsymbol{K}}_0^{-1} \cdot \boldsymbol{F}^{\text{EXT}}$.

Linearizing Eqs.(2.48) leads to the coupled system of equations to solve for the iteration increments,

$$\begin{bmatrix} \frac{\partial \boldsymbol{F}^{\text{INT}}}{\partial \boldsymbol{d}} & -\boldsymbol{F}^{\text{EXT}} \\ \frac{\partial f}{\partial(\Delta \boldsymbol{d})} & \frac{\partial f}{\partial(\Delta\lambda)} \end{bmatrix}^k \cdot \begin{bmatrix} \delta\boldsymbol{d}^k \\ \delta\lambda^k \end{bmatrix} = \begin{bmatrix} -\boldsymbol{R}_{n+1}^k \\ \Delta a - f^k \end{bmatrix} \tag{2.50}$$

where

$$\frac{\partial f}{\partial(\Delta \boldsymbol{d})} = \left(\frac{(1-b)/f}{(\tilde{\boldsymbol{d}}_0)^T \cdot diag(\tilde{\boldsymbol{K}}_0) \cdot \tilde{\boldsymbol{d}}_0}\right)(\Delta \boldsymbol{d}^k)^T \cdot diag(\tilde{\boldsymbol{K}}_0) \tag{2.51}$$

$$\frac{\partial f}{\partial(\Delta \lambda)} = \frac{b}{f}\Delta\lambda^k \tag{2.52}$$

The values are then updated as follows,

$$\boldsymbol{d}_{n+1}^{k+1} = \boldsymbol{d}_{n+1}^{k} + \delta \boldsymbol{d}^k \ , \ \lambda_{n+1}^{k+1} = \lambda_{n+1}^{k} + \delta\lambda^k \tag{2.53}$$

$$\Delta \boldsymbol{d}^{k+1} = \Delta \boldsymbol{d}^k + \delta \boldsymbol{d}^k \ , \ \Delta\lambda^{k+1} = \Delta\lambda^k + \delta\lambda^k \tag{2.54}$$

Initialization of $\Delta \boldsymbol{d}^0$ and $\Delta\lambda^0$:

Procedure 1: (used also to initialize Procedure 2)

1.(a) Let $\tilde{\boldsymbol{d}}_n = \tilde{\boldsymbol{K}}_n^{-1} \cdot \boldsymbol{F}^{\mathrm{EXT}}$, where $\tilde{\boldsymbol{K}}_n = \partial \boldsymbol{F}^{\mathrm{INT}}(\boldsymbol{d}_n)/\partial \boldsymbol{d}$

1.(b) Let $\Delta \boldsymbol{d}^0 = \Delta\lambda^0 \tilde{\boldsymbol{d}}_n$.

1.(c) Solve for magnitude of $\Delta\lambda^0$:

$$f(\Delta \boldsymbol{d}^0, \Delta\lambda^0) = \Delta a \tag{2.55}$$

$$f(\Delta\lambda^0 \tilde{\boldsymbol{d}}_n, \Delta\lambda^0) = \Delta a \tag{2.56}$$

$$|\Delta\lambda^0| = \frac{\Delta a}{f(\tilde{\boldsymbol{d}}_n, 1)} \tag{2.57}$$

1.(d) Determine sign of $\Delta\lambda^0$ with these conditions: (i) if $\mathrm{sign}[\det \tilde{\boldsymbol{K}}_n] = -\ \mathrm{sign}[\det \tilde{\boldsymbol{K}}_{n-1}]$, and (ii) if $\det \tilde{\boldsymbol{K}}_{n-1}$ to $\det \tilde{\boldsymbol{K}}_n$ passes through 0 or ∞, then $\mathrm{sign}(\Delta\lambda_{n+1}^0) = -\ \mathrm{sign}(\Delta\lambda_n^0)$, else $\mathrm{sign}(\Delta\lambda_{n+1}^0) = \mathrm{sign}(\Delta\lambda_n^0)$. Then, $\Delta\lambda_{n+1}^0 = \mathrm{sign}(\Delta\lambda_{n+1}^0)|\Delta\lambda^0|$.

Procedure 2: Using the Lagrange polynomials, extrapolate to time t_{n+1} to initialize, such that,

$$\lambda_{n+1}^{(0)} = \ell_1^2(a_{n+1})\lambda_{n-2} + \ell_2^2(a_{n+1})\lambda_{n-1} + \ell_3^2(a_{n+1})\lambda_n \tag{2.58}$$

$$\boldsymbol{d}_{n+1}^{(0)} = \ell_1^2(a_{n+1})\boldsymbol{d}_{n-2} + \ell_2^2(a_{n+1})\boldsymbol{d}_{n-1} + \ell_3^2(a_{n+1})\boldsymbol{d}_n \tag{2.59}$$

where if the increments of arc-length a are constant (as for the single dof discussion), then $\ell_1^2(a_{n+1}) = 1$, $\ell_2^2(a_{n+1}) = -3$, and $\ell_3^2(a_{n+1}) = 3$. Now initialize $\Delta\lambda_{n+1}^{(0)} = \lambda_{n+1}^{(0)} - \lambda_n$ and $\Delta\boldsymbol{d}_{n+1}^{(0)} = \boldsymbol{d}_{n+1}^{(0)} - \boldsymbol{d}_n$.

Convergence Check: We have separate tolerances tol_R and tol_f for the balance equation residual and arc-length function, respectively, such that

$$\begin{aligned} \text{if } \frac{\|\boldsymbol{R}(\boldsymbol{d}_{n+1}^{k+1}, \lambda_{n+1}^{k+1})\|}{\|\boldsymbol{R}(\boldsymbol{d}_{n+1}^{0}, \lambda_{n+1}^{0})\|} &< tol_R \\ \text{and } \frac{f_{n+1}^{k+1} - \Delta a}{\Delta a} &< tol_f \end{aligned} \tag{2.60}$$

then converged, else iterate.

In summary, arc-length methods are used when pure load control cannot converge to the actual force-displacement path (such as for buckling, or localized deformation and failure). Pure displacement control is preferred for this reason, but if force or pressure is applied (or gravity) and buckling or failure could occur, arc-length methods are used to *continue* the solution.

Arc-length algorithm for single dof problem: What follows is the outline of an algorithm you can use to write your 1D code to solve a nonlinear single dof problem using Newton-Raphson with Arc-Length control:

```
n=1
d(n)=0
lambda(n)=0
Fext=8
b=0.5
Delta_a=0.1
while d(n) < 7
Ktilde=?
dtilde=Fext/Ktilde
f_arc=?  function of (dtilde,1)
k=1
(initialization)
if n<3
Delta_lambda = Delta_a / f_arc
Delta_d = (Delta_lambda)*dtilde
lambda = lambda(n) + Delta_lambda
d = d(n) + Delta_d
else
lambda = lambda(n-2) - 3*lambda(n-1) + 3*lambda(n)
d = d(n-2) - 3*d(n-1) + 3*d(n)
Delta_lambda = lambda - lambda(n)
Delta_d = d - d(n)
end
Fint=?
```

```
r=Fint-lambda*Fext

f_arc=?

while (convergence criteria)

(put Newton-Raphson here to update d and lambda)

k=k+1

end

n=n+1

d(n)=d

lambda(n)=lambda

end
```

2.1.6 Other Nonlinear Solution Algorithms

Here, we briefly introduce 'matrix-free' or 'indirect-iterative' nonlinear solution algorithms. They are attractive—if not necessary—for very large problems because no tangent needs to be calculated and no linear algebraic system of equations needs to be solved. They are specifically used for quasi-static problems, whereas for dynamic problems explicit time integrators are used (from which the Dynamic Relaxation algorithm is motivated).

1. **Nonlinear Conjugate Gradient (CG)**: This algorithm entails minimizing the energy functional $\Pi(\boldsymbol{d})$, where its gradient is negative the residual $\boldsymbol{R}(\boldsymbol{d})$. The method is similar to linear CG except that we iteratively solve for the line search parameter (or approximate it) and search directions are *approximately* orthogonal. Preconditioning becomes extremely important because many nonlinear problems are ill-conditioned (i.e., large spread in the eigenvalues of the underlying tangent). We want the eigenvalues of the underlying tangent to be as closely clustered as possible, where the perfect preconditioner is the inverse (i.e., consistent tangent) since the identity matrix has all eigenvalues = 1. Refer to [CG-Method].

2. **Dynamic Relaxation**: Fictitious mass and damping are introduced to form the dynamic problem which is then solved by an explicit time integrator, relaxing the dynamic equations until the quasi-static solution is obtained. Refer to Key et al. [1981], Underwood [1983] for more details.

2.2 Nonlinear Elastostatics of an Axially-Loaded Bar at Small Strain

Refer to Sects.3.2, 8.1, and 8.2 of Anandarajah [2010], among other references. This section is meant to provide a brief introduction to the nonlinear finite element method (FEM), formulating the Strong, Weak, Galerkin, and nonlinear finite element equations in residual form for solution by the Newton-Raphson method. We assume geometric linearity (small strain $\epsilon = du/dx$), but material nonlinearity (axial stress $\sigma(\epsilon)$ is a nonlinear function of axial strain ϵ). An example of a two-element discretization of an axially-loaded one-dimensional (1D) bar is provided, with a nonlinear elastic constitutive relation for axial stress $\sigma(\epsilon)$. Refer to CVEN 5511 notes (or other introductory FEM books or notes) for a review of the linear FEM for an axially-loaded bar.

2.2.1 Strong Form

The strong form of the problem is a formal statement of the governing differential equation(s) and boundary conditions. It is called "strong" because the differential equation is satisfied pointwise, in this case at every point x in the domain $\bar{\Omega}$ (more below). Here, our governing differential equation is the balance of linear momentum *without* inertia terms. For the axially-loaded bar shown in Fig.2.8, the strong form (S) may be stated as,

$$\text{Find } u(x) : \bar{\Omega} \mapsto \mathbb{R} \text{ such that}$$

$$-\frac{d}{dx}(\sigma A) = f \quad x \in \Omega \tag{2.61}$$

$$(\sigma A)_L = F \quad x = L \tag{2.62}$$

$$u = g \quad x = 0 \tag{2.63}$$

where the internal axial force $N(x) = \sigma(x)A(x)$ (see CVEN 5511 notes), the axial displacement $u(x) : \bar{\Omega} \mapsto \mathbb{R}$ reads as "the domain of $u(x)$ for x is $\bar{\Omega} = [0, L]$ or $0 \leq x \leq L$, and the range of u is the set of real numbers $\mathbb{R}$," and $\Omega = (0, L)$ where $x \in \Omega$ reads "x in Ω" or $0 < x < L$. A natural (or Neumann) BC is applied at $x = L$, and an essential (or Dirichlet) BC is applied at $x = 0$. Refer to Fig.2.8 for definition of terms in the Strong Form (S).

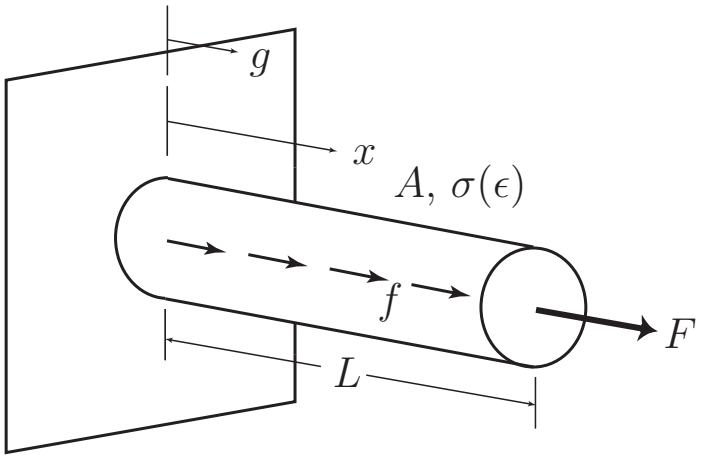

Figure 2.8. Axially-loaded bar with cross-sectional area A (m^2), length L (m), axial stress σ (Pa) which may be a nonlinear function of axial strain $\epsilon = du/dx$, axial displacement $u(x)$, concentrated force F (N) at $x = L$, distributed axial force f (N/m), and prescribed axial displacement g (m) at $x = 0$.

2.2.2 Weak Form

To formulate the weak or variational form, we write the differential equation in residual form using the Method of Weighted Residuals, such as,

$$\int_0^L w \left[\frac{d}{dx}(\sigma A) + f \right] dx = 0 \tag{2.64}$$

where $w(x)$ is called the weighting function. We next integrate by parts, which will provide us (i) a bilinear form (symmetry, typically), and (ii) provide the natural BC. After integrating

by parts using the chain rule

$$\frac{d}{dx}\left[w(\sigma A)\right] = \frac{dw}{dx}(\sigma A) + w\frac{d(\sigma A)}{dx} \tag{2.65}$$

and applying the Divergence Theorem, we have

$$\int_0^L \frac{dw}{dx}\sigma A dx = \int_0^L wf dx + w(L)F \tag{2.66}$$

Recall that we integrate by parts to reach a bilinear form and also to provide the natural BC [Hughes, 1987]. Thus, we can state the weak (or variational) form (W) as,

$$\begin{gathered} \text{Find } u(x) \in \mathcal{S} \text{ such that} \\ \int_0^L \frac{dw}{dx}\sigma A dx = \int_0^L wf dx + w(L)F \\ \text{holds for all } w(x) \in \mathcal{V} \end{gathered} \tag{2.67}$$

where the trial solution space is $\mathcal{S} = \{u(x) : \bar{\Omega} \mapsto \mathbb{R}, u(0) = g\}$ and weighting function space is $\mathcal{V} = \{w(x) : \bar{\Omega} \mapsto \mathbb{R}, w(0) = 0\}$. It can be shown that the weak and strong forms are equivalent [Hughes, 1987]. It is called the "weak" form because the differential equation is satisfied in integral (or average) form.

2.2.3 Galerkin Form

The Galerkin form is a discrete approximation to the weak form, as demonstrated in Fig.2.9. There are two traditional Galerkin methods [Hughes, 1987]: the Bubnov-Galerkin and Petrov-Galerkin methods. The Bubnov-Galerkin method assumes the class of functions for the weighting function and trial solution (displacement) are the same (e.g., linear shape functions for both), whereas the Petrov-Galerkin method is more general and allows their

function classes to be different. We will use the Bubnov-Galerkin method (which is normally just called the "Galerkin" method). An advantage computationally to Bubnov-Galerkin is that the tangent stiffness matrix is symmetric, if the material tangent matrix is symmetric. This symmetry will break down for non-associative plasticity (used for most geomaterials) as well as anisotropy due to fabric or texture effects.

The Galerkin form involves discretizing spatially the domain, in this case the bar of length L, into discrete segments with characteristic length h. The discrete trial solution and weighting function spaces $\mathcal{S}^h$ and $\mathcal{V}^h$, respectively, in turn are finite dimensional subspaces of their continuous counterparts: $\mathcal{S}^h \subset \mathcal{S}$, $\mathcal{V}^h \subset \mathcal{V}$. The Galerkin form (G) is a restatement of the weak form in finite dimensional space as,

$$\begin{gathered} \text{Find } u^h(x) \in \mathcal{S}^h \text{ such that} \\ \int_{\Omega^h} \frac{dw^h}{dx} \sigma(\epsilon^h) A dx = \int_{\Omega^h} w^h f dx + w^h(L) F \\ \text{holds for all } w^h(x) \in \mathcal{V}^h \end{gathered} \tag{2.68}$$

where axial strain $\epsilon^h = du^h/dx$, and h is the characteristic length of the finite element (indicating that the variable is discrete). The finite dimensional trial solution space is $\mathcal{S}^h = \{u^h(x) : \bar{\Omega}^h \mapsto \mathbb{R}, u^h(0) = g\}$ and weighting function space is $\mathcal{V}^h = \{w^h(x) : \bar{\Omega}^h \mapsto \mathbb{R}, w^h(0) = 0\}$, where $\bar{\Omega}^h = [0, L]$. For this 1D problem, $\bar{\Omega}^h = \bar{\Omega}$, but this is usually not the case for 2D and 3D problems, where $\bar{\Omega}^h \subset \bar{\Omega}$, i.e., the mesh is an approximation (typically a sub-domain) of the physical spatial (geometric) domain.

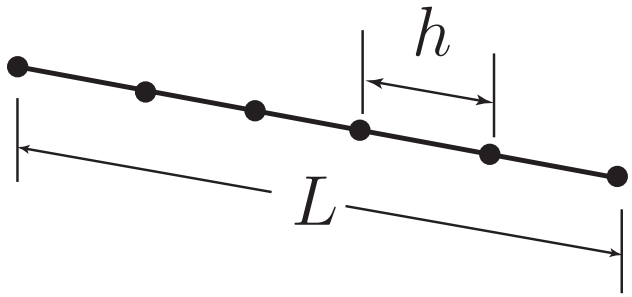

Figure 2.9. Discretization of bar for Galerkin form, given discretization parameter h.

2.2.4 Finite Element Form

The next step in formulating the nonlinear finite element equations is to further discretize the problem into finite elements, such that,

$$\Omega^h = \mathop{\mathbf{A}}_{e=1}^{n_{\text{el}}} \Omega^e \tag{2.69}$$

where $\mathop{\mathbf{A}}_{e=1}^{n_{\text{el}}}$ is called the element assembly operator, $\Omega^e = (x_1^e, x_2^e)$, n_{el} is the number of finite elements, and e indicates the element number. The domain of element e is shown in Fig.2.10 for the global coordinate system x as well as the natural coordinate system ξ.

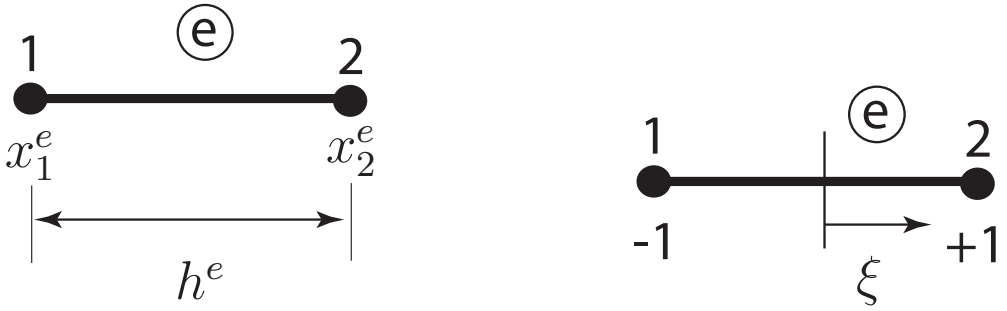

Figure 2.10. Linear 2-noded finite element in global coordinate x and natural coordinate ξ. Element length $h^e = x_2^e - x_1^e$. x_a^e is global coordinate of local node a, where $a = 1, 2$.

We will use an isoparametric formulation for the global coordinate x, weighting function w,

and displacement u such that,

$$x^{h^e}(\xi) = \sum_{a=1}^{2} N_a(\xi) x_a^e \tag{2.70}$$

$$w^{h^e}(\xi) = \sum_{a=1}^{2} N_a(\xi) c_a^e \tag{2.71}$$

$$u^{h^e}(\xi) = \sum_{a=1}^{2} N_a(\xi) d_a^e \tag{2.72}$$

where the shape functions are shown in Fig.2.11, c_a^e are the local nodal weighting function values, and d_a^e are the local nodal displacements shown in Fig.2.12. The formulation is called "isoparametric" because the coordinate x and weighting function w and displacement u are all interpolated with the *same* shape functions.

Figure 2.11. Linear shape functions for 2-noded element in natural coordinate ξ. $N_1 = (1-\xi)/2$, $N_2 = (1+\xi)/2$.

Figure 2.12. Nodal values of weighting function c_a^e and displacement d_a^e, local node $a = 1, 2$.

To express in matrix-vector form, we carry out the summation and write,

$$x^{h^e}(\xi) = \left[\begin{array}{cc} N_1 & N_2 \end{array}\right] \left[\begin{array}{c} x_1^e \\ x_2^e \end{array}\right] = \boldsymbol{N}^e(\xi) \cdot \boldsymbol{x}^e \tag{2.73}$$

$$w^{h^e}(\xi) = \left[\begin{array}{cc} N_1 & N_2 \end{array}\right] \left[\begin{array}{c} c_1^e \\ c_2^e \end{array}\right] = \boldsymbol{N}^e(\xi) \cdot \boldsymbol{c}^e = (\boldsymbol{c}^e)^T \cdot (\boldsymbol{N}^e)^T(\xi) \tag{2.74}$$

$$u^{h^e}(\xi) = \left[\begin{array}{cc} N_1 & N_2 \end{array}\right] \left[\begin{array}{c} d_1^e \\ d_2^e \end{array}\right] = \boldsymbol{N}^e(\xi) \cdot \boldsymbol{d}^e \tag{2.75}$$

When calculating the spatial derivatives of the weighting function and displacement field, we use the Jacobian of coordinate transformation j^e:

$$\frac{dw^{h^e}(\xi)}{dx} = \frac{d\boldsymbol{N}^e(\xi)}{dx} \cdot \boldsymbol{c}^e = \boldsymbol{B}^e \cdot \boldsymbol{c}^e = (\boldsymbol{c}^e)^T \cdot (\boldsymbol{B}^e)^T \tag{2.76}$$

$$\boldsymbol{B}^e = \frac{d\boldsymbol{N}^e(\xi)}{dx} = \frac{d\boldsymbol{N}^e(\xi)}{d\xi}\frac{d\xi}{dx} \tag{2.77}$$

$$j^e = \frac{dx^{h^e}}{d\xi} = \frac{\partial N_1}{\partial \xi}x_1^e + \frac{\partial N_2}{\partial \xi}x_2^e = -\frac{1}{2}x_1^e + \frac{1}{2}x_2^e = h^e/2 \tag{2.78}$$

$$\Longrightarrow \quad \boldsymbol{B}^e = \frac{1}{h^e}\left[\begin{array}{cc} -1 & 1 \end{array}\right] \tag{2.79}$$

We likewise transform the integration as,

$$\int_{\Omega^e} (\bullet) dx = \int_{-1}^{1} (\bullet) j^e d\xi \tag{2.80}$$

We rewrite the discrete variational equation in element form as

$$\int_{\Omega^h} \frac{dw^h}{dx}\sigma(\epsilon^h) A dx = \int_{\Omega^h} w^h f dx + w^h(L)F \tag{2.81}$$

$$\mathop{\mathsf{A}}_{e=1}^{n_{\text{el}}} \left\{ \int_{\Omega^e} \frac{dw^{h^e}}{dx}\sigma(\epsilon^{h^e}) A dx = \int_{\Omega^e} w^{h^e} f dx + w^{h^e}(L)F \right\} \tag{2.82}$$

Substituting the shape functions, we have

$$\mathop{\mathbf{A}}_{e=1}^{n_{\text{el}}} (\boldsymbol{c}^e)^T \cdot \left\{ \underbrace{\int_{-1}^{1} (\boldsymbol{B}^e)^T \sigma(\epsilon^{h^e}) A j^e d\xi}_{\boldsymbol{f}^{e,\text{INT}}(\boldsymbol{d}^e)} = \underbrace{\underbrace{\int_{-1}^{1} (\boldsymbol{N}^e)^T f j^e d\xi}_{\boldsymbol{f}_f^e} + \boldsymbol{f}_F^e}_{\boldsymbol{f}^{e,\text{EXT}}} \right\} \tag{2.83}$$

$$\mathop{\mathbf{A}}_{e=1}^{n_{\text{el}}} (\boldsymbol{c}^e)^T \cdot \left\{ \boldsymbol{f}^{e,\text{INT}}(\boldsymbol{d}^e) = \boldsymbol{f}^{e,\text{EXT}} \right\} \tag{2.84}$$

where $\boldsymbol{f}^{e,\text{INT}}(\boldsymbol{d}^e)$ is the internal element force vector, and $\boldsymbol{f}^{e,\text{EXT}}$ is the external element force vector. After assembly and application of BCs, we have,

$$\boldsymbol{c}^T \cdot \left[\boldsymbol{F}^{\text{INT}}(\boldsymbol{d}) - \boldsymbol{F}^{\text{EXT}} \right] = 0 \tag{2.85}$$

which must hold **for all** $\boldsymbol{c}$ (all w^h), which implies that $\boldsymbol{c}$ is arbitrary, except for nodes where we have essential B.C.s, $c_A = 0$ if $d_A = g$ at global node A. Thus, for equilibrium to be satisfied after applying essential B.C.s, then the following equation must hold

$$\boldsymbol{F}^{\text{INT}}(\boldsymbol{d}) = \boldsymbol{F}^{\text{EXT}} \tag{2.86}$$

or in residual form

$$\boldsymbol{R}(\boldsymbol{d}) = \boldsymbol{F}^{\text{INT}}(\boldsymbol{d}) - \boldsymbol{F}^{\text{EXT}} = \boldsymbol{0} \tag{2.87}$$

which is a system of nonlinear equations that can be solved by the Newton-Raphson method we presented in Sect.2.1.

2.2.5 Consistent Tangent

The main ingredient needed for a Newton-Raphson solution method is the consistent tangent. In this case, the global consistent tangent is written as,

$$\frac{\partial \boldsymbol{R}}{\partial \boldsymbol{d}} = \frac{\partial \boldsymbol{F}^{\mathrm{INT}}(\boldsymbol{d})}{\partial \boldsymbol{d}} = \mathop{\mathsf{A}}_{e=1}^{n_{\mathrm{el}}} \frac{\partial [\boldsymbol{f}^e(\boldsymbol{d}^e)]^{\mathrm{INT}}}{\partial \boldsymbol{d}^e} \tag{2.88}$$

where, using $\epsilon^{h^e} = du^{h^e}/dx = \boldsymbol{B}^e \cdot \boldsymbol{d}^e$, and assuming the cross-sectional area A is not a function of axial displacement,

$$\frac{\partial [\boldsymbol{f}^e(\boldsymbol{d}^e)]^{\mathrm{INT}}}{\partial \boldsymbol{d}^e} = \frac{\partial}{\partial \boldsymbol{d}^e}\left(\int_{-1}^{1} (\boldsymbol{B}^e)^T \sigma(\epsilon^{h^e}) A j^e d\xi\right) \tag{2.89}$$

$$= \int_{-1}^{1} (\boldsymbol{B}^e)^T \frac{\partial \sigma(\epsilon^{h^e})}{\partial \boldsymbol{d}^e} A j^e d\xi \tag{2.90}$$

where by the chain rule

$$\frac{\partial \sigma(\epsilon^{h^e})}{\partial \boldsymbol{d}^e} = \frac{\partial \sigma(\epsilon^{h^e})}{\partial \epsilon^{h^e}} \frac{\partial \epsilon^{h^e}}{\partial \boldsymbol{d}^e} = \frac{\partial \sigma(\epsilon^{h^e})}{\partial \epsilon^{h^e}} \boldsymbol{B}^e \tag{2.91}$$

and

$$\frac{\partial [\boldsymbol{f}^e(\boldsymbol{d}^e)]^{\mathrm{INT}}}{\partial \boldsymbol{d}^e} = \int_{-1}^{1} (\boldsymbol{B}^e)^T \boldsymbol{B}^e \frac{\partial \sigma(\epsilon^{h^e})}{\partial \epsilon^{h^e}} A j^e d\xi \tag{2.92}$$

where for a linear element with constant cross-sectional area A and constant axial strain ϵ^{h^e},

$$\frac{\partial [\boldsymbol{f}^e(\boldsymbol{d}^e)]^{\mathrm{INT}}}{\partial \boldsymbol{d}^e} = \frac{\partial \sigma(\epsilon^{h^e})}{\partial \epsilon^{h^e}} \frac{A}{h^e} \begin{bmatrix} 1 & -1 \\ -1 & 1 \end{bmatrix} \tag{2.93}$$

If we assume linear elasticity with Young's modulus E, $\sigma(\epsilon^{h^e}) = E\epsilon^{h^e}$ and $\partial\sigma/\partial\epsilon^{h^e} = E$, as expected.

2.2.6 Summary of the Newton-Raphson method for nonlinear elastostatic finite element method

Here, the solution of the nonlinear FEM using the Newton-Raphson method is summarized.

0. **initialize:** $k = 0$, $\boldsymbol{R}(\boldsymbol{d}^0) = \boldsymbol{F}^{\mathrm{INT}}(\boldsymbol{d}^0) - \boldsymbol{F}^{\mathrm{EXT}}$

1. **solve for increment during iteration:**

$$\delta \boldsymbol{d}^k = \left(\frac{\partial \boldsymbol{R}(\boldsymbol{d}^k)}{\partial \boldsymbol{d}} \right)^{-1} \cdot (-\boldsymbol{R}^k) \tag{2.94}$$

2. **update:**

$$\boldsymbol{d}^{k+1} = \boldsymbol{d}^k + \delta \boldsymbol{d}^k \tag{2.95}$$

$$\boldsymbol{R}(\boldsymbol{d}^{k+1}) = \boldsymbol{F}^{\mathrm{INT}}(\boldsymbol{d}^{k+1}) - \boldsymbol{F}^{\mathrm{EXT}} \tag{2.96}$$

3. **check for convergence:** `tol` = 1e-8, `tol` = 1e-16, ..., your choice

$$\begin{aligned} &\texttt{if} \quad \frac{\|\boldsymbol{R}(\boldsymbol{d}^{k+1})\|}{\|\boldsymbol{R}(\boldsymbol{d}^0)\|} < \texttt{tol},\ \boldsymbol{d}^* = \boldsymbol{d}^{k+1},\ \texttt{exit} \\ &\texttt{else} \quad k = k+1,\ \texttt{iterate} \rightarrow \texttt{step}\,1 \end{aligned}$$

2.2.7 Nonlinear elasticity

The form of material nonlinearity we will consider as a first example is nonlinear elasticity. Later, elastoplasticity (and elastodamage) could be a source of material nonlinearity. Figure

2.13 shows (a) linear elasticity and (b) one choice for nonlinear elasticity†:

$$\text{linear} \quad \sigma(\epsilon) = \quad E\epsilon \Longrightarrow \frac{\partial \sigma}{\partial \epsilon} = E \tag{2.97}$$

$$\text{exponential} \quad \sigma(\epsilon) = \quad \sigma_{\text{sat}}(1 - \exp[-B\epsilon]) \Longrightarrow \frac{\partial \sigma}{\partial \epsilon} = B\sigma_{\text{sat}} \exp[-B\epsilon] \tag{2.98}$$

where B is a parameter controlling how quickly the saturated stress σ_{sat} is reached (like approaching a perfectly-plastic limit but with no irrecoverable deformation).

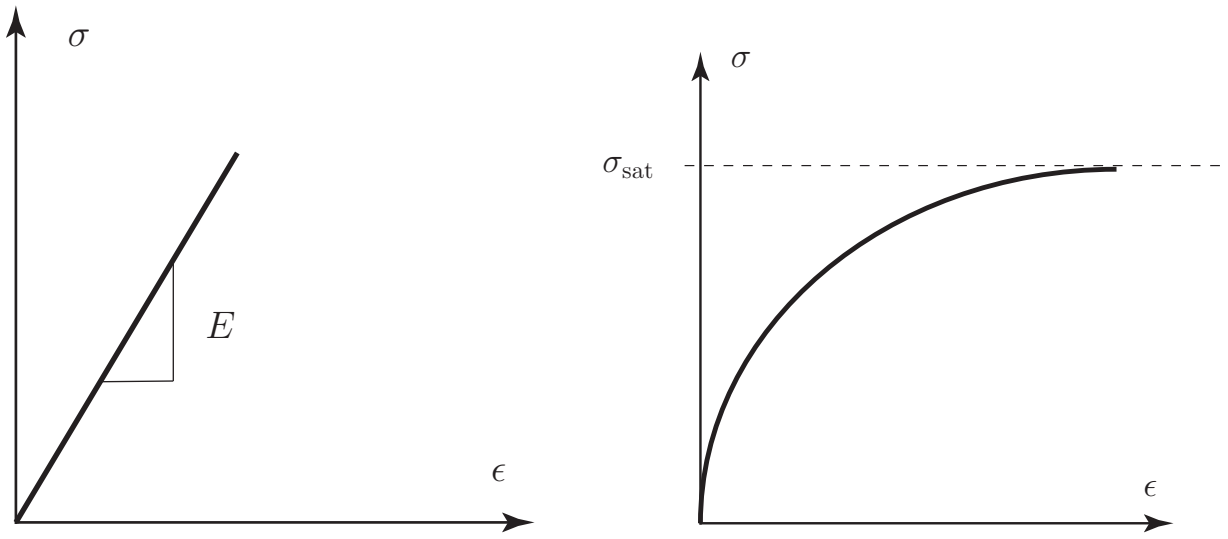

Figure 2.13. (a) Hooke's law. Linear elasticity. (b) Nonlinear elasticity.

2.2.8 Example

Let us consider a two linear element discretization of the axially loaded bar as shown in Fig.2.14. We assume $u = g = 0$ at $x = 0$. The 'external' force $\boldsymbol{f}^{e,\text{EXT}}$ at the element level is the sum of the force due to a uniformly distributed force f and concentrated force F, such

†This model is contrived and not indicative of any real material behavior, except it does combine nonlinear elasticity with perfect-plasticity-like behavior which will be useful when testing an arc-length method under load control.

that,

$$\boldsymbol{f}^{e,\mathrm{EXT}} = \boldsymbol{f}^e_f + \boldsymbol{f}^e_F \tag{2.99}$$

$$\boldsymbol{f}^1_f = \boldsymbol{f}^2_f = \int_{-1}^{1} \begin{bmatrix} (1-\xi)/2 \\ (1+\xi)/2 \end{bmatrix} f(h^e/2)d\xi = \frac{fh^e}{2}\begin{bmatrix} 1 \\ 1 \end{bmatrix} \tag{2.100}$$

$$\boldsymbol{f}^1_F = \begin{bmatrix} F^R_1 \\ 0 \end{bmatrix};\ \boldsymbol{f}^2_F = \begin{bmatrix} 0 \\ F \end{bmatrix} \tag{2.101}$$

where F^R_1 is the reaction force at dof $d_1 = 0$.

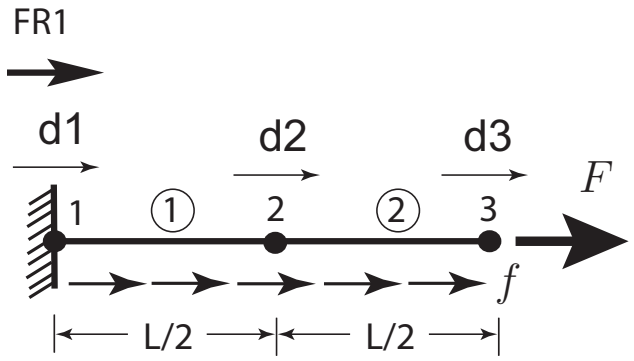

Figure 2.14. Two linear element discretization of bar.

For a simple 1D problem like this, the element assembly process for the external force $\boldsymbol{F}^{\mathrm{EXT}}$ is straightforward:

$$\boldsymbol{F}^{\mathrm{EXT}} = \frac{fL}{4}\begin{bmatrix} 1 \\ 1 \\ 0 \end{bmatrix} + \frac{fL}{4}\begin{bmatrix} 0 \\ 1 \\ 1 \end{bmatrix} + \begin{bmatrix} F^R_1 \\ 0 \\ F \end{bmatrix} = \frac{fL}{4}\begin{bmatrix} 1 \\ 2 \\ 1 \end{bmatrix} + \begin{bmatrix} F^R_1 \\ 0 \\ F \end{bmatrix} \tag{2.102}$$

The internal force for element e is calculated as

$$\boldsymbol{f}^{e,\mathrm{INT}}(\boldsymbol{d}^e) = \int_{-1}^{1} (\boldsymbol{B}^e)^T \sigma(\epsilon^{h^e}) A (h^e/2)\, d\xi \tag{2.103}$$

$$(\boldsymbol{B}^e)^T = \begin{bmatrix} dN_1/dx \\ dN_2/dx \end{bmatrix} = \frac{1}{h^e} \begin{bmatrix} -1 \\ 1 \end{bmatrix} \tag{2.104}$$

$$\boldsymbol{f}^{e,\mathrm{INT}}(\boldsymbol{d}^e) = \sigma(\boldsymbol{d}^e) A \begin{bmatrix} -1 \\ 1 \end{bmatrix} \tag{2.105}$$

After assembly, the internal force vector $\boldsymbol{F}^{\mathrm{INT}}$ is

$$\boldsymbol{F}^{\mathrm{INT}}(\boldsymbol{d}) = \sigma(\boldsymbol{d}^1) A \begin{bmatrix} -1 \\ 1 \\ 0 \end{bmatrix} + \sigma(\boldsymbol{d}^2) A \begin{bmatrix} 0 \\ -1 \\ 1 \end{bmatrix} \tag{2.106}$$

Note that the axial stresses in element 1 $\sigma(\boldsymbol{d}^1)$ and element 2 $\sigma(\boldsymbol{d}^2)$ may be different. Recall the consistent tangent for a 2-noded linear element with constant cross-sectional area A, such as

$$\frac{\partial \boldsymbol{f}^{e,\mathrm{INT}}}{\partial \boldsymbol{d}^e} = \frac{\partial \sigma(\boldsymbol{d}^e)}{\partial \epsilon^{h^e}} \frac{A}{h^e} \begin{bmatrix} 1 & -1 \\ -1 & 1 \end{bmatrix} \tag{2.107}$$

Then, the assembly of the full consistent tangent is

$$\frac{\partial \boldsymbol{R}}{\partial \boldsymbol{d}} = \frac{\partial \sigma(\boldsymbol{d}^1)}{\partial \epsilon^{h^e}} \frac{2A}{L} \begin{bmatrix} 1 & -1 & 0 \\ -1 & 1 & 0 \\ 0 & 0 & 0 \end{bmatrix} + \frac{\partial \sigma(\boldsymbol{d}^2)}{\partial \epsilon^{h^e}} \frac{2A}{L} \begin{bmatrix} 0 & 0 & 0 \\ 0 & 1 & -1 \\ 0 & -1 & 1 \end{bmatrix} \tag{2.108}$$

Recall the Galerkin form in vector form

$$\boldsymbol{c}^T \cdot \left[\boldsymbol{F}^{\mathrm{INT}}(\boldsymbol{d}) - \boldsymbol{F}^{\mathrm{EXT}}\right] = \boldsymbol{c}^T \cdot \boldsymbol{R} = \begin{bmatrix} c_1 & c_2 & c_3 \end{bmatrix} \cdot \begin{bmatrix} R_1 \\ R_2 \\ R_3 \end{bmatrix} = 0 \tag{2.109}$$

Since $d_1 = 0$, then $c_1 = 0$, and the first row of $\boldsymbol{R}$ is removed (but R_1 will $= 0$ as a post processing step such that $F_1^R = F_1^{INT}(\boldsymbol{d}) - fL/4$ is the reaction force), and the first row and column of $\partial\boldsymbol{R}/\partial\boldsymbol{d}$ are removed. The degrees of freedom left to be solved are d_2 and d_3.

What if $u = g$ at $x = L$ instead of a concentrated force F? Then, $c_1 = c_3 = 0$, and reaction force F_3^R takes the place of F in $\boldsymbol{F}^{\mathrm{EXT}} = \begin{bmatrix} F_1^R & 0 & F_3^R \end{bmatrix}^T$, the first and third rows of $\boldsymbol{R}$ are removed, along with the first and third rows and columns of $\partial\boldsymbol{R}/\partial\boldsymbol{d}$. Note that for element 2, the local element displacement vector $\boldsymbol{d}^{e=2} = [d_2\ d_3]^T = [d_2\ g]^T$. In this case, there is only one degree of freedom to be solved, d_2. Also, there are now two reaction forces (F_1^R and F_3^R) that may be determined as a post-processing step as $F_1^R = F_1^{INT}(\boldsymbol{d}) - fL/4$ and $F_3^R = F_3^{INT}(\boldsymbol{d}) - fL/4$ where $\boldsymbol{d} = [0\ d_2\ g]^T$ such that d_2 is the only unknown dof.

We will revisit this example in a problem set.

2.3 Nonlinear Elastodynamics of an Axially Loaded Bar at Small Strain

Refer to Hughes [1987] for details of the linear elastodynamic finite element method (FEM) and Belytschko et al. [2000] for an overview of the nonlinear FEM. This section is meant to serve as a brief introduction to the nonlinear elastodynamic FEM, formulating the Strong, Weak, Galerkin, and nonlinear finite element equations in residual form after time integration (using the Newmark and Runge-Kutta time integration methods) for solution by the Newton-Raphson method (Runge-Kutta is explicit and thus does not require a nonlinear interative solution). We assume geometric linearity (small strain $\epsilon(x,t) = \partial u(x,t)/\partial x$), but material nonlinearity (axial stress $\sigma(\epsilon)$ is a nonlinear function of axial strain ϵ). Refer to CVEN 5511 notes (or other introductory FEM books) for a review of the linear FEM for a dynamic axially-loaded bar.

2.3.1 Strong Form

The strong form of the problem is a formal statement of the governing partial differential equation with boundary conditions and initial conditions. It is called "strong" because the differential equation is satisfied pointwise, in this case at every point x in the domain $\bar{\Omega}$ (more below). Here, our governing partial differential equation is the balance of linear momentum *with* inertia terms. For the axially-loaded bar shown in Fig.2.15, the strong form (S) may

be stated as follows,

$$\text{Find } u(x,t) : \bar{\Omega} \times [0,T] \mapsto \mathbb{R} \text{ such that}$$

$$\rho(x)A(x)\frac{\partial^2 u(x,t)}{\partial t^2} - \frac{\partial}{\partial x}[\sigma(\epsilon)A] = f(x,t) \qquad x \in \Omega \qquad t \in (0,T) \tag{2.110}$$

$$(\sigma A)_L = F(t) \qquad x = L \qquad t \in (0,T) \tag{2.111}$$

$$u(0,t) = g(t) \qquad x = 0 \qquad t \in (0,T) \tag{2.112}$$

$$u(x,0) = u_0(x) \quad x \in (0,L) \quad t = 0 \tag{2.113}$$

$$\dot{u}(x,0) = \dot{u}_0(x) \quad x \in (0,L) \quad t = 0 \tag{2.114}$$

where the internal axial force $N(x,t) = \sigma(x,t)A(x)$ (see CVEN 5511 notes), the axial displacement $u(x,t) : \bar{\Omega} \times [0,T] \mapsto \mathbb{R}$ reads "the domain of $u(x,t)$ for x is $\bar{\Omega} = [0,L]$ and for t is $[0,T]$, or $0 \leq x \leq L$ and $0 \leq t \leq T$, and the range of u is the set of real numbers $\mathbb{R}$," and $\Omega = (0,L)$ where $x \in \Omega$ reads "x in Ω" or $0 < x < L$. A natural (or Neumann) concentrated force boundary condition (BC) $F(t)$ is applied at $x = L$, and an essential (or Dirichlet) displacement BC $g(t)$ is applied at $x = 0$. Note that the BCs may be functions of time t. Initial displacement $u_0(x)$ and initial velocity $\dot{u}_0(x)$ along the bar coordinate x are applied at $t = 0$. Refer to Fig.2.15 for illustration of terms in the Strong Form (S).

2.3.2 Weak Form

To formulate the weak or variational form, we write the differential equation in residual form using the Method of Weighted Residuals as,

$$\int_0^L w(x) \left[-\rho(x)A(x)\frac{\partial^2 u(x,t)}{\partial t^2} + \frac{\partial}{\partial x}[\sigma(\epsilon(x,t))A(x)] + f(x,t) \right] dx = 0 \tag{2.115}$$

where $w(x)$ is the weighting function which is not a function of time t as it is arbitrary, except where the essential BC is applied where it is zero. We next integrate by parts, which

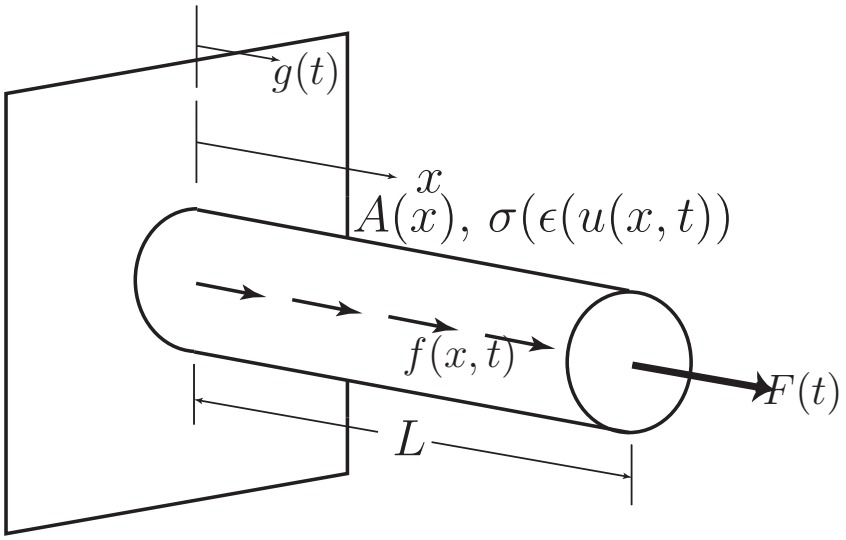

Figure 2.15. Axially-loaded bar with cross-sectional area $A(x)$ (m^2), length L (m), axial stress $\sigma(x,t)$ (Pa) which may be a nonlinear function of axial strain $\epsilon(x,t) = \partial u(x,t)/\partial x$, axial displacement $u(x,t)$, concentrated force $F(t)$ (N) at $x = L$, distributed axial force $f(x,t)$ (N/m), and prescribed axial displacement $g(t)$ (m) at $x = 0$.

will give us (i) a bilinear form (symmetry, typically), and (ii) provide the natural BC. After integrating by parts using the chain rule,

$$\frac{\partial}{\partial x}\left[w(\sigma A)\right] = \frac{\partial w}{\partial x}(\sigma A) + w\frac{\partial(\sigma A)}{\partial x} \tag{2.116}$$

and applying the Divergence Theorem, we have,

$$\int_0^L \left[w(x)\rho(x)A(x)\frac{\partial^2 u(x,t)}{\partial t^2} + \frac{\partial w(x)}{\partial x}\sigma(\epsilon(x,t))A(x)\right] dx = \int_0^L w(x)f(x,t)dx + w(L)F(t) \tag{2.117}$$

Recall that we integrate by parts to reach a bilinear form and also to provide the natural BC [Hughes, 1987]. Thus, we can state the weak, or variational, form (W) as,

$$\begin{aligned} & \text{Find } u(x,t) \in \mathcal{S} \text{ such that} \\ \int_0^L \left[w(x)\rho(x)A(x)\frac{\partial^2 u(x,t)}{\partial t^2} + \frac{\partial w(x)}{\partial x}\sigma(\epsilon(x,t))A(x) \right] dx &= \\ & \int_0^L w(x)f(x,t)dx + w(L)F(t) \\ & \text{holds for all } w(x) \in \mathcal{V} \end{aligned} \tag{2.118}$$

where the trial solution space is $\mathcal{S} = \{u(x,t) : \bar{\Omega} \times [0,T] \mapsto \mathbb{R}, u(0,t) = g(t)\}$ and weighting function space is $\mathcal{V} = \{w(x) : \bar{\Omega} \mapsto \mathbb{R}, w(0) = 0\}$. It can be shown that the weak and strong forms are equivalent [Hughes, 1987]. It is called the "weak" form because the partial differential equation is satisfied in integral (or average) form.

2.3.3 Galerkin Form

The Galerkin form is a discrete approximation to the weak form, as demonstrated in Fig.2.9 for the elastostatic problem. As for elastostatics, similarly for elastodynamics we will use the Bubnov-Galerkin formulation.

The Galerkin form involves discretizing spatially the domain, in this case the bar of length L, into discrete length segments with characteristic length h. The discrete trial solution and weighting function spaces $\mathcal{S}^h$ and $\mathcal{V}^h$, respectively, in turn are finite dimensional subspaces of their continuous counterparts: $\mathcal{S}^h \subset \mathcal{S}$, $\mathcal{V}^h \subset \mathcal{V}$. The Galerkin form (G) is a restatement

of the weak form in finite dimensional space as,

$$\begin{aligned} &\text{Find } u^h(x,t) \in \mathcal{S}^h \text{ such that} \\ \int_0^L \left[w^h(x)\rho(x)A(x)\frac{\partial^2 u^h(x,t)}{\partial t^2} + \frac{\partial w^h(x)}{\partial x}\sigma(\epsilon^h(x,t))A(x) \right] dx &= \\ &\int_0^L w^h(x) f(x,t) dx + w^h(L)F(t) \\ &\text{holds for all } w^h(x) \in \mathcal{V}^h \end{aligned} \tag{2.119}$$

where axial strain $\epsilon^h(x,t) = \partial u^h(x,t)/\partial x$, and h is the characteristic length of the finite element (indicating that the variable is discrete). The finite dimensional trial solution space is $\mathcal{S}^h = \{u^h(x,t) : \bar{\Omega}^h \mapsto \mathbb{R}, u^h(0,t) = g(t)\}$ and weighting function space is $\mathcal{V}^h = \{w^h(x) : \bar{\Omega}^h \mapsto \mathbb{R}, w^h(0) = 0\}$, where $\bar{\Omega}^h = [0, L]$. For this 1D problem, $\bar{\Omega}^h = \bar{\Omega}$, but this is usually not the case for 2D and 3D problems, where $\bar{\Omega}^h \subset \bar{\Omega}$, i.e., the mesh is an approximation (typically a sub-domain) of the physical spatial (geometric) domain.

2.3.4 Finite Element Form

The next step in formulating the nonlinear finite element elastodynamic equations, is to discretize the 1D bar into finite elements, such that,

$$\Omega^h = \mathop{\mathbf{A}}_{e=1}^{n_{\text{el}}} \Omega^e \tag{2.120}$$

where $\mathop{\mathbf{A}}_{e=1}^{n_{\text{el}}}$ is called the element assembly operator, $\Omega^e = (x_1^e, x_2^e)$ is the element domain, n_{el} is the number of finite elements, and e denotes the element number. The domain of element e is shown in Fig.2.10 for the global coordinate system x as well as the natural coordinate system ξ.

We use an isoparametric formulation for the global coordinate x, weighting function w,

displacement u, velocity $\dot{u}$ (when include viscoelasticity or mass-proportional damping), and acceleration $\ddot{u}$ such as,

$$x^{h^e}(\xi) = \sum_{a=1}^{2} N_a(\xi) x_a^e \tag{2.121}$$

$$w^{h^e}(\xi) = \sum_{a=1}^{2} N_a(\xi) c_a^e \tag{2.122}$$

$$u^{h^e}(\xi, t) = \sum_{a=1}^{2} N_a(\xi) d_a^e(t) \tag{2.123}$$

$$\dot{u}^{h^e}(\xi, t) = \sum_{a=1}^{n_{en}=2} N_a(\xi) \dot{d}_a^e(t) \tag{2.124}$$

$$\ddot{u}^{h^e}(\xi, t) = \sum_{a=1}^{n_{en}=2} N_a(\xi) \ddot{d}_a^e(t) \tag{2.125}$$

where the shape functions are shown in Fig.2.11, c_a^e are the local nodal weighting function values, and $d_a^e(t)$ the local nodal displacements shown in Fig.2.12. $\dot{d}_a^e(t)$ is the axial velocity at local node a, and $\ddot{d}_a^e(t)$ is the axial acceleration. Note that the time derivatives on axial displacement $u^{h^e}(\xi, t)$ to determine the axial velocity $\dot{u}^{h^e}(\xi, t)$ and axial acceleration $\ddot{u}^{h^e}(\xi, t)$ are applied to the nodal degree of freedom $d_a^e(t)$. The formulation is called "isoparametric" because the coordinate x and weighting function and displacement are all interpolated with the *same* shape functions.

To place in vector form for nonlinear solution, we carry out the summation and write as,

$$x^{h^e}(\xi) = \left[\begin{array}{cc} N_1 & N_2 \end{array}\right] \left[\begin{array}{c} x_1^e \\ x_2^e \end{array}\right] = \boldsymbol{N}^e(\xi) \cdot \boldsymbol{x}^e \tag{2.126}$$

$$w^{h^e}(\xi) = \left[\begin{array}{cc} N_1 & N_2 \end{array}\right] \left[\begin{array}{c} c_1^e \\ c_2^e \end{array}\right] = \boldsymbol{N}^e(\xi) \cdot \boldsymbol{c}^e = (\boldsymbol{c}^e)^T \cdot (\boldsymbol{N}^e)^T(\xi) \tag{2.127}$$

$$u^{h^e}(\xi,t) = \left[\begin{array}{cc} N_1 & N_2 \end{array}\right] \left[\begin{array}{c} d_1^e(t) \\ d_2^e(t) \end{array}\right] = \boldsymbol{N}^e(\xi) \cdot \boldsymbol{d}^e(t) \tag{2.128}$$

$$\dot{u}^{h^e}(\xi,t) = \left[\begin{array}{cc} N_1 & N_2 \end{array}\right] \left[\begin{array}{c} \dot{d}_1^e(t) \\ \dot{d}_2^e(t) \end{array}\right] = \boldsymbol{N}^e(\xi) \cdot \dot{\boldsymbol{d}}^e(t) \tag{2.129}$$

$$\ddot{u}^{h^e}(\xi,t) = \left[\begin{array}{cc} N_1 & N_2 \end{array}\right] \left[\begin{array}{c} \ddot{d}_1^e(t) \\ \ddot{d}_2^e(t) \end{array}\right] = \boldsymbol{N}^e(\xi) \cdot \ddot{\boldsymbol{d}}^e(t) \tag{2.130}$$

When calculating the spatial derivatives of the weighting function and displacement field (or velocity field for viscoelasticity), we use the Jacobian of coordinate transformation j^e:

$$\frac{\partial w^{h^e}(\xi)}{\partial x} = \frac{\partial \boldsymbol{N}^e(\xi)}{\partial x} \cdot \boldsymbol{c}^e = \boldsymbol{B}^e \cdot \boldsymbol{c}^e = (\boldsymbol{c}^e)^T \cdot (\boldsymbol{B}^e)^T \tag{2.131}$$

$$\boldsymbol{B}^e = \frac{\partial \boldsymbol{N}^e(\xi)}{\partial x} = \frac{\partial \boldsymbol{N}^e(\xi)}{\partial \xi}\frac{\partial \xi}{\partial x} \tag{2.132}$$

$$j^e = \frac{dx^{h^e}}{d\xi} = \frac{\partial N_1}{\partial \xi}x_1^e + \frac{\partial N_2}{\partial \xi}x_2^e = -\frac{1}{2}x_1^e + \frac{1}{2}x_2^e = h^e/2 \tag{2.133}$$

$$\Longrightarrow \quad \boldsymbol{B}^e = \frac{1}{h^e}\left[\begin{array}{cc} -1 & 1 \end{array}\right] \tag{2.134}$$

$$\epsilon^{h^e}(\xi,t) = \frac{\partial u^{h^e}(\xi,t)}{\partial x} = \boldsymbol{B}^e \cdot \boldsymbol{d}^e(t) \tag{2.135}$$

$$\dot{\epsilon}^{h^e}(\xi,t) = \frac{\partial \dot{u}^{h^e}(\xi,t)}{\partial x} = \boldsymbol{B}^e \cdot \dot{\boldsymbol{d}}^e(t) \tag{2.136}$$

We likewise transform the spatial integration as,

$$\int_{\Omega^e} (\bullet) dx = \int_{-1}^{1} (\bullet) j^e d\xi \tag{2.137}$$

We rewrite the discrete variational equation in finite element form, first recalling the Galerkin form as,

$$\int_{\Omega^h} \left[w^h(x) \rho A(x) \frac{\partial^2 u^h(x,t)}{\partial t^2} + \frac{\partial w^h(x)}{\partial x} \sigma(\epsilon^h(x,t)) A(x) \right] dx = \int_{\Omega^h} w^h(x) f(x,t) dx + w^h(L) F(t) \tag{2.138}$$

and leaving off the arguments (x,t),

$$\mathop{\mathsf{A}}_{e=1}^{n_{\text{el}}} \left\{ \int_{\Omega^e} \left[w^{h^e} \rho A \frac{\partial^2 u^{h^e}}{\partial t^2} + \frac{\partial w^{h^e}}{\partial x} \sigma(\epsilon^{h^e}) A \right] dx = \int_{\Omega^e} w^{h^e} f dx + w^{h^e}(L) F \right\} \tag{2.139}$$

Substituting the shape functions, we have,

$$\mathop{\mathsf{A}}_{e=1}^{n_{\text{el}}} (\boldsymbol{c}^e)^T \cdot \left\{ \left(\underbrace{\int_{-1}^{1} (\boldsymbol{N}^e)^T \rho A j^e \boldsymbol{N}^e d\xi}_{\boldsymbol{m}^e} \right) \cdot \ddot{\boldsymbol{d}}^e(t) + \underbrace{\int_{-1}^{1} (\boldsymbol{B}^e)^T \sigma(\epsilon^{h^e}) A j^e d\xi}_{\boldsymbol{f}^{e,\text{INT}}(\boldsymbol{d}^e{}_{(t)})} = \underbrace{\underbrace{\int_{-1}^{1} (\boldsymbol{N}^e)^T f j^e d\xi}_{\boldsymbol{f}^e_f(t)} + \boldsymbol{f}^e_F(t)}_{\boldsymbol{f}^{e,\text{EXT}}{}_{(t)}} \right\} \tag{2.140}$$

$$\mathop{\mathsf{A}}_{e=1}^{n_{\text{el}}} (\boldsymbol{c}^e)^T \cdot \left\{ \boldsymbol{m}^e \cdot \ddot{\boldsymbol{d}}^e(t) + \boldsymbol{f}^{e,\text{INT}}(\boldsymbol{d}^e(t)) = \boldsymbol{f}^{e,\text{EXT}}(t) \right\} \tag{2.141}$$

where $\boldsymbol{m}^e$ is the element mass matrix, $\boldsymbol{f}^{e,\text{INT}}(\boldsymbol{d}^e(t))$ is the internal element force vector, and $\boldsymbol{f}^{e,\text{EXT}}(t)$ is the external element force vector which may be a function of time t. After assembly and application of BCs, we have

$$\boldsymbol{c}^T \cdot \left[\boldsymbol{M} \cdot \ddot{\boldsymbol{d}}(t) + \boldsymbol{F}^{\text{INT}}(\boldsymbol{d}(t)) - \boldsymbol{F}^{\text{EXT}}(t) \right] = 0 \tag{2.142}$$

which must hold **for all** $\boldsymbol{c}$ (all w^h), which implies that $\boldsymbol{c}$ is arbitrary, except for nodes where we have essential B.C.s, $c_A = 0$ if $d_A(t) = g(t)$ at global node A. Thus, for equilibrium to be satisfied after applying essential B.C.s with $\boldsymbol{c}$ arbitrary at all other nodal degrees of freedom, then the following equation must hold:

$$\boldsymbol{M} \cdot \ddot{\boldsymbol{d}}(t) + \boldsymbol{F}^{\mathrm{INT}}(\boldsymbol{d}(t)) = \boldsymbol{F}^{\mathrm{EXT}}(t) \tag{2.143}$$

Before placing in residual form for solution by the Newton-Raphson method (assuming an implicit time integration scheme), we apply the Newmark time integration scheme [Hughes, 1987] by writing Eq.(2.143) at current time $t_{n+1} = t_n + \Delta t$, where Δt is the time increment, such that,

$$\boldsymbol{M} \cdot \ddot{\boldsymbol{d}}(t_{n+1}) + \boldsymbol{F}^{\mathrm{INT}}(\boldsymbol{d}(t_{n+1})) = \boldsymbol{F}^{\mathrm{EXT}}(t_{n+1}) \tag{2.144}$$

or

$$\boldsymbol{M} \cdot \boldsymbol{a}_{n+1} + \boldsymbol{F}^{\mathrm{INT}}(\boldsymbol{d}_{n+1}) = \boldsymbol{F}^{\mathrm{EXT}}_{n+1} \tag{2.145}$$

where the nodal acceleration vector $\boldsymbol{a}_{n+1} = \ddot{\boldsymbol{d}}(t_{n+1})$. For Newmark time integration, the finite difference in time equations are,

$$\boldsymbol{d}_{n+1} = \boldsymbol{d}_n + \Delta t \boldsymbol{v}_n + \frac{\Delta t^2}{2}\left[(1-2\beta)\boldsymbol{a}_n + 2\beta \boldsymbol{a}_{n+1}\right] \tag{2.146}$$

$$\boldsymbol{v}_{n+1} = \boldsymbol{v}_n + \Delta t\left[(1-\gamma)\boldsymbol{a}_n + \gamma \boldsymbol{a}_{n+1}\right] \tag{2.147}$$

where γ and β are integration parameters, $\boldsymbol{v}_{n+1} = \dot{\boldsymbol{d}}(t_{n+1})$ is the velocity vector at time t_{n+1}, and values at previous time t_n are known. We can substitute to solve for $\boldsymbol{a}^{k+1}_{n+1}$ using Newton-Raphson (current iteration $k+1$), and then update $\boldsymbol{d}^{k+1}_{n+1}$ and $\boldsymbol{v}^{k+1}_{n+1}$ during iteration as follows. First, we introduce the "predictors" from known values at time t_n as,

$$\tilde{\boldsymbol{d}}_{n+1} = \boldsymbol{d}_n + \Delta t \boldsymbol{v}_n + \frac{\Delta t^2}{2}(1-2\beta)\boldsymbol{a}_n \tag{2.148}$$

$$\tilde{\boldsymbol{v}}_{n+1} = \boldsymbol{v}_n + \Delta t(1-\gamma)\boldsymbol{a}_n \tag{2.149}$$

such that the update during iteration becomes,

$$\boldsymbol{d}_{n+1}^{k+1} = \tilde{\boldsymbol{d}}_{n+1} + \beta \Delta t^2 \boldsymbol{a}_{n+1}^{k+1} \tag{2.150}$$

$$\boldsymbol{v}_{n+1}^{k+1} = \tilde{\boldsymbol{v}}_{n+1} + \gamma \Delta t \boldsymbol{a}_{n+1}^{k+1} \tag{2.151}$$

To initialize time-stepping, we must solve for initial acceleration $\boldsymbol{a}_0$ from the FE equation,

$$\boldsymbol{M} \cdot \boldsymbol{a}_0 = \boldsymbol{F}_0^{EXT} - \boldsymbol{F}^{INT}(\boldsymbol{d}_0) \tag{2.152}$$

We rewrite in residual form, and solve via Newton-Raphson as,

$$\boldsymbol{R}(\boldsymbol{a}_{n+1}^{k+1}) = \boldsymbol{M} \cdot \boldsymbol{a}_{n+1}^{k+1} + \boldsymbol{F}^{INT}(\boldsymbol{d}_{n+1}^{k+1}) - \boldsymbol{F}_{n+1}^{EXT} = \boldsymbol{0} \tag{2.153}$$

2.3.5 Consistent Tangent

To solve Eq.(2.153) via the Newton-Raphson solution method, we need the consistent tangent. In this case, the global consistent tangent with respect to acceleration solution $\boldsymbol{a}$ is (assuming evaluated at iteration k at time step $n+1$),

$$\frac{\partial \boldsymbol{R}}{\partial \boldsymbol{a}} = \boldsymbol{M} + \frac{\partial \boldsymbol{F}^{\mathrm{INT}}(\boldsymbol{d})}{\partial \boldsymbol{d}} \frac{\partial \boldsymbol{d}}{\partial \boldsymbol{a}} = \mathop{\mathsf{A}}_{e=1}^{n_{\mathrm{el}}} \left[\boldsymbol{m}^e + \frac{\partial \boldsymbol{f}^{e,\mathrm{INT}}(\boldsymbol{d}^e)}{\partial \boldsymbol{d}^e} (\beta \Delta t^2) \right] \tag{2.154}$$

where, using $\epsilon^{h^e} = \partial u^{h^e}/\partial x = \boldsymbol{B}^e \cdot \boldsymbol{d}^e$, and assuming the cross-sectional area A is not a function of axial displacement,

$$\frac{\partial \boldsymbol{f}^{e,\mathrm{INT}}(\boldsymbol{d}^e)}{\partial \boldsymbol{d}^e} = \frac{\partial}{\partial \boldsymbol{d}^e} \left(\int_{-1}^{1} (\boldsymbol{B}^e)^T \sigma(\epsilon^{h^e}) A j^e d\xi \right) \tag{2.155}$$

$$= \int_{-1}^{1} (\boldsymbol{B}^e)^T \frac{\partial \sigma(\epsilon^{h^e})}{\partial \boldsymbol{d}^e} A j^e d\xi \tag{2.156}$$

where by the chain rule

$$\frac{\partial \sigma(\epsilon^{h^e})}{\partial \boldsymbol{d}^e} = \frac{\partial \sigma(\epsilon^{h^e})}{\partial \epsilon^{h^e}} \frac{\partial \epsilon^{h^e}}{\partial \boldsymbol{d}^e} = \frac{\partial \sigma(\epsilon^{h^e})}{\partial \epsilon^{h^e}} \boldsymbol{B}^e \tag{2.157}$$

and

$$\frac{\partial \boldsymbol{f}^{e,\mathrm{INT}}(\boldsymbol{d}^e)}{\partial \boldsymbol{d}^e} = \int_{-1}^{1} (\boldsymbol{B}^e)^T \boldsymbol{B}^e \frac{\partial \sigma(\epsilon^{h^e})}{\partial \epsilon^{h^e}} A j^e d\xi \tag{2.158}$$

where for a linear element with constant cross-sectional area A and constant axial strain ϵ^{h^e},

$$\frac{\partial \boldsymbol{f}^{e,\mathrm{INT}}(\boldsymbol{d}^e)}{\partial \boldsymbol{d}^e} = \frac{\partial \sigma(\epsilon^{h^e})}{\partial \epsilon^{h^e}} \frac{A}{h^e} \begin{bmatrix} 1 & -1 \\ -1 & 1 \end{bmatrix} \tag{2.159}$$

If we assume linear elasticity with Young's modulus E, $\sigma(\epsilon^{h^e}) = E\epsilon^{h^e}$ and $\partial\sigma/\partial\epsilon^{h^e} = E$, as expected, but we will leave the formulation general to be able to accomodate nonlinear constitutive models.

2.3.6 Summary of the Newton-Raphson method for nonlinear elastodynamic finite element method

Here, the nonlinear solution using the Newton-Raphson method is summarized in the context of our current discussion of nonlinear elastodynamic FEM (assuming all quantities evaluated at time step $n+1$ unless otherwise indicated).

Determine the predictors:

$$\tilde{\boldsymbol{d}} = \boldsymbol{d}_n + \Delta t \boldsymbol{v}_n + \frac{\Delta t^2}{2}(1-2\beta)\boldsymbol{a}_n$$
$$\tilde{\boldsymbol{v}} = \boldsymbol{v}_n + \Delta t(1-\gamma)\boldsymbol{a}_n$$

0. **initialize iteration:** $k = 0$, $\boldsymbol{R}(\boldsymbol{a}^0) = \boldsymbol{M} \cdot \boldsymbol{a}^0 + \boldsymbol{F}^{\mathrm{INT}}(\boldsymbol{d}^0) - \boldsymbol{F}^{\mathrm{EXT}}$, where $\boldsymbol{a}^0 = \boldsymbol{a}_n$ and

$\boldsymbol{d}^0 = \boldsymbol{d}_n$, and $\boldsymbol{F}^{\rm EXT}_{n+1}$ and/or g_{n+1} are incremented to drive the solution (subscript $n+1$ implied in the equations).

1. **solve for increment:**

$$\left(\frac{\partial \boldsymbol{R}(\boldsymbol{a}^k)}{\partial \boldsymbol{a}}\right) \cdot \delta \boldsymbol{a}^k = -\boldsymbol{R}^k \tag{2.160}$$

2. **update:**

$$\begin{aligned} \boldsymbol{a}^{k+1} &= \boldsymbol{a}^k + \delta \boldsymbol{a}^k && (2.161)\\ \boldsymbol{d}^{k+1} &= \tilde{\boldsymbol{d}} + \beta \Delta t^2 \boldsymbol{a}^{k+1} && (2.162)\\ \boldsymbol{v}^{k+1} &= \tilde{\boldsymbol{v}} + \gamma \Delta t \boldsymbol{a}^{k+1} && (2.163)\\ \boldsymbol{R}(\boldsymbol{a}^{k+1}) &= \boldsymbol{M} \cdot \boldsymbol{a}^{k+1} + \boldsymbol{F}^{\rm INT}(\boldsymbol{d}^{k+1}) - \boldsymbol{F}^{\rm EXT} && (2.164) \end{aligned}$$

3. **check for convergence:** `tol` = 1e-8, `tol` = 1e-16, ..., your choice

$$\begin{aligned} \texttt{if} \quad & \frac{\|\boldsymbol{R}(\boldsymbol{a}^{k+1})\|}{\|\boldsymbol{R}(\boldsymbol{a}^0)\|} < \texttt{tol},\ \boldsymbol{a}^* = \boldsymbol{a}^{k+1},\ \texttt{exit} \\ \texttt{else} \quad & k = k+1,\ \texttt{iterate} \rightarrow \texttt{step}\,1 \end{aligned}$$

We will consider a dynamic loading example in a future problem set, first with analytical solution assuming linear elasticity (but with full nonlinear solution with Newmark time integration), and then with nonlinear elasticity (and later inelasticity such as elastoplasticity, elastodamage, etc.).

2.3.7 Runge-Kutta adaptive time step integration for nonlinear elastodynamic finite element method

Within the Newmark time integration scheme, when selecting the integration parameters to be $\beta = 0$ and $\gamma = 1/2$ this leads to the well-known Central Difference time integration method, which is explicit and thus conditionally stable on the selection of time increment Δt. Explicit time integration schemes as applied to nonlinear elastodynamics, such as in Eq.(2.143) in our case, do not require iterative nonlinear solution via Newton-Raphson or other Newton-like method, and in turn do not require a linear matrix equation solution at each iteration. This is appealing when time increment Δt is required to be small to resolve the physics, such as simulating a car crash for designing safer cars, or helmet-head impact to design safer helmets and lessen the likelihood of Traumatic Brain Injury (TBI). However, for "slower" dynamic activities such as normal running and jumping, or earthquake loading, implicit time integration schemes which are unconditionally stable such as Newmark's parameters $\beta = 0.3025$ and $\gamma = 0.6$ (with a small amount of algorithmic damping) or Trapezoidal Rule $\beta = 1/4$ and $\gamma = 1/2$ (no algorithmic damping) are appealing, but require Newton-Rapshon or other Newton-like method to iteratively solve the nonlinear equations. Whether explicit or implicit time integration of nonlinear elastodynamics equations, having an adaptive time-stepping procedure to increase Δt when possible for faster solution and decrease Δt when needed for stability is appealing. There are various adaptive time-stepping procedures available for both explicit and implicit time integration schemes, and the purpose of this section is not to provide a review of the various available procedures. We instead focus on one adaptive time-stepping procedue for a higher-order explicit time integration scheme, the well-known Runge-Kutta(RK)-Fehlberg scheme (cite?). The adaptivity stems from error control based on fourth and fifth order accurate multi-stage RK methods. These multi-stage methods are applied to first order ordinary differential equations (ODEs). Thus,

Eq.(2.143) must be recast as a first order ODE in the following form:

$$\dot{\boldsymbol{z}} = \boldsymbol{f}(t, \boldsymbol{z}) \tag{2.165}$$

for unknown degree of freedom vector $\boldsymbol{z}$ with right hand side vector equation $\boldsymbol{f}(t, \boldsymbol{z})$. This may be accomplished by setting,

$$\boldsymbol{z} = \begin{bmatrix} \boldsymbol{z}_d \\ \boldsymbol{z}_{\dot{d}} \end{bmatrix} = \begin{bmatrix} \boldsymbol{d} \\ \dot{\boldsymbol{d}} \end{bmatrix} \tag{2.166}$$

which upon taking the time derivative becomes,

$$\dot{\boldsymbol{z}} = \begin{bmatrix} \dot{\boldsymbol{z}}_d \\ \dot{\boldsymbol{z}}_{\dot{d}} \end{bmatrix} = \begin{bmatrix} \dot{\boldsymbol{d}} \\ \ddot{\boldsymbol{d}} \end{bmatrix} \tag{2.167}$$

where $\dot{\boldsymbol{z}}_d = \boldsymbol{z}_{\dot{d}}$, the first term in the left hand side of Eq.(2.165). To find the second term in the left hand side of Eq.(2.165), we rearrange Eq.(2.143) to read as,

$$\ddot{\boldsymbol{d}} = \boldsymbol{M}^{-1} \cdot \left(\boldsymbol{F}^{EXT} - \boldsymbol{F}^{INT}(\boldsymbol{d}) \right) \tag{2.168}$$

or rewritten in terms of $\boldsymbol{z}$ as,

$$\dot{\boldsymbol{z}}_{\dot{d}} = \boldsymbol{M}^{-1} \cdot \left(\boldsymbol{F}^{EXT} - \boldsymbol{F}^{INT}(\boldsymbol{z}_d) \right) \tag{2.169}$$

Equation (2.165) then becomes,

$$\begin{bmatrix} \dot{\boldsymbol{z}}_d \\ \dot{\boldsymbol{z}}_{\dot{d}} \end{bmatrix} = \begin{bmatrix} \boldsymbol{z}_{\dot{d}} \\ \boldsymbol{M}^{-1} \cdot \left(\boldsymbol{F}^{EXT} - \boldsymbol{F}^{INT}(\boldsymbol{z}_d) \right) \end{bmatrix} \tag{2.170}$$

which is a first order ODE we can solve with an adaptive time-stepping multi-stage RK method. If the mass matrix is lumped (such as through nodal integration Hughes [1987]) and in turn $\boldsymbol{M}$ becomes diagonal, then $\boldsymbol{M}^{-1}$ is trivial to evaluate.

enter more details here

This page intentionally left blank.

Chapter 3

One-Dimensional Constitutive Modeling at Small Strain

Much of the material in this chapter is taken from Simo and Hughes [1998], Borja [2013].

This chapter will primarily focus on steps 1-5 of a typical modeling procedure if you are developing your own inelastic constitutive model. We start with a simple form of inelastic constitute model: small strain elastoplasticity with linear hardening. These steps are outlined as follows:

1. **kinematics:** We assume small strains, such that an additive decomposition of axial strain ϵ into elastic and plastic parts is appropriate:

$$\begin{aligned} \epsilon &= \epsilon^{\mathrm{e}} + \epsilon^{\mathrm{p}} \\ \text{total strain} \quad & \epsilon = du/dx \\ \text{elastic strain} \quad & \epsilon^{\mathrm{e}} \text{ (recoverable deformation)} \\ \text{plastic strain} \quad & \epsilon^{\mathrm{p}} \text{ (permanent/irrecoverable deformation)} \end{aligned} \tag{3.1}$$

where $\dot{\epsilon}^{\mathrm{p}}$ will be defined through a **flow rule**, from which ϵ^{p} can be integrated in time. Then, given the total strain ϵ from the finite element calculation, we can calculate the elastic strain as $\epsilon^{\mathrm{e}} = \epsilon - \epsilon^{\mathrm{p}}$.* Consider Fig.3.1 for an elastic-perfectly-plastic model (hardening modulus $H = 0$).

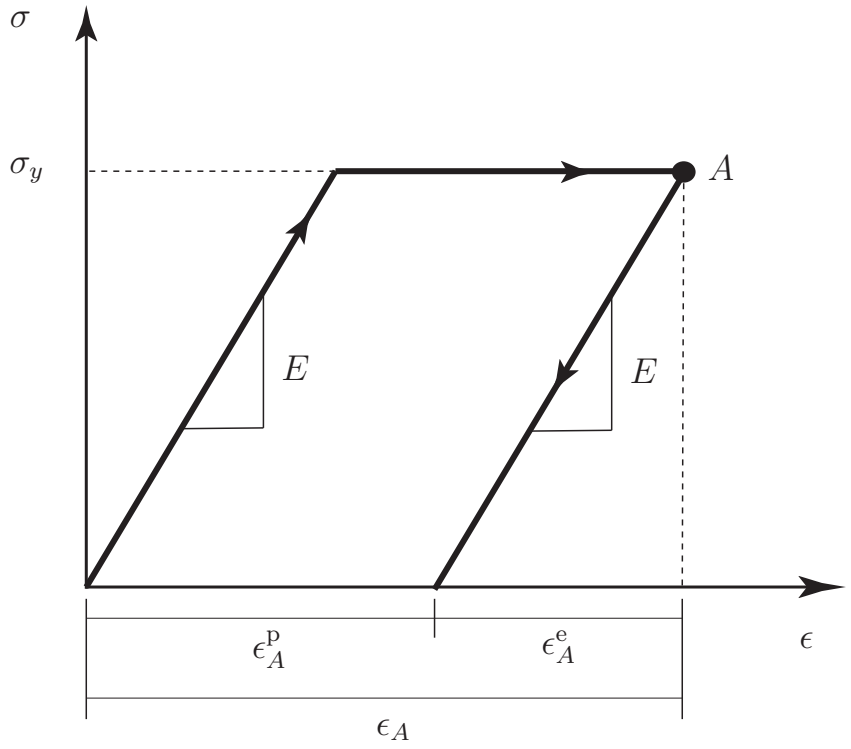

Figure 3.1. Linear elastic, perfectly plastic, stress-strain response showing additive decomposition of strain at point A: $\epsilon_A = \epsilon^{\mathrm{e}}_A + \epsilon^{\mathrm{p}}_A$.

2. **balance equations and thermodynamics:** These equations will involve derivation of the following: (1) balance of mass (use for fluid flow, mixture theory, etc., not here), (2) balance of linear momentum (solve for displacement), (3) balance of angular momentum (leads to symmetric stress for non-polar media), (4) balance of energy (first law of thermodynamics; solve for temperature), (5) second law of thermodynamics (constrains inelastic constitutive model formulation; requires non-negative energy dis-

*At this time, I do not have a satisfactory solution to the challenge of using (1) roman font superscript e to denote *elastic* strain ϵ^{e}, and (2) italic font superscript e to denote finite *element* quantity, such as *element* characteristic length h^e, or *element* displacement vector $\boldsymbol{d}^e$.

sipation). We focus on (4) and (5) for constitutive modeling purposes in this chapter. For further information, refer to continuum mechanics textbooks, such as Malvern [1969], Holzapfel [2000].

3. **constitutive equations:** For elastoplasticity, we need constitutive equations for stress (e.g., linear elasticity $\sigma = E\epsilon^{\mathrm{e}}$), a yield function $f(\sigma, \boldsymbol{q}^{\zeta}) = 0$ and plastic potential function $g(\sigma, \boldsymbol{q}^{\zeta})$, internal state variable (ISV) evolution equations (e.g., hardening, perfect, or softening plasticity) for a stress-like ISV vector $\boldsymbol{q}^{\zeta}$. Superscript ζ implies that $\boldsymbol{q}^{\zeta}$ is a stress-like ISV vector, as opposed to the heat flux vector $\boldsymbol{q}$.

   We ignore damage for now, which could degrade the elastic modulus and lead to softening and/or fracture.

   The ISVs attempt to represent phenomenologically the evolution of the underlying microstructure as it relates to the experimentally-observed behavior (e.g., motion and piling up of dislocations at obstacles in metals leading to hardening; compaction of pore space in sand leading to reduced volume and increased shear strength and hardening; shear bands in metals and particulate materials leading to post-peak softening and failure, ...).

4. **numerical integration in time:** Certain constitutive equations will be expressed in rate form (e.g., stress rate $\dot{\sigma} = d\sigma/dt$ and plastic strain rate $\dot{\epsilon}^{\mathrm{p}}$) to account for *evolution of solid material properties over time due to deformation and load history.* We must integrate numerically in time before we can implement these equations into a nonlinear finite element (FE) program. In rate form, the stress equation for constant Young's modulus reads,

$$\begin{aligned} \dot{\sigma} &= E\dot{\epsilon}^{\mathrm{e}} \\ \dot{\epsilon}^{\mathrm{e}} &= \dot{\epsilon} - \dot{\epsilon}^{\mathrm{p}} \end{aligned} \tag{3.2}$$

where $\dot{\epsilon}$ is the strain rate provided by the FE program, leading to what we call a "strain-driven" problem $\dot{\epsilon} \approx \Delta\epsilon/\Delta t$, where $\Delta\epsilon = d(\Delta u)/dx$ and $\Delta t = t_{n+1} - t_n$ is the time increment. The evolution equations (rate form of constitutive equations) are usually first order ordinary differential equations (ODEs) in time t, thus we may use a generalized trapezoidal rule to integrate in time (e.g., Backward Euler, Forward Euler, trapezoidal rule). If only plasticity is history dependent (i.e., no viscoelasticity), then we can write $\sigma = E\epsilon^{\mathrm{e}}$, $\epsilon^{\mathrm{e}} = \epsilon - \epsilon^{\mathrm{p}}$, $\epsilon^{\mathrm{p}} = \int_{t_0}^{t_1} \dot{\epsilon}^{\mathrm{p}} dt$.

5. **FE implementation, consistent tangent:** The axial 1D stress σ (and 3D stress tensor σ_{ij}) will be a nonlinear function of the element displacement: $\sigma(\boldsymbol{d}^e)$, where e denotes element, NOT elastic. Then, the formulation of the consistent tangent for Newton-Raphson solution can be more involved than for nonlinear elasticity:

$$\frac{\partial \boldsymbol{f}^{e,\mathrm{INT}}(\boldsymbol{d}^e)}{\partial \boldsymbol{d}^e} = \dots \tag{3.3}$$

   We will show such details after we present the 1D elastoplasticity theory, time integration, and local material consistent tangent $\partial\sigma^h/\partial\epsilon^h$.

6. **verification:** *verify* implemented model (compare to analytical closed-form solution, if have one, or other numerical nonlinear solution) or 'manufactured analytical solutions' [Schwer, 2007].

7. **calibrate constitutive parameters** from laboratory experimental data

8. **validation:** attempt to *validate* model using FE simulation of more complex experimental data (geotechnical centrifuge test, structural lab test, realistic component loading, etc.) with quantified uncertainty; is your constitutive model predictive?

9. **analyze problem of interest using FEA and constitutive model.**

3.1 Experimental Evidence

For a discussion of the stress-strain response of solid materials under tension and/or compression, refer to Ch.2 of Lubliner [1990] (pg71, here as Fig.3.2), or Ch.5 of Desai and Siriwardane [1984] for geomaterials, as well as other papers and books on materials of interest to you.

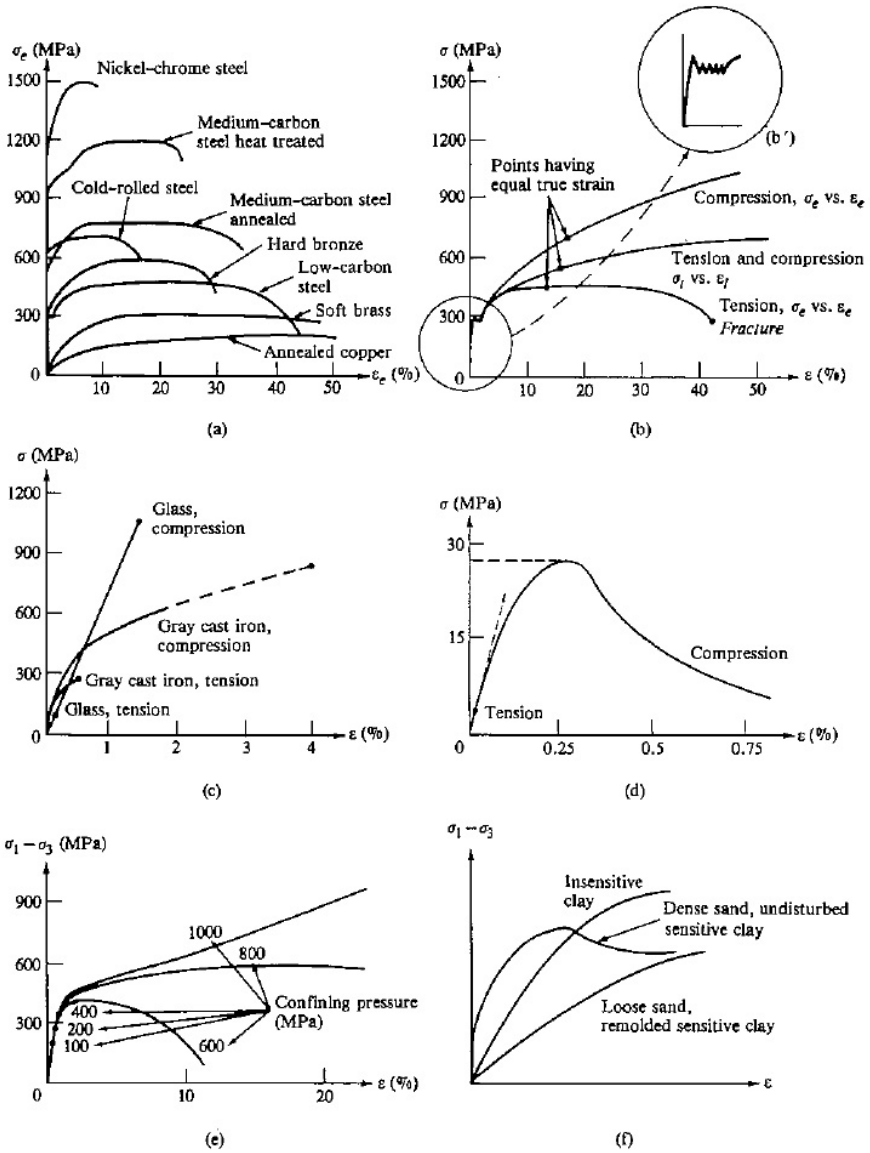

Figure 2.1.1. Stress-strain diagrams: (a) ductile metals, simple tension; (b) ductile metal (low-carbon steel), simple tension and compression; (b') yield-point phenomenon; (c) cast iron and glass, simple compression and tension; (d) typical concrete or rock, simple compression and tension; (e) rock (limestone), triaxial compression; (f) soils, triaxial compression.

Figure 3.2. Example experimental curves demonstrating elasto-plasticity. Taken from Figure 2.1.1 of Lubliner [1990].

3.2 Balance Equations and Thermodynamics

We start by writing the **balance of linear momentum** in 3D and 1D (uniaxial stress) for a single phase solid material as

$$3D \quad \rho \ddot{u}_i = \sigma_{ij,j} + \rho b_i \tag{3.4}$$

$$1D \quad (\rho A)\ddot{u} = (\sigma A)_{,x} + f \tag{3.5}$$

where, ρ = mass density (kg/m^3), $\ddot{u}_i$ = acceleration vector (m/s^2), $\sigma_{ij,j} = \partial \sigma_{ij}/\partial x_j$, σ_{ij} = symmetric stress (Pa), b_i = body force vector per unit mass (N/kg = m/s^2), $(\sigma A)_{,x} = \partial(\sigma A)/\partial x$, $\ddot{u}$ = axial acceleration (m/s^2), A = cross-sectional area of axially-loaded bar (m^2), f = distributed load along axially-loaded bar (N/m). The **balance of angular momentum** for a non-polar medium leads to symmetry of the stress tensor as $\sigma_{ij} = \sigma_{ji}$.

We may state the **balance of energy** (first law of thermodynamics) for a body $\mathcal{B}$ in Fig.3.3, in terms of its rate as

$$\begin{aligned} \text{total energy rate} &= \text{power input} + \text{heat input rate} \\ \dot{E}_{\text{total}} &= P_{\text{input}} + Q_{\text{input}} \end{aligned} \tag{3.6}$$

where $E_{\text{total}} = K + U$ is the total energy of the system, K is the kinetic energy, U is the potential energy, P_{input} is the power input as a result of external tractions and body force, and Q_{input} is the heat input rate due to heat conduction at the surface $\partial\mathcal{B}$ and distributed internal heat source within the body $\mathcal{B}$.

The power input term P_{input} warrants more attention. Note that it is composed of a traction

power term and body force power term as follows,

$$P_{\text{input}} = \int_{\partial\mathcal{B}} t_i^{\sigma} v_i da + \int_{\mathcal{B}} \rho b_i v_i dv \tag{3.7}$$

where the traction power term may be reformated as,

$$\begin{aligned} \int_{\partial\mathcal{B}} t_i^{\sigma} v_i da &= \int_{\partial\mathcal{B}} (\sigma_{ij} n_j) v_i da = \int_{\partial\mathcal{B}} (\sigma_{ij} v_i) n_j da \\ &= \int_{\mathcal{B}} \frac{\partial(\sigma_{ij} v_i)}{\partial x_j} dv = \int_{\mathcal{B}} (\sigma_{ij,j} v_i + \sigma_{ij} v_{i,j}) dv \end{aligned} \tag{3.8}$$

Recall from the balance of linear momentum,

$$\sigma_{ij,j} = \rho \dot{v}_i - \rho b_i \tag{3.9}$$

and the small strain rate,

$$\dot{\epsilon}_{ij} = \frac{1}{2}(v_{i,j} + v_{j,i}) \tag{3.10}$$

Given the symmetry of the Cauchy stress, we may write,

$$\sigma_{ij} v_{i,j} = \sigma_{ij} \dot{\epsilon}_{ij} \tag{3.11}$$

Substituting, recognizing that $D(\frac{1}{2} v_i v_i)/Dt = \dot{v}_i v_i$, and using again the conservation of solid phase mass $D\rho_0/Dt = 0$ (recall $dv = JdV$ and $\rho_0 = J\rho$), we may write,

$$\begin{aligned} P_{\text{input}} &= \int_{\mathcal{B}} \rho \dot{v}_i v_i dv - \int_{\mathcal{B}} \rho b_i v_i dv + \int_{\mathcal{B}} \sigma_{ij} \dot{\epsilon}_{ij} dv + \int_{\mathcal{B}} \rho b_i v_i dv \\ &= \frac{D}{Dt} \int_{\mathcal{B}} \frac{1}{2} \rho v_i v_i dv + \int_{\mathcal{B}} \sigma_{ij} \dot{\epsilon}_{ij} dv \end{aligned} \tag{3.12}$$

In summary, in integral form over the body $\mathcal{B}$, we have,

$$\dot{E}_{\text{total}} = \frac{D}{Dt}\int_{\mathcal{B}}\left(\frac{1}{2}\rho v_i v_i + \rho e\right)dv = \frac{D}{Dt}\int_{\mathcal{B}}\frac{1}{2}\rho v_i v_i dv + \int_{\mathcal{B}}\rho\dot{e}dv \tag{3.13}$$

$$P_{\text{input}} = \frac{D}{Dt}\int_{\mathcal{B}}\frac{1}{2}\rho v_i v_i dv + \int_{\mathcal{B}}\sigma_{ij}\dot{\epsilon}_{ij}dv \tag{3.14}$$

$$Q_{\text{input}} = \int_{\partial\mathcal{B}}(-q_i n_i)da + \int_{\mathcal{B}}\rho r dv = -\int_{\mathcal{B}}q_{i,i}dv + \int_{\mathcal{B}}\rho r dv \tag{3.15}$$

where $D(\bullet)/Dt$ is the material time derivative with respect to the motion of the solid (refer to Sect.2.3 of Holzapfel [2000]), we have employed the balance of mass of the solid (assuming single phase material) $D\rho_0/Dt = 0$, reference mass density $\rho_0 = J\rho$, J is the Jacobian of deformation, ρ is the mass density (kg/m^3), v_i is the velocity vector (m/s), e is the internal energy per unit mass (J/kg)[†], q_i is the heat flux vector into $\mathcal{B}$ (W/m^2), r is the internal heat supply per unit mass (W/kg). Substituting, canceling terms, and localizing the integral leads to the balance of energy equation as

$$3D \quad \rho\dot{e} = \sigma_{ij}\dot{\epsilon}_{ij} + \rho r - q_{i,i} \tag{3.16}$$

$$1D \quad \rho\dot{e} = \sigma\dot{\epsilon} + \rho r - q_{,x} \quad \text{(per unit volume)} \tag{3.17}$$

The **second law of thermodynamics** in 3D states that,

$$\begin{aligned} \text{rate of entropy increase} &\geq \text{entropy input rate} \\ \frac{D}{Dt}\int_{\mathcal{B}}\rho\eta dv &\geq \int_{\mathcal{B}}\rho\frac{r}{\theta}dv - \int_{\partial\mathcal{B}}\frac{1}{\theta}q_i n_i da \end{aligned} \tag{3.18}$$

where η is the entropy per unit mass (J/(K.kg)), θ is the temperature (K), and n_i is the unit

[†]yet another usage of italic e!

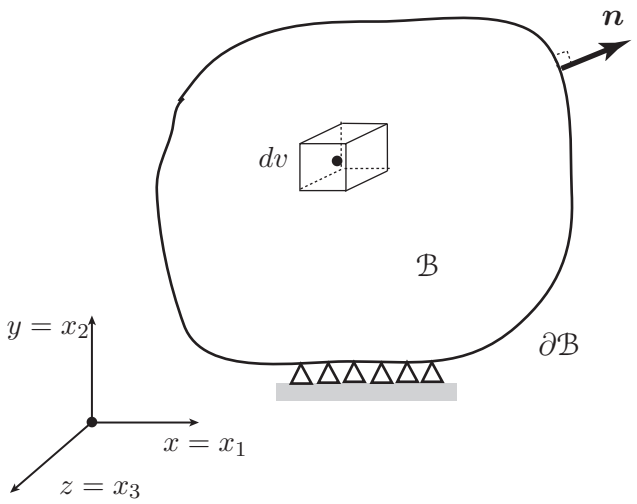

Figure 3.3. Continuum body $\mathcal{B}$ with boundary $\partial\mathcal{B}$.

normal vector to the surface $\partial\mathcal{B}$. After localizing the integral, we have,

$$\rho\theta\dot{\eta} \quad \geq \quad \rho r - q_{i,i} + \frac{1}{\theta} q_i \theta_{,i} \tag{3.19}$$

We assume the existence of a Helmholtz free energy function per unit mass ψ (important for non-isothermal problems) as follows,

$$\psi = e - \eta\theta \tag{3.20}$$

After substituting for ψ, and $\rho\dot{e}$ from the first law (3.16) leads to the Clausius-Duhem inequality (check the derivation yourself) as,

$$\sigma_{ij}\dot{\epsilon}_{ij} - \rho\dot{\psi} - \rho\eta\dot{\theta} - \frac{1}{\theta} q_i \theta_{,i} \geq 0 \tag{3.21}$$

For isothermal ($\dot{\theta} = 0$) and homogeneous temperature ($\theta_{,i} = 0$) problems, the Clausius-

Duhem inequality is written as

$$3D \quad \sigma_{ij}\dot{\epsilon}_{ij} - \rho\dot{\psi} \geq 0 \tag{3.22}$$

$$1D \quad \sigma\dot{\epsilon} - \rho\dot{\psi} \geq 0 \quad \text{(per unit volume)} \tag{3.23}$$

3.3 Constitutive Equations for 1D Elastoplasticity

We outline the topic coverage for 1D classical (inviscid or rate-independent) elastoplasticity as [Simo and Hughes, 1998, Anandarajah, 2010, Borja, 2013]

(i) Helmholtz free energy function

(ii) yield and plastic potential functions

(iii) evolution equations for ISVs

(iv) Kuhn-Tucker optimality conditions

(v) consistency condition

(vi) continuum elastoplastic tangent

(vii) isotropic/kinematic hardening

(viii) convexity of yield surface

(ix) uniqueness (Hill's stability postulate, softening plasticity)

In more detail, we have

(i) **Helmholtz free energy function:** The Helmholtz free energy function ψ per unit mass is additively decomposed ("energy separable" processes, which is a constitutive assumption in and of itself) into elastic e and plastic p parts as,

$$\rho\psi(\epsilon^{\mathrm{e}}, \zeta) \;\; = \;\; \rho\psi^{\mathrm{e}}(\epsilon^{\mathrm{e}}) + \rho\psi^{\mathrm{p}}(\zeta) \tag{3.24}$$

where ϵ^{e} is the elastic strain, and ζ is a strain-like ISV, not necessarily the plastic strain, although in our case for 1D elastoplasticity it will end up being the magnitude of the axial plastic strain $|\epsilon^{\mathrm{p}}|$. Taking the material time derivative (refer to Sect.2.3 of Holzapfel [2000], and we will discuss more when we discuss mixture theory), we have from the chain rule,

$$\frac{D(\rho\psi)}{Dt} = \dot{\rho}\psi + \rho\dot{\psi} \tag{3.25}$$

where $\dot{\rho} \approx 0$ for a single phase solid material deformed at small strain. This will not be the case for multiphase materials treated by mixture theory (we will discuss later), and also for finite strain conditions. Then, we see that,

$$\rho\dot{\psi} = \frac{D(\rho\psi)}{Dt} = \frac{\partial(\rho\psi)}{\partial\epsilon^{\mathrm{e}}}\dot{\epsilon}^{\mathrm{e}} + \frac{\partial(\rho\psi)}{\partial\zeta}\dot{\zeta} \tag{3.26}$$

We substitute this into the Clausius-Duhem inequality and rearrange terms to obtain the following,

$$\left(\sigma - \frac{\partial(\rho\psi)}{\partial\epsilon^{\mathrm{e}}}\right)\dot{\epsilon}^{\mathrm{e}} + \sigma\dot{\epsilon}^{\mathrm{p}} - \frac{\partial(\rho\psi)}{\partial\zeta}\dot{\zeta} \geq 0 \tag{3.27}$$

Coleman and Noll [1963], Coleman and Gurtin [1967] argued that the elastic strain rate $\dot{\epsilon}^{\mathrm{e}}$ can be an independent process from the plastic strain rate $\dot{\epsilon}^{\mathrm{p}}$ and ISV rate $\dot{\zeta}$, thus for (3.27) to hold, we have an equation for the stress σ as,

$$\sigma - \frac{\partial(\rho\psi)}{\partial\epsilon^{\mathrm{e}}} = 0 \implies \sigma = \frac{\partial(\rho\psi)}{\partial\epsilon^{\mathrm{e}}} \tag{3.28}$$

If (3.28) holds, such that the stress σ is derived from a Helmholtz free energy function, then the constitutive model is said to be "hyperelastic." Also, a thermodynamically-conjugate stress-like ISV κ can be defined as

$$\kappa := \frac{\partial(\rho\psi)}{\partial\zeta} \tag{3.29}$$

(which is related to the yield stress) such that the **reduced dissipation inequality** $\mathcal{D}$ becomes the difference between plastic power per unit volume (which when integrated over time leads to plastic work) and rate of stored work of plastic ISV evolution as,

$$\mathcal{D} := \sigma\dot{\epsilon}^{\mathrm{p}} - \kappa\dot{\zeta} \geq 0 \tag{3.30}$$

We make a **constitutive assumption for the Helmholtz free energy function** ψ (per unit mass) that leads to linear elasticity and linear hardening/softening as,

$$\rho\psi(\epsilon^{\mathrm{e}}, \zeta) = \frac{1}{2}E(\epsilon^{\mathrm{e}})^2 + \frac{1}{2}H^{\kappa}\zeta^2 \tag{3.31}$$

Then, assuming mass density ρ is constant, we have

$$\sigma = \frac{\partial(\rho\psi)}{\partial\epsilon^{\mathrm{e}}} = E\epsilon^{\mathrm{e}} \tag{3.32}$$

$$\kappa = \frac{\partial(\rho\psi)}{\partial\zeta} = H^{\kappa}\zeta \tag{3.33}$$

Assuming constant elastic modulus E and constant hardening/softening modulus H^{κ}, we express the stress equations in rate form as

$$\dot{\sigma} = E\dot{\epsilon}^{\mathrm{e}} = E(\dot{\epsilon} - \dot{\epsilon}^{\mathrm{p}}) \tag{3.34}$$

$$\dot{\kappa} = H^{\kappa}\dot{\zeta} \tag{3.35}$$

The axial strain rate $\dot{\epsilon}$ will be provided numerically by the finite element solution, and thus we need **evolution equations** for $\dot{\epsilon}^{\text{p}}$ and $\dot{\zeta}$, as well as **yield and plastic potential functions**, in order to calculate stress σ and stress-like ISV κ.

(ii) **yield and plastic potential functions:** We define a yield function f to determine when the stress reaches plastic yielding along the stress-strain curve, where we have,

$$\begin{aligned} f(\sigma, \kappa) &= |\sigma| - \kappa \leq 0 \\ & \quad f < 0 \text{ elastic} \\ & \quad f = 0 \text{ plastic} \end{aligned} \tag{3.36}$$

We can define the initial value of the stress-like ISV κ to be the initial yield stress in compression or tension of the 1D axially loaded bar, such that $\kappa_0 = \kappa(t = 0) = \sigma_{y0}$. We can look at the yield surface in 1D in Fig.3.4. In 1D, the elastic region is the portion of the real number line where the axial stress σ lies between the values of κ in positive (tension) and negative (compression) directions. In 1D, the plastic region is the value of stress that equals the stress-like ISV, such as $|\sigma| = \kappa$. In Fig.3.4, the initial position of the yield surface is shown.

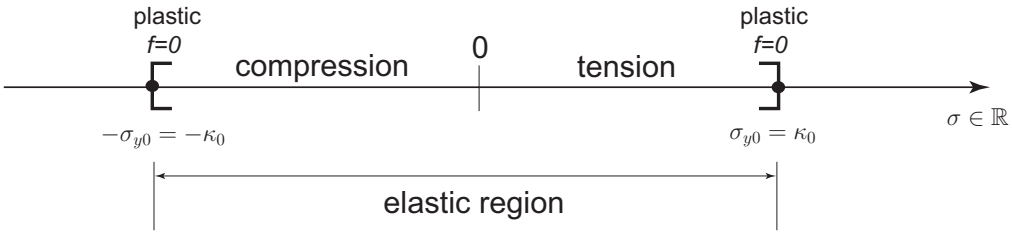

Figure 3.4. Yield surface in 1D, where the axial stress is in the set of real numbers: $\sigma \in \mathbb{R}$. We will discuss the stress-path using this figure and a stress-strain plot.

A plastic potential function g is defined similar to the yield function f, but is used to govern the plastic flow, or plastic strain rate, where the yield function f is used to govern the admissible stress state (whether elastic or elastoplastic loading). There are

two choices for the plastic potential function g: (1) if $g = f$, then we have **associative plastic flow**; (2) if $g \neq f$, then we have **non-associative plastic flow** (typical for geomaterials and concrete based on plastic volume change predicted by $\partial g/\partial \boldsymbol{\sigma}$; discussed in Chapter 5).

(iii) **evolution equations:** Now we define the evolution equations starting with the **plastic flow rule**. We assume associative flow $g = f$ for 1D plasticity (and 3D isochoric plasticity, later) for now, such that

$$\dot{\epsilon}^{\mathrm{p}} = \dot{\gamma}\frac{\partial g}{\partial \sigma} \implies \dot{\sigma} = E\left(\dot{\epsilon} - \dot{\gamma}\frac{\partial g}{\partial \sigma}\right) \tag{3.37}$$

$$g = f = |\sigma| - \kappa \tag{3.38}$$

$$\frac{\partial g}{\partial \sigma} = \frac{\partial |\sigma|}{\partial \sigma} = \mathrm{sign}(\sigma) \tag{3.39}$$

$$\implies \dot{\epsilon}^{\mathrm{p}} = \dot{\gamma}\,\mathrm{sign}(\sigma) \tag{3.40}$$

where $\dot{\gamma}$ is the plastic multiplier or consistency parameter. Notice that $\dot{\gamma} = |\dot{\epsilon}^{\mathrm{p}}| > 0$, where plastic flow (deformation or strain) is in the direction of stress, which in 1D is sign(σ) (i.e., "+" for tension, and "−" for compression). We likewise define an **evolution equation for the strain-like ISV**, such as

$$\dot{\zeta} = \dot{\gamma}h(\sigma, \kappa) \implies \dot{\kappa} = H^{\kappa}\dot{\gamma}h(\sigma, \kappa) \tag{3.41}$$

where $h(\sigma, \kappa)$ is the hardening function. For simplicity, we assume $h(\sigma, \kappa) = -\frac{\partial g}{\partial \kappa} = 1 \implies \dot{\zeta} = \dot{\gamma} = |\dot{\epsilon}^{\mathrm{p}}|$. *We will show later that* $h(\sigma, \kappa) = -\frac{\partial f}{\partial \kappa}$ *results from satisfying the principle of maximum plastic dissipation, where also associative plasticity* $g = f$ *likewise results. It is important to recognize that the principle of maximum plastic dissipation is NOT the same as the second law of thermodynamics, which we will not violate. However, for geomaterials, experimental data dictate non-associative plasticity, which violates the principle of maximum plastic dissipation, but not the second law of*

thermodynamics. More later.

We summarize the constitutive and evolution equations as

$$\dot{\sigma} = E\dot{\epsilon}^{\mathrm{e}} = E\left(\dot{\epsilon} - \dot{\epsilon}^{\mathrm{p}}\right) \tag{3.42}$$

$$\dot{\epsilon}^{\mathrm{p}} = \dot{\gamma}\,\mathrm{sign}(\sigma) \tag{3.43}$$

$$\dot{\kappa} = H^{\kappa}|\dot{\epsilon}^{\mathrm{p}}| = H^{\kappa}\dot{\gamma} \tag{3.44}$$

where hardening, softening, and perfect plasticity for κ are shown in Fig.3.5. Note that the abscissa in Fig.3.5 is the plastic strain magnitude $|\epsilon^{\mathrm{p}}|$, and not the total strain ϵ. We will solve for $\dot{\gamma}$ from the consistency condition.

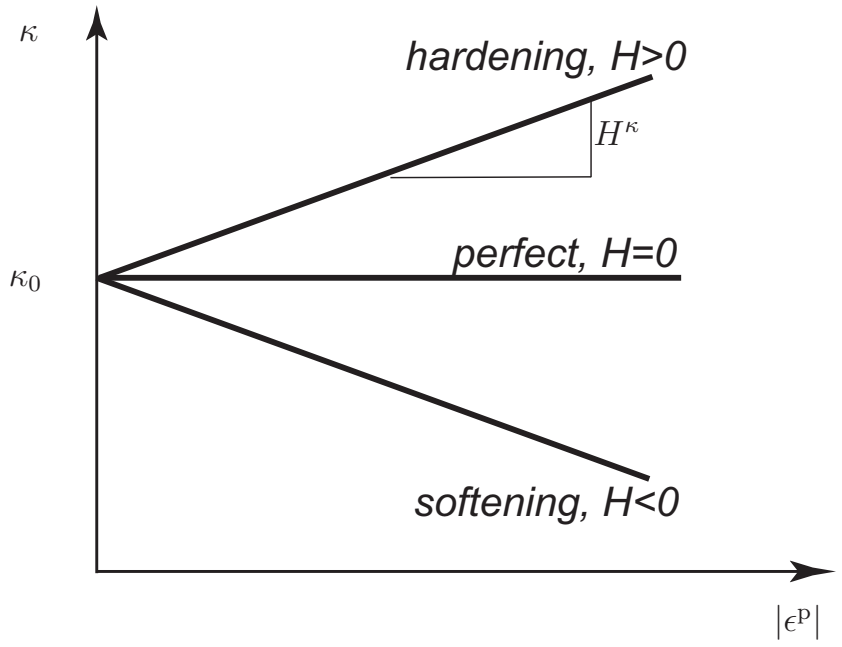

Figure 3.5. Evolution of ISV κ for linear hardening/softening with hardening/softening modulus H^{κ}.

(iv) **Kuhn-Tucker optimality conditions:** We know the following conditions separately: (a) $\dot{\gamma} \geq 0$, that the plastic multiplier is positive ($\dot{\gamma} > 0$, plastic loading) or zero ($\dot{\gamma} = 0$, elastic loading/unloading); and (b) $f \leq 0$, the yield function is negative ($f < 0$, elastic loading/unloading) or zero ($f = 0$, plastic loading). Then, together, these two

conditions are combined as $\dot{\gamma} f = 0$, such that if $\dot{\gamma} > 0$ then $f = 0$ and we have plastic loading, where then the stress state is on the yield surface in Fig.3.6.

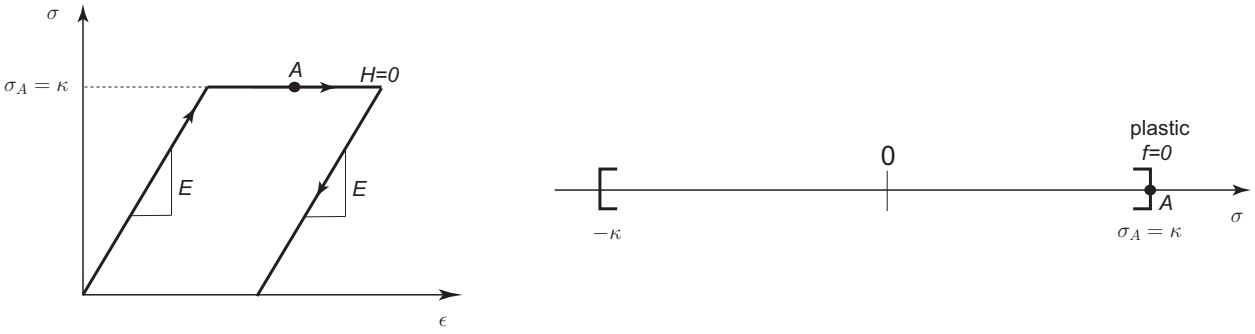

Figure 3.6. Stress state is plastic, said to be "plastic loading" at $\sigma_A = \kappa$.

If $f < 0$ then $\dot{\gamma} = 0$, then we have elastic loading/unloading as shown in Fig.3.7.

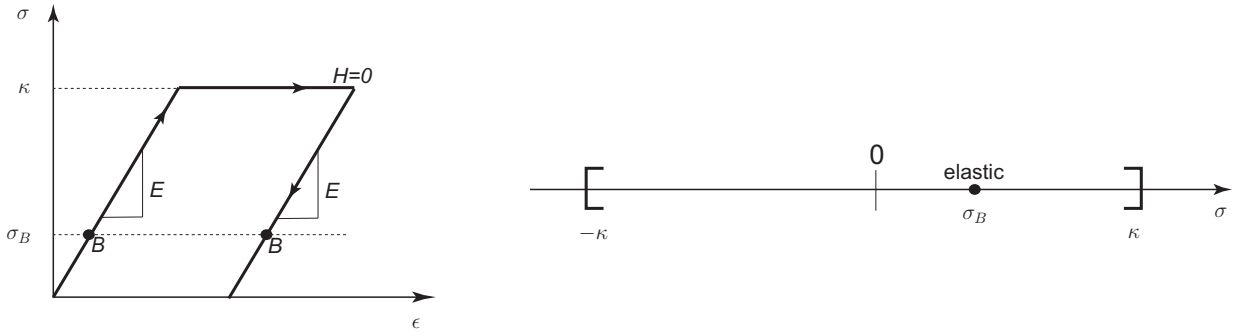

Figure 3.7. Stress state is elastic, said to be "elastic loading or unloading" at σ_B.

These conditions are called the **Kuhn-Tucker optimality conditions** written as

$$\dot{\gamma} \geq 0 \ , \ f \leq 0 \ , \ \dot{\gamma} f = 0 \tag{3.45}$$

(v) **consistency condition:** When loading plastically[‡], $f = 0$, or in rate form $\dot{f} = 0$ (stress state persists on yield surface). When loading or unloading elastically, $f < 0$, or in rate form $\dot{f} < 0$ (or $\dot{f} > 0$). Combined, these conditions read as (i) plastic loading:

[‡]Strictly speaking, the loading is always elastoplastic because the elasticity and plasticity are coupled as the stress is calculated from the elastic strain as $\sigma = E\epsilon^{\mathrm{e}} = E(\epsilon - \epsilon^{\mathrm{p}})$.

$\dot{\gamma} > 0$ implies $\dot{f} = 0$; (ii) elastic unloading/loading: $\dot{f} < 0$ (or $\dot{f} > 0$) implies $\dot{\gamma} = 0$. Then, together, these two conditions are combined into the **consistency condition:**

$$\dot{\gamma}\dot{f} = 0 \tag{3.46}$$

oftentimes written for plastic loading ($\dot{\gamma} > 0$) as simply $\dot{f} = 0$. **We solve for $\dot{\gamma}$ from the consistency condition during plastic loading** ($\dot{\gamma} > 0$ and $\dot{f} = 0$). Using the chain rule

$$\dot{f}(\sigma, \kappa) = \frac{\partial f}{\partial \sigma}\dot{\sigma} + \frac{\partial f}{\partial \kappa}\dot{\kappa} = 0 \tag{3.47}$$

and substituting evolution equations leads to the solution for $\dot{\gamma}$ as

$$\frac{\partial f}{\partial \sigma} E \left(\dot{\epsilon} - \dot{\gamma}\frac{\partial g}{\partial \sigma} \right) + \frac{\partial f}{\partial \kappa} H^{\kappa} h(\sigma, \kappa)\dot{\gamma} = 0 \tag{3.48}$$

$$\dot{\gamma} = \frac{\frac{\partial f}{\partial \sigma} E \dot{\epsilon}}{\frac{\partial f}{\partial \sigma} E \frac{\partial g}{\partial \sigma} - \frac{\partial f}{\partial \kappa} H^{\kappa} h} \tag{3.49}$$

For our example, as we will see, the plastic multiplier becomes,

$$\dot{\gamma} = \frac{E\dot{\epsilon}[\text{sign}(\sigma)]}{E + H^{\kappa}} \tag{3.50}$$

(vi) **continuum elastoplastic tangent:** Substituting the solution for $\dot{\gamma}$ back into the stress evolution equation, we obtain an expression for the **continuum elastoplastic tangent** E^{ep}, which relates the **total stress rate** $\dot{\sigma}$ to the **total strain rate** $\dot{\epsilon}$ as

$$\dot{\sigma} = E \left(\dot{\epsilon} - \dot{\gamma}\frac{\partial g}{\partial \sigma} \right) \tag{3.51}$$

$$= \underbrace{\left(E - \frac{E \frac{\partial g}{\partial \sigma} \frac{\partial f}{\partial \sigma} E}{\frac{\partial f}{\partial \sigma} E \frac{\partial g}{\partial \sigma} - \frac{\partial f}{\partial \kappa} H h} \right)}_{E^{\text{ep}}} \dot{\epsilon} \tag{3.52}$$

$$= E^{\text{ep}}\dot{\epsilon} \tag{3.53}$$

For our example,

$$\frac{\partial f}{\partial \sigma} = \frac{\partial g}{\partial \sigma} = \text{sign}(\sigma) \tag{3.54}$$

$$\frac{\partial f}{\partial \kappa} = -1 \tag{3.55}$$

$$h(\sigma, \kappa) = 1 \tag{3.56}$$

then, we have

$$\dot{\sigma} = E^{\text{ep}} \dot{\epsilon} \ , \ E^{\text{ep}} = \frac{E H^{\kappa}}{E + H^{\kappa}} \tag{3.57}$$

For bilinear hardening/softening (which we have assumed), the stress-strain response is illustrated in Fig.3.8.

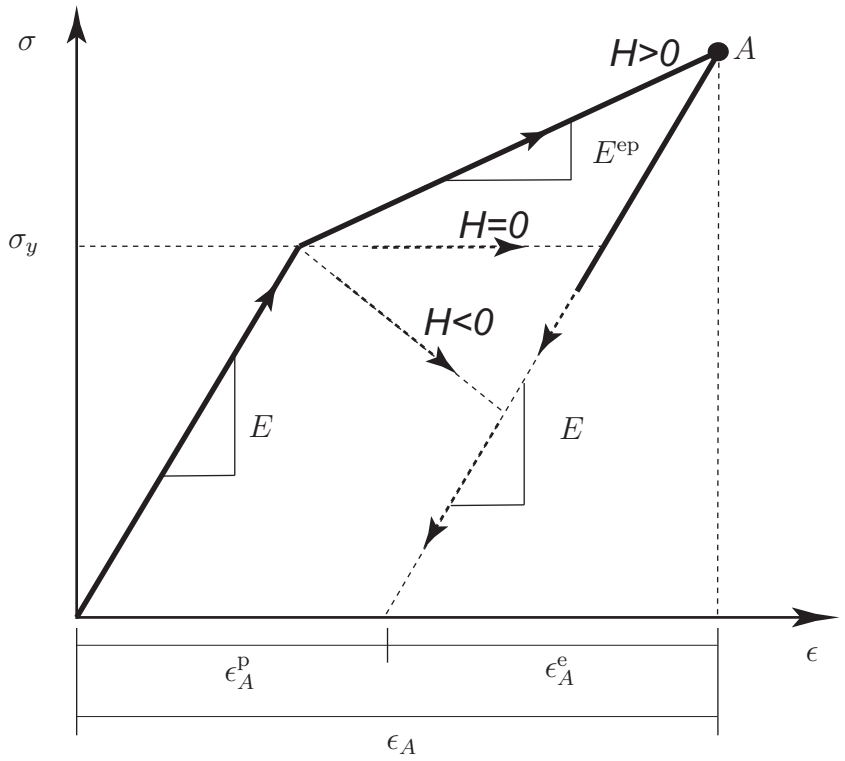

Figure 3.8. Linear elastic, hardening/perfect/softening plastic, stress-strain response showing additive decomposition of strain at point A: $\epsilon_A = \epsilon^{\text{e}}_A + \epsilon^{\text{p}}_A$. The slope of the plastic loading curve is the elasto-plastic modulus E^{ep}.

(vii) **combined isotropic and kinematic hardening:** Until now, we considered only

isotropic hardening through stress-like ISV κ, such as in Fig.3.9.

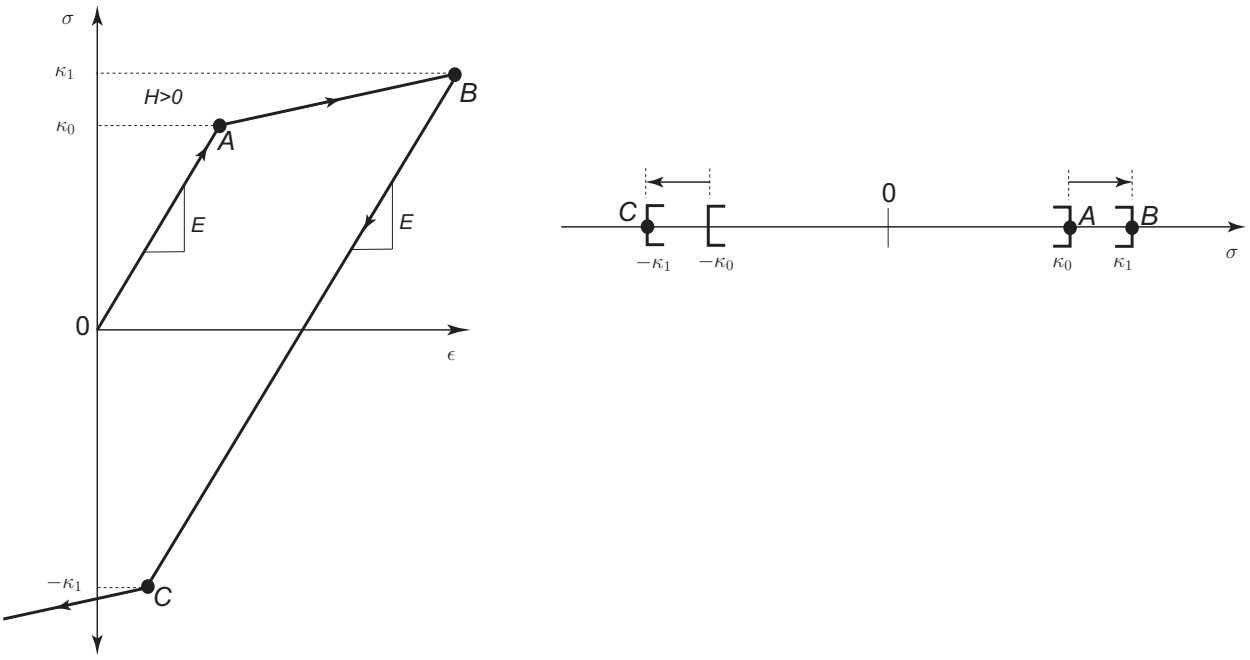

Figure 3.9. Linear elastic, hardening plasticity response showing evolution of isotropic ISV κ from κ_0 to κ_1 on stress-strain curve and yield surface stress space σ. This is **isotropic hardening**.

As shown in Fig.3.9, if κ increases or decreases, the elastic domain increases or decreases symmetrically about the stress origin (Fig.3.9 shows an increase in the elastic domain). But certain experimental data have shown that upon unloading and reverse loading, yielding is not symmetric, which is called the *Bauschinger effect*, as illustrated in Fig.3.10.

Thus, we introduce a *backstress* α into the thermodynamics and yield function to account for unsymmetric yield about the stress origin, which is called **kinematic** hardening.

The Helmholtz free energy function ψ (per unit mass) is modified to include two other

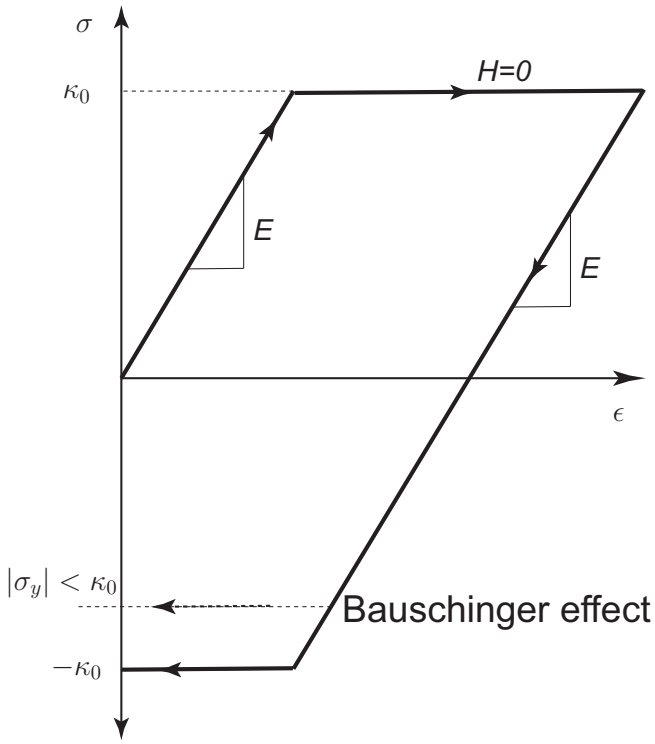

Figure 3.10. Linear elastic, perfectly-plastic response showing Bauschinger effect upon unloading and reloading where $|\sigma_y| < \kappa_0$. This experimentally-observed phenomenon motivates **kinematic hardening**.

ISVs (ζ^α and α) associated with kinematic hardening as

$$\rho\psi(\epsilon^{\mathrm{e}}, \boldsymbol{\zeta}) := \frac{1}{2}E(\epsilon^{\mathrm{e}})^2 + \frac{1}{2}\boldsymbol{\zeta}\cdot\boldsymbol{H}\cdot\boldsymbol{\zeta} \tag{3.58}$$

$$\boldsymbol{\zeta} = \begin{bmatrix} \zeta^\kappa \\ \zeta^\alpha \end{bmatrix}, \ \boldsymbol{H} = \begin{bmatrix} H^\kappa & 0 \\ 0 & H^\alpha \end{bmatrix} \tag{3.59}$$

where $\boldsymbol{\zeta}$ is now a vector of strain-like ISVs, and $\boldsymbol{H}$ is the hardening matrix. From the Clausius-Duhem inequality, we have an energy-conjugate vector $\boldsymbol{q}^\zeta$ of stress-like ISVs as

$$\boldsymbol{q}^\zeta = \frac{\partial(\rho\psi)}{\partial\boldsymbol{\zeta}} = \begin{bmatrix} \kappa \\ \alpha \end{bmatrix} = \boldsymbol{H}\cdot\boldsymbol{\zeta} \tag{3.60}$$

$$\dot{\boldsymbol{q}}^\zeta = \boldsymbol{H}\cdot\dot{\boldsymbol{\zeta}} \tag{3.61}$$

We introduce the backstress α into the yield function as follows

$$f(\sigma, \boldsymbol{q}^{\zeta}) = |\sigma - \alpha| - \kappa \leq 0 \tag{3.62}$$

When we analyze initial yield stress $\sigma_{y0} = \alpha_0 + \kappa_0 \text{sign}(\sigma - \alpha_0)$, we can see in Fig.3.11 the effect of the backstress α in shifting the yield surface. Think of the yield surface as translated ("kinematic") in stress space, in this case along the real number line as shown in Fig.3.11, where the elastic domain is centered about $\sigma = \alpha$.

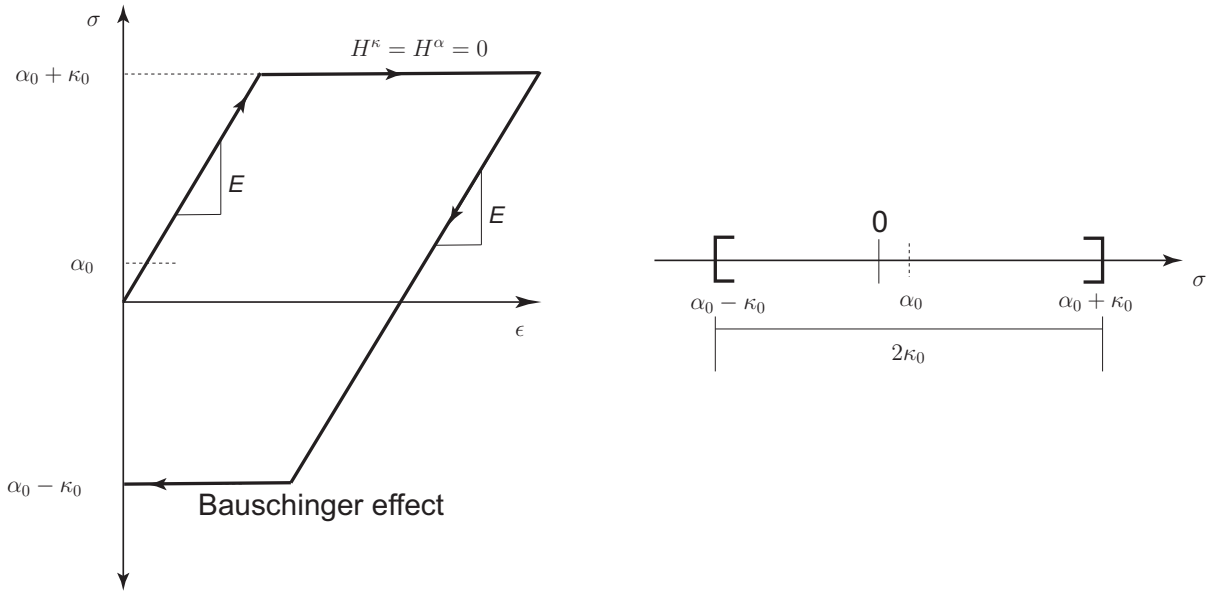

Figure 3.11. Linear elastic, perfectly-plastic response showing translated position of center of yield surface by backstress α_0. The size of the yield surface is still controlled by κ_0, where the size is $2\kappa_0$. This is **kinematic hardening** when the backstress α evolves and the yield surface translates.

If κ remains constant ($H^\kappa = 0$, $\kappa = \kappa_0$), but α is increasing by hardening ($H^\alpha > 0$), then the yield surface translates in stress space ($\sigma \in \mathbb{R}$), but does not grow or reduce in size as shown in Fig.3.12. We can confirm that the yield surface just translates in stress space without changing size by the following calculation:

$$\begin{aligned} (\alpha_0 + \kappa_0) - (\alpha_0 - \kappa_0) &= 2\kappa_0 \\ (\alpha_1 + \kappa_0) - (\alpha_1 - \kappa_0) &= 2\kappa_0 \end{aligned} \tag{3.63}$$

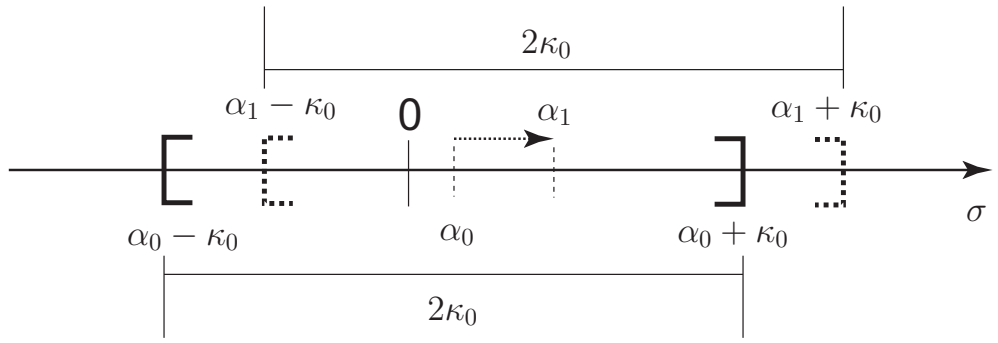

Figure 3.12. Kinematic hardening ($H^\alpha > 0$), but isotropic perfectly plastic ($H^\kappa = 0$), showing translated position of center of yield surface by backstress α_0 to hardened value α_1. The size of the yield surface is still controlled by κ_0, where the size is $2\kappa_0$ because $H^\kappa = 0$. *In class: we will draw a stress-path with corresponding stress-strain curve to illustrate this concept.*

We can write the evolution equation for the strain-like ISV vector $\boldsymbol{\zeta}$ as

$$\dot{\boldsymbol{\zeta}} = \dot{\gamma}\boldsymbol{h}(\sigma, \boldsymbol{q}^\zeta) \implies \dot{\boldsymbol{q}}^\zeta = \dot{\gamma}\boldsymbol{H} \cdot \boldsymbol{h}(\sigma, \boldsymbol{q}^\zeta) \tag{3.64}$$

For simplicity, let $\boldsymbol{h}(\sigma, \boldsymbol{q}^\zeta) = -\partial g/\partial \boldsymbol{q}^\zeta$ and $g = f$, such that

$$-\frac{\partial g}{\partial \boldsymbol{q}^\zeta} = -\begin{bmatrix} \frac{\partial g}{\partial \kappa} \\ \frac{\partial g}{\partial \alpha} \end{bmatrix} = \begin{bmatrix} 1 \\ \text{sign}(\sigma - \alpha) \end{bmatrix} \implies \begin{array}{l} \dot{\kappa} = H^\kappa \dot{\gamma} \\ \dot{\alpha} = H^\alpha \text{sign}(\sigma - \alpha)\dot{\gamma} \end{array} \tag{3.65}$$

$$\dot{\boldsymbol{\zeta}} = \begin{bmatrix} \dot{\zeta}^\kappa \\ \dot{\zeta}^\alpha \end{bmatrix} = \dot{\gamma} \begin{bmatrix} 1 \\ \text{sign}(\sigma - \alpha) \end{bmatrix} \tag{3.66}$$

We revisit the consistency condition:

$$\dot{f} = \frac{\partial f}{\partial \sigma}\dot{\sigma} + \frac{\partial f}{\partial \boldsymbol{q}^\zeta} \cdot \dot{\boldsymbol{q}}^\zeta = 0 \tag{3.67}$$

Upon substituting the evolution equations into the consistency condition equation leads

to the solution of the plastic multiplier $\dot{\gamma}$ as follows,

$$\frac{\partial f}{\partial \sigma} E \left(\dot{\epsilon} - \dot{\gamma} \frac{\partial g}{\partial \sigma} \right) + \frac{\partial f}{\partial \boldsymbol{q}^{\zeta}} \cdot \boldsymbol{H} \cdot \boldsymbol{h} \dot{\gamma} = 0 \tag{3.68}$$

$$\dot{\gamma} = \frac{\frac{\partial f}{\partial \sigma} E \dot{\epsilon}}{\frac{\partial f}{\partial \sigma} E \frac{\partial g}{\partial \sigma} - \frac{\partial f}{\partial \boldsymbol{q}^{\zeta}} \cdot \boldsymbol{H} \cdot \boldsymbol{h}} \tag{3.69}$$

More specifically, for our example of linear elasticity and linear hardening, we have

$$\frac{\partial f}{\partial \boldsymbol{q}^{\zeta}} = \begin{bmatrix} -1 \\ -\text{sign}(\sigma - \alpha) \end{bmatrix} \tag{3.70}$$

$$-\frac{\partial f}{\partial \boldsymbol{q}^{\zeta}} \cdot \boldsymbol{H} \cdot \boldsymbol{h} = H^{\kappa} + H^{\alpha} \tag{3.71}$$

Then, the continuum elastoplastic tangent results as (show the derivation yourself)

$$E^{\text{ep}} = \frac{E(H^{\kappa} + H^{\alpha})}{E + H^{\kappa} + H^{\alpha}} \tag{3.72}$$

(viii) **convexity of yield surface:** Convexity of the elastic domain in stress space (Fig.3.13) is required for proper formulation of an elastoplasticity model [Simo and Hughes, 1998]. In Fig.3.13, convex and non-convex yield surfaces are illustrated in principal stress space, where the two options are summarized: **convex** implies that all possible stress states lie within the elastic domain ($f < 0$), or on the yield surface ($f = 0$), whereas **non-convex** implies that it is possible for a stress state to lie outside the elastic domain (which is impossible for rate-independent plasticity because this violates one of the Kuhn-Tucker conditions, $f \leq 0$).

Mathematically, this can be proven as follows [Simo and Hughes, 1998]. Consider an elastic domain bounded by a yield surface

$$\mathbb{E}_{\sigma} = \left\{ \sigma \in \mathbb{R}, \boldsymbol{q}^{\zeta} \in \mathbb{R}^2, f(\sigma, \boldsymbol{q}^{\zeta}) \leq 0 \right\} \tag{3.73}$$

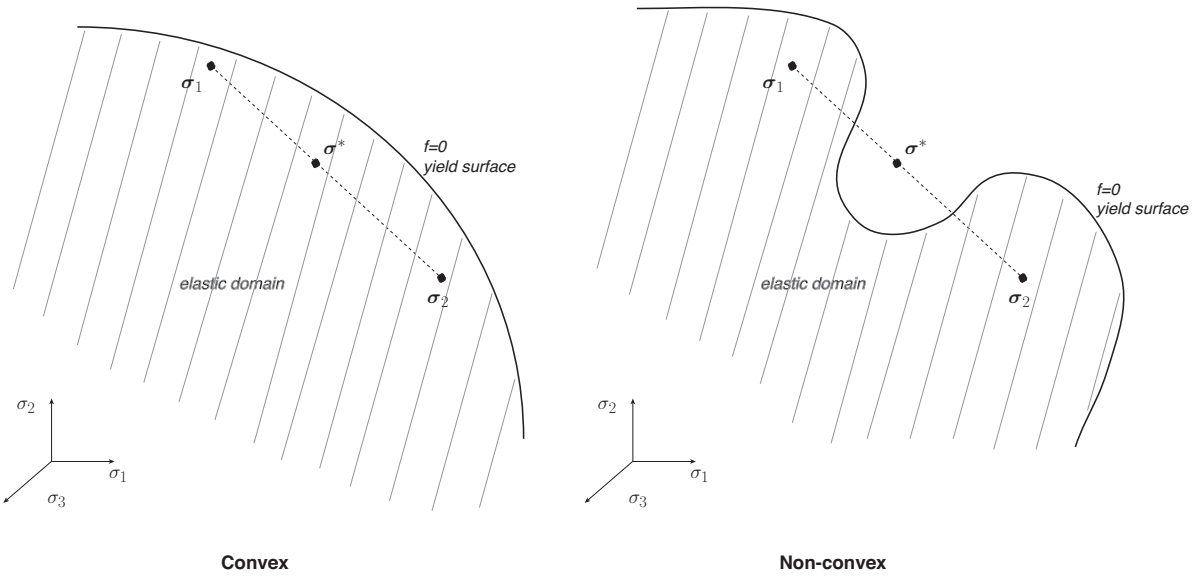

Figure 3.13. Illustration of convex (left) and non-convex (right) yield surfaces in 3D principal stress space. The concept is that for any two elastic stress states $\boldsymbol{\sigma}_1$ and $\boldsymbol{\sigma}_2$, a third elastic stress state can lie along a straight line in between, which we call $\boldsymbol{\sigma}^*$. If $\boldsymbol{\sigma}^*$ falls within the elastic domain, then the yield surface is convex, otherwise it is not. A mathematical proof is given in the notes.

We want to ensure convexity of f, thus we need to show that

$$f[\sigma^*, (\boldsymbol{q}^\zeta)^*] \leq \eta f(\sigma_1, \boldsymbol{q}_1^\zeta) + (1-\eta) f(\sigma_2, \boldsymbol{q}_2^\zeta) \quad \forall \eta \in [0,1] \tag{3.74}$$

$$\sigma^* = \eta\sigma_1 + (1-\eta)\sigma_2 \text{ (linear interpolation)} \tag{3.75}$$

$$(\boldsymbol{q}^\zeta)^* = \eta \boldsymbol{q}_1^\zeta + (1-\eta)\boldsymbol{q}_2^\zeta \tag{3.76}$$

We can check this by applying the triangle inequality, $|a+b| \leq |a| + |b|$, such that

$$f[\sigma^*, (\boldsymbol{q}^\zeta)^*] = |\sigma^* - \alpha^*| - \kappa^* \tag{3.77}$$

$$= |\eta\sigma_1 + (1-\eta)\sigma_2 - \eta\alpha_1 - (1-\eta)\alpha_2| - \eta\kappa_1 - (1-\eta)\kappa_2 \tag{3.78}$$

$$\leq (\eta|\sigma_1 - \alpha_1| - \eta\kappa_1) + ((1-\eta)|\sigma_2 - \alpha_2| - (1-\eta)\kappa_2) \tag{3.79}$$

$$= \eta f(\sigma_1, \boldsymbol{q}_1^\zeta) + (1-\eta) f(\sigma_2, \boldsymbol{q}_2^\zeta) \tag{3.80}$$

$$q.e.d$$

Therefore, $f(\sigma, \boldsymbol{q}^\zeta)$ is convex for our simple 1D combined isotropic-kinematic hardening elastoplasticity model.

(ix) **uniqueness (Hill's stability postulate and softening plasticity):** Let us revisit the analysis of uniqueness for elastoplasticity on pg53 of Hill [1950]. Consider an elastoplastic bar in static equilibrium, with constant cross-sectional area A

$$\begin{aligned} \sigma_{,x} &= 0 \quad \text{for } x \in (0, L) \\ \sigma A &= F \quad \text{at } x = L \\ u &= g \quad \text{at } x = 0 \end{aligned} \tag{3.81}$$

Consider two possible distinct stress increments $\dot{\sigma}$ and $\dot{\sigma}^*$ resulting from two distinct strain increments $\dot{\epsilon}$ and $\dot{\epsilon}^*$, where

$$\begin{aligned} \dot{\sigma} &= E^{ep}\dot{\epsilon}, \quad \dot{\epsilon} = \dot{u}_{,x} \\ \dot{\sigma}^* &= E^{ep}\dot{\epsilon}^*, \quad \dot{\epsilon}^* = \dot{u}^*_{,x} \end{aligned} \tag{3.82}$$

The BCs are the same, where $\dot{\sigma}_{,x} = 0$ and $\dot{\sigma}^*_{,x} = 0$ for static equilibrium without a body force. Consider the derivative

$$\frac{\partial}{\partial x}\left[(\dot{\sigma} - \dot{\sigma}^*)(\dot{u} - \dot{u}^*)\right] = \frac{\partial(\dot{\sigma} - \dot{\sigma}^*)}{\partial x}(\dot{u} - \dot{u}^*) + (\dot{\sigma} - \dot{\sigma}^*)\frac{\partial(\dot{u} - \dot{u}^*)}{\partial x} \tag{3.83}$$

Then, integrating over the length L of the bar (to provide a strain energy difference), we have

$$\int_0^L (\dot{\sigma} - \dot{\sigma}^*)(\dot{\epsilon} - \dot{\epsilon}^*)dx = \int_0^L \frac{\partial}{\partial x}\left[(\dot{\sigma} - \dot{\sigma}^*)(\dot{u} - \dot{u}^*)\right]dx - \int_0^L \frac{\partial(\dot{\sigma} - \dot{\sigma}^*)}{\partial x}(\dot{u} - \dot{u}^*)dx \tag{3.84}$$

Let us analyze each term separately on the r.h.s. Using Green's theorem, and because the BCs are the same for each solution (i.e., the stresses at $x = L$ and displacements

at $x = 0$ are the same), we have

$$\int_0^L \frac{\partial}{\partial x} \left[(\dot{\sigma} - \dot{\sigma}^*)(\dot{u} - \dot{u}^*) \right] dx = \left[(\dot{\sigma} - \dot{\sigma}^*)(\dot{u} - \dot{u}^*) \right]_0^L = 0 \tag{3.85}$$

Also, because $\dot{\sigma}_{,x} = 0$ and $\dot{\sigma}^*_{,x} = 0$ for $x \in (0, L)$, we have

$$\int_0^L \frac{\partial(\dot{\sigma} - \dot{\sigma}^*)}{\partial x} (\dot{u} - \dot{u}^*) dx = 0 \tag{3.86}$$

Then, we are left with

$$\int_0^L (\dot{\sigma} - \dot{\sigma}^*)(\dot{\epsilon} - \dot{\epsilon}^*) dx = 0 \tag{3.87}$$

$$\int_0^L E^{\text{ep}} (\dot{\epsilon} - \dot{\epsilon}^*)^2 dx = 0 \tag{3.88}$$

which leads to the following **uniqueness conditions:**

$$\begin{aligned}
\text{elasticity} &\implies E^{\text{ep}} = E > 0 \implies \dot{\epsilon} = \dot{\epsilon}^* \text{ unique} \\
\text{hardening plasticity} &\implies E^{\text{ep}} > 0 \implies \dot{\epsilon} = \dot{\epsilon}^* \text{ unique} \\
\text{perfect plasticity} &\implies E^{\text{ep}} = 0 \implies \dot{\epsilon}\,,\ \dot{\epsilon}^* \text{ arbitrary , not unique}
\end{aligned} \tag{3.89}$$

We need another analysis for rate-independent softening plasticity (which is also non-unique).

For uniqueness and stability analysis of strain-softening, small strain elasto-plasticity theory, refer to Sandler and Wright [1976], Read and Hegemier [1984], Needleman [1988], Loret and Prevost [1991], Sluys and de Borst [1992]. Recall the balance of linear momentum in 1D for elastodynamics (without body force) as

$$\sigma_{,x} = \rho v_{,t} \tag{3.90}$$

where the axial velocity $v = u_{,t} = du/dt$. For isotropic hardening or softening, we have

$$\dot{\sigma} = E^{\text{ep}}\dot{\epsilon} = E^{\text{ep}}u_{,xt} = E^{\text{ep}}v_{,x} \tag{3.91}$$

Take the time derivative of the balance equation as,

$$\sigma_{,xt} = \rho v_{,tt} \tag{3.92}$$

$$E^{\text{ep}}v_{,xx} = \rho v_{,tt} \tag{3.93}$$

$$v_{,tt} - \frac{E^{\text{ep}}}{\rho}v_{,xx} = 0 \tag{3.94}$$

which is a form of the **wave equation** and is **hyperbolic**. We analyze characteristics of the partial differential equation (PDE) by introducing a new coordinate s (characteristic curve), such that,

$$\frac{d}{ds}\left(\frac{\partial v}{\partial t}\right) = \frac{\partial^2 v}{\partial t^2}\frac{dt}{ds} + \frac{\partial^2 v}{\partial t \partial x}\frac{dx}{ds} = 0 \tag{3.95}$$

$$\frac{d}{ds}\left(\frac{\partial v}{\partial x}\right) = \frac{\partial^2 v}{\partial t \partial x}\frac{dt}{ds} + \frac{\partial^2 v}{\partial x^2}\frac{dx}{ds} = 0 \tag{3.96}$$

The characteristic determinant of (3.94)-(3.96) is then

$$\begin{vmatrix} 1 & 0 & -\frac{E^{\text{ep}}}{\rho} \\ \frac{dt}{ds} & \frac{dx}{ds} & 0 \\ 0 & \frac{dt}{ds} & \frac{dx}{ds} \end{vmatrix} = \left(\frac{dx}{ds}\right)^2 - \frac{E^{\text{ep}}}{\rho}\left(\frac{dt}{ds}\right)^2 = 0 \tag{3.97}$$

where the characteristics are $\frac{dx}{dt} = \pm\sqrt{\frac{E^{\text{ep}}}{\rho}}$, which are the physical wave speeds. Consider the following three cases:

(a) <u>hardening plasticity</u> ($H^\kappa > 0$): $E^{\text{ep}} > 0 \implies$ wave speeds are real, and PDE is well-posed.

(b) <u>perfect plasticity</u> ($H^\kappa = 0$): $E^{\text{ep}} = 0 \implies$ wave speeds $= 0$, and PDE trans-

forms from hyperbolic to parabolic; ill-posed because initial disturbances cannot propagate through the body.

(c) softening plasticity ($H^\kappa < 0$): $E^{\rm ep} < 0 \implies$ imaginary wave speeds, and PDE transforms from hyperbolic to elliptic; ill-posed because initial disturbances cannot propagate through the body.

Rate-dependent plasticity (viscoplasticity) 'regularizes' the PDEs for softening plasticity such that the governing equation is well-posed (we will discuss in Sect.3.7).

3.4 Numerical Integration in Time of 1D Elastoplasticity

Refer to Simo and Hughes [1998]. We integrate in time the stress rate, evolution equations, and consistency condition, written together as,

$$\dot{\sigma} = E\dot{\epsilon}^{\rm e} = E(\dot{\epsilon} - \dot{\epsilon}^{\rm p}) = E\left(\dot{\epsilon} - \dot{\gamma}\frac{\partial g}{\partial \sigma}\right),\ \frac{\partial g}{\partial \sigma} = \text{sign}(\sigma - \alpha) \tag{3.98}$$

$$\dot{\kappa} = H^\kappa \dot{\gamma} \tag{3.99}$$

$$\dot{\alpha} = H^\alpha \text{sign}(\sigma - \alpha)\dot{\gamma} \tag{3.100}$$

$$\dot{\gamma}\dot{f} = 0 \tag{3.101}$$

There are 4 first-order ODEs, and 4 unknowns $(\sigma, \kappa, \alpha, \gamma)$. We use Backward Euler integration (implicit, first order accurate), which can be shown to be equivalent to the "return mapping algorithm" for certain constitutive models. Consider an example ("f" is a generic

function):

$$\dot{y} = f(y,t)\,, \quad y(0) = y_0 \tag{3.102}$$

$$\int_{t_n}^{t_{n+1}} \dot{y}dt = \int_{t_n}^{t_{n+1}} f(y,t)dt \tag{3.103}$$

$$y_{n+1} - y_n = \Delta t f(y_{n+1}, t_{n+1}) \tag{3.104}$$

$$y_{n+1} = y_n + \Delta t f(y_{n+1}, t_{n+1}) \tag{3.105}$$

Now, apply Backward Euler to our 4 ODEs as follows

$$\begin{aligned}
\sigma_{n+1} &= \sigma_n + E\left(\Delta\epsilon - \Delta\gamma\,\mathrm{sign}(\sigma_{n+1} - \alpha_{n+1})\right) \\
&\quad \Delta\epsilon = \epsilon_{n+1} - \epsilon_n \\
&\quad \Delta\gamma = \Delta t\dot{\gamma}_{n+1} = \gamma_{n+1} - \gamma_n \\
\sigma_{n+1} &= \sigma^{\mathrm{tr}}_{n+1} - E\Delta\gamma\,\mathrm{sign}(\sigma_{n+1} - \alpha_{n+1}) \qquad (3.106) \\
&\quad \sigma^{\mathrm{tr}}_{n+1} = \sigma_n + E\Delta\epsilon
\end{aligned}$$

$$\kappa_{n+1} = \kappa_n + H^{\kappa}\Delta\gamma \tag{3.107}$$

$$\alpha_{n+1} = \alpha_n + H^{\alpha}\Delta\gamma\,\mathrm{sign}(\sigma_{n+1} - \alpha_{n+1}) \tag{3.108}$$

$$\dot{\gamma}_{n+1}f_{n+1} - \dot{\gamma}_n f_n = 0 \Longrightarrow \dot{\gamma}_{n+1}f_{n+1} = 0 \Longrightarrow f_{n+1} = 0 \tag{3.109}$$

where $\sigma^{\mathrm{tr}}_{n+1}$ is the trial stress, and if there is elastoplastic loading at times t_n and t_{n+1} then $\dot{\gamma}_n > 0$, $f_n = 0$, $\dot{\gamma}_{n+1} > 0$, $f_{n+1} = 0$, else if elastic at time t_n and elastoplastic at time t_{n+1}, then $\dot{\gamma}_n = 0$, $f_n < 0$, $\dot{\gamma}_{n+1} > 0$, $f_{n+1} = 0$. Note that to reach the integrated form in Eq.(3.109), we apply the chain rule (with $u = \dot{\gamma}$, $v = f$, $a = t_n$, $b = t_{n+1}$) and Backward

Euler as follows:

$$\begin{aligned}
\frac{d(uv)}{dt} &= \frac{du}{dt}v + u\frac{dv}{dt} \\
\int_b^a \frac{d(uv)}{dt}dt &= \int_b^a \frac{du}{dt}v dt + \int_b^a u\frac{dv}{dt}dt \\
(\dot{\gamma}f)|_{t_n}^{t_{n+1}} &= \Delta t \frac{d\dot{\gamma}_{n+1}}{dt} f_{n+1} + \int_{t_n}^{t_{n+1}} \underbrace{\dot{\gamma}\dot{f}}_{=0} dt \\
\dot{\gamma}_{n+1}f_{n+1} - \dot{\gamma}_n f_n &= 0
\end{aligned}$$

where we used the consistency condition $\dot{\gamma}\dot{f} = 0$, and for a plastic state $f_{n+1} = 0$ or an elastic state $\dot{\gamma}_{n+1} = 0$.

Because these equations are linear, we may substitute the 3 evolution equations into $f_{n+1} = 0$ to solve for $\Delta\gamma$ as follows,

$$\begin{aligned}
f_{n+1} &= |\sigma_{n+1} - \alpha_{n+1}| - \kappa_{n+1} = 0 \qquad (3.110) \\
&\Longrightarrow \operatorname{sign}(\sigma_{n+1} - \alpha_{n+1}) \left[\sigma_{n+1}^{\mathrm{tr}} - E\Delta\gamma \operatorname{sign}(\sigma_{n+1} - \alpha_{n+1}) - \alpha_n \right. \\
&\qquad \left. - H^\alpha \Delta\gamma \operatorname{sign}(\sigma_{n+1} - \alpha_{n+1})\right] - \kappa_n - H^\kappa \Delta\gamma = 0 \\
&\Longrightarrow \operatorname{sign}(\sigma_{n+1} - \alpha_{n+1})[\sigma_{n+1}^{\mathrm{tr}} - \alpha_n] - \Delta\gamma(E + H^\kappa + H^\alpha) - \kappa_n = 0
\end{aligned}$$

We can show that $\operatorname{sign}(\sigma_{n+1} - \alpha_{n+1}) = \operatorname{sign}(\sigma_{n+1}^{\mathrm{tr}} - \alpha_n)$. [§] For example, assume perfect

[§]The "radial return" approximation would assume $\operatorname{sign}(\sigma_{n+1} - \alpha_{n+1}) \approx \operatorname{sign}(\sigma_{n+1}^{\mathrm{tr}} - \alpha_n)$.

plasticity for α, $H^\alpha = 0$, such that,

$$\begin{aligned}
\sigma_{n+1} - \alpha_{n+1} &= \sigma^{\text{tr}}_{n+1} - E\Delta\gamma\,\text{sign}(\sigma_{n+1} - \alpha_{n+1}) - \alpha_n \\
&= (\sigma^{\text{tr}}_{n+1} - \alpha_n) - E\Delta\gamma\,\text{sign}(\sigma_{n+1} - \alpha_{n+1}) \\
|\sigma_{n+1} - \alpha_{n+1}| &= \text{sign}(\sigma_{n+1} - \alpha_{n+1})(\sigma^{\text{tr}}_{n+1} - \alpha_n) - E\Delta\gamma \\
\underbrace{|\sigma_{n+1} - \alpha_{n+1}|}_{>0} &= \underbrace{\text{sign}(\sigma_{n+1} - \alpha_{n+1})\text{sign}(\sigma^{\text{tr}}_{n+1} - \alpha_n)}_{\text{must be } >0}\underbrace{|\sigma^{\text{tr}}_{n+1} - \alpha_n|}_{\geq 0} - \underbrace{E\Delta\gamma}_{>0} \\
&\quad \Longrightarrow \text{sign}(\sigma_{n+1} - \alpha_{n+1}) = \text{sign}(\sigma^{\text{tr}}_{n+1} - \alpha_n)
\end{aligned}$$

Then, we have the incremental plastic multiplier as,

$$\Delta\gamma = \frac{|\sigma^{\text{tr}}_{n+1} - \alpha_n| - \kappa_n}{E + H^\kappa + H^\alpha} = \frac{f^{\text{tr}}_{n+1}}{E + H^\kappa + H^\alpha} \tag{3.111}$$

Let us summarize the **return mapping algorithm:** given $\Delta\epsilon$ over a time step (from the nonlinear finite element solution), and σ_n, κ_n, α_n, γ_n from the past time step (you do not need to update $\gamma_{n+1} = \gamma_n + \Delta\gamma$, but it is useful for plotting an effective plastic strain magnitude), we follow these steps

1. **compute trial stress:** $\sigma^{\text{tr}}_{n+1} = \sigma_n + E\Delta\epsilon$

2. **check for yielding:** trial yield function $f^{\text{tr}}_{n+1} = |\sigma^{\text{tr}}_{n+1} - \alpha_n| - \kappa_n$

$$\begin{aligned}
\text{if} \quad f^{\text{tr}}_{n+1} > 0 \quad \text{plastic} \quad & \text{go to step 3} \\
\text{else} \quad f^{\text{tr}}_{n+1} < 0 \quad \text{elastic}: \quad & \sigma_{n+1} = \sigma^{\text{tr}}_{n+1} \\
& \alpha_{n+1} = \alpha_n \\
& \kappa_{n+1} = \kappa_n \\
& \gamma_{n+1} = \gamma_n
\end{aligned} \tag{3.112}$$

3. **compute** $\Delta\gamma = \frac{f^{\text{tr}}_{n+1}}{E+H^{\kappa}+H^{\alpha}}$, and **update**:

$$\begin{aligned}
\sigma_{n+1} &= \sigma^{\text{tr}}_{n+1} - E\Delta\gamma\,\text{sign}(\sigma^{\text{tr}}_{n+1} - \alpha_n) \\
\alpha_{n+1} &= \alpha_n + H^{\alpha}\Delta\gamma\,\text{sign}(\sigma^{\text{tr}}_{n+1} - \alpha_n) \\
\kappa_{n+1} &= \kappa_n + H^{\kappa}\Delta\gamma \\
\gamma_{n+1} &= \gamma_n + \Delta\gamma
\end{aligned} \tag{3.113}$$

We can visualize this algorithm in Fig.3.14 for the case of hardening. This strain increment $\Delta\epsilon$ loads the 1D elastoplastic bar from an elastic stress state at σ_n to an elastoplastic stress state at σ_{n+1}.

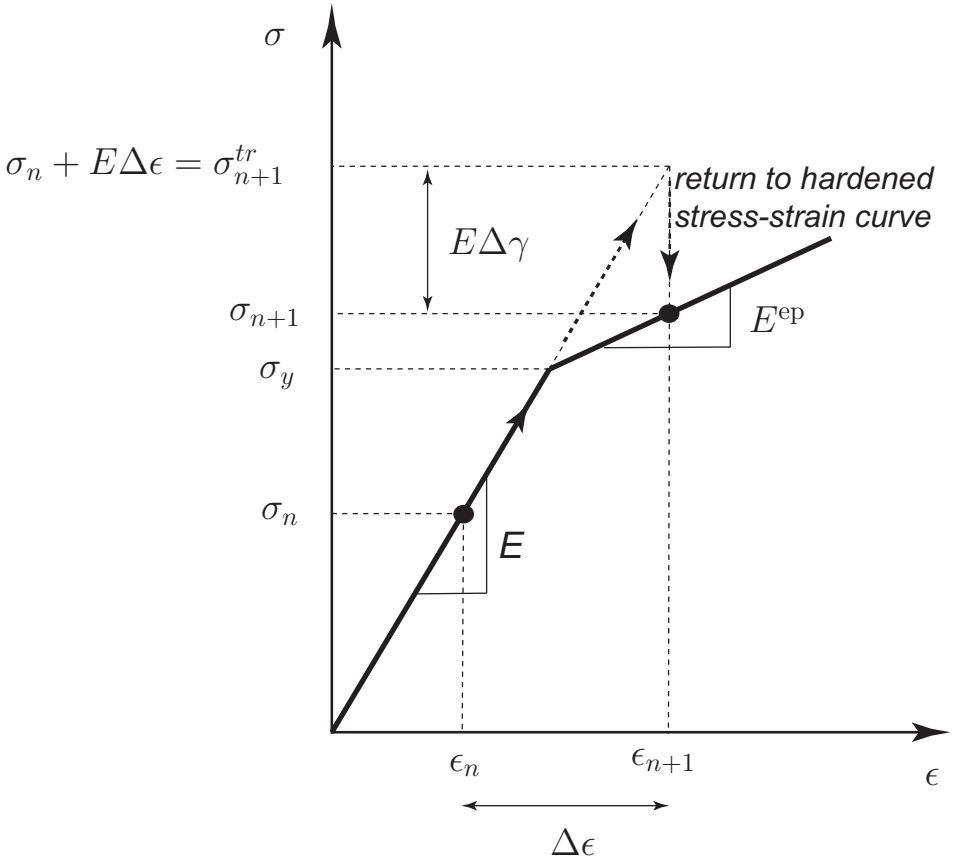

Figure 3.14. Illustration of return mapping algorithm (Backward Euler time integration) for hardening elastoplasticity.

3.5 Consistent Tangent for 1D Elastoplasticity

Recall the element level consistent tangent for the nonlinear axially-loaded bar as follows

$$\frac{\partial \boldsymbol{f}^{e,\mathrm{INT}}(\boldsymbol{d}^e)}{\partial \boldsymbol{d}^e} = \int_{-1}^{1} (\boldsymbol{B}^e)^T \boldsymbol{B}^e \frac{\partial \sigma^{h^e}}{\partial \epsilon^{h^e}} A j^e d\xi \tag{3.114}$$

Recall the stress evolution equation, and recognize that $\Delta\epsilon^{k+1} = \epsilon_{n+1}^{k+1} - \epsilon_n$, such that at a Gauss point in an element e, we have

$$\begin{aligned}
\sigma_{n+1}^{k+1} &= (\sigma_{n+1}^{k+1})^{\mathrm{tr}} - E\Delta\gamma^{k+1}\,\mathrm{sign}\left[(\sigma_{n+1}^{k+1})^{\mathrm{tr}} - \alpha_n\right] && (3.115)\\
(\sigma_{n+1}^{k+1})^{\mathrm{tr}} &= \sigma_n + E\Delta\epsilon^{k+1} && (3.116)\\
\Delta\gamma^{k+1} &= \frac{(f_{n+1}^{k+1})^{\mathrm{tr}}}{E + H^\kappa + H^\alpha} && (3.117)
\end{aligned}$$

or, without $(\bullet)_{n+1}^{k+1}$,

$$\begin{aligned}
\sigma &= \sigma^{\mathrm{tr}} - E\Delta\gamma\,\mathrm{sign}\left[\sigma^{\mathrm{tr}} - \alpha_n\right] && (3.118)\\
\sigma^{\mathrm{tr}} &= \sigma_n + E\Delta\epsilon && (3.119)\\
\Delta\gamma &= \frac{f^{\mathrm{tr}}}{E + H^\kappa + H^\alpha} && (3.120)
\end{aligned}$$

Then, the **material consistent tangent** may be calculated as

$$\begin{aligned}
\left(\frac{\partial \sigma^{h^e}}{\partial \epsilon^{h^e}}\right)_{n+1}^{k+1} &= \frac{\partial \sigma^{\mathrm{tr}}}{\partial \epsilon} - E\frac{\partial \Delta\gamma}{\partial \epsilon}\,\mathrm{sign}\left[\sigma^{\mathrm{tr}} - \alpha_n\right] && (3.121)\\
\frac{\partial \sigma^{\mathrm{tr}}}{\partial \epsilon} = E\ ,\ \frac{\partial \Delta\gamma}{\partial \epsilon} &= \frac{E\,\mathrm{sign}\left[\sigma^{\mathrm{tr}} - \alpha_n\right]}{E + H^\kappa + H^\alpha} && (3.122)\\
\left(\frac{\partial \sigma^{h^e}}{\partial \epsilon^{h^e}}\right)_{n+1}^{k+1} &= \frac{E(H^\kappa + H^\alpha)}{E + H^\kappa + H^\alpha} && (3.123)
\end{aligned}$$

Note: for simple 1D elastoplasticity, the continuum elastoplastic tangent E^{ep} and material consistent tangent $\left(\partial\sigma^{h^e}/\partial\epsilon^{h^e}\right)_{n+1}^{k+1}$ are the SAME. This will NOT be the case for higher

dimensional plasticity (2D and 3D).

3.6 Constitutive Equations for 1D Viscoelasticity

See Chp.10 of Simo and Hughes [1998]. 1D linear viscoelasticity will be similar to viscoplasticity (Sect.3.7), except that the relaxed solution is elastic as opposed to inviscid elastoplastic. We begin with the kinematics: $\epsilon^{\mathrm{e}} = \epsilon^{es} + \epsilon^{\mathrm{ve}}$ is the elastic strain for a standard linear solid, where the elastic-spring strain is ϵ^{es}, and the viscoelastic strain is ϵ^{ve} (Fig.3.15).

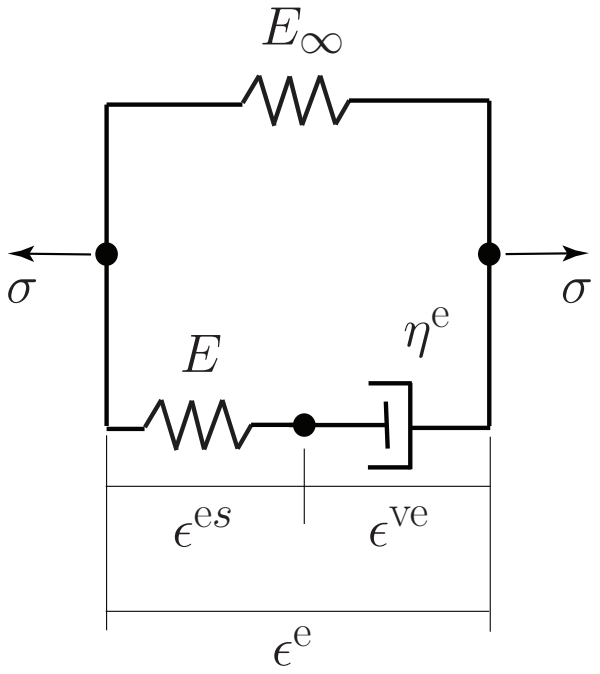

Figure 3.15. Illustration of 1D linear viscoelasticity.

The initial elastic modulus is $E_0 = E + E_\infty$, the long term elastic modulus is E_∞, and the elastic viscosity is η^{e} (Pa.s). The total axial stress is $\sigma = E_\infty \epsilon^{\mathrm{e}} + \sigma^{\mathrm{v}}$, where the viscous stress is $\sigma^{\mathrm{v}} = \eta^{\mathrm{e}} \dot{\epsilon}^{\mathrm{ve}} = E\epsilon^{es} = E(\epsilon^{\mathrm{e}} - \epsilon^{\mathrm{ve}})$, which leads to the ODE,

$$\dot{\epsilon}^{\mathrm{ve}} + \frac{1}{\tau^{\mathrm{e}}} \epsilon^{\mathrm{ve}} = \frac{1}{\tau^{\mathrm{e}}} \epsilon^{\mathrm{e}} \tag{3.124}$$

where the elastic relaxation time constant is $\tau^{\mathrm{e}} = \eta^{\mathrm{e}}/E$ (s). We solve analytically[¶] for $\epsilon^{\mathrm{ve}}(t)$ to solve for stress $\sigma(t)$. The solution of $\epsilon^{\mathrm{ve}}(t)$ can be obtained by using an integration factor $\exp(t/\tau^{\mathrm{e}})$ (check the derivation yourself), such that,

$$\begin{aligned}
\exp(t/\tau^{\mathrm{e}})\dot{\epsilon}^{\mathrm{ve}} + \frac{1}{\tau^{\mathrm{e}}}\exp(t/\tau^{\mathrm{e}})\epsilon^{\mathrm{ve}} &= \frac{1}{\tau^{\mathrm{e}}}\exp(t/\tau^{\mathrm{e}})\epsilon^{\mathrm{e}} && (3.125)\\
\int_{-\infty}^{t}\frac{d}{ds}\left[\exp(s/\tau^{\mathrm{e}})\epsilon^{\mathrm{ve}}(s)\right]ds &= \int_{-\infty}^{t}\frac{1}{\tau^{\mathrm{e}}}\exp(s/\tau^{\mathrm{e}})\epsilon^{\mathrm{e}}(s)ds && (3.126)\\
\exp(t/\tau^{\mathrm{e}})\epsilon^{\mathrm{ve}}(t) &= \frac{1}{\tau^{\mathrm{e}}}\int_{-\infty}^{t}\exp(s/\tau)\epsilon^{\mathrm{e}}(s)ds && (3.127)\\
\epsilon^{\mathrm{ve}}(t) &= \int_{-\infty}^{t}\frac{1}{\tau^{\mathrm{e}}}\exp((s-t)/\tau^{\mathrm{e}})\epsilon^{\mathrm{e}}(s)ds && (3.128)\\
\frac{d}{ds}\left[\exp((s-t)/\tau^{\mathrm{e}})\epsilon(s)\right] &= \frac{1}{\tau^{\mathrm{e}}}\exp((s-t)/\tau^{\mathrm{e}})\epsilon^{\mathrm{e}}(s) + \exp((s-t)/\tau^{\mathrm{e}})\dot{\epsilon}^{\mathrm{e}}(s)\\
\epsilon^{\mathrm{ve}}(t) &= \underbrace{\int_{-\infty}^{t}\frac{d}{ds}\left[\exp((s-t)/\tau^{\mathrm{e}})\epsilon^{\mathrm{e}}(s)\right]ds}_{\epsilon^{\mathrm{e}}(t)}\\
&\quad - \int_{-\infty}^{t}\exp((s-t)/\tau^{\mathrm{e}})\dot{\epsilon}^{\mathrm{e}}(s)ds && (3.129)
\end{aligned}$$

Then, the stress becomes

$$\begin{aligned}
\sigma(t) &= E_{\infty}\epsilon^{\mathrm{e}}(t) + E\int_{-\infty}^{t}\exp((s-t)/\tau^{\mathrm{e}})\dot{\epsilon}^{\mathrm{e}}(s)ds && (3.130)\\
&= \int_{-\infty}^{t}G(t-s)\dot{\epsilon}^{\mathrm{e}}(s)ds && (3.131)\\
&\quad G(t-s) = E_{\infty} + E\exp(-(t-s)/\tau^{\mathrm{e}}) && (3.132)
\end{aligned}$$

where $G(t-s)$ is the **relaxation function**. Note in this formulation there is no plastic strain ($\epsilon^{\mathrm{p}} = 0$), such that the total strain is the elastic strain, $\epsilon = \epsilon^{\mathrm{e}} + \epsilon^{\mathrm{p}} = \epsilon^{\mathrm{e}}$. Analytically, consider two loading conditions (numerically, we can consider more general loading conditions):

(i) **stress relaxation**: a step function for the total strain $\epsilon(t) = \epsilon_0 H(t)$ is introduced, such that $\dot{\epsilon}(t) = \epsilon_0\delta(t)$ (Fig.3.16), where $H(t)$ is the Heaviside function, and $\delta(t)$ is the

[¶]In Sect.3.6.1 we will solve these equations numerically.

Dirac-Delta function. We see that,

$$\sigma(t) = \int_{-\infty}^{t} G(t-s)\epsilon_0\delta(s)ds = \epsilon_0 G(t) \tag{3.133}$$

$$G(t) = E_\infty + E\exp(-t/\tau^{\mathrm{e}}) \tag{3.134}$$

We could also represent a generalized relaxation model with multiple spring-dashpots in parallel to provide a **Prony series** for $G(t)$ [Simo and Hughes, 1998].

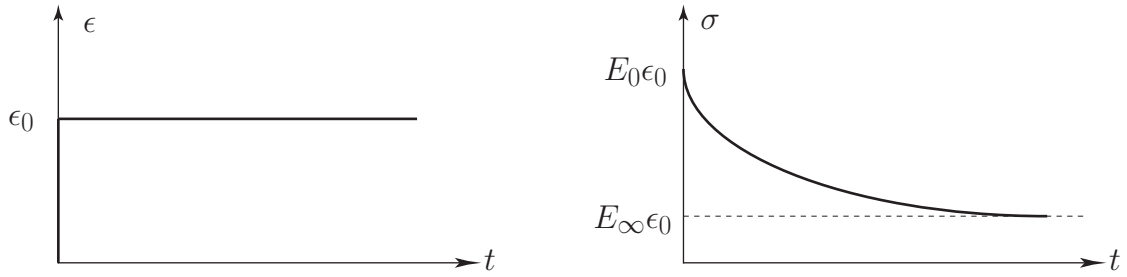

Figure 3.16. Illustration of stress relaxation under constant applied total strain ϵ_0 for 1D linear viscoelasticity.

(ii) **creep**: Alternatively, we can write the solution in terms of a **creep function** $J(t)$ (derive yourself), such that,

$$\epsilon(t) = \int_{-\infty}^{t} J(t-s)\dot{\sigma}(s)ds \tag{3.135}$$

$$J(t) = \frac{1}{E_\infty}\left[1 - \frac{E}{E_0}\exp\left(\frac{-E_\infty t}{E_0\tau^{\mathrm{e}}}\right)\right] \tag{3.136}$$

For example, consider a **creep strain**, where there is a step function for total stress $\sigma(t) = \sigma_0 H(t)$, $\dot{\sigma}(t) = \sigma_0\delta(t)$ (Fig.3.17), such that,

$$\epsilon(t) = \int_{-\infty}^{t} J(t-s)\sigma_0\,\delta(s)ds = \sigma_0 J(t) \tag{3.137}$$

Oftentimes, for viscoelastic response, you are provided data in the **frequency domain**,

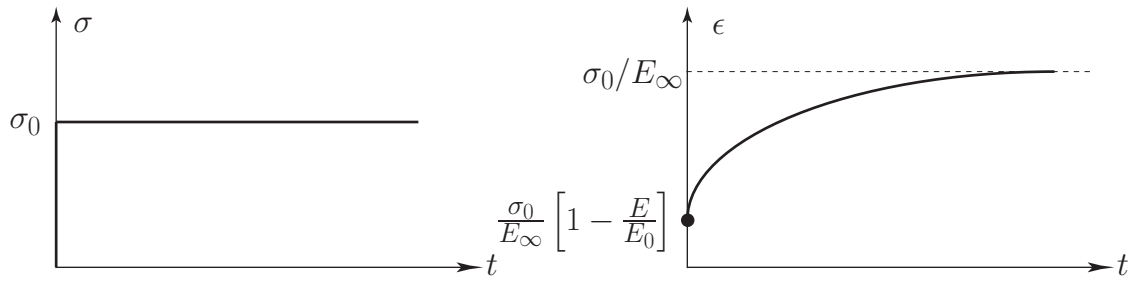

Figure 3.17. Illustration of strain creep under constant applied stress σ_0 for 1D linear viscoelasticity.

thus we must transform the equations from time to frequency domain. Consider an applied harmonic total strain, such as,

$$\epsilon(t) = \epsilon_0 \exp(i\omega t) \ , \ i = \sqrt{-1} \tag{3.138}$$

$$\dot{\epsilon}(t) = \epsilon_0 i\omega \exp(i\omega t) \tag{3.139}$$

where ω is the frequency, and i is the imaginary number. Then, the stress becomes

$$\sigma(t) = E_\infty \epsilon_0 \exp(i\omega t) + E \int_{-\infty}^{t} \exp((s-t)/\tau^{\mathrm{e}}) \epsilon_0 i\omega \exp(i\omega s) ds \tag{3.140}$$

$$= G^*(\omega)\epsilon(t) \tag{3.141}$$

$$G^*(\omega) = G_s(\omega) + iG_l(\omega) \tag{3.142}$$

$$G_s(\omega) = E_\infty + \frac{E(\omega\tau^{\mathrm{e}})^2}{1+(\omega\tau^{\mathrm{e}})^2} \tag{3.143}$$

$$G_l(\omega) = \frac{E\omega\tau^{\mathrm{e}}}{1+(\omega\tau^{\mathrm{e}})^2} \tag{3.144}$$

$$\text{loss factor} = \frac{G_l}{G_s} \tag{3.145}$$

3.6.1 Numerical time integration of 1D viscoelasticity

enter here

3.7 Constitutive Equations for 1D Viscoplasticity

Refer to Simo and Hughes [1998] and Fig.3.18 for the kinematics of a 1D rheological elasto-plastic model: $\epsilon = \epsilon^{\mathrm{e}} + \epsilon^{\mathrm{vp}}$, where $\epsilon = du/dx$ is the total strain, ϵ^{e} is the elastic strain, ϵ^{vp} is the **viscoplastic strain**, and η^{p} is the plastic viscosity (Pa.s).

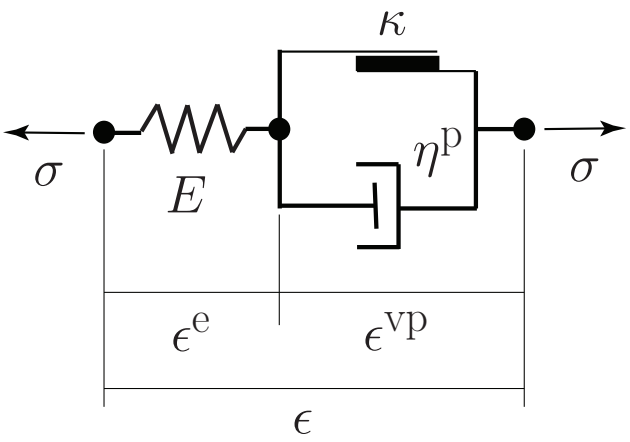

Figure 3.18. One degree of freedom illustration of viscoplasticity, where the total strain is additively decomposed into elastic and viscoplastic parts as $\epsilon = \epsilon^{\mathrm{e}} + \epsilon^{\mathrm{vp}}$. Viscosity η^{p} introduces the viscous effect into the plasticity, where κ is the stress-like ISV.

The Helmholtz free energy function per unit mass is the same as for rate-independent (inviscid) elastoplasticity: $\rho\psi(\epsilon^{\mathrm{e}}, \zeta) = \frac{1}{2}E(\epsilon^{\mathrm{e}})^2 + \frac{1}{2}H\zeta^2$, such that $\dot{\sigma} = E\dot{\epsilon}^{\mathrm{e}} = E(\dot{\epsilon} - \dot{\epsilon}^{\mathrm{vp}})$ and $\dot{\kappa} = H\dot{\zeta}$. The yield function is now replaced by a **loading function**: $f(\sigma, \kappa) = |\sigma| - \kappa$. The evolution equation for viscoplastic strain is then written as,

$$\begin{aligned} &\text{if} \quad f < 0 \quad \dot{\epsilon}^{\mathrm{vp}} = 0 \\ &\text{if} \quad f \geq 0 \quad \dot{\epsilon}^{\mathrm{vp}} = \tfrac{f}{\eta^{\mathrm{p}}}\mathrm{sign}(\sigma) \end{aligned} \tag{3.146}$$

We define an "extra stress" σ_{extra} that is the portion of the stress above the 'frictional' plastic-mechanism-governing ISV κ, that acts on the dashpot: $\sigma_{\mathrm{extra}} = \eta^{\mathrm{p}}\dot{\epsilon}^{\mathrm{vp}}$ (check units). For example, consider the 1D stress line for $f > 0$ in Fig.3.19.

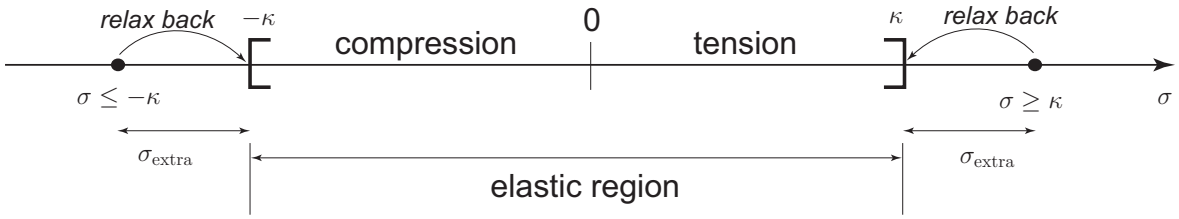

Figure 3.19. Illustration of viscoplasticity, with relaxation of stress state from σ_{extra} to inviscid yield surface at $\sigma = \kappa$.

We see that

$$\left.\begin{array}{ll} \sigma > \kappa, & \sigma_{\text{extra}} = \sigma - \kappa \\ \sigma \leq -\kappa, & \sigma_{\text{extra}} = \sigma - (-\kappa) \end{array}\right\} = (|\sigma| - \kappa)\text{sign}(\sigma) = f\text{sign}(\sigma) \tag{3.147}$$

and thus $\sigma_{\text{extra}} = f\text{sign}(\sigma) = \eta^{\text{p}}\dot{\epsilon}^{\text{vp}} \Longrightarrow \dot{\epsilon}^{\text{vp}} = \frac{f}{\eta^{\text{p}}}\text{sign}(\sigma)$. Generalizing for all stress states (elastic, and elasto-visco-plastic), we have

$$\dot{\epsilon}^{vp} = \frac{\langle f \rangle}{\eta}\text{sign}(\sigma) \tag{3.148}$$

$$\langle f \rangle = (f + |f|)/2 \tag{3.149}$$

For hardening, $\dot{\kappa} = H\dot{\zeta} = H|\dot{\epsilon}^{\text{vp}}| = H\langle f \rangle / \eta^{\text{p}}$, where $\langle \bullet \rangle$ is the Macaulay bracket. This is called the **Perzyna-type viscoplasticity** model.

Alternatively, introduce a relaxation time constant $\tau = \eta^{\text{p}}/E$, where

$$\begin{aligned} \dot{\epsilon}^{\text{vp}} &= \frac{1}{\tau^{\text{p}}E}(|\sigma| - \kappa)\text{sign}(\sigma) \\ &= \frac{1}{\tau^{\text{p}}E}(\sigma - \kappa\,\text{sign}(\sigma)) \end{aligned} \tag{3.150}$$

Recall that,

$$\begin{aligned} \dot{\sigma} = E\dot{\epsilon}^{\mathrm{e}} &= E(\dot{\epsilon} - \dot{\epsilon}^{\mathrm{vp}}) && (3.151) \\ &= E\left(\dot{\epsilon} - \frac{1}{\tau^{\mathrm{p}}E}(\sigma - \kappa\,\mathrm{sign}(\sigma))\right) \\ \dot{\sigma} + \frac{1}{\tau^{\mathrm{p}}}\sigma &= E\dot{\epsilon} + \frac{1}{\tau^{\mathrm{p}}}\kappa\,\mathrm{sign}(\sigma) && (3.152) \end{aligned}$$

For hardening (considering plastic loading), we have

$$\begin{aligned} \dot{\kappa} = \frac{H}{\tau^{\mathrm{p}}E}\langle f\rangle &= -\frac{H}{\tau^{\mathrm{p}}E}(\kappa - |\sigma|) && (3.153) \\ \dot{\kappa} + \frac{H}{\tau^{\mathrm{p}}E}\kappa &= \frac{H}{\tau^{\mathrm{p}}E}|\sigma| && (3.154) \end{aligned}$$

This is the **Duvaut-Lions form of viscoplasticity**. Furthermore, consider that as $t/\tau^{\mathrm{p}} \to \infty$ ($t \to \infty$ or $\tau^{\mathrm{p}} \to 0$), the viscoplastic solution approaches the rate-independent (inviscid) solution ($f = 0$ for plastic loading), such that we can rewrite the Duvaut-Lions form as

$$\begin{aligned} \dot{\sigma} + \frac{1}{\tau^{\mathrm{p}}}\sigma &= E\dot{\epsilon} + \frac{1}{\tau^{\mathrm{p}}}\sigma_{\mathrm{inv}} && (3.155) \\ \dot{\kappa} + \frac{H}{\tau^{\mathrm{p}}E}\kappa &= \frac{H}{\tau^{\mathrm{p}}E}\kappa_{\mathrm{inv}} && (3.156) \end{aligned}$$

where σ_{inv} and κ_{inv} are the inviscid solution. We note the following about the **Duvaut-Lions form of viscoplasticity**: Kuhn-Tucker conditions (there are none); consistency condition (there is none); continuum elastoplastic tangent (none, because no consistency condition); isotropic/kinematic hardening (we will stick with isotropic, but can generalize for combined isotropic-kinematic hardening); convexity of yield surface (there is no yield surface); and for a **uniqueness and stability analysis**, consider the numerically integrated form using

Backward Euler as

$$\frac{\sigma_{n+1}-\sigma_n}{\Delta t}+\frac{1}{\tau^{\mathrm{p}}}\sigma_{n+1} = E\frac{\Delta\epsilon}{\Delta t}+\frac{1}{\tau^{\mathrm{p}}}\sigma_{\mathrm{inv}} \tag{3.157}$$

$$\sigma_{n+1}\left(1+\frac{\Delta t}{\tau^{\mathrm{p}}}\right) = \underbrace{\sigma_n+E\Delta\epsilon}_{\sigma^{\mathrm{tr}}_{n+1}}+\frac{\Delta t}{\tau^{\mathrm{p}}}\sigma_{\mathrm{inv}} \tag{3.158}$$

We analyze the consistent tangent as,

$$\frac{\partial\sigma_{n+1}}{\partial\epsilon_{n+1}} = \frac{1}{1+\frac{\Delta t}{\tau^{\mathrm{p}}}}\left(E+\frac{\Delta t}{\tau^{\mathrm{p}}}\frac{EH^{\kappa}}{E+H^{\kappa}}\right) \tag{3.159}$$

$$\frac{\partial\sigma_{n+1}}{\partial\epsilon_{n+1}} = \frac{E}{1+\frac{\Delta t}{\tau^{\mathrm{p}}}}\left(1+\frac{\Delta t}{\tau^{\mathrm{p}}}\frac{H^{\kappa}}{E+H^{\kappa}}\right) \tag{3.160}$$

$$1+\frac{\Delta t}{\tau^{\mathrm{p}}}\frac{H^{\kappa}}{E+H^{\kappa}} = 1+\Delta t\frac{E^{\mathrm{ep}}}{\eta^{\mathrm{p}}}>0 \text{ for } \frac{\partial\sigma_{n+1}}{\partial\epsilon_{n+1}}>0 \tag{3.161}$$

$$\Delta t\frac{E^{\mathrm{ep}}}{\eta^{\mathrm{p}}}>-1 \tag{3.162}$$

$$0<\Delta t<-\frac{\eta^{\mathrm{p}}}{E^{\mathrm{ep}}} \text{ if } E^{\mathrm{ep}}<0 \tag{3.163}$$

where $E^{\mathrm{ep}} = EH^{\kappa}/(E+H^{\kappa})$ is the consistent (and continuum) elasto-plastic tangent for 1D inviscid isotropic hardening elastoplasticity. Thus, if we choose a time increment small enough, the numerical solution will remain stable for softening viscoplasticity. **Note:** viscous-regularization is just one approach to regularization of a strain-softening inviscid plasticity model. Other approaches include nonlocal plasticity (e.g., [Bazant and Jirasek, 2003]), strain-gradient plasticity (e.g., [R. de Borst and H. Mühlhaus, 1992]), and discrete fracture (e.g., cohesive zone models [Ortiz and Pandolfi, 1999]), etc.

3.8 Constitutive Equations for 1D Elastodamage

need content

3.9 Constitutive Equations for 1D Thermoelasticity

need content

This page intentionally left blank.

Chapter 4

3D Isochoric (Deviatoric) Rate-Independent Plasticity at Small Strain

Much of the material in this chapter is taken from Simo and Hughes [1998], Borja [2013]. This chapter will primarily focus on steps 1-5 of a typical modeling procedure if you are developing your own elastoplastic constitutive model (refer also to Ch.3 for more discussion in terms of 1D elastoplasticity). These steps are outlined as follows (same steps as for 1D elastoplasticity):

1. **kinematics:** We assume small strains, such that an additive decomposition of strain tensor $\boldsymbol{\epsilon}$ is appropriate:

$$
\begin{aligned}
&\boldsymbol{\epsilon} = \boldsymbol{\epsilon}^{\mathrm{e}} + \boldsymbol{\epsilon}^{\mathrm{p}} \\
\text{total strain} \quad &\boldsymbol{\epsilon} = \tfrac{1}{2}\left[\frac{\partial \boldsymbol{u}}{\partial \boldsymbol{x}} + \left(\frac{\partial \boldsymbol{u}}{\partial \boldsymbol{x}}\right)^T\right] = \begin{bmatrix} \epsilon_{11} & \epsilon_{12} & \epsilon_{13} \\ \epsilon_{12} & \epsilon_{22} & \epsilon_{23} \\ \epsilon_{13} & \epsilon_{23} & \epsilon_{33} \end{bmatrix} \\
&\epsilon_{ij} = \tfrac{1}{2}\left[u_{i,j} + u_{j,i}\right] \\
\text{elastic strain} \quad &\boldsymbol{\epsilon}^{\mathrm{e}} \text{ (recoverable deformation)} \\
\text{plastic strain} \quad &\boldsymbol{\epsilon}^{\mathrm{p}} \text{ (permanent deformation)}
\end{aligned}
\tag{4.1}
$$

   where $\dot{\boldsymbol{\epsilon}}^{\mathrm{p}}$ will be defined through a **flow rule**, from which $\boldsymbol{\epsilon}^{\mathrm{p}}$ can be integrated. Then, given the total strain tensor $\boldsymbol{\epsilon}$ from the finite element solution, we can calculate the elastic strain as $\boldsymbol{\epsilon}^{\mathrm{e}} = \boldsymbol{\epsilon} - \boldsymbol{\epsilon}^{\mathrm{p}}$.

2. **balance equations and thermodynamics:** We will revisit the balance equations and thermodynamics for a 3D solid continuum body at small strain: (1) balance of mass (use for fluid flow, mixture theory, etc.; not needed in this section), (2) balance of linear momentum (solve for displacement), (3) balance of angular momentum (leads to symmetric stress for non-polar media), (4) balance of energy (first law of thermodynamics; solve for temperature), (5) second law of thermodynamics (constrains elastoplasticity formulation; requires non-negative energy dissipation). We focus on (4) and (5) for constitutive modeling purposes in this Chapter. For further information, refer to continuum mechanics textbooks, such as Malvern [1969], Holzapfel [2000].

3. **constitutive equations:** We need constitutive equations for stress (e.g., linear isotropic elasticity $\boldsymbol{\sigma} = \boldsymbol{c}^{\mathrm{e}} : \boldsymbol{\epsilon}^{\mathrm{e}}$, or $\sigma_{ij} = c^{\mathrm{e}}_{ijkl}\epsilon^{\mathrm{e}}_{kl}$), where c^{e}_{ijkl} is the 4th order elastic modulus tensor, a yield function $f(\boldsymbol{\sigma}, \boldsymbol{q}^{\zeta}) = 0$ and plastic potential function $g(\boldsymbol{\sigma}, \boldsymbol{q}^{\zeta})$, internal state variable (ISV) evolution equations (e.g., hardening, perfect, or softening plasticity)

for a stress-like ISV vector $\boldsymbol{q}^\zeta$. As for 1D elastoplasticity, the ISVs attempt to represent phenomenologically the evolution of the underlying microstructure as it relates to the experimentally-observed behavior (e.g., motion and piling up of dislocations at obstacles in metals leading to hardening; compaction of pore space in sand leading to reduced volume and increased shear strength, hardening; shear-banding leading to post-peak softening and failure, ...).

4. **numerical integration in time:** Constitutive equations are expressed in rate form (e.g., $\dot{\boldsymbol{\sigma}} = D\boldsymbol{\sigma}/Dt$) to account for evolution of the solid material over time due to deformation and load history. We must integrate numerically in time before we can implement these equations in a nonlinear FE program. In rate form, the stress equation reads, assuming constant elastic modulus tensor $\boldsymbol{c}^e$,

$$\begin{aligned} \dot{\boldsymbol{\sigma}} &= \boldsymbol{c}^{\mathrm{e}} : \dot{\boldsymbol{\epsilon}}^{\mathrm{e}} \\ \dot{\boldsymbol{\epsilon}}^{\mathrm{e}} &= \dot{\boldsymbol{\epsilon}} - \dot{\boldsymbol{\epsilon}}^{\mathrm{p}} \end{aligned} \tag{4.2}$$

where $\dot{\boldsymbol{\epsilon}}$ is the prescribed strain rate tensor by the FE program, leading to what we call a "strain-driven" problem $\dot{\boldsymbol{\epsilon}} \approx \Delta\boldsymbol{\epsilon}/\Delta t$, where Δt is the time increment. The evolution equations (rate form of constitutive equations) are usually first order ordinary differential equations (ODEs) in time t, thus we may use a generalized trapezoidal rule to integrate in time (e.g., Backward Euler, Forward Euler, trapezoidal rule).

5. **FE implementation, consistent tangent:** The 3D stress tensor σ_{ij} will be a nonlinear function of the element displacement: $\boldsymbol{\sigma}(\boldsymbol{d}^e)$, where e denotes element, NOT elastic. Then, the formulation of the consistent tangent for Newton-Raphson solution will follow as,

$$\frac{\partial \boldsymbol{f}^{e,\mathrm{INT}}(\boldsymbol{d}^e)}{\partial \boldsymbol{d}^e} = \dots \tag{4.3}$$

We will show details after we present the 3D elastoplasticity theory, time integration,

and local material consistent tangent $\partial \boldsymbol{\sigma}^{h^e} / \partial \boldsymbol{\epsilon}^{h^e}$ at a Gauss point in element e.

4.1 Balance Equations and Thermodynamics

The **balance of linear momentum** in 3D for a single phase solid material is

$$\rho \ddot{u}_i = \sigma_{ij,j} + \rho b_i \tag{4.4}$$

where the divergence of the stress tensor is $\sigma_{ij,j} = \partial \sigma_{ij} / \partial x_j$, ρ is the mass density (kg/m^3), $\ddot{u}_i$ is the acceleration vector (m/s^2), σ_{ij} is the symmetric stress tensor (Pa), b_i is the body force vector per unit mass (N/kg = m/s^2). The **balance of angular momentum** for a non-polar solid leads to symmetry of the stress tensor as $\sigma_{ij} = \sigma_{ji}$.

Using the result from 1D elastoplasticity discussion in Ch.3, we may write the **balance of energy** pointwise for a body $\mathcal{B}$ in Fig.3.3 as

$$\rho \dot{e} = \sigma_{ij} \dot{\epsilon}_{ij} + \rho r - q_{i,i} \tag{4.5}$$

Likewise, for the second law of thermodynamics in 3D, we may write (from the result in 1D elastoplasticity)

$$\rho \theta \dot{\eta} \;\; \geq \;\; \rho r - q_{i,i} + \frac{1}{\theta} q_i \theta_{,i} \tag{4.6}$$

Recall we assume the existence of a Helmholtz free energy function per unit mass ψ (important for non-isothermal problems) as follows,

$$\psi = e - \eta \theta \tag{4.7}$$

After substituting for ψ, and $\rho\dot{e}$ from the first law leads to the Clausius-Duhem inequality (check the derivation yourself)

$$\sigma_{ij}\dot{\epsilon}_{ij} - \rho\dot{\psi} - \rho\eta\dot{\theta} - \frac{1}{\theta}q_i\theta_{,i} \geq 0 \tag{4.8}$$

For isothermal ($\dot{\theta} = 0$) and homogeneous temperature ($\theta_{,i} = 0$) problems, the Clausius-Duhem inequality is written as

$$\sigma_{ij}\dot{\epsilon}_{ij} - \rho\dot{\psi} \geq 0 \tag{4.9}$$

4.2 Constitutive Equations for 3D Elastoplasticity

We outline the topic coverage for 3D classical (inviscid, rate-independent) elastoplasticity as [Simo and Hughes, 1998, Anandarajah, 2010, Borja, 2013]

(i) Helmholtz free energy function

(ii) yield and plastic potential functions

(iii) evolution equations

(iv) Kuhn-Tucker optimality conditions

(v) consistency condition

(vi) continuum elastoplastic tangent

(vii) isotropic/kinematic hardening

(viii) convexity of yield surface

(ix) uniqueness (Hill's stability postulate, softening plasticity)

In more detail, we have

(i) **Helmholtz free energy function:** The Helmholtz free energy function ψ per unit mass is additively decomposed ("energy separable" processes, which is a constitutive assumption) into elastic e and plastic p parts as,

$$\rho\psi(\boldsymbol{\epsilon}^{\mathrm{e}}, \boldsymbol{\zeta}) \;\; = \;\; \rho\psi^{\mathrm{e}}(\boldsymbol{\epsilon}^{\mathrm{e}}) + \rho\psi^{\mathrm{p}}(\boldsymbol{\zeta}) \tag{4.10}$$

where $\boldsymbol{\epsilon}^{\mathrm{e}}$ is the elastic strain tensor, and $\boldsymbol{\zeta}$ is a strain-like ISV vector, not necessarily the plastic strain. Taking the material time derivative (refer to Sect.2.3 of Holzapfel [2000]), we have

$$\frac{D(\rho\psi)}{Dt} = \dot{\rho}\psi + \rho\dot{\psi} \tag{4.11}$$

where $\dot{\rho} \approx 0$ (conservation of mass) for a single phase solid material deformed at small strain. This will not be the case for multiphase materials treated by mixture theory (we will discuss later), and also for finite strain conditions. Then, we see that

$$\rho\dot{\psi} = \frac{D(\rho\psi)}{Dt} = \frac{\partial(\rho\psi)}{\partial\boldsymbol{\epsilon}^{\mathrm{e}}} : \dot{\boldsymbol{\epsilon}}^{\mathrm{e}} + \frac{\partial(\rho\psi)}{\partial\boldsymbol{\zeta}} \cdot \dot{\boldsymbol{\zeta}} \tag{4.12}$$

We substitute this into the Clausius-Duhem inequality and rearrange terms to obtain the following

$$\left(\boldsymbol{\sigma} - \frac{\partial(\rho\psi)}{\partial\boldsymbol{\epsilon}^{\mathrm{e}}}\right) : \dot{\boldsymbol{\epsilon}}^{\mathrm{e}} + \boldsymbol{\sigma} : \dot{\boldsymbol{\epsilon}}^{\mathrm{p}} - \frac{\partial(\rho\psi)}{\partial\boldsymbol{\zeta}} \cdot \dot{\boldsymbol{\zeta}} \geq 0 \tag{4.13}$$

Coleman and Noll [1963], Coleman and Gurtin [1967] argued that the elastic strain rate tensor $\dot{\boldsymbol{\epsilon}}^{\mathrm{e}}$ could be an independent process from the plastic strain rate tensor $\dot{\boldsymbol{\epsilon}}^{\mathrm{p}}$ and ISV rate vector $\dot{\boldsymbol{\zeta}}$. Thus for (4.13) to hold, we must have an equation for the stress $\boldsymbol{\sigma}$ as,

$$\boldsymbol{\sigma} - \frac{\partial(\rho\psi)}{\partial\boldsymbol{\epsilon}^{\mathrm{e}}} = \mathbf{0} \implies \boldsymbol{\sigma} = \frac{\partial(\rho\psi)}{\partial\boldsymbol{\epsilon}^{\mathrm{e}}} \tag{4.14}$$

If (4.14) holds, such that the stress tensor $\boldsymbol{\sigma}$ is derived from a Helmholtz free energy

function, then the constitutive model is said to be "hyperelastic." Also, a thermodynamically-conjugate stress-like ISV vector $\boldsymbol{q}^{\zeta}$ can be defined as

$$\boldsymbol{q}^{\zeta} := \frac{\partial(\rho\psi)}{\partial\boldsymbol{\zeta}} \tag{4.15}$$

(which is related to the isotropic stress-like ISV κ and backstress $\boldsymbol{\alpha}$) such that the **reduced dissipation inequality** $\mathcal{D}$ results as the difference between plastic power per unit volume (which when integrated over time leads to plastic work per unit volume) and rate of stored work of plastic ISV evolution as,

$$\mathcal{D} := \boldsymbol{\sigma} : \dot{\boldsymbol{\epsilon}}^{\mathrm{p}} - \boldsymbol{q}^{\zeta} \cdot \dot{\boldsymbol{\zeta}} \geq 0 \ , \ \sigma_{ij}\dot{\epsilon}^{\mathrm{p}}_{ij} - q^{\zeta}_{A}\dot{\zeta}_{A} \geq 0 \tag{4.16}$$

where $A = 1, \ldots,$ number of ISV components. We make a **constitutive assumption for the Helmholtz free energy function** ψ (per unit mass) that leads to linear isotropic elasticity and linear hardening/softening as

$$\rho\psi(\boldsymbol{\epsilon}^{\mathrm{e}}, \boldsymbol{\zeta}) = \frac{1}{2}\boldsymbol{\epsilon}^{\mathrm{e}} : \boldsymbol{c}^{\mathrm{e}} : \boldsymbol{\epsilon}^{\mathrm{e}} + \frac{1}{2}\boldsymbol{\zeta} \cdot \boldsymbol{H} \cdot \boldsymbol{\zeta} = \frac{1}{2}\epsilon^{\mathrm{e}}_{ij} c^{\mathrm{e}}_{ijkl} \epsilon^{\mathrm{e}}_{kl} + \frac{1}{2}\zeta_A H_{AB} \zeta_B \tag{4.17}$$

Then, we have

$$\boldsymbol{\sigma} = \frac{\partial(\rho\psi)}{\partial\boldsymbol{\epsilon}^{\mathrm{e}}} = \boldsymbol{c}^{\mathrm{e}} : \boldsymbol{\epsilon}^{\mathrm{e}} \tag{4.18}$$

$$\boldsymbol{c}^{\mathrm{e}} = \lambda \boldsymbol{1} \otimes \boldsymbol{1} + 2\mu \boldsymbol{I} \tag{4.19}$$

$$c^{\mathrm{e}}_{ijkl} = \lambda\delta_{ij}\delta_{kl} + \mu(\delta_{ik}\delta_{jl} + \delta_{il}\delta_{jk}) \tag{4.20}$$

$$(\boldsymbol{1})_{ij} = \delta_{ij} \ , \ (\boldsymbol{I})_{ijkl} = \frac{1}{2}(\delta_{ik}\delta_{jl} + \delta_{il}\delta_{jk}) \tag{4.21}$$

$$\boldsymbol{q}^{\zeta} = \frac{\partial(\rho\psi)}{\partial\boldsymbol{\zeta}} = \boldsymbol{H} \cdot \boldsymbol{\zeta} \tag{4.22}$$

where $\boldsymbol{c}^{\mathrm{e}}$ is the isotropic elastic modulus, λ and μ are the Lamé parameters, $\boldsymbol{1}$ is the 2nd order identity tensor, $\boldsymbol{I}$ the 4th order identity tensor, δ_{ij} the Kronecker-delta operator,

and $\boldsymbol{H}$ is the hardening modulus matrix. Assuming constant moduli, we express the stress equations in rate form as

$$\dot{\boldsymbol{\sigma}} = \boldsymbol{c}^{\mathrm{e}} : \dot{\boldsymbol{\epsilon}}^{\mathrm{e}} = \boldsymbol{c}^{\mathrm{e}} : (\dot{\boldsymbol{\epsilon}} - \dot{\boldsymbol{\epsilon}}^{\mathrm{p}}) \tag{4.23}$$

$$\dot{\boldsymbol{q}}^{\zeta} = \boldsymbol{H} \cdot \dot{\boldsymbol{\zeta}} \tag{4.24}$$

The strain rate tensor $\dot{\boldsymbol{\epsilon}}$ will be provided numerically (in incremental form) by the finite element solution, and thus we need **evolution equations** for $\dot{\boldsymbol{\epsilon}}^{\mathrm{p}}$ and $\dot{\boldsymbol{\zeta}}$, as well as **yield and plastic potential functions**, in order to calculate stress $\boldsymbol{\sigma}$ and stress-like ISV $\boldsymbol{q}^{\zeta}$.

(ii) **yield and plastic potential functions (for isotropic plasticity):** We define a yield function f to indicate the transition from elastic to elastoplastic response as,

$$\begin{aligned} f(\boldsymbol{\sigma}, \kappa) &= \|\boldsymbol{s}\| - \kappa \leq 0 \\ & \quad f < 0 \text{ elastic} \\ & \quad f = 0 \text{ elastoplastic} \end{aligned} \tag{4.25}$$

which is known as "J_2" or "von Mises" plasticity, because the J2 stress is defined as $J_2 = \frac{1}{2}\|\boldsymbol{s}\|^2$, and the von Mises stress $= \sqrt{\frac{3}{2}}\|\boldsymbol{s}\| = \sqrt{3J_2}$, where $\|\boldsymbol{s}\| = \sqrt{s_{ij}s_{ij}}$ is the L2 norm of the deviatoric stress tensor $\boldsymbol{s} = \boldsymbol{\sigma} - \frac{1}{3}tr(\boldsymbol{\sigma})\mathbf{1}$ or $s_{ij} = \sigma_{ij} - p\delta_{ij}$, with mean stress $p = \sigma_{kk}/3$; note that $\boldsymbol{s}$ is traceless, i.e., $\mathrm{tr}\boldsymbol{s} = s_{ii} = \sigma_{ii} - 3p = 0$. In terms of principal stresses, the yield function becomes

$$f(\sigma_1, \sigma_2, \sigma_3, \kappa) = \frac{1}{\sqrt{3}}\left[(\sigma_1 - \sigma_2)^2 + (\sigma_2 - \sigma_3)^2 + (\sigma_1 - \sigma_3)^2\right]^{1/2} - \kappa \leq 0 \tag{4.26}$$

We typically visualize the yield surface $f = 0$ in the π-plane ($\sigma_1 + \sigma_2 + \sigma_3 = 0$) in principal stress space (Fig.4.1). Note that the yield function is independent of the mean

stress p (and thus independent of changes in hydrostatic stress state $\sigma_1 = \sigma_2 = \sigma_3$), i.e., it is deviatoric. The elastic domain is written as

$$\mathbb{E}_\sigma = \{(\boldsymbol{\sigma}, \kappa) \in \mathbb{S} \times \mathbb{R}, f(\boldsymbol{\sigma}, \kappa) \leq 0\} \tag{4.27}$$

where $\mathbb{S}$ is the space of symmetric second order tensors, and $\mathbb{R}$ is the space of real numbers. We may plot the yield surface $f = 0$ in principal stress space as in Fig.4.1.

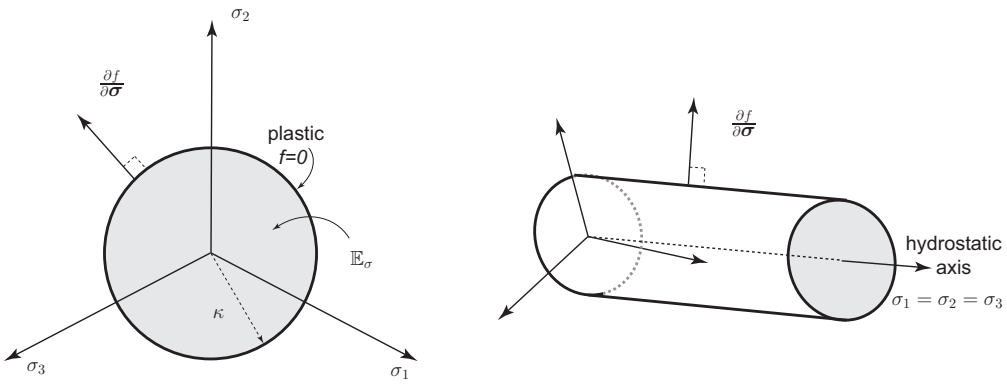

Figure 4.1. Yield surface in 3D: (left) π-plane, and (right), 3D principal stress space.

We define the initial value of the stress-like ISV κ to be the initial yield stress in the π-plane. For example, consider axial stress loading ('triaxial' or unconfined compression or tension). In (i) triaxial compression (Fig.4.2, assuming frictionless top and bottom boundaries, which experimentally is not possible even when attempted with grease or other lubricant), the axial stress $\sigma_3 = \sigma_a < 0$, and radial stress $\sigma_1 = \sigma_2 = \sigma_r < 0$; the radial stress is the confining stress. For (ii) uniaxial stress in tension $\sigma_2 = \sigma_3 = \sigma_r = 0$, $\sigma_1 = \sigma_a > 0$, then the initial value of κ can be solved from (4.26) as

$$\kappa_0 = \sqrt{\frac{2}{3}} |\sigma_a - \sigma_r|_y \tag{4.28}$$

which is the radius of the yield surface in the π-plane in Fig.4.1, where $|\sigma_a - \sigma_r|_y$ is taken at yield from an experimentally-determined stress-strain curve.

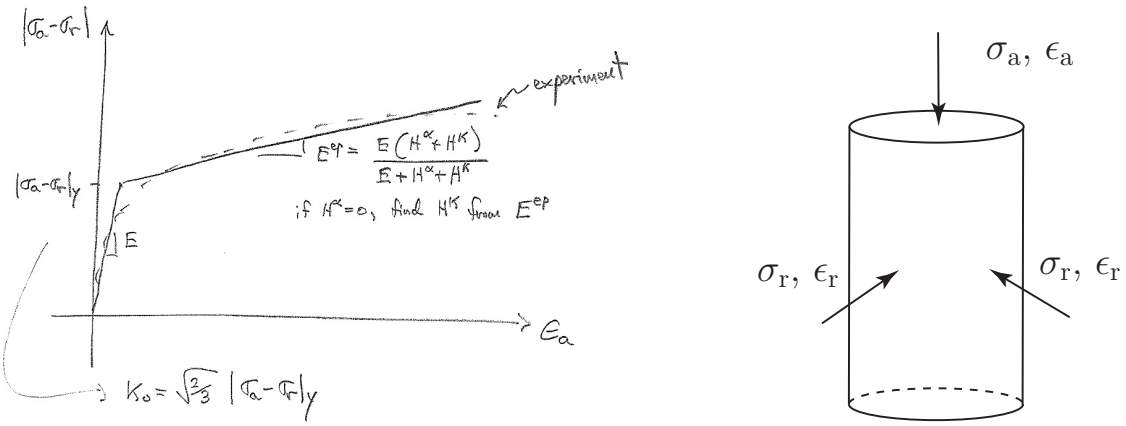

Figure 4.2. Cylindrical specimen (metal, soil, rock, concrete, foam, ...) in compression or tension.

The plastic potential function g can be defined such that if $g = f$, we have associative plastic flow, whereas if $g \neq f$, then we have non-associative plastic flow (typical for geomaterials and concrete, i.e., frictional strength defined differently than volumetric plastic strain). Here, for J_2 flow, we will assume associative plastic flow, $g = f$. Chapter 5 considers non-associative plastic flow constitutive models for geomaterials.

(iii) **evolution equations (in rate form):** Now, we define the evolution equations, starting with the **plastic flow rule**. We assume associative flow $g = f$ for 3D isochoric plasticity, such that

$$\dot{\boldsymbol{\epsilon}}^p = \dot{\gamma}\frac{\partial g}{\partial \boldsymbol{\sigma}} \implies \dot{\boldsymbol{\sigma}} = \boldsymbol{c}^{\mathrm{e}} : \left(\dot{\boldsymbol{\epsilon}} - \dot{\gamma}\frac{\partial g}{\partial \boldsymbol{\sigma}}\right) \tag{4.29}$$

$$\frac{\partial g}{\partial \boldsymbol{\sigma}} = \frac{\partial \|\boldsymbol{s}\|}{\partial \boldsymbol{\sigma}} \tag{4.30}$$

where $\dot{\gamma}$ is the plastic multiplier or consistency parameter. To find $\partial g/\partial \boldsymbol{\sigma}$, we carry

out the stress derivative in index notation as follows

$$\frac{\partial g}{\partial \sigma_{ij}} = \frac{\partial \sqrt{s_{ab}s_{ab}}}{\partial \sigma_{ij}} = \frac{1/2}{\|\boldsymbol{s}\|}\left(2\frac{\partial s_{ab}}{\partial \sigma_{ij}}s_{ab}\right) \tag{4.31}$$

$$s_{ab} = \sigma_{ab} - \frac{1}{3}\sigma_{kk}\delta_{ab} \tag{4.32}$$

$$\frac{\partial s_{ab}}{\partial \sigma_{ij}} = \frac{\partial \sigma_{ab}}{\partial \sigma_{ij}} - \frac{1}{3}\frac{\partial \sigma_{kk}}{\partial \sigma_{ij}}\delta_{ab} = \delta_{ai}\delta_{bj} - \frac{1}{3}\delta_{ij}\delta_{ab} \tag{4.33}$$

$$\Longrightarrow \quad \frac{\partial s_{ab}}{\partial \sigma_{ij}}s_{ab} = s_{ij} \tag{4.34}$$

$$\Longrightarrow \quad \dot{\epsilon}^p_{ij} = \dot{\gamma}\frac{s_{ij}}{\|\boldsymbol{s}\|} = \dot{\gamma}\hat{n}_{ij} \tag{4.35}$$

where $\hat{\boldsymbol{n}}$ is the **direction of plastic flow**. Note that for deviatoric plastic flow, the volumetric plastic flow is zero (Fig.4.1): $\dot{\epsilon}^{\mathrm{p}}_v = \dot{\epsilon}^{\mathrm{p}}_{ii} = \dot{\gamma}\frac{s_{ii}}{\|\boldsymbol{s}\|} = 0$. Note that the plastic multiplier is the magnitude of the plastic strain rate tensor: $\dot{\gamma} = \|\dot{\boldsymbol{\epsilon}}^{\mathrm{p}}\| > 0$, and plastic flow is in the direction of deviatoric stress $\hat{\boldsymbol{n}}$.

For the strain-like ISV ζ, we let

$$\dot{\zeta} = \dot{\gamma}h(\boldsymbol{\sigma}, \kappa) \Longrightarrow \dot{\kappa} = H^{\kappa}\dot{\gamma}h(\boldsymbol{\sigma}, \kappa) \tag{4.36}$$

where $h(\boldsymbol{\sigma}, \kappa)$ is the hardening function, and for simplicity, we assume $h(\boldsymbol{\sigma}, \kappa) = -\frac{\partial g}{\partial \kappa} = 1 \Longrightarrow \dot{\zeta} = \dot{\gamma}$. Thus, for a summary of the evolution equations, we have

$$\dot{\boldsymbol{\sigma}} = \boldsymbol{c}^{\mathrm{e}} : \dot{\boldsymbol{\epsilon}}^{\mathrm{e}} = \boldsymbol{c}^{\mathrm{e}} : (\dot{\boldsymbol{\epsilon}} - \dot{\boldsymbol{\epsilon}}^{\mathrm{p}}) \tag{4.37}$$

$$\dot{\boldsymbol{\epsilon}}^{\mathrm{p}} = \dot{\gamma}\frac{\boldsymbol{s}}{\|\boldsymbol{s}\|} = \dot{\gamma}\hat{\boldsymbol{n}} \tag{4.38}$$

$$\dot{\kappa} = H^{\kappa}\dot{\gamma} \tag{4.39}$$

(iv) **Kuhn-Tucker optimality conditions:** The **Kuhn-Tucker optimality conditions** are written the same as for 1D elastoplasticity as,

$$\dot{\gamma} \geq 0 \ , \ f \leq 0 \ , \ \dot{\gamma}f = 0 \tag{4.40}$$

(v) **consistency condition:** The **consistency condition** is the same as for 1D elastoplasticity,

$$\dot{\gamma}\dot{f} = 0 \tag{4.41}$$

oftentimes written for plastic loading ($\dot{\gamma} > 0$) as simply $\dot{f} = 0$. **We solve for $\dot{\gamma}$ from the consistency condition during plastic loading** ($\dot{\gamma} > 0$ and $\dot{f} = 0$). Using the chain rule

$$\dot{f} = \frac{\partial f}{\partial \boldsymbol{\sigma}} : \dot{\boldsymbol{\sigma}} + \frac{\partial f}{\partial \kappa}\dot{\kappa} = 0 \tag{4.42}$$

and substituting the evolution equations leads to solution of the plastic multiplier $\dot{\gamma}$ as

$$\frac{\partial f}{\partial \boldsymbol{\sigma}} : \boldsymbol{c}^{\mathrm{e}} : \left(\dot{\boldsymbol{\epsilon}} - \dot{\gamma}\frac{\partial g}{\partial \boldsymbol{\sigma}}\right) + \frac{\partial f}{\partial \kappa}H^{\kappa}h(\boldsymbol{\sigma}, \kappa)\dot{\gamma} = 0 \tag{4.43}$$

$$\dot{\gamma} = \frac{\frac{\partial f}{\partial \boldsymbol{\sigma}} : \boldsymbol{c}^{\mathrm{e}} : \dot{\boldsymbol{\epsilon}}}{\frac{\partial f}{\partial \boldsymbol{\sigma}} : \boldsymbol{c}^{\mathrm{e}} : \frac{\partial g}{\partial \boldsymbol{\sigma}} - \frac{\partial f}{\partial \kappa}H^{\kappa}h} = \frac{1}{\chi}\frac{\partial f}{\partial \boldsymbol{\sigma}} : \boldsymbol{c}^{\mathrm{e}} : \dot{\boldsymbol{\epsilon}} \tag{4.44}$$

(vi) **continuum elastoplastic tangent $\boldsymbol{c}^{\mathrm{ep}}$**: The derivation of the continuum elastoplastic tangent is a little more involved than for 1D elastoplasticity (because we work in tensor notation for 3D elastoplasticity here) whereby substituting the solution for $\dot{\gamma}$ back into the stress evolution equation, we obtain an expression for the **continuum elastoplastic tangent $\boldsymbol{c}^{\mathrm{ep}}$**, which relates the **total stress rate $\dot{\boldsymbol{\sigma}}$** to the **total strain rate $\dot{\boldsymbol{\epsilon}}$** as

$$\dot{\boldsymbol{\sigma}} = \boldsymbol{c}^{\mathrm{e}} : \left(\dot{\boldsymbol{\epsilon}} - \frac{1}{\chi}\left[\frac{\partial f}{\partial \boldsymbol{\sigma}} : \boldsymbol{c}^{e} : \dot{\boldsymbol{\epsilon}}\right]\frac{\partial g}{\partial \boldsymbol{\sigma}}\right) \tag{4.45}$$

$$\dot{\sigma}_{ij} = c^{\mathrm{e}}_{ijkl}\left(\dot{\epsilon}_{kl} - \frac{1}{\chi}\left[\frac{\partial f}{\partial \sigma_{ab}}c^{\mathrm{e}}_{abcd}\dot{\epsilon}_{cd}\right]\frac{\partial g}{\partial \sigma_{kl}}\right) \tag{4.46}$$

$$\dot{\sigma}_{ij} = c^{\mathrm{e}}_{ijkl}\dot{\epsilon}_{kl} - \frac{1}{\chi}c^{\mathrm{e}}_{ijkl}\frac{\partial g}{\partial \sigma_{kl}}\frac{\partial f}{\partial \sigma_{ab}}c^{\mathrm{e}}_{abcd}\dot{\epsilon}_{cd} \tag{4.47}$$

$$\dot{\sigma}_{ij} = \left(c^{\mathrm{e}}_{ijcd} - \frac{1}{\chi}c^{\mathrm{e}}_{ijkl}\frac{\partial g}{\partial \sigma_{kl}}\frac{\partial f}{\partial \sigma_{ab}}c^{\mathrm{e}}_{abcd}\right)\dot{\epsilon}_{cd} \tag{4.48}$$

$$\dot{\boldsymbol{\sigma}} = \left(\boldsymbol{c}^{\mathrm{e}} - \frac{1}{\chi}\boldsymbol{c}^{\mathrm{e}} : \frac{\partial g}{\partial \boldsymbol{\sigma}} \otimes \frac{\partial f}{\partial \boldsymbol{\sigma}} : \boldsymbol{c}^{\mathrm{e}}\right) : \dot{\boldsymbol{\epsilon}} \tag{4.49}$$

$$\dot{\boldsymbol{\sigma}} = \boldsymbol{c}^{\mathrm{ep}} : \dot{\boldsymbol{\epsilon}} \tag{4.50}$$

where recall that repeated indices are dummy indices, such that we sum over them. The free indices determine the order of the tensor (i.e, 1 free index denotes a 1st order tensor or vector, 2 free indices denote a 2nd order tensor or matrix, 3 free indices denote a 3rd order tensor, ...). For our example, (rederive these steps yourself)

$$\frac{\partial f}{\partial \boldsymbol{\sigma}} = \frac{\partial g}{\partial \boldsymbol{\sigma}} = \frac{\boldsymbol{s}}{\|\boldsymbol{s}\|} = \hat{\boldsymbol{n}} \tag{4.51}$$

$$\frac{\partial f}{\partial \kappa} = -1 \tag{4.52}$$

$$h(\boldsymbol{\sigma}, \kappa) = 1 \tag{4.53}$$

$$\frac{\partial f}{\partial \boldsymbol{\sigma}} : \boldsymbol{c}^{\mathrm{e}} : \frac{\partial g}{\partial \boldsymbol{\sigma}} = 2\mu \hat{\boldsymbol{n}} : \hat{\boldsymbol{n}} = 2\mu \tag{4.54}$$

$$\chi = \frac{\partial f}{\partial \boldsymbol{\sigma}} : \boldsymbol{c}^{\mathrm{e}} : \frac{\partial g}{\partial \boldsymbol{\sigma}} - \frac{\partial f}{\partial \kappa} H^{\kappa} h(\boldsymbol{\sigma}, \kappa) = 2\mu + H^{\kappa} \tag{4.55}$$

then, we have

$$\boldsymbol{c}^{\mathrm{ep}} = \boldsymbol{c}^{\mathrm{e}} - \frac{(2\mu)^2}{2\mu + H^{\kappa}} \hat{\boldsymbol{n}} \otimes \hat{\boldsymbol{n}} \tag{4.56}$$

(vii) **combined isotropic/kinematic hardening:** The Helmholtz free energy function ψ (per unit mass) is modified to include two other ISVs ($\boldsymbol{\zeta}^{\alpha}$ and $\boldsymbol{\alpha}$) associated with kinematic hardening as

$$\rho\psi(\boldsymbol{\epsilon}^{\mathrm{e}}, \boldsymbol{\zeta}) = \frac{1}{2}\boldsymbol{\epsilon}^{\mathrm{e}} : \boldsymbol{c}^{\mathrm{e}} : \boldsymbol{\epsilon}^{\mathrm{e}} + \frac{1}{2}\boldsymbol{\zeta} \cdot \boldsymbol{H} \cdot \boldsymbol{\zeta} \tag{4.57}$$

where the linear isotropic elastic modulus is $\boldsymbol{c}^{\mathrm{e}}$, and $\boldsymbol{H}$ is the hardening modulus matrix,

where we have

$$\boldsymbol{\sigma} = \frac{\partial(\rho\psi)}{\partial\boldsymbol{\epsilon}^{\mathrm{e}}} = \boldsymbol{c}^{\mathrm{e}} : \boldsymbol{\epsilon}^{\mathrm{e}} \tag{4.58}$$

$$\boldsymbol{q}^{\zeta} = \frac{\partial(\rho\psi)}{\partial\boldsymbol{\zeta}} = \begin{bmatrix} \kappa \\ \boldsymbol{\alpha} \end{bmatrix} = \boldsymbol{H} \cdot \boldsymbol{\zeta} \tag{4.59}$$

$$\boldsymbol{H} = \begin{bmatrix} H^{\kappa} & \mathbf{0}^{T} \\ \mathbf{0} & H^{\alpha}\mathbf{1} \end{bmatrix} \tag{4.60}$$

We introduce the backstress $\boldsymbol{\alpha}$ into the yield function as follows

$$f(\boldsymbol{\sigma}, \boldsymbol{q}^{\zeta}) = \|\boldsymbol{\xi}\| - \kappa = 0 \tag{4.61}$$

where $\boldsymbol{\xi} = \boldsymbol{s} - \boldsymbol{\alpha}$ is the deviatoric "relative" stress; or sometimes $\boldsymbol{\xi} = \boldsymbol{s} - \frac{2}{3}\boldsymbol{\alpha}$ is defined as the deviatoric relative stress, wherein the 2/3 factor is introduced to allow the 3D model to reduce to a 1D uniaxial stress form as in Ch.3. Let us visualize the shifted yield surface in the π-plane in Fig.4.3, where the elastic domain is centered about $\boldsymbol{\alpha}$, which is defined as

$$\mathbb{E}_{\sigma} = \{(\boldsymbol{\sigma}, \boldsymbol{\alpha}, \kappa) \in \mathbb{S} \times \mathbb{S} \times \mathbb{R}, f(\boldsymbol{\sigma}, \boldsymbol{\alpha}, \kappa) \leq 0\} \tag{4.62}$$

Note that the radius of the yield surface is still controlled by κ, such that for plasticity $f = 0 \Longrightarrow \|\boldsymbol{\xi}\| = \kappa$.

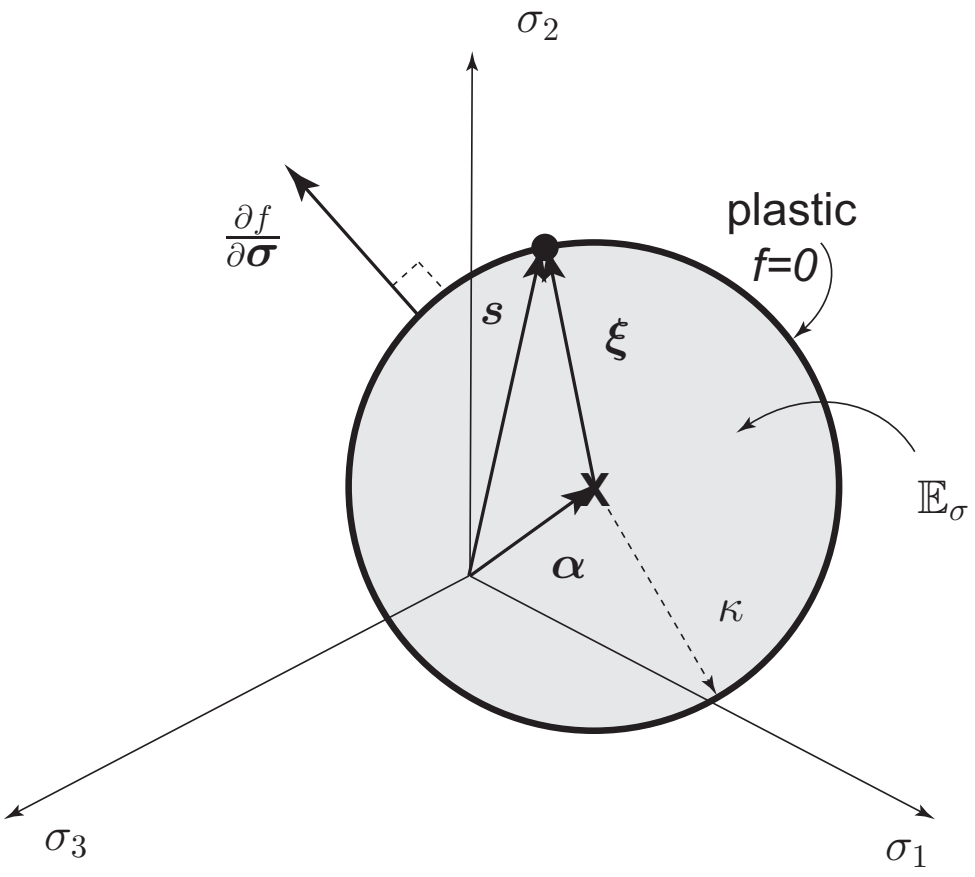

Figure 4.3. Yield surface in π-plane, centered about $\boldsymbol{\alpha}$.

Evolution equations:

For the plastic strain evolution, we have

$$\dot{\boldsymbol{\epsilon}}^{\mathrm{p}} = \dot{\gamma}\frac{\partial g}{\partial \boldsymbol{\sigma}} = \dot{\gamma}\frac{\boldsymbol{\xi}}{\|\boldsymbol{\xi}\|} = \dot{\gamma}\hat{\boldsymbol{n}} \tag{4.63}$$

and the evolution of the strain-like ISV vector is

$$\dot{\boldsymbol{\zeta}} = \dot{\gamma}\boldsymbol{h}(\boldsymbol{\sigma}, \boldsymbol{q}^{\zeta}) \implies \dot{\boldsymbol{q}}^{\zeta} = \boldsymbol{H}\cdot\dot{\boldsymbol{\zeta}} = \dot{\gamma}\boldsymbol{H}\cdot\boldsymbol{h}(\boldsymbol{\sigma}, \boldsymbol{q}^{\zeta}) \tag{4.64}$$

For simplicity, let $\boldsymbol{h}(\boldsymbol{\sigma}, \boldsymbol{q}^{\zeta}) = -\partial g/\partial \boldsymbol{q}^{\zeta}$ and $g = f$, such that

$$-\frac{\partial g}{\partial \boldsymbol{q}^{\zeta}} = -\begin{bmatrix} \frac{\partial g}{\partial \kappa} \\ \frac{\partial g}{\partial \boldsymbol{\alpha}} \end{bmatrix} = \begin{bmatrix} 1 \\ \hat{\boldsymbol{n}} \end{bmatrix} \implies \begin{array}{l} \dot{\kappa} = H^{\kappa}\dot{\gamma} \\ \dot{\boldsymbol{\alpha}} = H^{\alpha}\dot{\gamma}\hat{\boldsymbol{n}} \end{array} \tag{4.65}$$

$$\dot{\boldsymbol{\zeta}} = \begin{bmatrix} \dot{\zeta}^{\kappa} \\ \dot{\boldsymbol{\zeta}}^{\alpha} \end{bmatrix} = \dot{\gamma}\begin{bmatrix} 1 \\ \hat{\boldsymbol{n}} \end{bmatrix} = \begin{bmatrix} \|\dot{\boldsymbol{\epsilon}}^{\mathrm{p}}\| \\ \dot{\boldsymbol{\epsilon}}^{\mathrm{p}} \end{bmatrix} \tag{4.66}$$

We revisit the consistency condition as,

$$\dot{f} = \frac{\partial f}{\partial \boldsymbol{\sigma}} : \dot{\boldsymbol{\sigma}} + \frac{\partial f}{\partial \boldsymbol{q}^{\zeta}} \cdot \dot{\boldsymbol{q}}^{\zeta} = 0 \tag{4.67}$$

where substituting the evolution equations leads to a solution for the plastic multiplier $\dot{\gamma}$ as

$$\frac{\partial f}{\partial \boldsymbol{\sigma}} : \boldsymbol{c}^{e} : \left(\dot{\boldsymbol{\epsilon}} - \dot{\gamma}\frac{\partial g}{\partial \boldsymbol{\sigma}}\right) + \frac{\partial f}{\partial \boldsymbol{q}^{\zeta}} \cdot \boldsymbol{H}\cdot\boldsymbol{h}\dot{\gamma} = 0 \tag{4.68}$$

$$\dot{\gamma} = \frac{\frac{\partial f}{\partial \boldsymbol{\sigma}} : \boldsymbol{c}^{\mathrm{e}} : \dot{\boldsymbol{\epsilon}}}{\frac{\partial f}{\partial \boldsymbol{\sigma}} : \boldsymbol{c}^{\mathrm{e}} : \frac{\partial g}{\partial \boldsymbol{\sigma}} - \frac{\partial f}{\partial \boldsymbol{q}^{\zeta}} \cdot \boldsymbol{H}\cdot\boldsymbol{h}} \tag{4.69}$$

For our example, we have

$$\frac{\partial f}{\partial \boldsymbol{q}^\zeta} = \begin{bmatrix} -1 \\ -\frac{\boldsymbol{\xi}}{\|\boldsymbol{\xi}\|} \end{bmatrix} = \begin{bmatrix} -1 \\ -\hat{\boldsymbol{n}} \end{bmatrix} \tag{4.70}$$

$$-\frac{\partial f}{\partial \boldsymbol{q}^\zeta} \cdot \boldsymbol{H} \cdot \boldsymbol{h} = H^\kappa + H^\alpha \tag{4.71}$$

Then, the continuum elastoplastic tangent becomes

$$\boldsymbol{c}^{\mathrm{ep}} = \boldsymbol{c}^{\mathrm{e}} - \frac{(2\mu)^2}{2\mu + H^\alpha + H^\kappa} \hat{\boldsymbol{n}} \otimes \hat{\boldsymbol{n}} \tag{4.72}$$

(viii) **convexity of yield surface:** Convexity of the elastic domain in stress space (Fig.3.13) is required for proper formulation of an elastoplasticity model [Simo and Hughes, 1998]. Mathematically, this can be proven as follows [Simo and Hughes, 1998]. Consider an elastic domain bounded by a yield surface

$$\mathbb{E}_\sigma = \{(\boldsymbol{\sigma}, \boldsymbol{\alpha}, \kappa) \in \mathbb{S} \times \mathbb{S} \times \mathbb{R}, f(\boldsymbol{\sigma}, \boldsymbol{\alpha}, \kappa) \leq 0\} \tag{4.73}$$

To ensure convexity of f, we need to show that

$$f[\boldsymbol{\sigma}^*, (\boldsymbol{q}^\zeta)^*] \leq \eta f(\boldsymbol{\sigma}_1, \boldsymbol{q}_1^\zeta) + (1-\eta) f(\boldsymbol{\sigma}_2, \boldsymbol{q}_2^\zeta) \quad \forall \eta \in [0,1] \tag{4.74}$$

$$\boldsymbol{\sigma}^* = \eta \boldsymbol{\sigma}_1 + (1-\eta)\boldsymbol{\sigma}_2 \tag{4.75}$$

$$(\boldsymbol{q}^\zeta)^* = \eta \boldsymbol{q}_1^\zeta + (1-\eta)\boldsymbol{q}_2^\zeta \tag{4.76}$$

We apply the triangle inequality, $\|\boldsymbol{a}+\boldsymbol{b}\| \leq \|\boldsymbol{a}\| + \|\boldsymbol{b}\|$, such that

$$\begin{aligned} f[\boldsymbol{\sigma}^*, (\boldsymbol{q}^\zeta)^*] &= \|\boldsymbol{\xi}^*\| - \kappa^* = \|\boldsymbol{s}^* - \boldsymbol{\alpha}^*\| - \kappa^* && (4.77)\\ &\leq \eta\|\boldsymbol{s}_1 - \boldsymbol{\alpha}_1\| - \eta\kappa_1 + (1-\eta)\|\boldsymbol{s}_2 - \boldsymbol{\alpha}_2\| - (1-\eta)\kappa_2 && (4.78)\\ &= \eta f(\boldsymbol{\sigma}_1, \boldsymbol{q}_1^\zeta) + (1-\eta) f(\boldsymbol{\sigma}_2, \boldsymbol{q}_2^\zeta) && (4.79)\\ & \quad q.e.d \end{aligned}$$

Therefore, $f(\boldsymbol{\sigma}, \boldsymbol{q}^\zeta)$ is convex.

(ix) **uniqueness (Hill's stability postulate) and the principle of maximum plastic dissipation:** Recall the reduced dissipation inequality as,

$$\mathcal{D} = \boldsymbol{\sigma} : \dot{\boldsymbol{\epsilon}}^{\mathrm{p}} - \boldsymbol{q}^\zeta \cdot \dot{\boldsymbol{\zeta}} \geq 0 \tag{4.80}$$

where $\mathcal{D}$ is the dissipation function.

Statement of the Principle of Maximum Plastic Dissipation: of all possible stress states $\boldsymbol{\sigma}^*$ and $(\boldsymbol{q}^\zeta)^*$ that satisfy $f(\boldsymbol{\sigma}^*, (\boldsymbol{q}^\zeta)^*) = 0$, the one state that maximizes the dissipation function $\mathcal{D}$ is the physical state $(\boldsymbol{\sigma}, \boldsymbol{q}^\zeta)$, such that

$$\mathcal{D}(\boldsymbol{\sigma}, \boldsymbol{q}^\zeta) \geq \mathcal{D}(\boldsymbol{\sigma}^*, (\boldsymbol{q}^\zeta)^*) \tag{4.81}$$

We can restate this rule as a constrained minimization problem with constraint $f(\boldsymbol{\sigma}^*, (\boldsymbol{q}^\zeta)^*) = 0$ (yield function = 0) and multiplier $\dot{\gamma}$ (the plastic multiplier), where we define a "Lagrangian" as

$$\mathcal{L} := -\mathcal{D}(\boldsymbol{\sigma}^*, (\boldsymbol{q}^\zeta)^*) + \dot{\gamma} f(\boldsymbol{\sigma}^*, (\boldsymbol{q}^\zeta)^*) \tag{4.82}$$

where the "$-$" sign makes it a minimization problem. For minimization, we apply the

stationarity condition, such that

$$\delta\mathcal{L} = \frac{\partial\mathcal{L}}{\partial\boldsymbol{\sigma}^*} : \delta\boldsymbol{\sigma}^* + \frac{\partial\mathcal{L}}{\partial(\boldsymbol{q}^\zeta)^*} \cdot \delta(\boldsymbol{q}^\zeta)^* + \frac{\partial\mathcal{L}}{\partial\dot{\gamma}}\delta\dot{\gamma} = 0 \tag{4.83}$$

Thus, for arbitrary $\delta\boldsymbol{\sigma}^*$, $\delta(\boldsymbol{q}^\zeta)^*$, and $\delta\dot{\gamma}$, we have three conditions,

$$\frac{\partial\mathcal{L}}{\partial\boldsymbol{\sigma}^*} = \mathbf{0}\,,\ \frac{\partial\mathcal{L}}{\partial(\boldsymbol{q}^\zeta)^*} = \mathbf{0}\,,\ \frac{\partial\mathcal{L}}{\partial\dot{\gamma}} = 0 \tag{4.84}$$

Thus, for the actual state $(\boldsymbol{\sigma}, \boldsymbol{q}^\zeta)$, we have

$$\frac{\partial\mathcal{L}}{\partial\boldsymbol{\sigma}^*} = -\underbrace{\frac{\partial\mathcal{D}}{\partial\boldsymbol{\sigma}^*}}_{\dot{\boldsymbol{\epsilon}}^p} + \dot{\gamma}\frac{\partial f}{\partial\boldsymbol{\sigma}^*} = 0 \tag{4.85}$$

$$\Longrightarrow \boxed{\dot{\boldsymbol{\epsilon}}^p = \dot{\gamma}\frac{\partial f}{\partial\boldsymbol{\sigma}}} \tag{4.86}$$

$$\frac{\partial\mathcal{L}}{\partial(\boldsymbol{q}^\zeta)^*} = -\underbrace{\frac{\partial\mathcal{D}}{\partial(\boldsymbol{q}^\zeta)^*}}_{\dot{\boldsymbol{\zeta}}} + \dot{\gamma}\frac{\partial f}{\partial(\boldsymbol{q}^\zeta)^*} = 0 \tag{4.87}$$

$$\Longrightarrow \boxed{\dot{\boldsymbol{\zeta}} = -\dot{\gamma}\frac{\partial f}{\partial\boldsymbol{q}^\zeta}} \tag{4.88}$$

$$\frac{\partial\mathcal{L}}{\partial\dot{\gamma}} = f(\boldsymbol{\sigma}^*, (\boldsymbol{q}^\zeta)^*) = 0 \tag{4.89}$$

$$\Longrightarrow \boxed{f(\boldsymbol{\sigma}, \boldsymbol{q}^\zeta) = 0} \tag{4.90}$$

If we assume the constraint is $f(\boldsymbol{\sigma}^*, (\boldsymbol{q}^\zeta)^*) \leq 0$ rather than $f(\boldsymbol{\sigma}^*, (\boldsymbol{q}^\zeta)^*) = 0$, then after constrained minimization, $f(\boldsymbol{\sigma}, \boldsymbol{q}^\zeta) \leq 0$, and the Kuhn-Tucker conditions result as

$$\dot{\gamma} \geq 0\ ,\ f \leq 0\ ,\ \dot{\gamma}f = 0 \tag{4.91}$$

Let us revisit **convexity.** The principle of maximum plastic dissipation states that

$$\mathcal{D}(\boldsymbol{\sigma}, \boldsymbol{q}^\zeta) \geq \mathcal{D}(\boldsymbol{\sigma}^*, (\boldsymbol{q}^\zeta)^*) \tag{4.92}$$

which can be rewritten as

$$(\boldsymbol{\sigma}^* - \boldsymbol{\sigma}) : \dot{\boldsymbol{\epsilon}}^{\mathrm{p}} - ((\boldsymbol{q}^{\zeta})^* - \boldsymbol{q}^{\zeta}) \cdot \dot{\boldsymbol{\zeta}} \leq 0 \tag{4.93}$$

where after substituting the results, we have

$$(\boldsymbol{\sigma}^* - \boldsymbol{\sigma}) : \frac{\partial f}{\partial \boldsymbol{\sigma}} + ((\boldsymbol{q}^{\zeta})^* - \boldsymbol{q}^{\zeta}) \cdot \frac{\partial f}{\partial \boldsymbol{q}^{\zeta}} \leq 0 \tag{4.94}$$

This is an alternate statement of convexity by considering perfect plasticity $(\boldsymbol{q}^{\zeta})^* = \boldsymbol{q}^{\zeta}$, and the stress vectors in Fig.4.4.

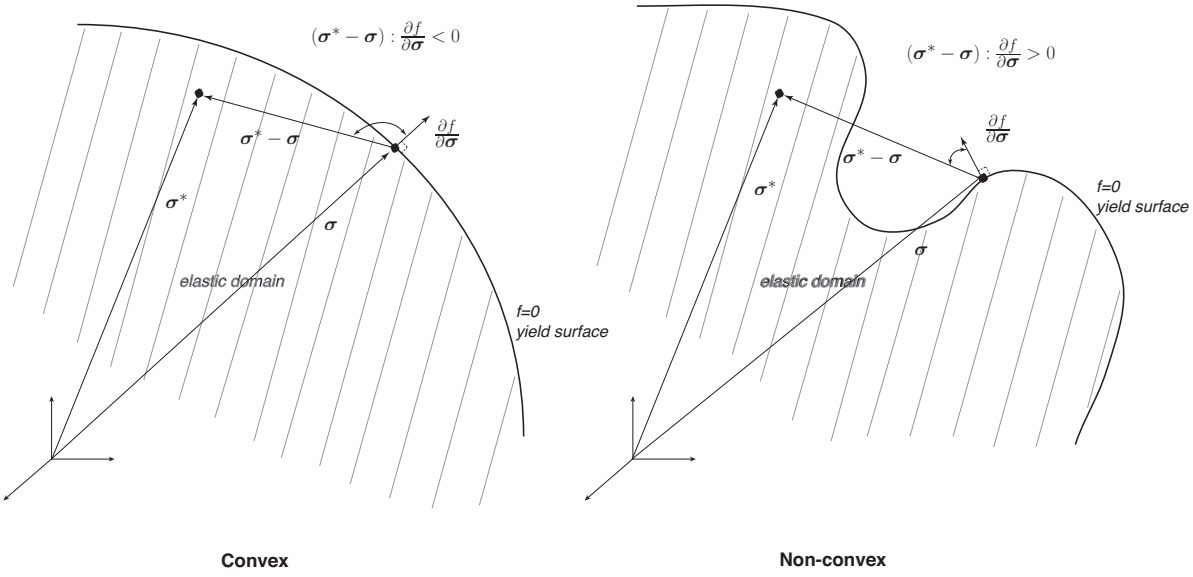

Figure 4.4. Convexity of the yield surface implies that the principle of maximum plastic dissipation is satisfied, assuming also that plasticity is associative, i.e., $g = f$.

Thus, the **principle of maximum plastic dissipation** results in the following:

(a) associative plastic flow and hardening

(b) Kuhn-Tucker loading/unloading conditions

(c) convexity of $\mathbb{E}_{\sigma}$

For geomaterials, we usually do not satisfy condition (a) and thus use non-associative

plastic flow $g \neq f$. It is possible to trigger loss of ellipticity (non-uniqueness) with non-associative plastic flow, but it is not always the case. Not satisfying the principle of maximum plastic dissipation DOES NOT MEAN that the reduced dissipation inequality (and in turn the second law of thermodynamics) is not satisfied. Thus, non-associativity plastic flow rules must still satisfy the reduced dissipation inequality.

4.3 Numerical Integration in Time of 3D Elastoplasticity

Refer to Simo and Hughes [1998]. We integrate in time the stress tensor rate, evolution equations, and consistency condition, written together as

$$\dot{\boldsymbol{\sigma}} = \boldsymbol{c}^{\mathrm{e}} : \dot{\boldsymbol{\epsilon}}^{\mathrm{e}} = \boldsymbol{c}^{\mathrm{e}} : (\dot{\boldsymbol{\epsilon}} - \dot{\boldsymbol{\epsilon}}^{\mathrm{p}}) = \boldsymbol{c}^{\mathrm{e}} : \left(\dot{\boldsymbol{\epsilon}} - \dot{\gamma} \underbrace{\frac{\boldsymbol{\xi}}{\|\boldsymbol{\xi}\|}}_{\hat{\boldsymbol{n}}} \right) \tag{4.95}$$

$$\dot{\kappa} = H^{\kappa} \dot{\gamma} \tag{4.96}$$

$$\dot{\boldsymbol{\alpha}} = H^{\alpha} \dot{\gamma} \underbrace{\frac{\boldsymbol{\xi}}{\|\boldsymbol{\xi}\|}}_{\hat{\boldsymbol{n}}} \tag{4.97}$$

$$\dot{\gamma} \dot{f} = 0 \tag{4.98}$$

There are 4 first-order ODEs, and 4 unknowns $(\boldsymbol{\sigma}, \kappa, \boldsymbol{\alpha}, \gamma)$. We use Backward Euler integration (implicit, first order accurate), which can be shown to be equivalent to the "return mapping algorithm" for certain constitutive models, including this one. Apply

Backward Euler to the 4 ODEs (check the math), such that

$$\begin{aligned}
\boldsymbol{\sigma}_{n+1} &= \boldsymbol{\sigma}_n + \boldsymbol{c}^e : \left(\Delta\boldsymbol{\epsilon} - \Delta\gamma \left[\frac{\boldsymbol{\xi}}{\|\boldsymbol{\xi}\|} \right]_{n+1} \right) \\
& \quad \Delta\boldsymbol{\epsilon} = \boldsymbol{\epsilon}_{n+1} - \boldsymbol{\epsilon}_n \ , \ \Delta\gamma = \Delta t \dot{\gamma}_{n+1} \\
& \quad \boldsymbol{c}^{\mathrm{e}} : \boldsymbol{\xi} = \lambda tr(\boldsymbol{\xi})\mathbf{1} + 2\mu\boldsymbol{\xi} = 2\mu\boldsymbol{\xi} \\
\boldsymbol{\sigma}_{n+1} &= \boldsymbol{\sigma}^{\mathrm{tr}}_{n+1} - 2\mu\Delta\gamma \left[\frac{\boldsymbol{\xi}}{\|\boldsymbol{\xi}\|} \right]_{n+1} \qquad (4.99) \\
& \quad \boldsymbol{\sigma}^{\mathrm{tr}}_{n+1} = \boldsymbol{\sigma}_n + \boldsymbol{c}^{\mathrm{e}} : \Delta\boldsymbol{\epsilon} \\
& \quad tr(\boldsymbol{\sigma}_{n+1}) = tr(\boldsymbol{\sigma}^{\mathrm{tr}}_{n+1}) \Longrightarrow p_{n+1} = \frac{1}{3} tr(\boldsymbol{\sigma}_{n+1}) = \frac{1}{3} tr(\boldsymbol{\sigma}^{\mathrm{tr}}_{n+1}) \\
& \quad \boldsymbol{s}_{n+1} = \boldsymbol{s}^{\mathrm{tr}}_{n+1} - 2\mu\Delta\gamma \left[\frac{\boldsymbol{\xi}}{\|\boldsymbol{\xi}\|} \right]_{n+1} \qquad (4.100) \\
\kappa_{n+1} &= \kappa_n + H^{\kappa}\Delta\gamma \qquad (4.101) \\
\boldsymbol{\alpha}_{n+1} &= \boldsymbol{\alpha}_n + H^{\alpha}\Delta\gamma \left[\frac{\boldsymbol{\xi}}{\|\boldsymbol{\xi}\|} \right]_{n+1} \qquad (4.102) \\
f_{n+1} &= \|\boldsymbol{\xi}_{n+1}\| - \kappa_{n+1} = 0 \qquad (4.103)
\end{aligned}$$

We now analyze the direction of plastic flow $\left[\frac{\boldsymbol{\xi}}{\|\boldsymbol{\xi}\|} \right]_{n+1}$ as

$$\begin{aligned}
\boldsymbol{\xi}_{n+1} = \boldsymbol{s}_{n+1} - \boldsymbol{\alpha}_{n+1} &= \underbrace{\boldsymbol{s}^{\mathrm{tr}}_{n+1} - \boldsymbol{\alpha}_n}_{\boldsymbol{\xi}^{\mathrm{tr}}_{n+1}} - \Delta\gamma(2\mu + H^{\alpha}) \frac{\boldsymbol{\xi}_{n+1}}{\|\boldsymbol{\xi}_{n+1}\|} \qquad (4.104) \\
\underbrace{\left(1 + \frac{\Delta\gamma(2\mu + H^{\alpha})}{\|\boldsymbol{\xi}_{n+1}\|} \right)}_{>0} \boldsymbol{\xi}_{n+1} &= \boldsymbol{\xi}^{\mathrm{tr}}_{n+1} \qquad (4.105) \\
\Longrightarrow \frac{\boldsymbol{\xi}_{n+1}}{\|\boldsymbol{\xi}_{n+1}\|} &= \frac{\boldsymbol{\xi}^{\mathrm{tr}}_{n+1}}{\|\boldsymbol{\xi}^{\mathrm{tr}}_{n+1}\|} \qquad (4.106) \\
\Longrightarrow \boldsymbol{\xi}_{n+1} &= \left(1 - \frac{\Delta\gamma(2\mu + H^{\alpha})}{\|\boldsymbol{\xi}^{\mathrm{tr}}_{n+1}\|} \right) \boldsymbol{\xi}^{\mathrm{tr}}_{n+1} \qquad (4.107) \\
\|\boldsymbol{\xi}_{n+1}\| &= \|\boldsymbol{\xi}^{\mathrm{tr}}_{n+1}\| - \Delta\gamma(2\mu + H^{\alpha}) \qquad (4.108)
\end{aligned}$$

Thus, the current and trial directions of plastic flow are the same $\hat{\boldsymbol{n}}_{n+1} = \hat{\boldsymbol{n}}^{\mathrm{tr}}$, making **Backward Euler equivalent to the return mapping algorithm for small strain J2 plasticity**. Because these equations are linear, we may substitute $\|\boldsymbol{\xi}_{n+1}\|$ and κ_{n+1}

into $f_{n+1} = 0$ to solve for $\Delta\gamma$, such that

$$\|\boldsymbol{\xi}^{\text{tr}}_{n+1}\| - \Delta\gamma(2\mu + H^\alpha) - \kappa_n - H^\kappa \Delta\gamma = 0 \tag{4.109}$$

$$\Longrightarrow \quad \Delta\gamma = \frac{\|\boldsymbol{\xi}^{\text{tr}}_{n+1}\| - \kappa_n}{2\mu + H^\alpha + H^\kappa} = \frac{f^{\text{tr}}_{n+1}}{2\mu + H^\alpha + H^\kappa} \tag{4.110}$$

We summarize the **return mapping algorithm** as follows: given $\Delta\boldsymbol{\epsilon}$ over the time increment, and $\boldsymbol{\sigma}_n$, κ_n, $\boldsymbol{\alpha}_n$, γ_n from the converged past time step, we have

(a) compute trial stress: $\boldsymbol{\sigma}^{\text{tr}}_{n+1} = \boldsymbol{\sigma}_n + \boldsymbol{c}^e : \Delta\boldsymbol{\epsilon}$, and $p_{n+1} = \frac{1}{3} tr(\boldsymbol{\sigma}^{\text{tr}}_{n+1})$, $\boldsymbol{s}^{\text{tr}}_{n+1} = \boldsymbol{\sigma}^{\text{tr}}_{n+1} - p_{n+1}\mathbf{1}$, $\boldsymbol{\xi}^{\text{tr}}_{n+1} = \boldsymbol{s}^{\text{tr}}_{n+1} - \boldsymbol{\alpha}_n$, $\hat{\boldsymbol{n}}^{\text{tr}} = \boldsymbol{\xi}^{\text{tr}}_{n+1}/\|\boldsymbol{\xi}^{\text{tr}}_{n+1}\|$

(b) check for yielding: trial yield function $f^{\text{tr}}_{n+1} = \|\boldsymbol{\xi}^{\text{tr}}_{n+1}\| - \kappa_n$

$$\begin{array}{rlll} \text{if} & f^{\text{tr}}_{n+1} > 0 & \text{plastic} & \text{go to step 3} \\ \text{else} & f^{\text{tr}}_{n+1} < 0 & \text{elastic}: & \boldsymbol{\sigma}_{n+1} = \boldsymbol{\sigma}^{\text{tr}}_{n+1} \\ & & & \boldsymbol{\alpha}_{n+1} = \boldsymbol{\alpha}_n \\ & & & \kappa_{n+1} = \kappa_n \\ & & & \gamma_{n+1} = \gamma_n \end{array} \tag{4.111}$$

(c) compute: $\Delta\gamma = \frac{f^{\text{tr}}_{n+1}}{2\mu + H^\alpha + H^\kappa}$, and update:

$$\begin{aligned} \boldsymbol{s}_{n+1} &= \boldsymbol{s}^{\text{tr}}_{n+1} - 2\mu\Delta\gamma\hat{\boldsymbol{n}}^{\text{tr}} \\ \boldsymbol{\alpha}_{n+1} &= \boldsymbol{\alpha}_n + H^\alpha\Delta\gamma\hat{\boldsymbol{n}}^{\text{tr}} \\ \kappa_{n+1} &= \kappa_n + H^\kappa\Delta\gamma \\ \gamma_{n+1} &= \gamma_n + \Delta\gamma \end{aligned} \tag{4.112}$$

We can visualize the **return mapping algorithm** in the π-plane, with $H^\kappa = 0$ (i.e., $\kappa_{n+1} = \kappa_n$) and $H^\alpha > 0$, as shown in Figs.4.5-4.7. Note the trial direction of plastic flow is $\hat{\boldsymbol{n}}^{\text{tr}} = \boldsymbol{\xi}^{\text{tr}}_{n+1}/\|\boldsymbol{\xi}^{\text{tr}}_{n+1}\|$.

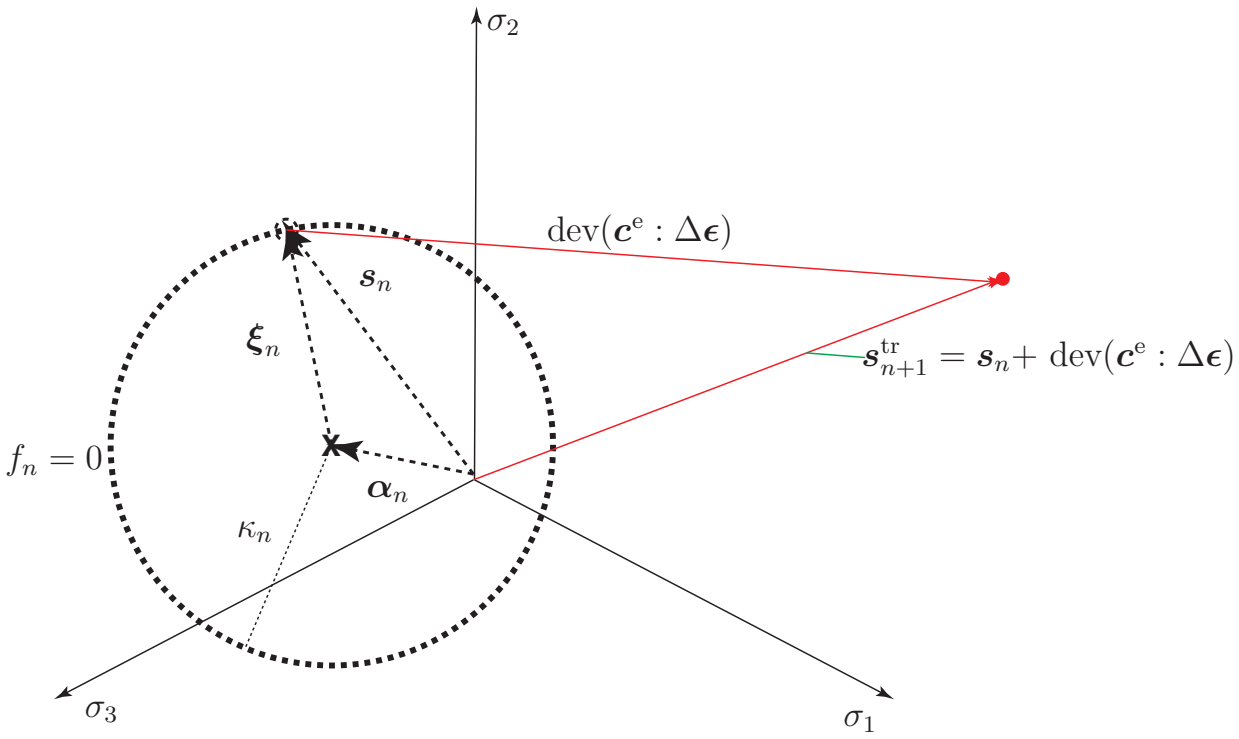

Figure 4.5. Yield surface in π-plane, centered about $\boldsymbol{\alpha}_n$ at time t_n, with incremental stress $\mathrm{dev}(\boldsymbol{c}^{\mathrm{e}} : \Delta\boldsymbol{\epsilon})$ (red arrow) applied to calculate trial deviatoric stress $\boldsymbol{s}^{\mathrm{tr}}_{n+1}$ (red arrow).

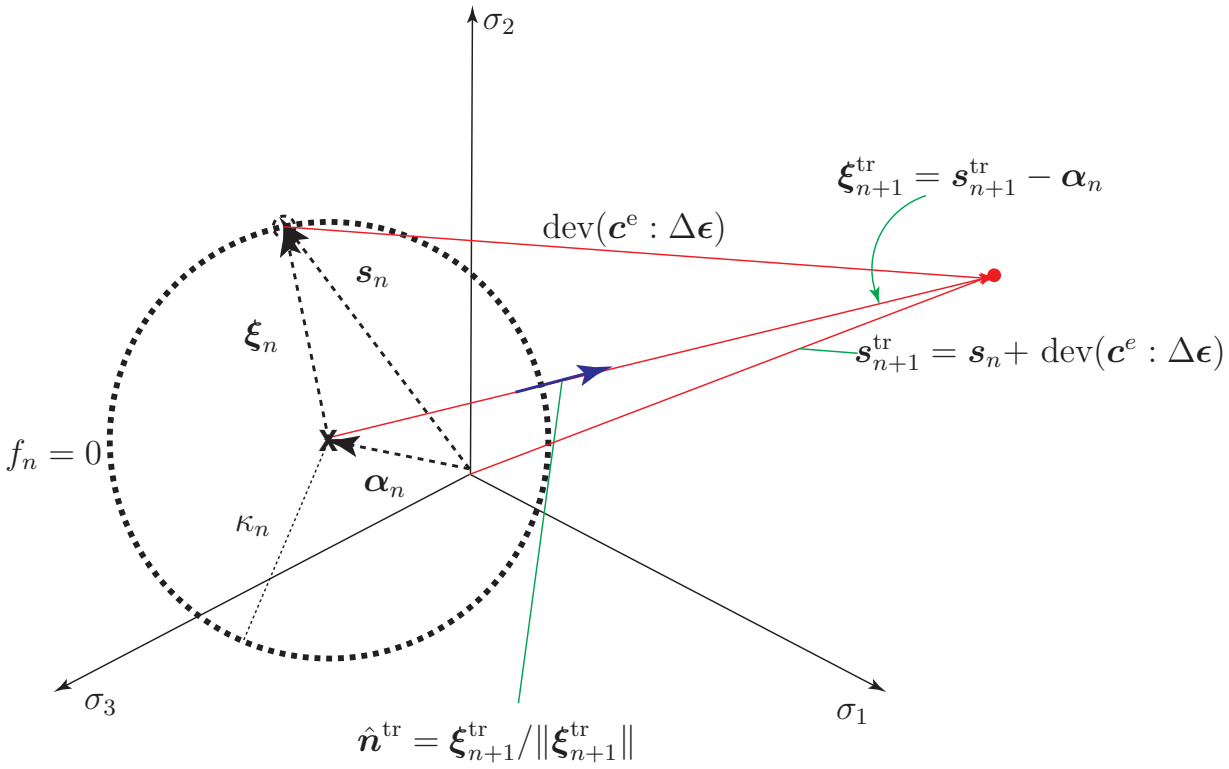

Figure 4.6. Yield surface in π-plane, centered about $\boldsymbol{\alpha}_n$ at time t_n, showing calculation of relative trial stress $\boldsymbol{\xi}^{\rm tr}_{n+1}$ (red arrow) and the direction of plastic flow $\hat{\boldsymbol{n}}^{\rm tr}$ (as short blue arrow).

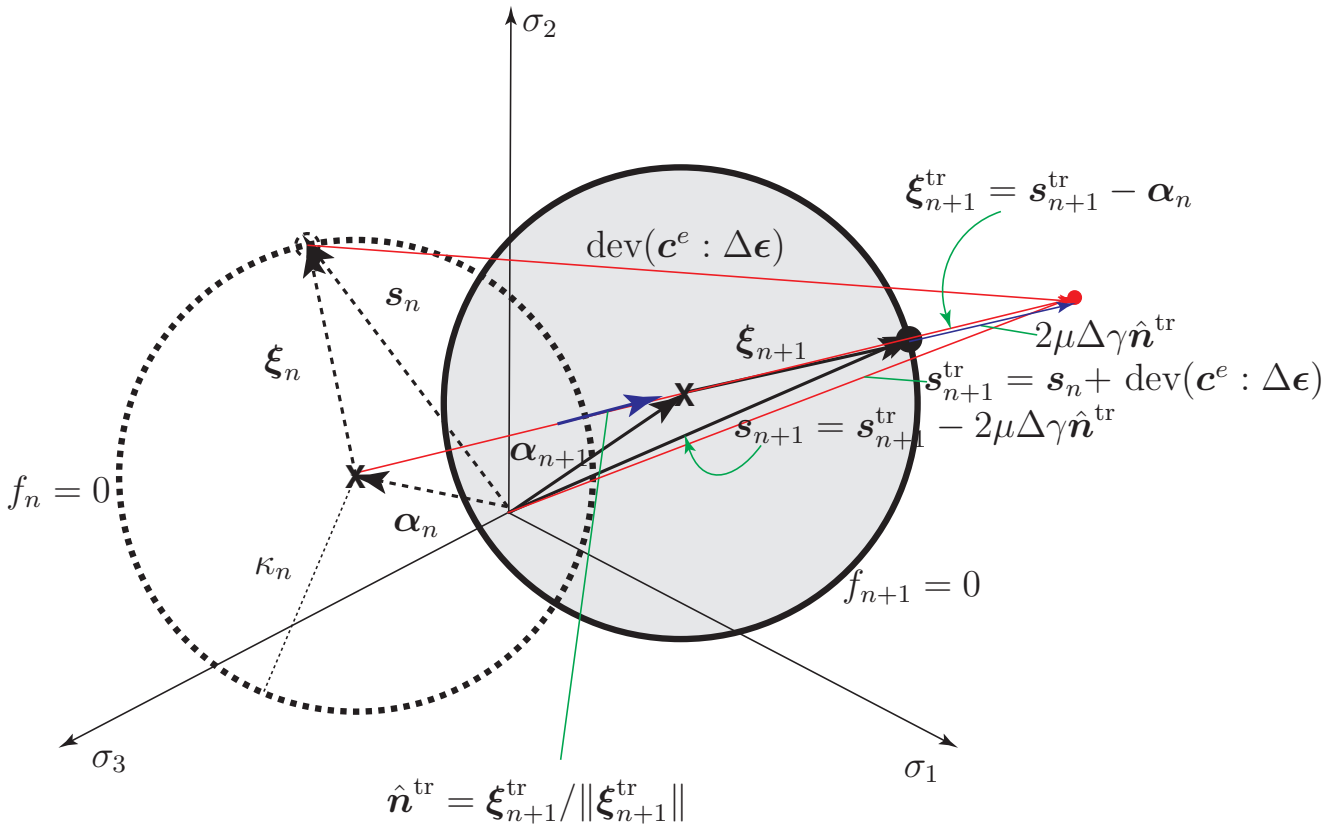

Figure 4.7. Yield surface in π-plane, centered about $\boldsymbol{\alpha}_n$ at time t_n, that is translated to center $\boldsymbol{\alpha}_{n+1} = \boldsymbol{\alpha}_n + H^{\alpha}(\Delta\gamma)\,\hat{\boldsymbol{n}}^{\mathrm{tr}}$ at t_{n+1} through kinematic hardening.

4.4 Consistent Tangent for 3D Elastoplasticity

Recall the element level consistent tangent for a 3D finite element as follows

$$\frac{\partial \boldsymbol{f}^{e,\mathrm{INT}}(\boldsymbol{d}^e)}{\partial \boldsymbol{d}^e} = \int_{-1}^{1}\int_{-1}^{1}\int_{-1}^{1} (\boldsymbol{B}^e)^T \cdot \frac{\partial \boldsymbol{\sigma}}{\partial \boldsymbol{\epsilon}} \cdot \boldsymbol{B}^e j^e d\xi d\eta d\zeta \tag{4.113}$$

We first derive the material consistent tangent $\frac{\partial \boldsymbol{\sigma}}{\partial \boldsymbol{\epsilon}}$ in tensor form (4th order), then we convert into a 6×6 matrix form for FE implementation. Recall the stress evolution equation, and recognize that $\Delta\boldsymbol{\epsilon}^{k+1} = \boldsymbol{\epsilon}_{n+1}^{k+1} - \boldsymbol{\epsilon}_n$, such that

$$\begin{aligned}
\boldsymbol{\sigma}_{n+1}^{k+1} &= (\boldsymbol{\sigma}_{n+1}^{k+1})^{\mathrm{tr}} - 2\mu\Delta\gamma^{k+1}\left(\frac{\boldsymbol{\xi}_{n+1}^{k+1}}{\|\boldsymbol{\xi}_{n+1}^{k+1}\|}\right)^{\mathrm{tr}} && (4.114)\\
(\boldsymbol{\sigma}_{n+1}^{k+1})^{\mathrm{tr}} &= \boldsymbol{\sigma}_n + \boldsymbol{c}^e : \Delta\boldsymbol{\epsilon}^{k+1} && (4.115)\\
(p_{n+1}^{k+1})^{\mathrm{tr}} &= \frac{1}{3} tr(\boldsymbol{\sigma}_{n+1}^{k+1})^{\mathrm{tr}} && (4.116)\\
(\boldsymbol{s}_{n+1}^{k+1})^{\mathrm{tr}} &= (\boldsymbol{\sigma}_{n+1}^{k+1})^{\mathrm{tr}} - (p_{n+1}^{k+1})^{\mathrm{tr}}\mathbf{1} && (4.117)\\
(\boldsymbol{\xi}_{n+1}^{k+1})^{\mathrm{tr}} &= (\boldsymbol{s}_{n+1}^{k+1})^{\mathrm{tr}} - \boldsymbol{\alpha}_n && (4.118)
\end{aligned}$$

For ease of notation, leave off the subscript and superscript $(\bullet)_{n+1}^{k+1}$, such that

$$\begin{aligned}
\boldsymbol{\sigma} &= \boldsymbol{\sigma}^{\mathrm{tr}} - 2\mu\Delta\gamma\hat{\boldsymbol{n}}^{\mathrm{tr}} && (4.119)\\
\boldsymbol{\sigma}^{\mathrm{tr}} &= \boldsymbol{\sigma}_n + \boldsymbol{c}^e : \Delta\boldsymbol{\epsilon} && (4.120)\\
p^{\mathrm{tr}} &= \frac{1}{3} tr\boldsymbol{\sigma}^{\mathrm{tr}} && (4.121)\\
\boldsymbol{s}^{\mathrm{tr}} &= \boldsymbol{\sigma}^{\mathrm{tr}} - p^{\mathrm{tr}}\mathbf{1} && (4.122)\\
\boldsymbol{\xi}^{\mathrm{tr}} &= \boldsymbol{s}^{\mathrm{tr}} - \boldsymbol{\alpha}_n && (4.123)
\end{aligned}$$

Then, the **material consistent tangent** may be calculated as (check the math)

$$\frac{\partial \boldsymbol{\sigma}}{\partial \boldsymbol{\epsilon}} = \frac{\partial \boldsymbol{\sigma}^{\mathrm{tr}}}{\partial \boldsymbol{\epsilon}} - 2\mu \hat{\boldsymbol{n}}^{\mathrm{tr}} \otimes \frac{\partial \Delta\gamma}{\partial \boldsymbol{\epsilon}} - 2\mu\Delta\gamma \frac{\partial \hat{\boldsymbol{n}}^{\mathrm{tr}}}{\partial \boldsymbol{\epsilon}} \tag{4.124}$$

$$\frac{\partial \Delta\gamma}{\partial \boldsymbol{\epsilon}} = \frac{1}{2\mu + H^{\alpha} + H^{\kappa}} \underbrace{\frac{\partial \|\boldsymbol{\xi}^{\mathrm{tr}}\|}{\partial \boldsymbol{\epsilon}}}_{\hat{\boldsymbol{n}}^{\mathrm{tr}} : \frac{\partial \boldsymbol{\xi}^{\mathrm{tr}}}{\partial \boldsymbol{\epsilon}} = 2\mu \hat{\boldsymbol{n}}^{\mathrm{tr}}} \tag{4.125}$$

$$\frac{\partial \boldsymbol{\xi}^{\mathrm{tr}}}{\partial \boldsymbol{\epsilon}} = \frac{\partial \boldsymbol{s}^{\mathrm{tr}}}{\partial \boldsymbol{\epsilon}} = \frac{\partial \boldsymbol{\sigma}^{\mathrm{tr}}}{\partial \boldsymbol{\epsilon}} - \mathbf{1} \otimes \frac{\partial p^{\mathrm{tr}}}{\partial \boldsymbol{\epsilon}}$$

$$\frac{\partial \boldsymbol{\sigma}^{\mathrm{tr}}}{\partial \boldsymbol{\epsilon}} = \boldsymbol{c}^{\mathrm{e}}$$

$$\left(\frac{\partial p^{\mathrm{tr}}}{\partial \boldsymbol{\epsilon}}\right)_{kl} = \frac{1}{3} c^{\mathrm{e}}_{iikl} = \frac{1}{3}\left(3\lambda\delta_{kl} + \mu(\delta_{ik}\delta_{il} + \delta_{il}\delta_{ik})\right) = (\lambda + \frac{2}{3}\mu)\delta_{kl}$$

$$= K\delta_{kl}$$

$$\frac{\partial \boldsymbol{\xi}^{\mathrm{tr}}}{\partial \boldsymbol{\epsilon}} = \lambda \mathbf{1} \otimes \mathbf{1} + 2\mu \boldsymbol{I} - (\lambda + \frac{2}{3}\mu)\mathbf{1} \otimes \mathbf{1} = 2\mu(\boldsymbol{I} - \frac{1}{3}\mathbf{1} \otimes \mathbf{1}) \tag{4.126}$$

$$\text{example} : a_{ij}(I_{ijkl} - \frac{1}{3}\delta_{ij}\delta_{kl}) = \mathrm{dev}[\mathrm{symm}(\boldsymbol{a})]_{kl}$$

$$\implies \frac{\partial \Delta\gamma}{\partial \boldsymbol{\epsilon}} = \frac{2\mu}{2\mu + H^{\alpha} + H^{\kappa}} \hat{\boldsymbol{n}}^{\mathrm{tr}} \tag{4.127}$$

where K is the bulk modulus, and

$$\frac{\partial \hat{\boldsymbol{n}}^{\mathrm{tr}}}{\partial \boldsymbol{\epsilon}} = \boldsymbol{\xi}^{\mathrm{tr}} \otimes \frac{\partial}{\partial \boldsymbol{\epsilon}}\left(\frac{1}{\|\boldsymbol{\xi}^{\mathrm{tr}}\|}\right) + \frac{1}{\|\boldsymbol{\xi}^{\mathrm{tr}}\|}\frac{\partial \boldsymbol{\xi}^{\mathrm{tr}}}{\partial \boldsymbol{\epsilon}} \tag{4.128}$$

$$\frac{\partial}{\partial \boldsymbol{\epsilon}}\left(\frac{1}{\|\boldsymbol{\xi}^{\mathrm{tr}}\|}\right) = \frac{-1}{\|\boldsymbol{\xi}^{\mathrm{tr}}\|(\boldsymbol{\xi}^{\mathrm{tr}} : \boldsymbol{\xi}^{\mathrm{tr}})} \underbrace{\boldsymbol{\xi}^{\mathrm{tr}} : \frac{\partial \boldsymbol{\xi}^{\mathrm{tr}}}{\partial \boldsymbol{\epsilon}}}_{2\mu \boldsymbol{\xi}^{\mathrm{tr}}} = \frac{-1}{\boldsymbol{\xi}^{\mathrm{tr}} : \boldsymbol{\xi}^{\mathrm{tr}}} 2\mu \hat{\boldsymbol{n}}^{\mathrm{tr}}$$

$$= \frac{-2\mu}{\boldsymbol{\xi}^{\mathrm{tr}} : \boldsymbol{\xi}^{\mathrm{tr}}} \boldsymbol{\xi}^{\mathrm{tr}} \otimes \hat{\boldsymbol{n}}^{\mathrm{tr}} + \frac{2\mu}{\|\boldsymbol{\xi}^{\mathrm{tr}}\|}(\boldsymbol{I} - \frac{1}{3}\mathbf{1} \otimes \mathbf{1})$$

$$= \frac{2\mu}{\|\boldsymbol{\xi}^{\mathrm{tr}}\|}\left(\boldsymbol{I} - \frac{1}{3}\mathbf{1} \otimes \mathbf{1} - \hat{\boldsymbol{n}}^{\mathrm{tr}} \otimes \hat{\boldsymbol{n}}^{\mathrm{tr}}\right) \tag{4.129}$$

Then the **material consistent elastoplastic tangent** is

$$\begin{aligned}\frac{\partial \boldsymbol{\sigma}}{\partial \boldsymbol{\epsilon}} &= \boldsymbol{c}^{\mathrm{e}} - 2\mu\left(\frac{2\mu}{2\mu + H^{\alpha} + H^{\kappa}}\right)\hat{\boldsymbol{n}}^{\mathrm{tr}} \otimes \hat{\boldsymbol{n}}^{\mathrm{tr}} \\ &\quad -2\mu\Delta\gamma\frac{2\mu}{\|\boldsymbol{\xi}^{\mathrm{tr}}\|}\left(\boldsymbol{I} - \frac{1}{3}\mathbf{1}\otimes\mathbf{1} - \hat{\boldsymbol{n}}^{\mathrm{tr}} \otimes \hat{\boldsymbol{n}}^{\mathrm{tr}}\right) \end{aligned} \tag{4.130}$$

Recall the **continuum elasto-plastic tangent** as

$$\boldsymbol{c}^{\mathrm{ep}} = \boldsymbol{c}^{\mathrm{e}} - \frac{1}{\chi}\boldsymbol{c}^{\mathrm{e}} : \frac{\partial g}{\partial \boldsymbol{\sigma}} \otimes \frac{\partial f}{\partial \boldsymbol{\sigma}} : \boldsymbol{c}^{\mathrm{e}} \tag{4.131}$$

$$\frac{\partial f}{\partial \boldsymbol{\sigma}} = \frac{\partial g}{\partial \boldsymbol{\sigma}} = \frac{\boldsymbol{\xi}}{\|\boldsymbol{\xi}\|} = \hat{\boldsymbol{n}} = \hat{\boldsymbol{n}}^{\mathrm{tr}} \tag{4.132}$$

$$\boldsymbol{c}^{\mathrm{e}} : \hat{\boldsymbol{n}}^{\mathrm{tr}} = 2\mu\hat{\boldsymbol{n}}^{\mathrm{tr}} \tag{4.133}$$

$$\frac{\partial f}{\partial \boldsymbol{\sigma}} : \boldsymbol{c}^{\mathrm{e}} : \frac{\partial g}{\partial \boldsymbol{\sigma}} = 2\mu\hat{\boldsymbol{n}}^{\mathrm{tr}} : \hat{\boldsymbol{n}}^{\mathrm{tr}} = 2\mu \tag{4.134}$$

$$\chi = \frac{\partial f}{\partial \boldsymbol{\sigma}} : \boldsymbol{c}^{\mathrm{e}} : \frac{\partial g}{\partial \boldsymbol{\sigma}} - \frac{\partial f}{\partial \boldsymbol{q}^{\zeta}} \cdot \boldsymbol{H} \cdot \boldsymbol{h}(\boldsymbol{\sigma}, \boldsymbol{q}^{\zeta}) = 2\mu + H^{\alpha} + H^{\kappa} \tag{4.135}$$

$$\boldsymbol{c}^{\mathrm{ep}} = \boldsymbol{c}^{\mathrm{e}} - \frac{(2\mu)^2}{2\mu + H^{\alpha} + H^{\kappa}}\hat{\boldsymbol{n}}^{\mathrm{tr}} \otimes \hat{\boldsymbol{n}}^{\mathrm{tr}} \tag{4.136}$$

Then, we can rewrite the consistent tangent as

$$\frac{\partial \boldsymbol{\sigma}}{\partial \boldsymbol{\epsilon}} = \boldsymbol{c}^{\mathrm{ep}} - \Delta\gamma\frac{(2\mu)^2}{\|\boldsymbol{\xi}^{\mathrm{tr}}\|}\left(\boldsymbol{I} - \frac{1}{3}\mathbf{1}\otimes\mathbf{1} - \hat{\boldsymbol{n}}^{\mathrm{tr}} \otimes \hat{\boldsymbol{n}}^{\mathrm{tr}}\right) \tag{4.137}$$

For small time steps, $\Delta t \to 0 \Longrightarrow \Delta\gamma \to 0$, such that in the limit, we have

$$\lim_{\Delta\gamma\to 0}\left(\frac{\partial \boldsymbol{\sigma}}{\partial \boldsymbol{\epsilon}}\right)_{n+1}^{k+1} = \boldsymbol{c}^{\mathrm{ep}} \tag{4.138}$$

Note: the continuum elastoplastic tangent $\boldsymbol{c}^{ep}$ and material consistent tangent $(\partial\boldsymbol{\sigma}/\partial\boldsymbol{\epsilon})_{n+1}^{k+1}$ are, in general, NOT the same. The advantage of the consistent tangent is that it will allow your Newton-Raphson algorithm to demonstrate quadratic convergence (and, possibly, convergence versus non-convergence if the problem is highly nonlinear), whereas the continuum tangent usually only provides linear convergence.

This page intentionally left blank.

Chapter 5

3D Pressure-Sensitive Plasticity at Small Strain

Much of the material in this chapter is taken from Borja [2013]. Following on Chapter 4, we focus this chapter on the differences in constitutive modeling for pressure-sensitive plasticity for geomaterials like soil, rock, and concrete, and other particulate materials. We motivate first the need for pressure-sensitive plasticity with some experimentally-observed behavior, and then focus our attention on the different non-associative plasticity models, with various definitions of yield function f and plastic potential function g, starting with Mohr-Coulomb (M-C) plasticity [Vermeer and de Borst, 1984]. Note that MC plasticity, and its follow-on variations such as Drucker-Prager (DP) plasticity, are "strength" models suitable for modeling small elastic deformations and failure in stiff geomaterials such as heavily overconsolidated clays, dense sands, rocks, and concrete. Whereas for softer soils such normally-consolidated clays, other constitutive models such as Modified Cam-Clay elasto-plasticity are better suited for modeling both deformation and failure [Borja, 2013].

With this in mind, we summarize traditional laboratory mechanical testing of geomaterials

(soil, rock) and other pressure-sensitive materials (e.g., concrete) for constitutive model development of failure (peak load) and parameter determination. Assumptions made are the following for these examples: (1) drained condition (all stresses are "effective" with respect to the effective stress principle [Terzaghi, 1943]); (2) solid mechanics sign convention: $\sigma > 0$ tension, $\sigma < 0$ compression; and (3) compressive principal stresses: $0 \geq \sigma_1 \geq \sigma_2 \geq \sigma_3$. Figure 5.1 illustrates the various mechanical loading conditions typical for testing geomaterials in the laboratory, which are pressure-sensitive, thus control of the mean effective stress is important for calibrating material constitutive parameters.

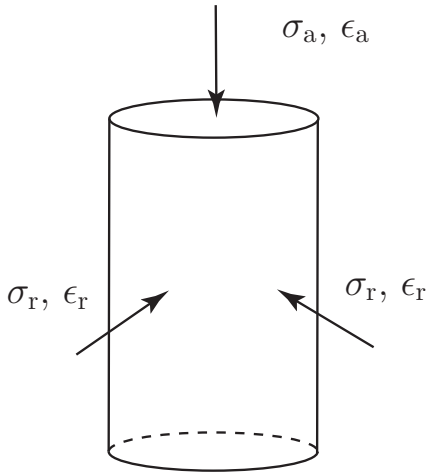

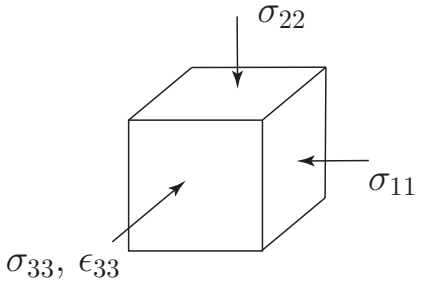

- "triaxial" compression (TC):
  $\sigma_3 = \sigma_\mathrm{a}$, $\sigma_1 = \sigma_2 = \sigma_\mathrm{r}$, $0 \geq \sigma_r \geq \sigma_a$, $|\sigma_a| \geq |\sigma_r|$
- "triaxial" extension (TE):
  $\sigma_1 = \sigma_\mathrm{a}$, $\sigma_2 = \sigma_3 = \sigma_\mathrm{r}$, $0 \geq \sigma_a \geq \sigma_r$, $|\sigma_r| \geq |\sigma_a|$
- uniaxial stress (unconfined) compression:
  $\sigma_\mathrm{a} < 0$, $\sigma_\mathrm{r} = 0$
- uniaxial strain (oedometer) compression:
  $\sigma_\mathrm{a} < 0$, $\sigma_\mathrm{r} < 0$, $\epsilon_\mathrm{r} = 0$
- true triaxial compression: $\sigma_{11} \neq \sigma_{22} \neq \sigma_{33}$
- plane strain (biaxial) compression:
  $\sigma_{11} \neq \sigma_{22} \neq \sigma_{33}$, $\epsilon_{33} = 0$
- plane stress compression:
  $\sigma_{11} \neq \sigma_{22}$, $\sigma_{33} = 0$, $\epsilon_{33} \neq 0$
- isotropic (hydrostatic) compression:
  $\sigma_{11} = \sigma_{22} = \sigma_{33} = \sigma$

Figure 5.1. Different experimental conditions for laboratory testing of geomaterials.

In Fig.5.2, we illustrate the typical stress-strain behavior of soil [Atkinson, 1993]. 'WET' and 'DRY' refer to the critical state of a soil, which is the state at which upon continuous shearing there is no more volumetric strain (or change in void ratio). For example, for a water-saturated soil, if 'WET' of critical state, its void ratio $e = V_v/V_s$ will contract and water will be pressed out of the void space (assuming drained condition). If 'DRY' of critical state, its void ratio will initially contract and then begin to dilate and take in more water into its void space as its volume increases. $e_{\rm cr}$ is the void ratio at critical state.

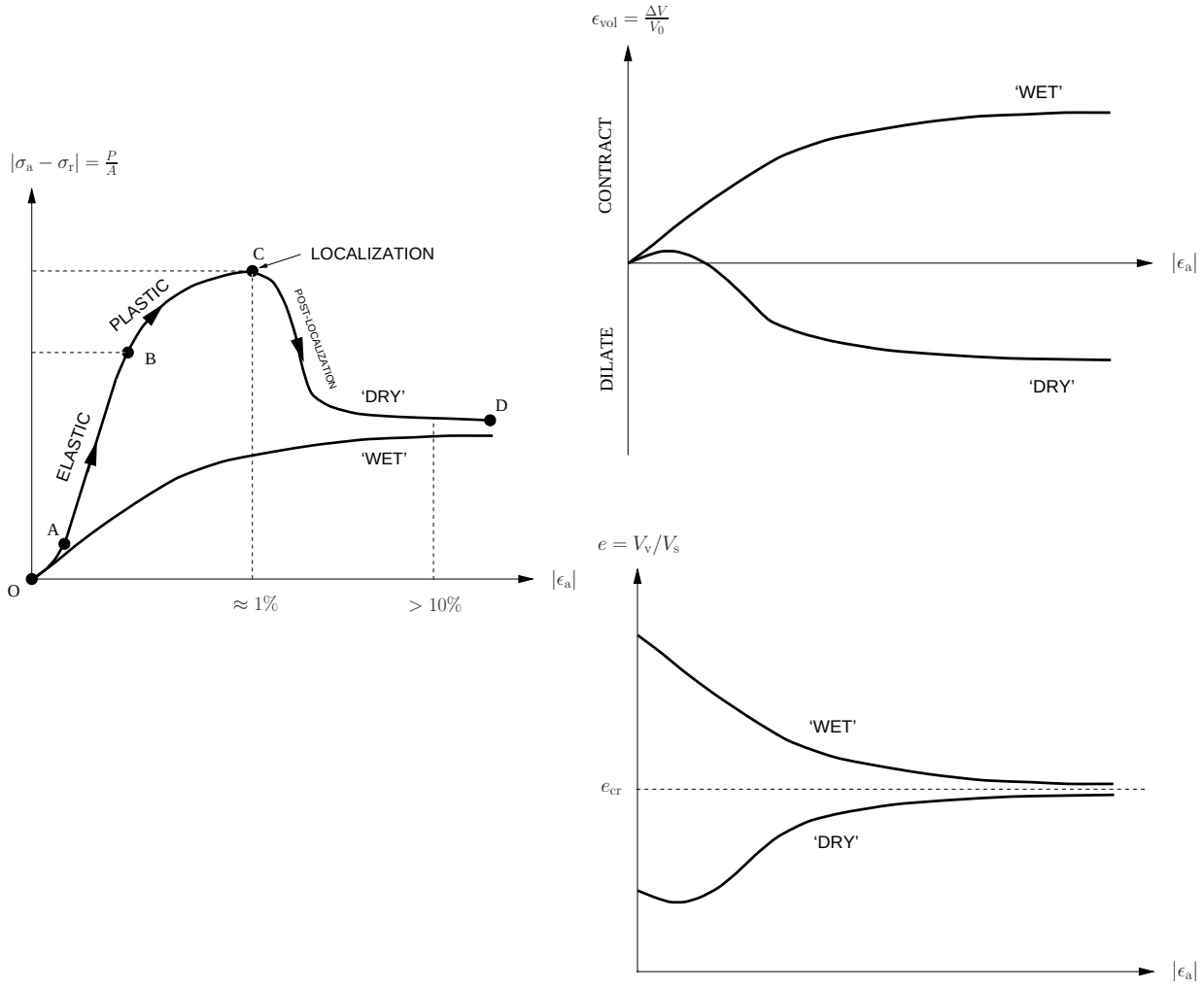

Figure 5.2. Typical stress-strain behavior of soil [Atkinson, 1993].

In Fig.5.3, we see shear banding in a dense sand [Vardoulakis et al., 1978, Vardoulakis and Goldschieder, 1981] with clear peak load and post-peak softening associated with development of the shear band.

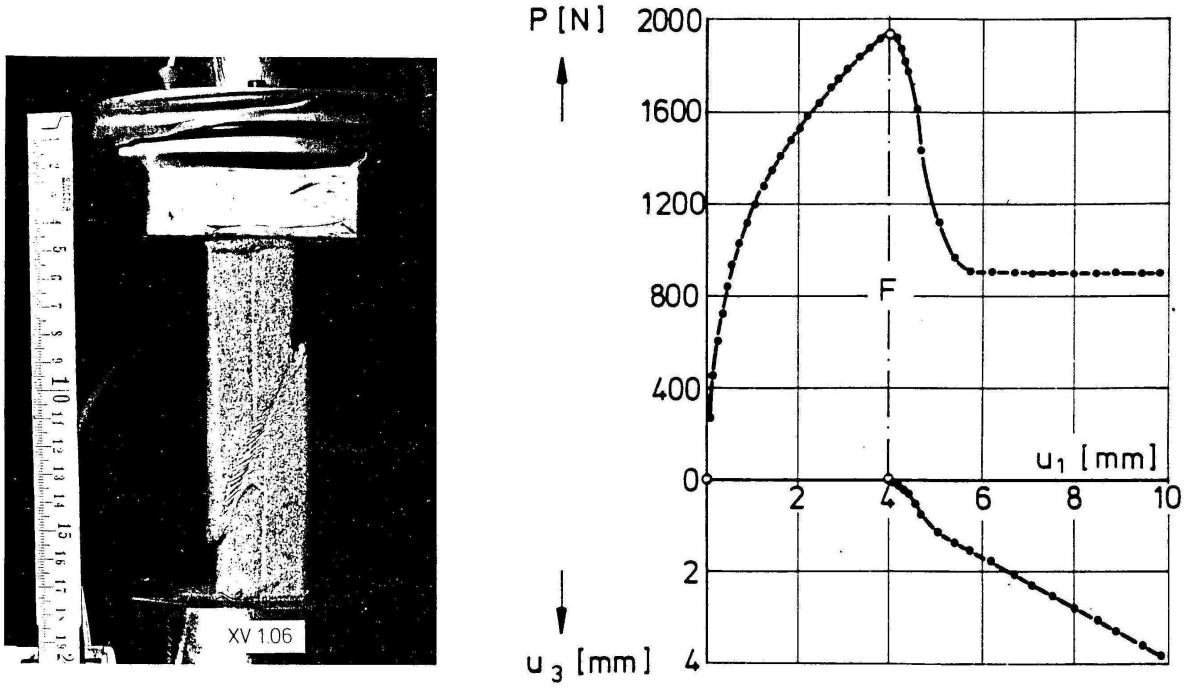

Figure 5.3. Shear banding in dense sand [Vardoulakis et al., 1978, Vardoulakis and Goldschieder, 1981].

In Fig.5.4, we illustrate the typical stress-strain behavior of rock [Jaeger and Cook, 1976]. Rocks do not exhibit a critical state as do certain soils. The main difference between soil and rock is that soil is particulate in nature allowing grains to slide over and past each other and fluid to occupy its voids, whereas rock is typically composed of a strongly cemented aggregate of crystals and amorphous grains not allowing grain sliding or easy occupation of the pore space by a fluid. The dilatancy observed in rock is due to opening of microcracks, forming and extending.

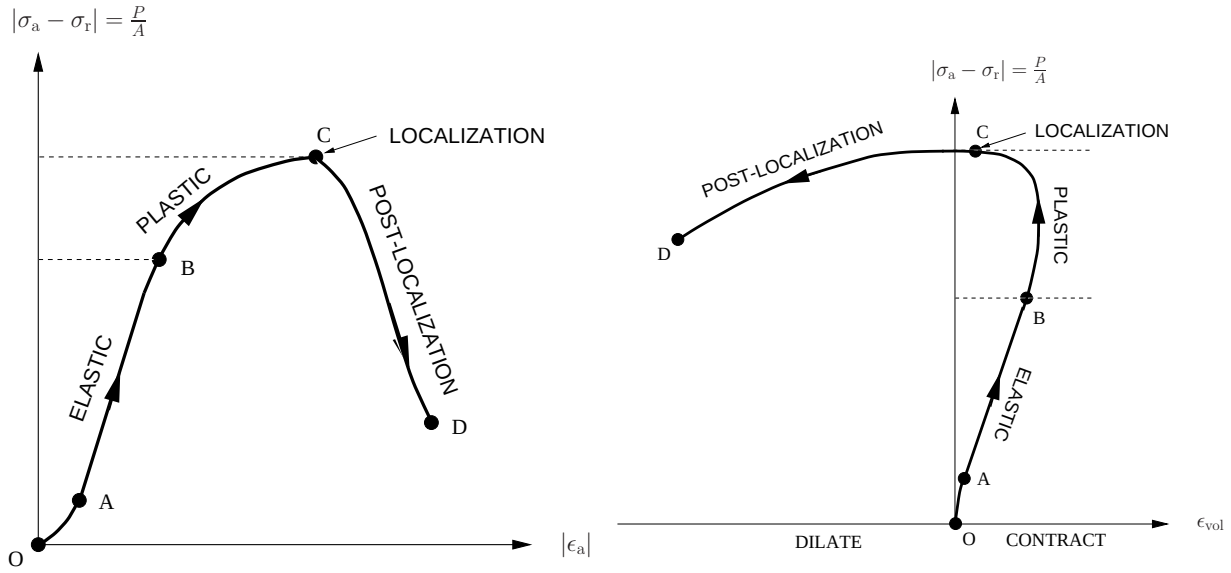

Figure 5.4. Typical stress-strain behavior of rock [Jaeger and Cook, 1976].

As an example, consider the failure of Tennesse marble observed in Fig.5.5 (courtesy of David Holcomb, Sandia National Laboratories).

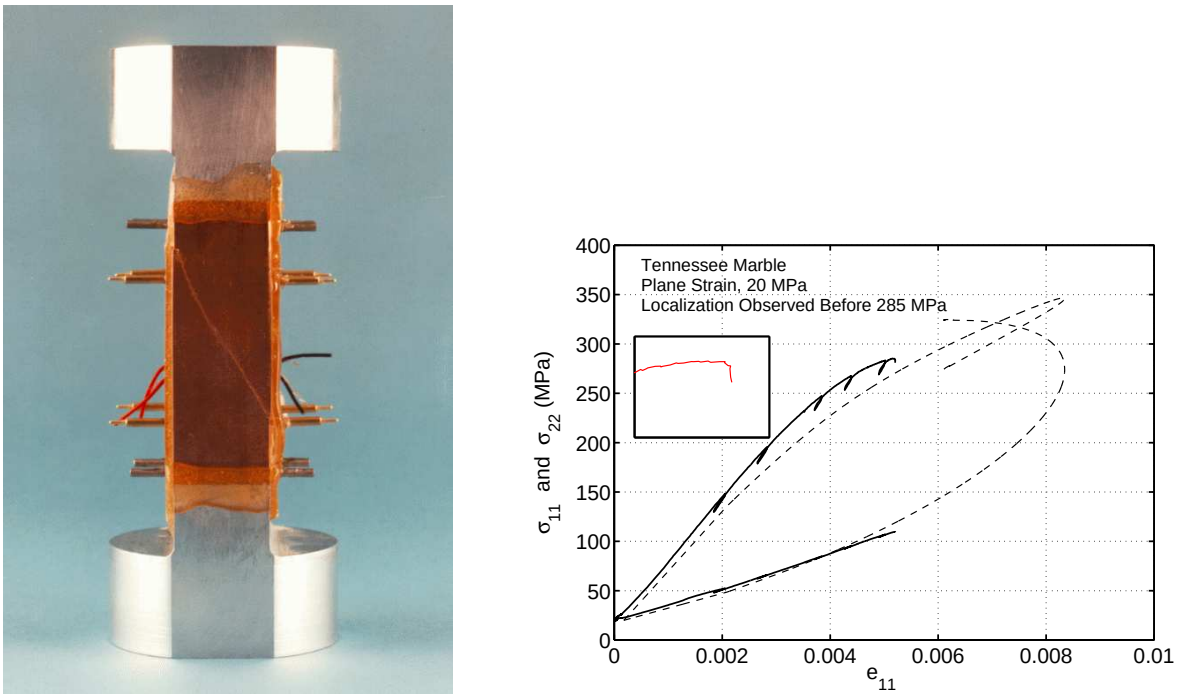

Figure 5.5. Rock failure: Tennesse marble (courtesy of D. Holcomb, Sandia).

5.1 Mohr-Coulomb (MC) plasticity

For Mohr-Coulomb (MC) plasticity, we recall the MC yield (or failure) criterion as

$$\tau_y = c - \sigma_y \tan\phi \tag{5.1}$$

where τ_y is the shear stress at yield on the failure plane, σ_y is the normal stress at yield on the failure plane, c is the cohesion (Pa), and ϕ is the friction angle (rad). Let us consider a sequence of Mohr-Circles at yield for various confining pressures with center $C = (\sigma_1 + \sigma_3)/2$ and radius $R = (\sigma_1 - \sigma_3)/2$, in Fig.5.6.

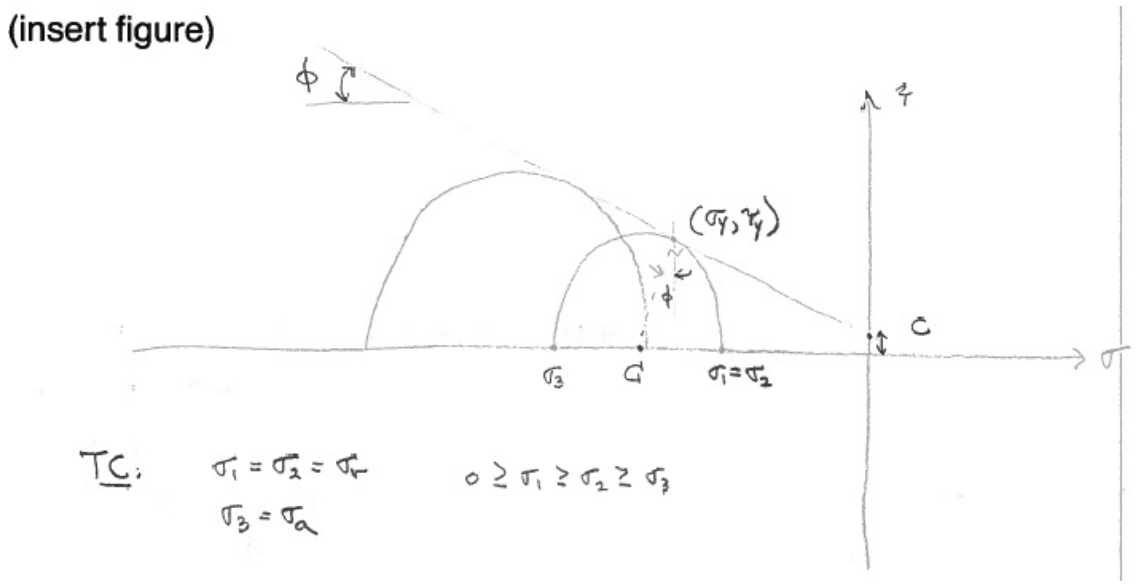

Figure 5.6. Plot of MC yield criterion.

Note that $\sin\phi = (\sigma_y - C)/R$ and $\cos\phi = \tau_y/R$. Substituting into the MC yield criterion,

we have

$$\tau_y = c - \sigma_y \tan\phi \tag{5.2}$$

$$\cos\phi(\sigma_1 - \sigma_3)/2 = c - \tan\phi(\sigma_1 + \sigma_3)/2 - (\sin^2\phi/\cos\phi)(\sigma_1 - \sigma_3)/2 \tag{5.3}$$

$$(\sigma_1 - \sigma_3) = 2c\cos\phi - (\sigma_1 + \sigma_3)\sin\phi \tag{5.4}$$

$$f(\sigma_1, \sigma_3) = (\sigma_1 - \sigma_3) - 2c\cos\phi + (\sigma_1 + \sigma_3)\sin\phi = 0 \tag{5.5}$$

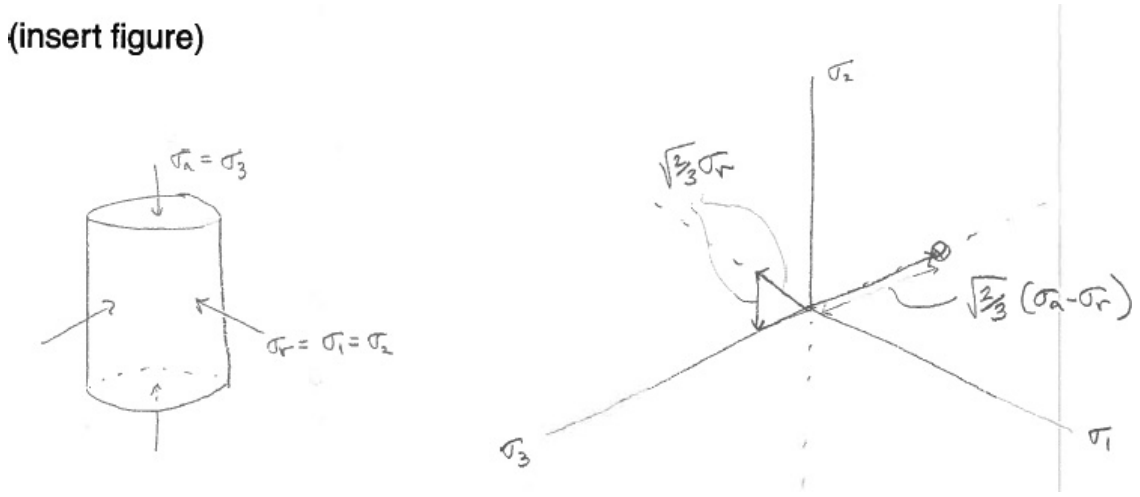

Figure 5.7. Stress path for conventional triaxial compression (TC).

Now, generalizing for 3D, we can write (at yield)

$$f(\sigma_1, \sigma_2, \sigma_3) = |\sigma_A - \sigma_B| - 2c\cos\phi + (\sigma_A + \sigma_B)\sin\phi = 0 \tag{5.6}$$

where $A, B = 1, 2, 3$, $A \neq B$, and for triaxial compression (TC), $\sigma_1 = \sigma_2 = \sigma_r$, $\sigma_3 = \sigma_a$ (decreases, increases in magnitude; see Fig.5.7), such that

$$|\sigma_1 - \sigma_3| = 2c\cos\phi - (\sigma_1 + \sigma_3)\sin\phi \tag{5.7}$$

$$|\sigma_2 - \sigma_3| = 2c\cos\phi - (\sigma_2 + \sigma_3)\sin\phi \tag{5.8}$$

For triaxial extension (TE), we have $\sigma_1 = \sigma_a$, $\sigma_2 = \sigma_3 = \sigma_r$ (decreases, increases in magnitude), such that

$$|\sigma_3 - \sigma_1| = 2c\cos\phi - (\sigma_3 + \sigma_1)\sin\phi \tag{5.9}$$

$$|\sigma_2 - \sigma_1| = 2c\cos\phi - (\sigma_2 + \sigma_1)\sin\phi \tag{5.10}$$

Figure 5.8 shows the two stress paths for TC and TE, and the difference in yield strength for these two loading conditions (if plotted on the same octahedral plane). Note that at the vertices, $\frac{\partial f}{\partial \boldsymbol{\sigma}}$ (or $\frac{\partial g}{\partial \boldsymbol{\sigma}}$) will be undefined (analytically). See Fig.5.9 for an illustration of the "Koiter fan."

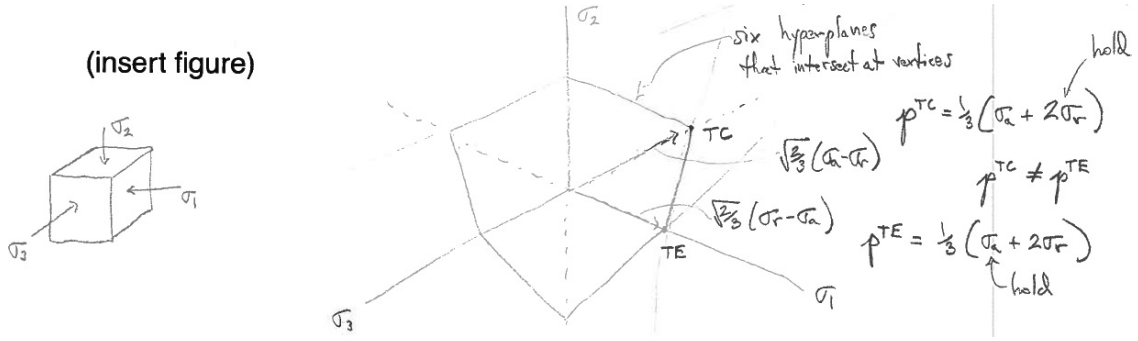

Figure 5.8. Stress path for conventional triaxial compression (TC) and triaxial extension (TE) for MC yield surface.

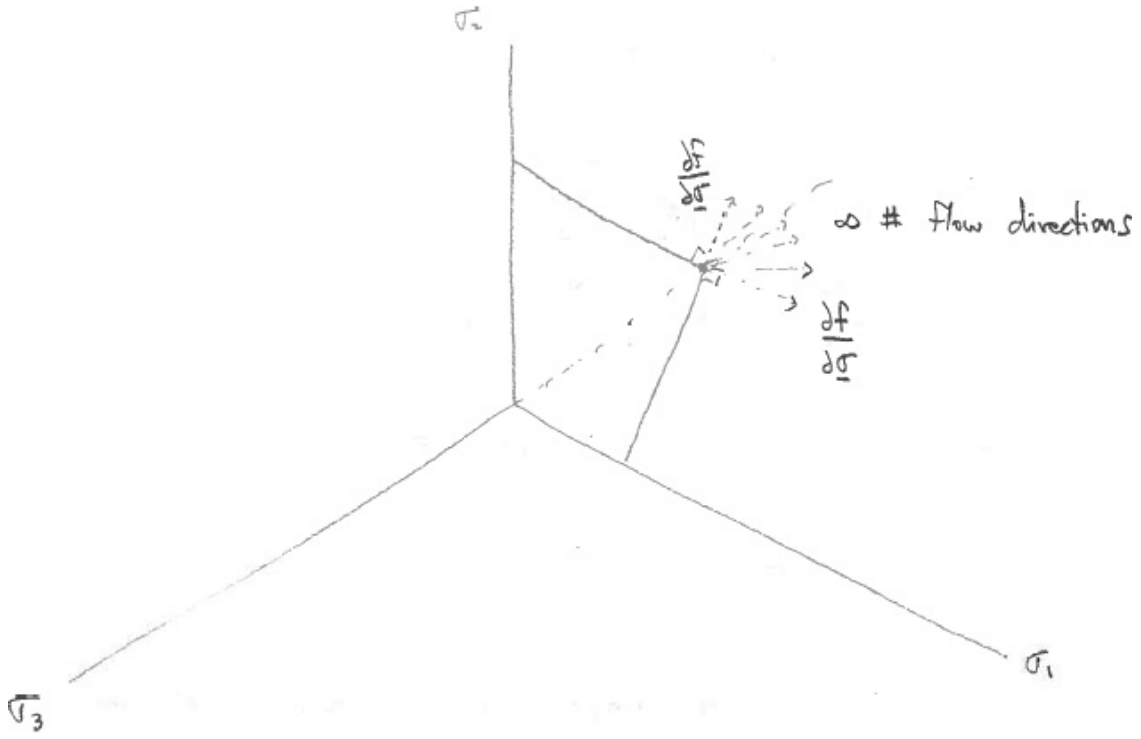

Figure 5.9. "Koiter fan" at vertex of MC yield surface. In theory, there are an infinite number of plastic flow directions at the vertices. For numerics, one gets chosen based on numerical precision.

We define a plastic potential function g as,

$$g(\sigma_1, \sigma_2, \sigma_3) = |\sigma_A - \sigma_B| - 2c\cos\psi + (\sigma_A + \sigma_B)\sin\psi \tag{5.11}$$

where $A, B = 1, 2, 3$, $A \neq B$, and $\psi < \phi$, where ψ is the dilation angle. Note that $g \neq f$ for non-associative plastic flow such that $\dot{\boldsymbol{\epsilon}}^p = \dot{\gamma}\frac{\partial g}{\partial \boldsymbol{\sigma}}$, and

$$\frac{\partial g}{\partial \sigma_A} = \text{sign}(\sigma_A - \sigma_B) + \sin\psi \ , \ \frac{\partial g}{\partial \sigma_B} = -\text{sign}(\sigma_A - \sigma_B) + \sin\psi \ , \ \frac{\partial g}{\partial \sigma_C} = 0 \tag{5.12}$$

where then

$$\dot{\epsilon}_v^{\text{p}} = tr(\dot{\boldsymbol{\epsilon}}^{\text{p}}) = 2\dot{\gamma}\sin\psi > 0 \text{ for } \psi > 0 \tag{5.13}$$

and

$$\dot{\epsilon}_A^p = \dot{\gamma}\frac{\partial g}{\partial \sigma_A} \ , \ \dot{\epsilon}_B^p = \dot{\gamma}\frac{\partial g}{\partial \sigma_B} \tag{5.14}$$

$$\text{shear} \implies \dot{\gamma} = \frac{(\dot{\epsilon}_A^{\text{p}} - \dot{\epsilon}_B^{\text{p}})/2}{\text{sign}(\sigma_A - \sigma_B)} = |\dot{\epsilon}_A^{\text{p}} - \dot{\epsilon}_B^{\text{p}}|/2 \tag{5.15}$$

$$\implies \sin\psi = \frac{\dot{\epsilon}_v^{\text{p}}}{2\dot{\gamma}} = \frac{\dot{\epsilon}_v^{\text{p}}}{|\dot{\epsilon}_A^{\text{p}} - \dot{\epsilon}_B^{\text{p}}|} > 0 \tag{5.16}$$

This is shear-induced dilation, illustrated in Fig.5.10.

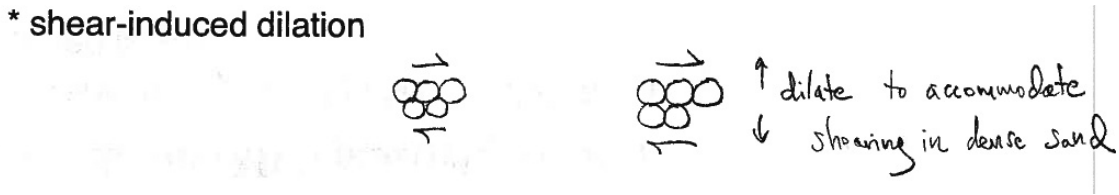

Figure 5.10. Demonstration of shear-induced dilatation for dense sand.

Now consider a constraint by the 2nd law of thermodynamics on the dilation angle ψ assuming perfect plasticity. The dissipation function $\mathcal{D}$ is written as,

$$\mathcal{D} = \boldsymbol{\sigma} : \dot{\boldsymbol{\epsilon}}^{\mathrm{p}} = \dot{\gamma} \sum_{A=1}^{3} \sigma_A \frac{\partial g}{\partial \sigma_A} \tag{5.17}$$

$$= \dot{\gamma} \left[|\sigma_A - \sigma_B| + (\sigma_A + \sigma_B) \sin\psi \right] \geq 0 \tag{5.18}$$

where for $f = 0$, $|\sigma_A - \sigma_B| = 2c\cos\phi - (\sigma_A + \sigma_B)\sin\phi$. Then

$$\dot{\gamma} \left[2c\cos\phi + (\sigma_A + \sigma_B)(\sin\psi - \sin\phi) \right] \geq 0 \tag{5.19}$$

where the Kuhn-Tucker conditions tell us $\dot{\gamma} \geq 0$, and for argument sake, assume cohesionless soil (e.g., sand, gravel) $c = 0$, then

$$\underbrace{(\sigma_A + \sigma_B)}_{<0}(\sin\psi - \sin\phi) \geq 0 \tag{5.20}$$

For positive plastic dissipation $\mathcal{D} \geq 0$, we have

$$\sin\psi - \sin\phi \leq 0 \Longrightarrow \sin\psi \leq \sin\phi \Longrightarrow \psi \leq \phi \tag{5.21}$$

The dilation angle ψ must be less than or equal to the friction angle ϕ to satisfy the Clausius-Duhem inequality (and second law of thermodynamics); the principle of maximum plastic dissipation is not satisfied by non-associative plasticity, but the plastic dissipation is positive, and the 2nd law is still satisfied.

5.2 Matsuoka-Nakai (MN) plasticity

We refer to Matsuoka and Nakai [1974], Borja et al. [2003] for a discussion of the Matsuoka-Nakai (MN) smooth yield surface approximation to the MC yield surface with vertices. The smooth approximation can make plasticity integration algorithms easier, not being concerned with vertices or the "Koiter fan" [Hughes, 1984] (i.e., infinite number of plastic flow directions at the vertex, in theory).

First, we define a stress $\bar{\boldsymbol{\sigma}} = \boldsymbol{\sigma} - \alpha \mathbf{1}$, where $\alpha = c \cot \phi$. Consider a spectral decomposition into principal stress directions $\boldsymbol{n}^A$ as

$$\bar{\boldsymbol{\sigma}} = \sum_{A=1}^{3} \bar{\sigma}_A \boldsymbol{m}^A \tag{5.22}$$

$$\bar{\sigma}_A = \sigma_A - \alpha \tag{5.23}$$

$$\boldsymbol{m}^A = \boldsymbol{n}^A \otimes \boldsymbol{n}^A \tag{5.24}$$

where $\bar{\sigma}_A$ is the eigenvalue, $\boldsymbol{n}^A$ the eigenvector, and $\boldsymbol{m}^A$ the spectral direction. Then the 3 stress invariants of $\bar{\boldsymbol{\sigma}}$ are

$$\bar{I}_1 = \bar{\sigma}_1 + \bar{\sigma}_2 + \bar{\sigma}_3 \tag{5.25}$$

$$\bar{I}_2 = \bar{\sigma}_1 \bar{\sigma}_2 + \bar{\sigma}_2 \bar{\sigma}_3 + \bar{\sigma}_1 \bar{\sigma}_3 \tag{5.26}$$

$$\bar{I}_3 = \bar{\sigma}_1 \bar{\sigma}_2 \bar{\sigma}_3 \tag{5.27}$$

These are used in formulating a yield function as (plotted by hand in Fig.5.11)

$$f = (\beta \bar{I}_3)^{1/3} - (\bar{I}_1 \bar{I}_2)^{1/3} \leq 0 \ , \quad \beta = \frac{9 - \sin^2 \phi}{1 - \sin^2 \phi} \tag{5.28}$$

where the plastic potential function $g = (b\bar{I}_3)^{1/3} - (\bar{I}_1 \bar{I}_2)^{1/3}$, and $b = \frac{9-\sin^2 \psi}{1-\sin^2 \psi}$, where $b \leq \beta$.

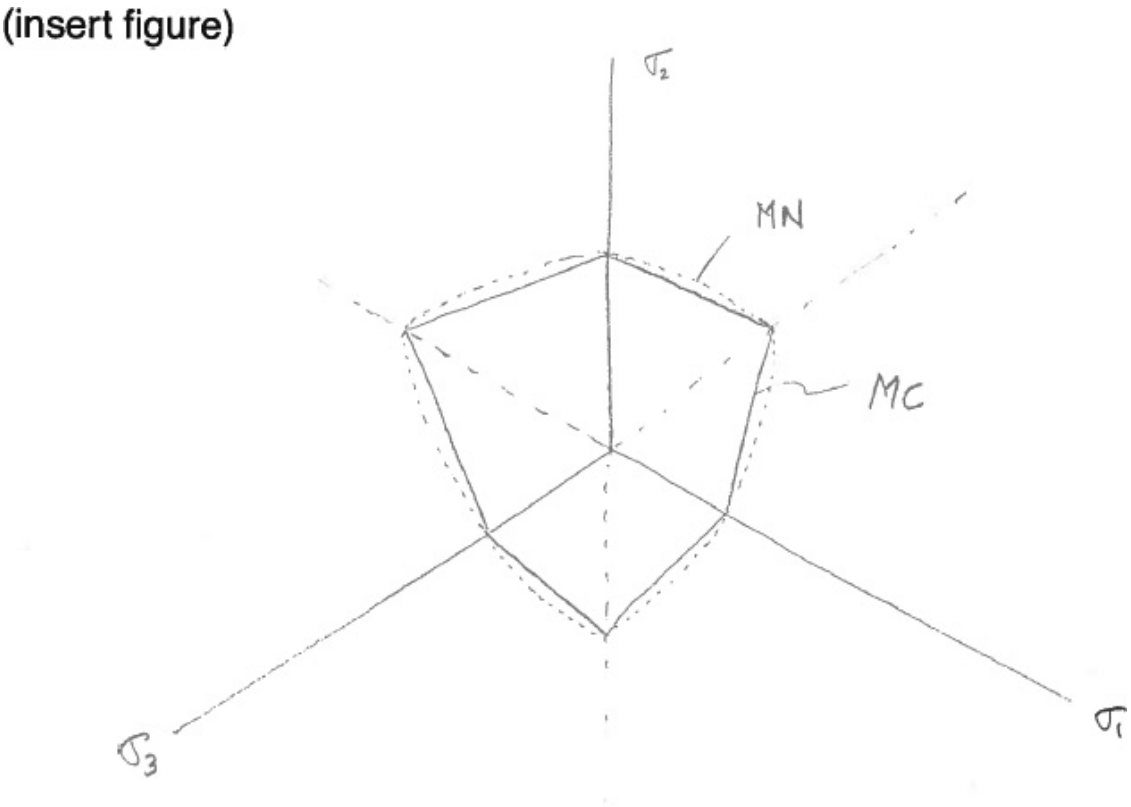

Figure 5.11. MN yield function smooth fit of MC yield surface vertices.

5.3 Drucker-Prager (DP) plasticity

Within the context of the MN yield function discussion in the previous section, we can write the yield function for Drucker-Prager (DP) plasticity [Drucker and Prager, 1952] which is also a smooth approximation to the MC yield surface as,

$$f = -(\beta \bar{I}_2)^{1/2} - \bar{I}_1 \leq 0 \tag{5.29}$$

$$\beta = \frac{(3+\sin\phi)^2}{3+2\sin\phi-\sin^2\phi} \quad \text{TE corner} \tag{5.30}$$

$$\beta = \frac{(3-\sin\phi)^2}{3-2\sin\phi-\sin^2\phi} \quad \text{TC corner} \tag{5.31}$$

See Fig.5.12 for a plot of $f = 0$ at the TE corner and TC corner.

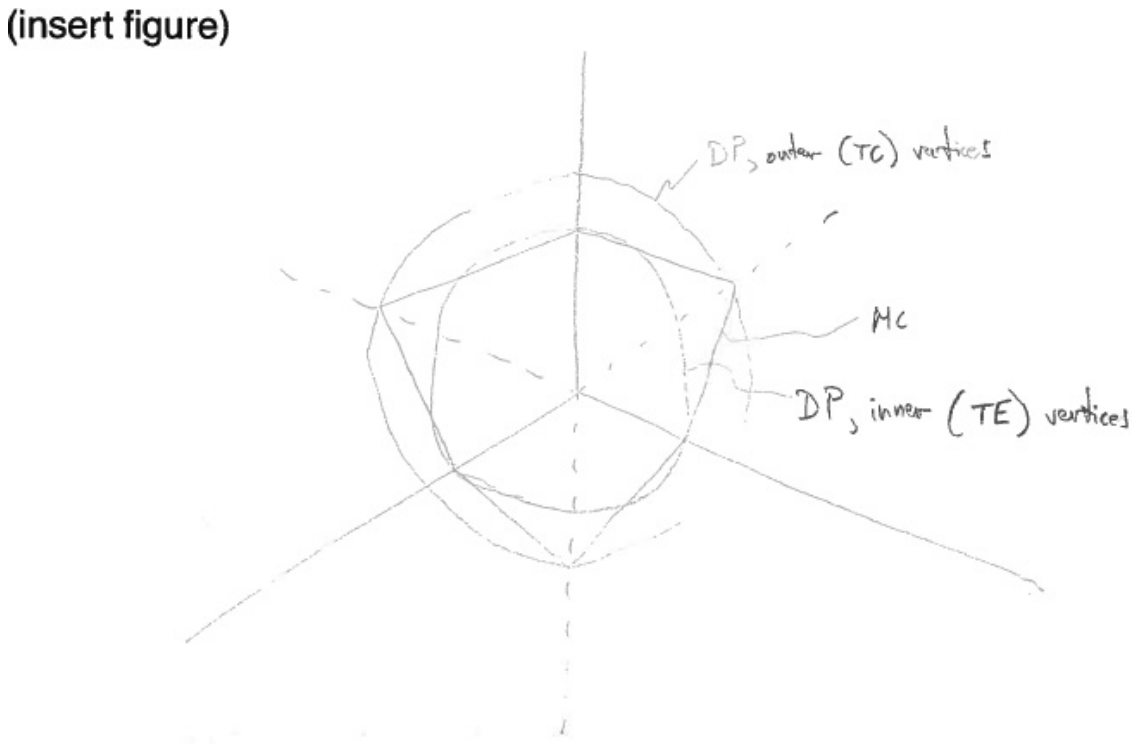

Figure 5.12. DP yield function smooth fit of MC yield surface vertices.

But we usually express the DP yield function differently as

$$f = \|\boldsymbol{s}\| - (A^{\phi}c - B^{\phi}p) \leq 0 \tag{5.32}$$

$$A^{\phi} = \frac{2\sqrt{6}\,\cos\phi}{3+\beta\sin\phi}\,, \quad B^{\phi} = \frac{2\sqrt{6}\sin\phi}{3+\beta\sin\phi}\,, \quad -1 \leq \beta \leq 1 \tag{5.33}$$

$$\beta = 1 \Longrightarrow \text{TE corner} \tag{5.34}$$

$$\beta = -1 \Longrightarrow \text{TC corner} \tag{5.35}$$

and for non-associative plastic flow (dilation angle $\psi \leq$ friction angle ϕ):

$$g = \|\boldsymbol{s}\| - (A^{\psi}c - B^{\psi}p) \tag{5.36}$$

$$A^{\psi} = \frac{2\sqrt{6}\,\cos\psi}{3+\beta\sin\psi}\,, \quad B^{\psi} = \frac{2\sqrt{6}\sin\psi}{3+\beta\sin\psi}\,, \quad -1 \leq \beta \leq 1 \tag{5.37}$$

If $\phi = \psi = 0$, we recover a form similar to J2 plasticity.

We will continue in more depth a presentation of the DP constitutive model equations, following the progression as presented for J2 plasticity.

The **Helmholtz free energy function** is written as

$$\rho\psi(\boldsymbol{\epsilon}^e, \boldsymbol{\zeta}) = \frac{1}{2}\boldsymbol{\epsilon}^{\mathrm{e}} : \boldsymbol{c}^{\mathrm{e}} : \boldsymbol{\epsilon}^{\mathrm{e}} + \frac{1}{2}\boldsymbol{\zeta}\cdot\boldsymbol{H}\cdot\boldsymbol{\zeta} \tag{5.38}$$

where then

$$\boldsymbol{\sigma} = \frac{\partial(\rho\psi)}{\partial\boldsymbol{\epsilon}^{\mathrm{e}}} = \boldsymbol{c}^{\mathrm{e}} : \boldsymbol{\epsilon}^{\mathrm{e}} \tag{5.39}$$

$$\boldsymbol{q}^{\zeta} = \frac{\partial(\rho\psi)}{\partial\boldsymbol{\zeta}} = \boldsymbol{H}\cdot\boldsymbol{\zeta} = \begin{bmatrix} c \\ \phi \\ \psi \\ \boldsymbol{\alpha} \end{bmatrix} \tag{5.40}$$

$$\boldsymbol{H} = \begin{bmatrix} H^{c} & & & \\ & H^{\phi} & & \\ & & H^{\psi} & \\ & & & H^{\alpha}\mathbf{1} \end{bmatrix} \tag{5.41}$$

The **yield and plastic potential functions** are written as

$$f(\boldsymbol{\sigma},\boldsymbol{q}^{\zeta}) = \|\boldsymbol{\xi}\| - (A^{\phi}c - B^{\phi}p) \leq 0 \tag{5.42}$$

$$g(\boldsymbol{\sigma},\boldsymbol{q}^{\zeta}) = \|\boldsymbol{\xi}\| - (A^{\psi}c - B^{\psi}p) \tag{5.43}$$

where then the **plastic flow rule** becomes

$$\dot{\boldsymbol{\epsilon}}^{\mathrm{p}} = \dot{\gamma}\frac{\partial g}{\partial\boldsymbol{\sigma}} = \dot{\gamma}\left(\frac{\partial\|\boldsymbol{\xi}\|}{\partial\boldsymbol{\sigma}} + B^{\psi}\frac{\partial p}{\partial\boldsymbol{\sigma}}\right) \tag{5.44}$$

$$= \dot{\gamma}\left(\hat{\boldsymbol{n}} + \frac{1}{3}B^{\psi}\mathbf{1}\right) \tag{5.45}$$

$$\dot{\epsilon}_{v}^{\mathrm{p}} = tr\dot{\boldsymbol{\epsilon}}^{\mathrm{p}} = \dot{\gamma}B^{\psi} \tag{5.46}$$

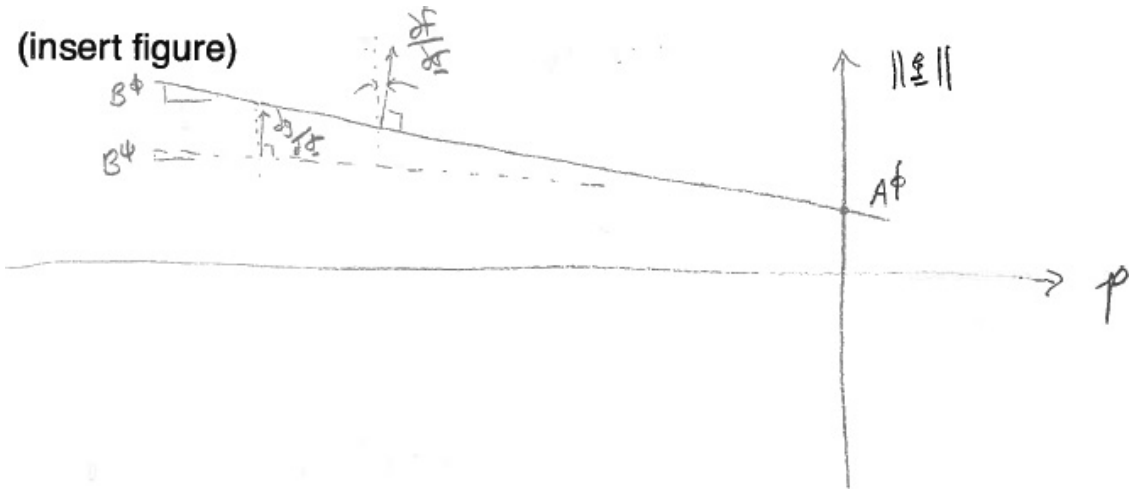

Figure 5.13. DP yield and plastic potential functions and non-associativity.

The **ISV evolution equations** are written as

$$\dot{\boldsymbol{\zeta}} = \dot{\gamma}\boldsymbol{h}(\boldsymbol{\sigma}, \boldsymbol{q}^\zeta) = \dot{\gamma}\begin{bmatrix} h_c(\boldsymbol{\sigma}, \boldsymbol{q}^\zeta) \\ h_\phi(\boldsymbol{\sigma}, \boldsymbol{q}^\zeta) \\ h_\psi(\boldsymbol{\sigma}, \boldsymbol{q}^\zeta) \\ \boldsymbol{h}_\alpha(\boldsymbol{\sigma}, \boldsymbol{q}^\zeta) \end{bmatrix} \tag{5.47}$$

$$\dot{\boldsymbol{q}}^\zeta = \dot{\gamma}\boldsymbol{H} \cdot \boldsymbol{h}(\boldsymbol{\sigma}, \boldsymbol{q}^\zeta) \tag{5.48}$$

Recall the principle of maximum plastic dissipation that states $\boldsymbol{h} = -\frac{\partial f}{\partial \boldsymbol{q}^\zeta}$. Because $\frac{\partial f}{\partial \psi} = 0$, we can make the modification $h_\psi = -\frac{\partial g}{\partial \psi}$, then

$$\boldsymbol{h} = \begin{bmatrix} -\frac{\partial f}{\partial c} \\ -\frac{\partial f}{\partial \phi} \\ -\frac{\partial g}{\partial \psi} \\ -\frac{\partial f}{\partial \boldsymbol{\alpha}} \end{bmatrix} = \begin{bmatrix} A^\phi \\ \frac{\partial A^\phi}{\partial \phi}c - \frac{\partial B^\phi}{\partial \phi}p \\ \frac{\partial A^\psi}{\partial \psi}c - \frac{\partial B^\psi}{\partial \psi}p \\ \hat{\boldsymbol{n}} \end{bmatrix}, \quad \dot{\boldsymbol{q}}^\zeta = \dot{\gamma}\underbrace{\begin{bmatrix} H^c A^\phi \\ H^\phi\left(\frac{\partial A^\phi}{\partial \phi}c - \frac{\partial B^\phi}{\partial \phi}p\right) \\ H^\psi\left(\frac{\partial A^\psi}{\partial \psi}c - \frac{\partial B^\psi}{\partial \psi}p\right) \\ H^\alpha \hat{\boldsymbol{n}} \end{bmatrix}}_{\boldsymbol{h}^q(\boldsymbol{\sigma}, \boldsymbol{q}^\zeta)} \tag{5.49}$$

We can then write the **consistency condition** $\dot{f} = 0$ as

$$\dot{\gamma} = \frac{1}{\chi}\frac{\partial f}{\partial \boldsymbol{\sigma}} : \boldsymbol{c}^{\mathrm{e}} : \dot{\boldsymbol{\epsilon}} \tag{5.50}$$

$$\chi = \frac{\partial f}{\partial \boldsymbol{\sigma}} : \boldsymbol{c}^{\mathrm{e}} : \frac{\partial g}{\partial \boldsymbol{\sigma}} - \frac{\partial f}{\partial \boldsymbol{q}^{\zeta}} \cdot \boldsymbol{H} \cdot \boldsymbol{h} \tag{5.51}$$

$$\boldsymbol{c}^{\mathrm{ep}} = \boldsymbol{c}^{\mathrm{e}} - \frac{1}{\chi}\boldsymbol{c}^{\mathrm{e}} : \frac{\partial g}{\partial \boldsymbol{\sigma}} \otimes \frac{\partial f}{\partial \boldsymbol{\sigma}} : \boldsymbol{c}^{\mathrm{e}} \tag{5.52}$$

For numerical integration and implementation, it turns out that the system of ODEs to solve using Backward Euler would be nonlinear, requiring Newton-Raphson to solve (we will show later how to setup this nonlinear solution algorithm). In order to simplify the formulation further to demonstrate the numerical integration, we can consider perfect plasticity for friction and dilation angles, such that $H^{\phi} = H^{\psi} = 0$. This leads to the following evolution equations to solve using Backward Euler:

$$\dot{\boldsymbol{\sigma}} = \boldsymbol{c}^{\mathrm{e}} : \left(\dot{\boldsymbol{\epsilon}} - \dot{\gamma}\frac{\partial g}{\partial \boldsymbol{\sigma}}\right) \tag{5.53}$$

$$\frac{\partial g}{\partial \boldsymbol{\sigma}} = \hat{\boldsymbol{n}} + \frac{1}{3}B^{\psi}\mathbf{1}$$

$$\dot{c} = \dot{\gamma}H^{c}A^{\phi} \tag{5.54}$$

$$\dot{\boldsymbol{\alpha}} = \dot{\gamma}H^{\alpha}\hat{\boldsymbol{n}} \tag{5.55}$$

$$\dot{f} = 0 \tag{5.56}$$

There are 4 first-order ODEs, and 4 unknowns $(\boldsymbol{\sigma}, c, \boldsymbol{\alpha}, \gamma)$ to solve. Using Backward Euler

integration (implicit, first order accurate) to numerically integrate in time, we have

$$\begin{aligned}
\boldsymbol{\sigma}_{n+1} &= \boldsymbol{\sigma}^{\mathrm{tr}}_{n+1} - \Delta\gamma\left(KB^{\psi}\mathbf{1} + 2\mu\hat{\boldsymbol{n}}_{n+1}\right) && (5.57)\\
&\quad \boldsymbol{\sigma}^{\mathrm{tr}}_{n+1} = \boldsymbol{\sigma}_n + \boldsymbol{c}^e : \Delta\boldsymbol{\epsilon}\\
&\quad p_{n+1} = p^{\mathrm{tr}}_{n+1} - KB^{\psi}\Delta\gamma\\
&\quad \boldsymbol{s}_{n+1} = \boldsymbol{s}^{\mathrm{tr}}_{n+1} - 2\mu\Delta\gamma\hat{\boldsymbol{n}}_{n+1} && (5.58)\\
c_{n+1} &= c_n + A^{\phi}H^c\Delta\gamma && (5.59)\\
\boldsymbol{\alpha}_{n+1} &= \boldsymbol{\alpha}_n + H^{\alpha}\Delta\gamma\hat{\boldsymbol{n}}_{n+1} && (5.60)\\
f_{n+1} &= \|\boldsymbol{\xi}_{n+1}\| - (A^{\phi}c_{n+1} - B^{\phi}p_{n+1}) = 0 && (5.61)
\end{aligned}$$

Again, it is possible to show that $\hat{\boldsymbol{n}}_{n+1} = \hat{\boldsymbol{n}}^{\mathrm{tr}}_{n+1}$ (show yourself).

We summarize the **return mapping algorithm** as follows: given $\Delta\boldsymbol{\epsilon}$ over a time step, and $\boldsymbol{\sigma}_n$, c_n, $\boldsymbol{\alpha}_n$, γ_n from the past coverged time t_n, we have

1. compute trial stress $\boldsymbol{\sigma}^{\mathrm{tr}}_{n+1} = \boldsymbol{\sigma}_n + \boldsymbol{c}^{\mathrm{e}} : \Delta\boldsymbol{\epsilon}$, and $p^{\mathrm{tr}}_{n+1} = \frac{1}{3}tr(\boldsymbol{\sigma}^{\mathrm{tr}}_{n+1})$, $\boldsymbol{s}^{\mathrm{tr}}_{n+1} = \boldsymbol{\sigma}^{\mathrm{tr}}_{n+1} - p^{\mathrm{tr}}_{n+1}\mathbf{1}$, $\boldsymbol{\xi}^{\mathrm{tr}}_{n+1} = \boldsymbol{s}^{\mathrm{tr}}_{n+1} - \boldsymbol{\alpha}_n$, $\hat{\boldsymbol{n}}^{\mathrm{tr}} = \boldsymbol{\xi}^{\mathrm{tr}}_{n+1}/\|\boldsymbol{\xi}^{\mathrm{tr}}_{n+1}\|$

2. check for yielding: trial yield function $f^{\mathrm{tr}}_{n+1} = \|\boldsymbol{\xi}^{\mathrm{tr}}_{n+1}\| - (A^{\phi}c_n - B^{\phi}p^{\mathrm{tr}}_{n+1})$

$$\begin{aligned}
\text{if}\quad & f^{\mathrm{tr}}_{n+1} > 0 \quad \text{plastic} && \text{go to step 3}\\
\text{else}\quad & f^{\mathrm{tr}}_{n+1} < 0 \quad \text{elastic}: && \boldsymbol{\sigma}_{n+1} = \boldsymbol{\sigma}^{\mathrm{tr}}_{n+1}\\
& && \boldsymbol{\alpha}_{n+1} = \boldsymbol{\alpha}_n \qquad (5.62)\\
& && c_{n+1} = c_n\\
& && \gamma_{n+1} = \gamma_n
\end{aligned}$$

3. compute $\Delta\gamma = \frac{f_{n+1}^{\rm tr}}{2\mu+KB^{\phi}B^{\psi}+H^{\alpha}+H^{c}(A^{\phi})^2}$, and update:

$$
\begin{aligned}
p_{n+1} &= p_{n+1}^{\rm tr} - KB^{\psi}\Delta\gamma \\
\boldsymbol{s}_{n+1} &= \boldsymbol{s}_{n+1}^{\rm tr} - 2\mu\Delta\gamma\hat{\boldsymbol{n}}^{\rm tr} \\
\boldsymbol{\alpha}_{n+1} &= \boldsymbol{\alpha}_{n} + H^{\alpha}\Delta\gamma\hat{\boldsymbol{n}}^{\rm tr} \\
c_{n+1} &= c_n + H^{c}A^{\phi}\Delta\gamma \\
\gamma_{n+1} &= \gamma_n + \Delta\gamma
\end{aligned}
\tag{5.63}
$$

Now, the **material consistent tangent** can be derived as follows,

$$
\boldsymbol{\sigma} = \boldsymbol{\sigma}^{\rm tr} - \Delta\gamma(KB^{\psi}\mathbf{1} + 2\mu\hat{\boldsymbol{n}}^{\rm tr}) \tag{5.64}
$$

$$
\frac{\partial\boldsymbol{\sigma}}{\partial\boldsymbol{\epsilon}} = \frac{\partial\boldsymbol{\sigma}^{\rm tr}}{\partial\boldsymbol{\epsilon}} - \underbrace{(KB^{\psi}\mathbf{1} + 2\mu\hat{\boldsymbol{n}}^{\rm tr})}_{(\hat{\boldsymbol{m}}^{\psi})^{\rm tr}} \otimes \frac{\partial\Delta\gamma}{\partial\boldsymbol{\epsilon}} - 2\mu\Delta\gamma\frac{\partial\hat{\boldsymbol{n}}^{\rm tr}}{\partial\boldsymbol{\epsilon}} \tag{5.65}
$$

$$
\frac{\partial\Delta\gamma}{\partial\boldsymbol{\epsilon}} = \frac{1}{\chi}\left(\frac{\partial\|\boldsymbol{\xi}^{\rm tr}\|}{\partial\boldsymbol{\epsilon}} + B^{\phi}\frac{\partial p^{\rm tr}}{\partial\boldsymbol{\epsilon}}\right) = \frac{1}{\chi}(\hat{\boldsymbol{m}}^{\phi})^{\rm tr} \tag{5.66}
$$

$$
\chi = 2\mu + KB^{\phi}B^{\psi} + H^{\alpha} + H^{c}(A^{\phi})^2 \tag{5.67}
$$

$$
\frac{\partial\|\boldsymbol{\xi}^{\rm tr}\|}{\partial\boldsymbol{\epsilon}} = 2\mu\hat{\boldsymbol{n}}^{\rm tr}\ , \quad \frac{\partial p^{\rm tr}}{\partial\boldsymbol{\epsilon}} = K\mathbf{1}
$$

$$
\frac{\partial\hat{\boldsymbol{n}}^{\rm tr}}{\partial\boldsymbol{\epsilon}} = \frac{2\mu}{\|\boldsymbol{\xi}^{\rm tr}\|}\left(\boldsymbol{I} - \frac{1}{3}\mathbf{1}\otimes\mathbf{1} - \hat{\boldsymbol{n}}^{\rm tr}\otimes\hat{\boldsymbol{n}}^{\rm tr}\right) \tag{5.68}
$$

$$
\begin{aligned}
\frac{\partial\boldsymbol{\sigma}}{\partial\boldsymbol{\epsilon}} &= \boldsymbol{c}^{\rm e} - \frac{1}{\chi}(\hat{\boldsymbol{m}}^{\psi})^{\rm tr}\otimes(\hat{\boldsymbol{m}}^{\phi})^{\rm tr} \\
&\quad -\frac{(2\mu)^2\Delta\gamma}{\|\boldsymbol{\xi}^{\rm tr}\|}\left(\boldsymbol{I} - \frac{1}{3}\mathbf{1}\otimes\mathbf{1} - \hat{\boldsymbol{n}}^{\rm tr}\otimes\hat{\boldsymbol{n}}^{\rm tr}\right)
\end{aligned}
\tag{5.69}
$$

Recall the continuum elastoplastic tangent as

$$\begin{aligned}
\boldsymbol{c}^{\mathrm{ep}} &= \boldsymbol{c}^{\mathrm{e}} - \frac{1}{\chi}\boldsymbol{c}^{\mathrm{e}} : \frac{\partial g}{\partial \boldsymbol{\sigma}} \otimes \frac{\partial f}{\partial \boldsymbol{\sigma}} : \boldsymbol{c}^{\mathrm{e}} && (5.70)\\
& \frac{\partial f}{\partial \boldsymbol{\sigma}} = \frac{1}{3}B^{\phi}\mathbf{1} + \hat{\boldsymbol{n}} \ , \quad \frac{\partial g}{\partial \boldsymbol{\sigma}} = \frac{1}{3}B^{\psi}\mathbf{1} + \hat{\boldsymbol{n}} && (5.71)\\
& \frac{\partial f}{\partial \boldsymbol{\sigma}} : \boldsymbol{c}^{\mathrm{e}} = (\hat{\boldsymbol{m}}^{\phi})^{\mathrm{tr}} \ , \quad \boldsymbol{c}^{\mathrm{e}} : \frac{\partial g}{\partial \boldsymbol{\sigma}} = (\hat{\boldsymbol{m}}^{\psi})^{\mathrm{tr}} && (5.72)\\
& \frac{\partial f}{\partial \boldsymbol{\sigma}} : \boldsymbol{c}^{\mathrm{e}} : \frac{\partial g}{\partial \boldsymbol{\sigma}} = KB^{\phi}B^{\psi} + 2\mu && (5.73)\\
& \chi = \frac{\partial f}{\partial \boldsymbol{\sigma}} : \boldsymbol{c}^{\mathrm{e}} : \frac{\partial g}{\partial \boldsymbol{\sigma}} - \frac{\partial f}{\partial \boldsymbol{q}^{\zeta}} \cdot \boldsymbol{H} \cdot \boldsymbol{h}(\boldsymbol{\sigma}, \boldsymbol{q}^{\zeta}) = 2\mu + KB^{\phi}B^{\psi} + H^{\alpha} + H^{c}(A^{\phi})^2 \\
\boldsymbol{c}^{\mathrm{ep}} &= \boldsymbol{c}^{\mathrm{e}} - \frac{1}{\chi}(\hat{\boldsymbol{m}}^{\psi})^{\mathrm{tr}} \otimes (\hat{\boldsymbol{m}}^{\phi})^{\mathrm{tr}} && (5.74)
\end{aligned}$$

Then, we can rewrite the consistent tangent as

$$\frac{\partial \boldsymbol{\sigma}}{\partial \boldsymbol{\epsilon}} = \boldsymbol{c}^{\mathrm{ep}} - \Delta\gamma \frac{(2\mu)^2}{\|\boldsymbol{\xi}^{\mathrm{tr}}\|}\left(\boldsymbol{I} - \frac{1}{3}\mathbf{1}\otimes\mathbf{1} - \hat{\boldsymbol{n}}^{\mathrm{tr}} \otimes \hat{\boldsymbol{n}}^{\mathrm{tr}}\right) \quad (5.75)$$

5.4 Nonlinear Drucker-Prager (DP) plasticity

Here, we consider the case of the fully nonlinear form of the Drucker-Prager (DP) plasticity model, where each ISV could be dependent upon the other. To start, recall the Backward Euler integrated evolution equations for the stress and ISVs, written in residual form, leaving off the $n+1$ subscript, as

$$\boldsymbol{R}(\boldsymbol{X}) = \boldsymbol{0} \quad , \qquad \boldsymbol{X} = \begin{bmatrix} \boldsymbol{\sigma} \\ \boldsymbol{q}^\zeta \\ \Delta\gamma \end{bmatrix} \tag{5.76}$$

$$\boldsymbol{R} = \begin{bmatrix} \boldsymbol{R}^\sigma \\ \boldsymbol{R}^q \\ R^\gamma \end{bmatrix} = \begin{bmatrix} \boldsymbol{\sigma} - \boldsymbol{\sigma}_n - \boldsymbol{c}^{\mathrm{e}} : \Delta\boldsymbol{\epsilon} + \Delta\gamma \boldsymbol{c}^{\mathrm{e}} : \frac{\partial g}{\partial \boldsymbol{\sigma}} \\ -\boldsymbol{q}^\zeta + \boldsymbol{q}_n^\zeta + \Delta\gamma \boldsymbol{h}^q \\ f \end{bmatrix} = \boldsymbol{0} \tag{5.77}$$

We then linearize for solution by the Newton-Raphson method for the unknown variable $\boldsymbol{X}$ (which contains the stress $\boldsymbol{\sigma}$, ISVs $\boldsymbol{q}^\zeta$, and increment of plastic multiplier $\Delta\gamma$) as

$$\boldsymbol{R}^{k+1} = \boldsymbol{R}^k + \left.\frac{\partial \boldsymbol{R}}{\partial \boldsymbol{X}}\right|_k \cdot \delta\boldsymbol{X} \approx \boldsymbol{0} \tag{5.78}$$

$$\frac{\partial \boldsymbol{R}}{\partial \boldsymbol{X}} = \begin{bmatrix} \frac{\partial \boldsymbol{R}^\sigma}{\partial \boldsymbol{\sigma}} & \frac{\partial \boldsymbol{R}^\sigma}{\partial \boldsymbol{q}^\zeta} & \frac{\partial \boldsymbol{R}^\sigma}{\partial \Delta\gamma} \\ \frac{\partial \boldsymbol{R}^q}{\partial \boldsymbol{\sigma}} & \frac{\partial \boldsymbol{R}^q}{\partial \boldsymbol{q}^\zeta} & \frac{\partial \boldsymbol{R}^q}{\partial \Delta\gamma} \\ \frac{\partial R^\gamma}{\partial \boldsymbol{\sigma}} & \frac{\partial R^\gamma}{\partial \boldsymbol{q}^\zeta} & \frac{\partial R^\gamma}{\partial \Delta\gamma} \end{bmatrix} \tag{5.79}$$

$$= \begin{bmatrix} \boldsymbol{I} + \Delta\gamma \boldsymbol{c}^{\mathrm{e}} : \frac{\partial^2 g}{\partial \boldsymbol{\sigma} \partial \boldsymbol{\sigma}} & \Delta\gamma \boldsymbol{c}^{\mathrm{e}} : \frac{\partial^2 g}{\partial \boldsymbol{\sigma} \partial \boldsymbol{q}^\zeta} & \boldsymbol{c}^{\mathrm{e}} : \frac{\partial g}{\partial \boldsymbol{\sigma}} \\ \Delta\gamma \frac{\partial \boldsymbol{h}^q}{\partial \boldsymbol{\sigma}} & -\boldsymbol{1} + \Delta\gamma \frac{\partial \boldsymbol{h}^q}{\partial \boldsymbol{q}^\zeta} & \boldsymbol{h}^q \\ \frac{\partial f}{\partial \boldsymbol{\sigma}} & \frac{\partial f}{\partial \boldsymbol{q}^\zeta} & 0 \end{bmatrix} \tag{5.80}$$

For iteration k, we rewrite the first two equations as

$$\begin{bmatrix} \boldsymbol{R}^{\sigma} \\ \boldsymbol{R}^{q} \end{bmatrix} + \boldsymbol{D} \cdot \begin{bmatrix} \delta\boldsymbol{\sigma} \\ \delta\boldsymbol{q}^{\zeta} \end{bmatrix} + \delta(\Delta\gamma) \begin{bmatrix} \boldsymbol{c}^{e} : \frac{\partial g}{\partial \boldsymbol{\sigma}} \\ \boldsymbol{h}^{q} \end{bmatrix} = \boldsymbol{0} \tag{5.81}$$

and then multiply by $\boldsymbol{D}^{-1}$ to obtain,

$$\boldsymbol{D}^{-1} \cdot \begin{bmatrix} \boldsymbol{R}^{\sigma} \\ \boldsymbol{R}^{q} \end{bmatrix} + \begin{bmatrix} \delta\boldsymbol{\sigma} \\ \delta\boldsymbol{q}^{\zeta} \end{bmatrix} + \delta(\Delta\gamma)\boldsymbol{D}^{-1} \cdot \begin{bmatrix} \boldsymbol{c}^{e} : \frac{\partial g}{\partial \boldsymbol{\sigma}} \\ \boldsymbol{h}^{q} \end{bmatrix} = \boldsymbol{0} \tag{5.82}$$

$$\delta(\Delta\gamma)\boldsymbol{D}^{-1} \cdot \begin{bmatrix} \boldsymbol{c}^{e} : \frac{\partial g}{\partial \boldsymbol{\sigma}} \\ \boldsymbol{h}^{q} \end{bmatrix} = -\boldsymbol{D}^{-1} \cdot \begin{bmatrix} \boldsymbol{R}^{\sigma} \\ \boldsymbol{R}^{q} \end{bmatrix} - \begin{bmatrix} \delta\boldsymbol{\sigma} \\ \delta\boldsymbol{q}^{\zeta} \end{bmatrix} \tag{5.83}$$

Then, multiply by $\begin{bmatrix} \frac{\partial f}{\partial \boldsymbol{\sigma}} & \frac{\partial f}{\partial \boldsymbol{q}^{\zeta}} \end{bmatrix}$ to obtain

$$\begin{aligned} \delta(\Delta\gamma) \begin{bmatrix} \frac{\partial f}{\partial \boldsymbol{\sigma}} & \frac{\partial f}{\partial \boldsymbol{q}^{\zeta}} \end{bmatrix} \cdot \boldsymbol{D}^{-1} \cdot \begin{bmatrix} \boldsymbol{c}^{e} : \frac{\partial g}{\partial \boldsymbol{\sigma}} \\ \boldsymbol{h}^{q} \end{bmatrix} = \\ - \begin{bmatrix} \frac{\partial f}{\partial \boldsymbol{\sigma}} & \frac{\partial f}{\partial \boldsymbol{q}^{\zeta}} \end{bmatrix} \cdot \boldsymbol{D}^{-1} \cdot \begin{bmatrix} \boldsymbol{R}^{\sigma} \\ \boldsymbol{R}^{q} \end{bmatrix} \underbrace{- \begin{bmatrix} \frac{\partial f}{\partial \boldsymbol{\sigma}} & \frac{\partial f}{\partial \boldsymbol{q}^{\zeta}} \end{bmatrix} \cdot \begin{bmatrix} \delta\boldsymbol{\sigma} \\ \delta\boldsymbol{q}^{\zeta} \end{bmatrix}}_{-f} \end{aligned} \tag{5.84}$$

We solve for the iteration increment of the time increment of the plastic mulitiplier $\delta(\Delta\gamma)$ as

$$\delta(\Delta\gamma) = \frac{f - \begin{bmatrix} \frac{\partial f}{\partial \boldsymbol{\sigma}} & \frac{\partial f}{\partial \boldsymbol{q}^\zeta} \end{bmatrix} \cdot \boldsymbol{D}^{-1} \cdot \begin{bmatrix} \boldsymbol{R}^\sigma \\ \boldsymbol{R}^q \end{bmatrix}}{\begin{bmatrix} \frac{\partial f}{\partial \boldsymbol{\sigma}} & \frac{\partial f}{\partial \boldsymbol{q}^\zeta} \end{bmatrix} \cdot \boldsymbol{D}^{-1} \cdot \begin{bmatrix} \boldsymbol{c}^e : \frac{\partial g}{\partial \boldsymbol{\sigma}} \\ \boldsymbol{h}^q \end{bmatrix}} \tag{5.85}$$

Then substitute back in to update the stress $\boldsymbol{\sigma}$ and ISVs $\boldsymbol{q}^\zeta$ as

$$\begin{bmatrix} \delta\boldsymbol{\sigma} \\ \delta\boldsymbol{q}^\zeta \end{bmatrix} = -\boldsymbol{D} \cdot \begin{bmatrix} \boldsymbol{R}^\sigma + \delta(\Delta\gamma)\boldsymbol{c}^e : \frac{\partial g}{\partial \boldsymbol{\sigma}} \\ \boldsymbol{R}^q + \delta(\Delta\gamma)\boldsymbol{h}^q \end{bmatrix} \tag{5.86}$$

Then check for convergence.

Now, we show how to calculate the **material consistent tangent** $\frac{\partial \boldsymbol{\sigma}}{\partial \boldsymbol{\epsilon}}$. Recall the residual form of the integrated equations, but pre-multiplying by $(\boldsymbol{c}^{\mathrm{e}})^{-1}$ as

$$\begin{bmatrix} (\boldsymbol{c}^{\mathrm{e}})^{-1} : \boldsymbol{\sigma} - (\boldsymbol{c}^{\mathrm{e}})^{-1} : \boldsymbol{\sigma}_n - \Delta\boldsymbol{\epsilon} + \Delta\gamma\frac{\partial g}{\partial \boldsymbol{\sigma}} \\ -\boldsymbol{q}^\zeta + \boldsymbol{q}_n^\zeta + \Delta\gamma\boldsymbol{h}^q \\ f \end{bmatrix} = \boldsymbol{0} \tag{5.87}$$

Take derivatives w.r.t. $\boldsymbol{\epsilon}$ at iteration $k+1$ and time t_{n+1} to obtain

$$\begin{bmatrix} (\boldsymbol{c}^{\mathrm{e}})^{-1} : \frac{\partial \boldsymbol{\sigma}}{\partial \boldsymbol{\epsilon}} - \boldsymbol{I} + \frac{\partial g}{\partial \boldsymbol{\sigma}} \otimes \frac{\partial \Delta\gamma}{\partial \boldsymbol{\epsilon}} + \Delta\gamma(\frac{\partial^2 g}{\partial \boldsymbol{\sigma} \partial \boldsymbol{q}^\zeta} \cdot \frac{\partial \boldsymbol{q}^\zeta}{\partial \boldsymbol{\epsilon}} + \frac{\partial^2 g}{\partial \boldsymbol{\sigma} \partial \boldsymbol{\sigma}} : \frac{\partial \boldsymbol{\sigma}}{\partial \boldsymbol{\epsilon}}) \\ -\frac{\partial \boldsymbol{q}^\zeta}{\partial \boldsymbol{\epsilon}} + \boldsymbol{h}^q \otimes \frac{\partial \Delta\gamma}{\partial \boldsymbol{\epsilon}} + \Delta\gamma(\frac{\partial \boldsymbol{h}^q}{\partial \boldsymbol{q}^\zeta} \cdot \frac{\partial \boldsymbol{q}^\zeta}{\partial \boldsymbol{\epsilon}} + \frac{\partial \boldsymbol{h}^q}{\partial \boldsymbol{\sigma}} : \frac{\partial \boldsymbol{\sigma}}{\partial \boldsymbol{\epsilon}}) \\ \frac{\partial f}{\partial \boldsymbol{q}^\zeta} \cdot \frac{\partial \boldsymbol{q}^\zeta}{\partial \boldsymbol{\epsilon}} + \frac{\partial f}{\partial \boldsymbol{\sigma}} : \frac{\partial \boldsymbol{\sigma}}{\partial \boldsymbol{\epsilon}} \end{bmatrix} = \boldsymbol{0}$$

$$\begin{bmatrix} (\boldsymbol{c}^{\mathrm{e}})^{-1} + \Delta\gamma \frac{\partial^2 g}{\partial \boldsymbol{\sigma} \partial \boldsymbol{\sigma}} & \Delta\gamma \frac{\partial^2 g}{\partial \boldsymbol{\sigma} \partial \boldsymbol{q}^\zeta} & \frac{\partial g}{\partial \boldsymbol{\sigma}} \\ \Delta\gamma \frac{\partial \boldsymbol{h}^q}{\partial \boldsymbol{\sigma}} & -\boldsymbol{1} + \Delta\gamma \frac{\partial \boldsymbol{h}^q}{\partial \boldsymbol{q}^\zeta} & \boldsymbol{h}^q \\ \frac{\partial f}{\partial \boldsymbol{\sigma}} & \frac{\partial f}{\partial \boldsymbol{q}^\zeta} & 0 \end{bmatrix} \cdot \begin{bmatrix} \frac{\partial \boldsymbol{\sigma}}{\partial \boldsymbol{\epsilon}} \\ \frac{\partial \boldsymbol{q}^\zeta}{\partial \boldsymbol{\epsilon}} \\ (\frac{\partial \Delta\gamma}{\partial \boldsymbol{\epsilon}})^T \end{bmatrix} = \begin{bmatrix} \boldsymbol{I} \\ \boldsymbol{0} \\ 0 \end{bmatrix} \tag{5.88}$$

We assign the following notation

$$\boldsymbol{B} = \begin{bmatrix} (\boldsymbol{c}^{\mathrm{e}})^{-1} + \Delta\gamma \frac{\partial^2 g}{\partial \boldsymbol{\sigma} \partial \boldsymbol{\sigma}} & \Delta\gamma \frac{\partial^2 g}{\partial \boldsymbol{\sigma} \partial \boldsymbol{q}^\zeta} \\ \Delta\gamma \frac{\partial \boldsymbol{h}^q}{\partial \boldsymbol{\sigma}} & -\boldsymbol{1} + \Delta\gamma \frac{\partial \boldsymbol{h}^q}{\partial \boldsymbol{q}^\zeta} \end{bmatrix} \tag{5.89}$$

and then,

$$\boldsymbol{B} \cdot \begin{bmatrix} \frac{\partial \boldsymbol{\sigma}}{\partial \boldsymbol{\epsilon}} \\ \frac{\partial \boldsymbol{q}^\zeta}{\partial \boldsymbol{\epsilon}} \end{bmatrix} + \begin{bmatrix} \frac{\partial g}{\partial \boldsymbol{\sigma}} \\ \boldsymbol{h}^q \end{bmatrix} \cdot \left(\frac{\partial \Delta\gamma}{\partial \boldsymbol{\epsilon}} \right)^T = \begin{bmatrix} \boldsymbol{I} \\ \boldsymbol{0} \end{bmatrix} \tag{5.90}$$

$$\begin{bmatrix} \frac{\partial f}{\partial \boldsymbol{\sigma}} & \frac{\partial f}{\partial \boldsymbol{q}^\zeta} \end{bmatrix} \cdot \begin{bmatrix} \frac{\partial \boldsymbol{\sigma}}{\partial \boldsymbol{\epsilon}} \\ \frac{\partial \boldsymbol{q}^\zeta}{\partial \boldsymbol{\epsilon}} \end{bmatrix} = 0 \tag{5.91}$$

We multiply by $\boldsymbol{B}^{-1}$ and $\left[\begin{array}{cc} \frac{\partial f}{\partial \boldsymbol{\sigma}} & \frac{\partial f}{\partial \boldsymbol{q}^\zeta} \end{array}\right]$ to obtain

$$\underbrace{\left[\begin{array}{cc} \frac{\partial f}{\partial \boldsymbol{\sigma}} & \frac{\partial f}{\partial \boldsymbol{q}^\zeta} \end{array}\right] \cdot \left[\begin{array}{c} \frac{\partial \boldsymbol{\sigma}}{\partial \boldsymbol{\epsilon}} \\ \frac{\partial \boldsymbol{q}^\zeta}{\partial \boldsymbol{\epsilon}} \end{array}\right]}_{=0} + \underbrace{\left[\begin{array}{cc} \frac{\partial f}{\partial \boldsymbol{\sigma}} & \frac{\partial f}{\partial \boldsymbol{q}^\zeta} \end{array}\right] \cdot \boldsymbol{B}^{-1} \cdot \left[\begin{array}{c} \frac{\partial g}{\partial \boldsymbol{\sigma}} \\ \boldsymbol{h}^q \end{array}\right]}_{e} \cdot (\frac{\partial \Delta\gamma}{\partial \boldsymbol{\epsilon}})^T =$$

$$\left[\begin{array}{cc} \frac{\partial f}{\partial \boldsymbol{\sigma}} & \frac{\partial f}{\partial \boldsymbol{q}^\zeta} \end{array}\right] \cdot \boldsymbol{B}^{-1} \cdot \left[\begin{array}{c} \boldsymbol{I} \\ \boldsymbol{0} \end{array}\right] \tag{5.92}$$

$$\Longrightarrow (\frac{\partial \Delta\gamma}{\partial \boldsymbol{\epsilon}})^T = \frac{1}{e} \left[\begin{array}{cc} \frac{\partial f}{\partial \boldsymbol{\sigma}} & \frac{\partial f}{\partial \boldsymbol{q}^\zeta} \end{array}\right] \cdot \boldsymbol{B}^{-1} \cdot \left[\begin{array}{c} \boldsymbol{I} \\ \boldsymbol{0} \end{array}\right] \tag{5.93}$$

We then substitute and solve for $\frac{\partial \boldsymbol{\sigma}}{\partial \boldsymbol{\epsilon}}$ as

$$\left[\begin{array}{c} \frac{\partial \boldsymbol{\sigma}}{\partial \boldsymbol{\epsilon}} \\ \frac{\partial \boldsymbol{q}^\zeta}{\partial \boldsymbol{\epsilon}} \end{array}\right] = \boldsymbol{B}^{-1} \cdot \left[\begin{array}{c} \boldsymbol{I} \\ \boldsymbol{0} \end{array}\right] - \frac{1}{e} \cdot \boldsymbol{B}^{-1} \cdot \left[\begin{array}{c} \frac{\partial g}{\partial \boldsymbol{\sigma}} \\ \boldsymbol{h}^q \end{array}\right] \cdot \left[\begin{array}{cc} \frac{\partial f}{\partial \boldsymbol{\sigma}} & \frac{\partial f}{\partial \boldsymbol{q}^\zeta} \end{array}\right] \cdot \boldsymbol{B}^{-1} \cdot \left[\begin{array}{c} \boldsymbol{I} \\ \boldsymbol{0} \end{array}\right] \tag{5.94}$$

We then take the upper 6×6 matrix for the 3D $\frac{\partial \boldsymbol{\sigma}}{\partial \boldsymbol{\epsilon}}$, after putting in vector-matrix form.

This page intentionally left blank.

Chapter 6

Mixture Theory, Poromechanics, and FE Implementation at Small Strain

Much of the content in this chapter is taken from Borja [2004], Li et al. [2004], de Boer [2005], Regueiro and Ebrahimi [2010], Regueiro et al. [2014].

We assume geometric linearity (i.e., small strains *and* small rotations). However, for discussion purposes, it is meaningful to introduce some nonlinear continuum mechanics concepts [Holzapfel, 2000].

An outline of the remaining sections is as follows:

1. formulate differential form of coupled balance of mass and linear momentum, and apply boundary conditions (BCs) to provide the Strong Form (S).

2. formulate coupled, variational, Weak Form (W).

3. state coupled, discrete, Galerkin Form (G).

4. formulate coupled, Finite Element (FE), Matrix-Vector form in 2D plane strain, using mixed quadrilateral element.

5. provide example of element assembly to obtain Global Matrix form, assuming linear isotropic elasticity and no dependence of porosity on solid skeleton volumetric strain ϵ_v.

6. conduct time integration using generalized trapezoidal rule.

7. include nonlinearity: porosity dependence on solid skeleton deformation (small strain), and nonlinear material constitutive model.

8. introduce inertia terms for dynamic mixture theory and FE implementation, and solution by Newmark time integration and Newton-Raphson.

6.1 Coupled balance of mass and linear momentum, Strong Form (S)

The concept of volume fraction for a solid and fluid mixture (porous solid skeleton saturated with a pore fluid) is shown in Fig.6.1.

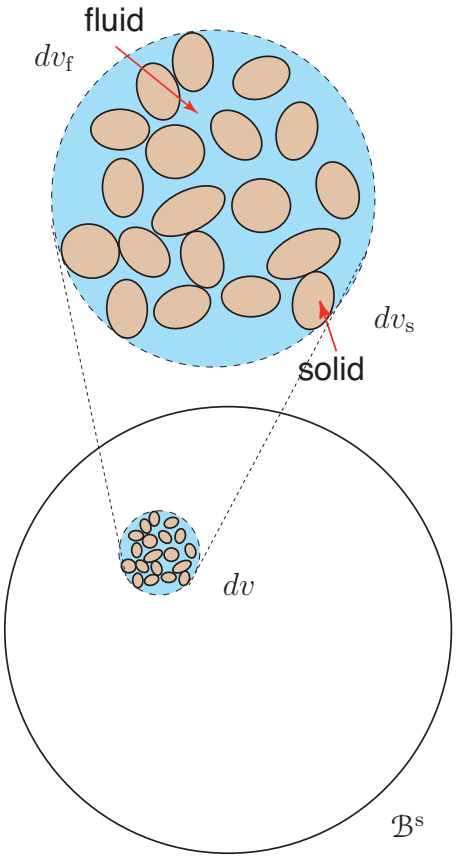

*theory of porous media assumes control space is that of the solid phase $\mathcal{B} = \mathcal{B}^{\mathrm{s}}$

$$
\begin{aligned}
n^{\alpha}(\boldsymbol{x},t) &= dv_{\alpha}/dv \\
&\sum_{\alpha} n^{\alpha} = 1\,, \quad n^{\mathrm{f}} + n^{\mathrm{s}} = 1 \\
&dv = \sum_{\alpha} dv_{\alpha}
\end{aligned}
$$

- $n^{\alpha}(\boldsymbol{x},t)$ = volume fraction of constituent α in $dv \subset \mathcal{B}$, where $\mathcal{B} = \mathcal{B}^{\mathrm{s}}$
- dv_{α} = differential volume of constituent α in dv

$$
\begin{aligned}
m_{\alpha} &= \int_{\mathcal{B}^{\alpha}} dm_{\alpha} = \int_{\mathcal{B}^{\alpha}} \rho^{\alpha R} dv_{\alpha} = \int_{\mathcal{B}} \rho^{\alpha R} n^{\alpha} dv = \int_{\mathcal{B}} \rho^{\alpha} dv \\
\rho^{\alpha R}(\boldsymbol{x},t) &= dm_{\alpha}/dv_{\alpha} \\
\rho^{\alpha}(\boldsymbol{x},t) &= dm_{\alpha}/dv = \rho^{\alpha R}(\boldsymbol{x},t) n^{\alpha}(\boldsymbol{x},t)
\end{aligned}
$$

- dm_{α} = differential mass of constituent α
- $\rho^{\alpha R}(\boldsymbol{x},t)$ = real mass density of constituent α
- $\rho^{\alpha}(\boldsymbol{x},t)$ = partial mass density of constituent α

Figure 6.1. Concept of volume fraction for biphasic (solid-fluid) mixture theory, showing solid skeleton composed of contacting grains. Mixture theory is a continuum assumption.

The kinematics of biphasic solid-fluid mixture theory are shown in Fig.6.2.

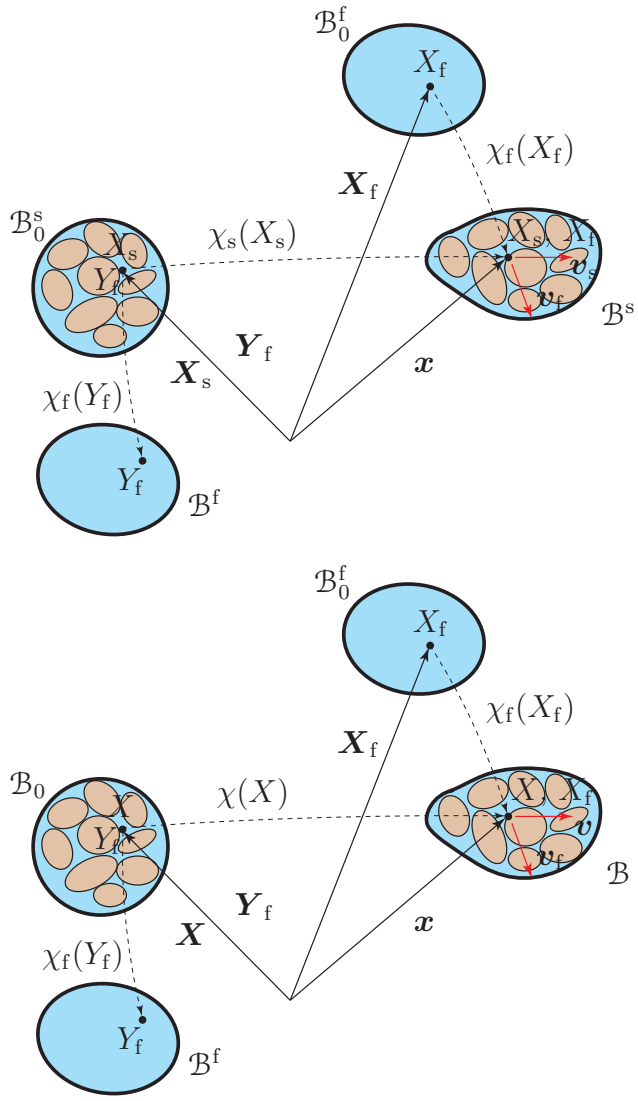

- $\boldsymbol{x}$ = spatial position vector, which is simultaneously occupied by all constituent material points $X_{\rm s}, X_{\rm f}$ of the mixture (homogenized, or smeared)

$$\boldsymbol{x} \;=\; \boldsymbol{\chi}_{\rm f}(\boldsymbol{X}_{\rm f}, t) = \boldsymbol{\chi}_{\rm s}(\boldsymbol{X}_{\rm s}, t)$$

- drop the s designation since control space is that of the solid skeleton

$$\boldsymbol{x} \;=\; \boldsymbol{\chi}_{\rm f}(\boldsymbol{X}_{\rm f}, t) = \boldsymbol{\chi}(\boldsymbol{X}, t)$$

Figure 6.2. Kinematics of a biphasic (solid-fluid) mixture theory, showing solid skeleton composed of contacting grains. The continuum assumption of mixture theory is evident in the assumption that solid and fluid constituents *coexist* at the current position $\boldsymbol{x}$.

Likewise, the volumetric deformation of a solid-fluid mixture, that is smeared in the current configuration at spatial position vector $\boldsymbol{x}$, is shown in Fig.6.3.

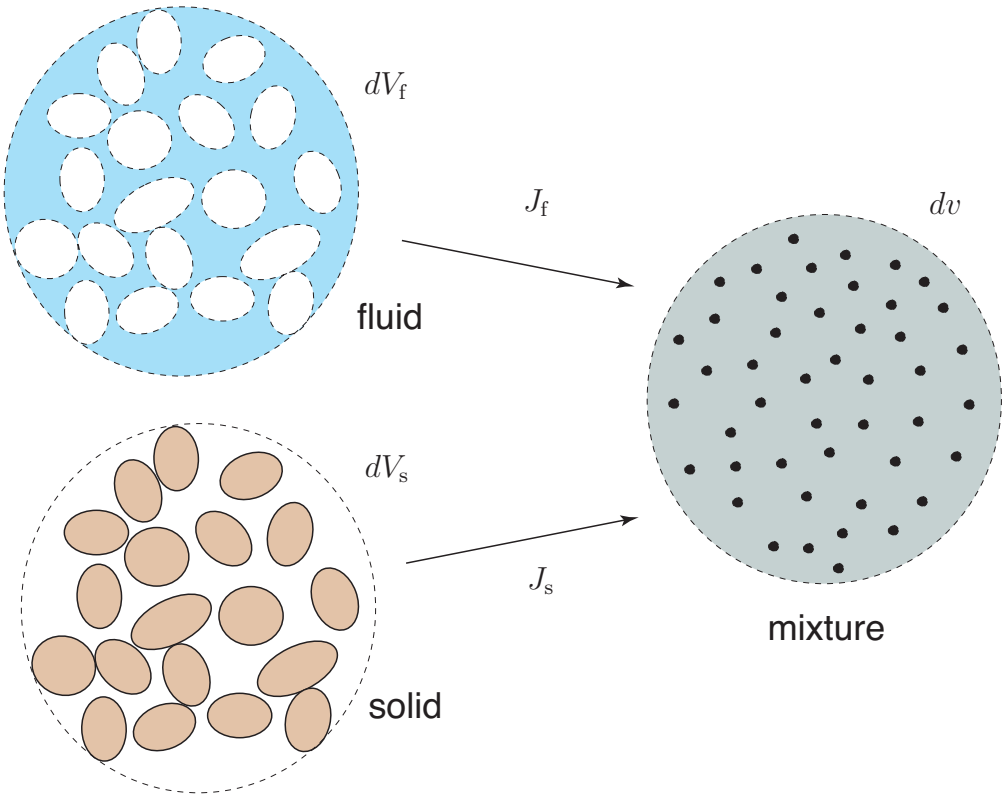

Figure 6.3. Volumetric deformation of solid and fluid constituents in a biphasic mixture (solid skeleton composed of contacting solid grains). Because the respective deformation gradients $\boldsymbol{F}_\mathrm{s}$ (or just $\boldsymbol{F}$) and $\boldsymbol{F}_\mathrm{f}$ map material points X_s (with differential volume dV_s, or dV) and Y_f (with differential volume dV_f) to current position $\boldsymbol{x}$ (with differential volume dv), the volumetric deformations through the Jacobians J_s (normally called J because in theory of porous media, one follows the motion of the solid skeleton) and J_f *smear the two constituents under volume change to the current differential volume* dv *at position* $\boldsymbol{x}$.

The Jacobian of deformation for the two constituents is written as

$$J_\mathrm{s} = \det\boldsymbol{F}_\mathrm{s} > 0\ ; \quad J_\mathrm{f} = \det\boldsymbol{F}_\mathrm{f} > 0 \tag{6.1}$$

$$dv = J_\mathrm{s} dV_\mathrm{s} = J_\mathrm{f} dV_\mathrm{f} \tag{6.2}$$

$$dv_\alpha = n^\alpha dv = n^\alpha J_\alpha dV_\alpha \tag{6.3}$$

$$dV_\mathrm{f} \subset \mathcal{B}_0^\mathrm{f}\ , \quad dV_\mathrm{s} \subset \mathcal{B}_0^\mathrm{s} \tag{6.4}$$

where we will typically drop the s superscripts and subscripts because the theory of porous

media assumes we follow the motion of the solid skeleton.

We can similarly reshow the three figures demonstrating the concept of volume fraction and kinematics for a biphasic solid-fluid mixture, but for the solid skeleton composed of alveolar tissue which makes up the lung parenchyma, Figs.6.4-6.6.

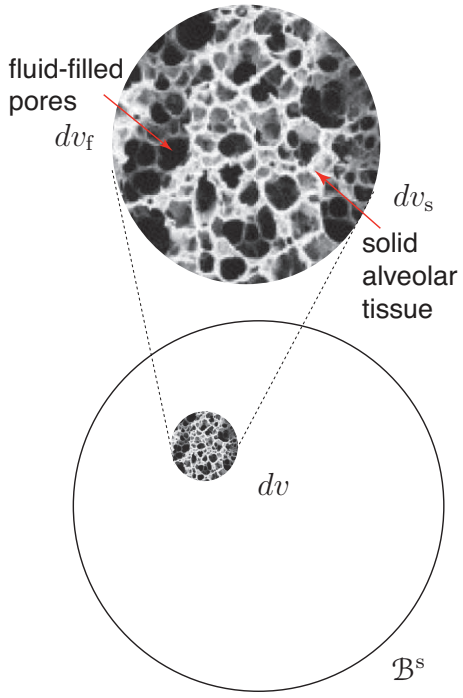

*theory of porous media assumes control space is that of the solid phase $\mathcal{B} = \mathcal{B}^{\mathrm{s}}$

$$
\begin{aligned}
n^{\alpha}(\boldsymbol{x},t) &= dv_{\alpha}/dv \\
&\sum_{\alpha} n^{\alpha} = 1\,, \quad n^{\mathrm{f}} + n^{\mathrm{s}} = 1 \\
&dv = \sum_{\alpha} dv_{\alpha}
\end{aligned}
$$

- $n^{\alpha}(\boldsymbol{x},t)$ = volume fraction of constituent α in $dv \subset \mathcal{B}$, where $\mathcal{B} = \mathcal{B}^{\mathrm{s}}$
- dv_{α} = differential volume of constituent α in dv

$$
\begin{aligned}
m_{\alpha} &= \int_{\mathcal{B}^{\alpha}} \rho^{\alpha R} dv_{\alpha} = \int_{\mathcal{B}} \rho^{\alpha R} n^{\alpha} dv = \int_{\mathcal{B}} \rho^{\alpha} dv \\
\rho^{\alpha R}(\boldsymbol{x},t) &= dm_{\alpha}/dv_{\alpha} \\
\rho^{\alpha}(\boldsymbol{x},t) &= dm_{\alpha}/dv = \rho^{\alpha R}(\boldsymbol{x},t) n^{\alpha}(\boldsymbol{x},t)
\end{aligned}
$$

- dm_{α} = differential mass of constituent α
- $\rho^{\alpha R}(\boldsymbol{x},t)$ = real mass density of constituent α
- $\rho^{\alpha}(\boldsymbol{x},t)$ = partial mass density of constituent α

Figure 6.4. Concept of volume fraction for biphasic (solid-fluid) mixture theory, showing solid skeleton composed of alveolar tissue.

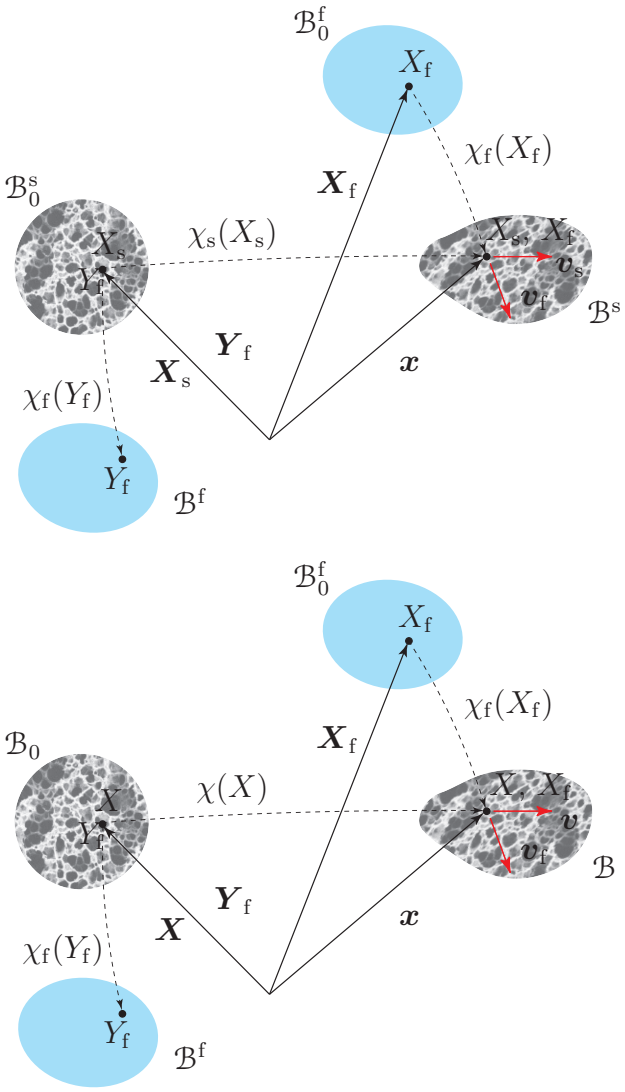

- $\boldsymbol{x}$ = spatial position vector, which is simultaneously occupied by all constituent material points $X_{\mathrm{s}}, X_{\mathrm{f}}$ of the mixture (homogenized, or smeared)

$$\boldsymbol{x} = \boldsymbol{\chi}_{\mathrm{f}}(\boldsymbol{X}_{\mathrm{f}}, t) = \boldsymbol{\chi}_{\mathrm{s}}(\boldsymbol{X}_{\mathrm{s}}, t) \qquad (6.5)$$

  *material point X_{s} is mapped from reference position $\boldsymbol{X}_{\mathrm{s}}$ to current position $\boldsymbol{x}$ through mapping χ_{s}

  *can define inverse map $\boldsymbol{X}_\alpha = \boldsymbol{\chi}_\alpha^{-1}(\boldsymbol{x}, t)$, assuming smoothly differentiable fields

- deformation gradient:

$$\boldsymbol{F}_\alpha = \frac{\partial \boldsymbol{\chi}_\alpha}{\partial \boldsymbol{X}_\alpha}\,, \quad \boldsymbol{F}_\alpha^{-1} = \frac{\partial \boldsymbol{X}_\alpha}{\partial \boldsymbol{x}}$$

- drop the s designation since control space is that of the solid skeleton: $\boldsymbol{x} = \boldsymbol{\chi}_{\mathrm{f}}(\boldsymbol{X}_{\mathrm{f}}, t) = \boldsymbol{\chi}(\boldsymbol{X}, t)$

Figure 6.5. Kinematics of a biphasic (solid-fluid) mixture theory, showing solid skeleton composed of alveolar tissue. The continuum assumption of mixture theory is evident in the assumption that solid and fluid constituents *coexist* at the current position $\boldsymbol{x}$.

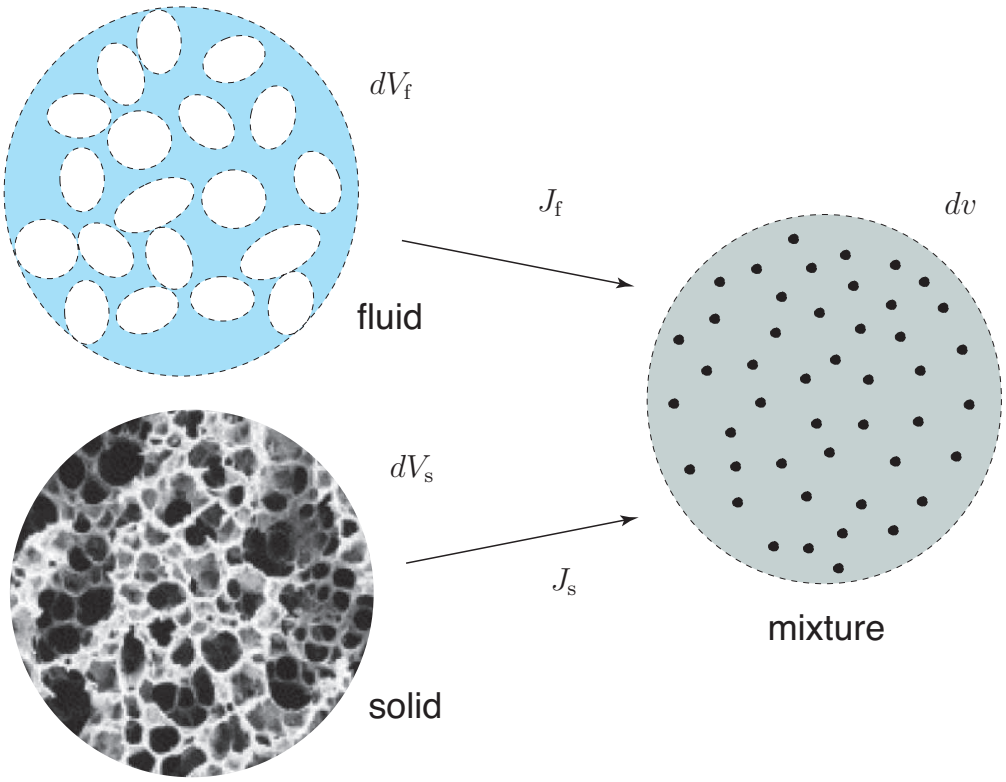

Figure 6.6. Volumetric deformation of solid and fluid constituents in a biphasic mixture (solid skeleton composed of alveolar tissue of the lung parenchyma).

Material time derivative of scalar spatial field $\psi(\boldsymbol{x},t)$, referring to Holzapfel [2000], de Boer [2005], is written **following the solid skeleton motion** as,

$$\frac{D^{\mathrm{s}}\psi(\boldsymbol{\chi}_{\mathrm{s}}(\boldsymbol{X}_{\mathrm{s}},t),t)}{Dt}=\frac{\partial\psi(\boldsymbol{x},t)}{\partial t}+\frac{\partial\psi(\boldsymbol{x},t)}{\partial\boldsymbol{x}}\frac{\partial\boldsymbol{\chi}_{\mathrm{s}}}{\partial t}=\frac{\partial\psi}{\partial t}+\mathrm{grad}\psi\cdot\boldsymbol{v}_{\mathrm{s}} \tag{6.6}$$

where we will drop the s designation because we follow the motion of the solid skeleton. **Following the pore fluid motion**, it is written as,

$$\frac{D^{\mathrm{f}}\psi(\boldsymbol{\chi}_{\mathrm{f}}(\boldsymbol{X}_{\mathrm{f}},t),t)}{Dt}=\frac{\partial\psi(\boldsymbol{x},t)}{\partial t}+\frac{\partial\psi(\boldsymbol{x},t)}{\partial\boldsymbol{x}}\frac{\partial\boldsymbol{\chi}_{\mathrm{f}}}{\partial t}=\frac{\partial\psi}{\partial t}+\mathrm{grad}\psi\cdot\boldsymbol{v}_{\mathrm{f}} \tag{6.7}$$

For the **balance of mass of the mixture**, we write separately the balance of mass of each constituent, solid and fluid, expressing all material time derivatives in terms of the solid skeleton motion, and then add the two equations together to obtain the balance of mass of the mixture. The total mass of constituent α in $\mathcal{B}$ is written as

$$m_{\alpha}=\int_{\mathcal{B}}\rho^{\alpha}dv=\int_{\mathcal{B}_0^{\alpha}}\rho^{\alpha}J_{\alpha}dV_{\alpha} \tag{6.8}$$

Taking the material time derivative of this spatial field with respect to the motion of constituent α, we can express the balance of mass of constituent α as

$$\frac{D^{\alpha}m_{\alpha}}{Dt}=\int_{\mathcal{B}_0^{\alpha}}\frac{D^{\alpha}(\rho^{\alpha}J_{\alpha})}{Dt}dV_{\alpha}=0 \tag{6.9}$$

where we currently ignore sources and sinks for now, and ignore chemical reaction between constituents (i.e., no mass exchange between constituents, such as dissolving solid into fluid, or precipitating fluid into solid). We can find that $D^{\alpha}J_{\alpha}/Dt=J_{\alpha}\mathrm{div}\boldsymbol{v}_{\alpha}$ [Holzapfel, 2000, de Boer, 2005] from,

$$\frac{D^{\alpha}J_{\alpha}}{Dt}=\frac{D^{\alpha}(\det\boldsymbol{F}_{\alpha})}{Dt}=J_{\alpha}\boldsymbol{F}_{\alpha}^{-T}:\frac{D^{\alpha}\boldsymbol{F}_{\alpha}}{Dt}=J_{\alpha}\frac{\partial X_{I(\alpha)}}{\partial x_i}\frac{\partial v_{i(\alpha)}(\boldsymbol{X}_{\alpha},t)}{\partial X_{I(\alpha)}}=J_{\alpha}\mathrm{div}\boldsymbol{v}_{\alpha} \tag{6.10}$$

We have

$$\frac{D^\alpha m_\alpha}{Dt} = \int_{\mathcal{B}} \left(\frac{D^\alpha \rho^\alpha}{Dt} + \rho^\alpha \mathrm{div} \boldsymbol{v}_\alpha \right) dv = 0 \tag{6.11}$$

and localizing the integral,

$$\frac{D^\alpha \rho^\alpha}{Dt} + \rho^\alpha \mathrm{div} \boldsymbol{v}_\alpha = 0 \tag{6.12}$$

Then, for each solid and fluid constituent, the balance of mass is written as,

$$\frac{D^\mathrm{s} \rho^\mathrm{s}}{Dt} + \rho^\mathrm{s} \mathrm{div} \boldsymbol{v}_\mathrm{s} = 0 \text{ , or } \frac{D \rho^\mathrm{s}}{Dt} + \rho^\mathrm{s} \mathrm{div} \boldsymbol{v} = 0 \tag{6.13}$$

$$\frac{D^\mathrm{f} \rho^\mathrm{f}}{Dt} + \rho^\mathrm{f} \mathrm{div} \boldsymbol{v}_\mathrm{f} = 0 \tag{6.14}$$

where $\boldsymbol{v}$ (or $\boldsymbol{v}_\mathrm{s}$) is the velocity of the solid skeleton, and $\boldsymbol{v}_\mathrm{f}$ is the velocity of the pore fluid. For eventual Lagrangian finite element implementation, where the mesh deforms with the solid skeleton deformation (tracked by solid skeleton displacement $\boldsymbol{u}$), we would like to express the material time derivatives solely in terms of the solid skeleton motion, and we recognize the following:

$$\frac{D^\mathrm{f} \rho^\mathrm{f}}{Dt} = \frac{D^\mathrm{s} \rho^\mathrm{f}}{Dt} + \mathrm{grad} \rho^\mathrm{f} \cdot \tilde{\boldsymbol{v}}_\mathrm{f} \tag{6.15}$$

$$\tilde{\boldsymbol{v}}_\mathrm{f} = \boldsymbol{v}_\mathrm{f} - \boldsymbol{v}_\mathrm{s} = \boldsymbol{v}_\mathrm{f} - \boldsymbol{v} \tag{6.16}$$

where $\tilde{\boldsymbol{v}}_\mathrm{f}$ is the relative velocity vector of the fluid with respect to the solid skeleton motion. Then the balance of mass for each constituent solid and fluid can be written with respect to

the solid skeleton motion as

$$\frac{D^{\mathrm{s}}\rho^{\mathrm{s}}}{Dt} + \rho^{\mathrm{s}}\mathrm{div}\boldsymbol{v} = 0 \tag{6.17}$$

$$\frac{D^{\mathrm{s}}\rho^{\mathrm{f}}}{Dt} + \rho^{\mathrm{f}}\mathrm{div}\boldsymbol{v} = -\mathrm{div}(\rho^{\mathrm{f}}\tilde{\boldsymbol{v}}_{\mathrm{f}}) \tag{6.18}$$

where $\mathrm{div}(\rho^{\mathrm{f}}\tilde{\boldsymbol{v}}_{\mathrm{f}})$ is the net mass flux of fluid through the solid skeleton (by the Divergence theorem). Using $\rho = \rho^{\mathrm{s}} + \rho^{\mathrm{f}}$, then the balance of mass for the mixture (summing each constituent balance of mass equation) is

$$\frac{D^{\mathrm{s}}\rho}{Dt} + \rho\mathrm{div}\boldsymbol{v} = -\mathrm{div}(\rho^{\mathrm{f}}\tilde{\boldsymbol{v}}_{\mathrm{f}}) \tag{6.19}$$

This is general for deformable constituents. However, oftentimes the constituents themselves are nearly incompressible with respect to the compressibility of the solid skeleton; e.g., a sand saturated with water, where water and the sand grains themselves are nearly incompressible as compared to the compressibility of the sand skeleton. This rationale can also apply to spongy soft biological tissues such as the brain and the lung parenchyma, wherein the saturating fluid is water and/or air, and the collagenous solid constituent is nearly incompressible when compared to the compressibility of the solid skeleton collagenous matrix (sometimes called the extracellular matrix (ECM)). Thus, we can consider a simpler case for which the solid and fluid constituents are incompressible. We start by substituting $\rho^{\mathrm{s}} = n^{\mathrm{s}}\rho^{\mathrm{sR}}$ and $\rho^{\mathrm{f}} = n^{\mathrm{f}}\rho^{\mathrm{fR}}$ into the separate constituent balance of mass equations,

$$\frac{\partial(n^{\mathrm{s}}\rho^{\mathrm{sR}})}{\partial t} + \mathrm{div}(n^{\mathrm{s}}\rho^{\mathrm{sR}}\boldsymbol{v}) = 0 \tag{6.20}$$

$$\frac{\partial(n^{\mathrm{f}}\rho^{\mathrm{fR}})}{\partial t} + \mathrm{div}(n^{\mathrm{f}}\rho^{\mathrm{fR}}\boldsymbol{v}) = -\mathrm{div}(n^{\mathrm{f}}\rho^{\mathrm{fR}}\tilde{\boldsymbol{v}}_{\mathrm{f}}) \tag{6.21}$$

We assume the solid and fluid constituents are incompressible (for saturated soils, or soft biological tissues), such that the real mass densities ρ^{sR} and ρ^{fR} are constant with respect to

time and space:

$$\rho^{\mathrm{sR}}\frac{\partial n^{\mathrm{s}}}{\partial t}+\rho^{\mathrm{sR}}\mathrm{div}(n^{\mathrm{s}}\boldsymbol{v}) = 0 \tag{6.22}$$

$$\rho^{\mathrm{fR}}\frac{\partial n^{\mathrm{f}}}{\partial t}+\rho^{\mathrm{fR}}\mathrm{div}(n^{\mathrm{f}}\boldsymbol{v}) = -\rho^{\mathrm{fR}}\mathrm{div}(n^{\mathrm{f}}\tilde{\boldsymbol{v}}_{\mathrm{f}}) \tag{6.23}$$

Recall the volume fraction relation $n^{\mathrm{s}}=1-n^{\mathrm{f}}$, where we then have

$$-\frac{\partial n^{\mathrm{f}}}{\partial t}+\mathrm{div}((1-n^{\mathrm{f}})\boldsymbol{v}) = 0 \tag{6.24}$$

$$\frac{\partial n^{\mathrm{f}}}{\partial t}+\mathrm{div}(n^{\mathrm{f}}\boldsymbol{v}) = -\mathrm{div}(n^{\mathrm{f}}\tilde{\boldsymbol{v}}_{\mathrm{f}}) \tag{6.25}$$

Summing these two balance equations leads to the balance of mass for a mixture composed of incompressible solid and fluid constituents as

$$\mathrm{div}\boldsymbol{v}+\mathrm{div}(n^{\mathrm{f}}\tilde{\boldsymbol{v}}_{\mathrm{f}})=0 \tag{6.26}$$

where $\boldsymbol{v}=\dot{\boldsymbol{u}}=D\boldsymbol{u}/Dt$ is the velocity of the solid skeleton following the solid skeleton motion, and $n^{\mathrm{f}}\tilde{\boldsymbol{v}}_{\mathrm{f}}=\tilde{\boldsymbol{v}}_{\mathrm{f}}^{\mathrm{Darcy}}$ is the superficial (Darcy seepage) fluid velocity. The balance of mass can be rewritten (assuming no interconversion of solid to fluid or fluid to solid constituents, i.e., ignore chemical reactions) as

$$\mathrm{div}\tilde{\boldsymbol{v}}_{\mathrm{f}}^{\mathrm{Darcy}}=-\mathrm{div}\dot{\boldsymbol{u}} \tag{6.27}$$

We can physically interpret this equation in various ways:

1. <u>locally undrained</u>: zero solid skeleton volumetric deformation with zero fluid flux

$$\mathrm{div}\tilde{\boldsymbol{v}}_{\mathrm{f}}^{\mathrm{Darcy}}=-\mathrm{div}\dot{\boldsymbol{u}}=0 \tag{6.28}$$

2. rate of fluid storage (in flow) equals rate of solid skeleton dilatation:

$$\mathrm{div}\tilde{\boldsymbol{v}}_{\mathrm{f}}^{\mathrm{Darcy}} < 0 \quad \text{flow in}\,, \quad \mathrm{div}\dot{\boldsymbol{u}} > 0 \quad \text{dilate} \tag{6.29}$$

3. rate of fluid depletion (out flow) equals rate of solid skeleton compaction:

$$\mathrm{div}\tilde{\boldsymbol{v}}_{\mathrm{f}}^{\mathrm{Darcy}} > 0 \quad \text{flow out}\,, \quad \mathrm{div}\dot{\boldsymbol{u}} < 0 \quad \text{compact} \tag{6.30}$$

Next, the **balance of linear momentum of the biphasic solid-fluid mixture** is derived. The balance of linear momentum for constituent α (α =s,f), ignoring inertia terms, may be written as:

$$\mathrm{div}\boldsymbol{\sigma}^{\alpha} + \rho^{\alpha}\boldsymbol{b}^{\alpha} + \boldsymbol{h}^{\alpha} \;=\; \boldsymbol{0} \tag{6.31}$$

where $\boldsymbol{\sigma}^{\alpha}$ is the partial stress for the α phase, such that $\boldsymbol{\sigma} = \boldsymbol{\sigma}^{\mathrm{s}} + \boldsymbol{\sigma}^{\mathrm{f}}$, ρ^{α} is the partial mass density such that $\rho = \rho^{\mathrm{s}} + \rho^{\mathrm{f}}$, $\boldsymbol{b}^{\alpha}$ is the body force per unit mass on constituent α (we assume the same body force for each constituent, such as acceleration of gravity, $\boldsymbol{b}^{\alpha} = \boldsymbol{b} = \boldsymbol{g}$), and $\boldsymbol{h}^{\alpha}$ is the internal body force drag of other constituents on constituent α. We note that the internal body forces due to drag between constituents sum to zero (equal and opposite; Newton's third law of motion), and thus do not affect the mixture as a whole:

$$\boldsymbol{h}^{\mathrm{s}} + \boldsymbol{h}^{\mathrm{f}} \;=\; \boldsymbol{0} \tag{6.32}$$

where $\boldsymbol{h}^{\mathrm{s}}$ is the body force drag of pore fluid on the solid skeleton, and $\boldsymbol{h}^{\mathrm{f}}$ is the body force drag of the solid skeleton on the pore fluid. Thus, when summing the individual balance of linear momentum equations for solid and fluid constituents, we have the balance of linear momentum equation for the mixture:

$$\mathrm{div}\boldsymbol{\sigma} + \rho\boldsymbol{g} \;=\; \boldsymbol{0} \tag{6.33}$$

This looks the same as a single constituent/phase medium, but we recognize the additive decomposition of the stress and mass density into its respective components for each constituent. The **balance of angular momentum** for non-polar constituents states that the respective partial stresses (and, in turn, the total stress) are symmetric: $\boldsymbol{\sigma}^\alpha = (\boldsymbol{\sigma}^\alpha)^T$.

It is now relevant to discuss a principle that allows us to distinguish stress acting on the solid skeleton, and the pressure acting on the pore fluid (assuming the fluid is nearly inviscid, such as water). We apply the effective stress principle (assuming Biot coefficient $B = 1$), which can be credited to Terzaghi [1943] (pg12) (among others), that states,

$$\boldsymbol{\sigma} = \boldsymbol{\sigma}' - p_{\mathrm{f}}\mathbf{1} \tag{6.34}$$

where the real (Cauchy) pore fluid pressure $p_{\mathrm{f}} = \frac{1}{n^{\mathrm{f}}}\left(\frac{-1}{3}\mathrm{tr}(\boldsymbol{\sigma}^{\mathrm{f}})\right)$ is positive in compression, and the mean effective stress is positive in tension $p' = \frac{1}{3}\mathrm{tr}(\boldsymbol{\sigma}')$, where $\boldsymbol{\sigma}'$ is the **effective stress**, or the stress acting on the solid skeleton, for which we will apply our solid skeleton constitutive equations. We assume a nearly inviscid (no shear stress) isotropic fluid (e.g., water), where then,

$$\boldsymbol{\sigma}^{\mathrm{f}} = p^{\mathrm{f}}\mathbf{1} \implies p_{\mathrm{f}} = \frac{1}{n^{\mathrm{f}}}(-p^{\mathrm{f}}) \tag{6.35}$$

and

$$\boldsymbol{\sigma}^{\mathrm{s}} = \boldsymbol{\sigma}' + p^{\mathrm{f}}\left(\frac{1}{n^{\mathrm{f}}} - 1\right)\mathbf{1} \tag{6.36}$$

Thus, we note that the partial solid stress $\boldsymbol{\sigma}^{\mathrm{s}}$ is NOT equal to the effective stress $\boldsymbol{\sigma}'$, $\boldsymbol{\sigma}^{\mathrm{s}} \neq \boldsymbol{\sigma}'$, unless the pore fluid pressure $p_{\mathrm{f}} = 0$. The effective stress principle is useful for introducing constitutive equations for the solid skeleton separate from the pore fluid, but it requires more study for application to materials other than soils or rocks, such as soft biological tissues. For rocks, we introduce the Biot coefficient B, recognizing that the stiffness of the rock solid skeleton is on the same order of magnitude as the rock solid constituent; for soils, foams, and soft biological tissues, $B \approx 1$.

Thus, we may state the coupled Strong Form (balance of mass and linear momentum) for the solid-fluid mixture with incompressible constituents, ignoring inertia terms, as

$$
(S)\left\{\begin{array}{rcll}
\text{Find } u_i(\boldsymbol{x},t):\bar{\Omega}\times[0,T]\mapsto\mathbb{R}^{n_{sd}}, & & & \\
\quad\text{and } p_{\mathrm{f}}(\boldsymbol{x},t):\bar{\Omega}\times[0,T]\mapsto\mathbb{R}, & & \text{such that} & \\
\sigma_{ij,j}+\rho b_i & = & 0 & \in\Omega \\
u_i & = & g_i^u & \text{on}\,\Gamma_u \\
\sigma'_{ij}n_j & = & t_i^{\sigma'} & \text{on}\,\Gamma_t \\
u_i(\boldsymbol{x},0) & = & u_{0i} & \in\Omega \\
\dot{u}_{i,i}+\tilde{v}^{\mathrm{Darcy}}_{i(\mathrm{f}),i} & = & 0 & \in\Omega_{\mathrm{f}} \\
p_{\mathrm{f}} & = & r & \text{on}\,\Gamma_r\,(\text{and}\,\Gamma_t) \\
-n_i\tilde{v}^{\mathrm{Darcy}}_{i(\mathrm{f})} & = & s & \text{on}\,\Gamma_s \\
p_{\mathrm{f}}(\boldsymbol{x},0) & = & p_{\mathrm{f}0} & \in\Omega_{\mathrm{f}}
\end{array}\right. \tag{6.37}
$$

where the BCs on a mixture body are shown in Fig.6.7.

Constitutive Equations:

Before we introduce constitutive equations, we present the thermodynamics (Clausius-Duhem inequality) for a biphasic mixture. The **balance of energy for constituent** α in the current configuration $\mathcal{B}$ is written as

$$
\rho^\alpha\frac{D^\alpha e^\alpha}{Dt}-\boldsymbol{\sigma}^\alpha:\dot{\boldsymbol{\epsilon}}^\alpha+\mathrm{div}\boldsymbol{q}^\alpha-\rho^\alpha r^\alpha \tag{6.38}
$$

$$
=\hat{e}^\alpha+\gamma^\alpha\left(\frac{1}{2}\boldsymbol{v}_\alpha\cdot\boldsymbol{v}_\alpha-e^\alpha\right)-\boldsymbol{v}_\alpha\cdot\boldsymbol{h}^\alpha \tag{6.39}
$$

where e^α is the internal energy per unit mass of constituent α, $\boldsymbol{q}^\alpha$ is the heat flux of constituent α, r^α is the heat input per unit mass of constituent α, and $\hat{e}^\alpha$ is the energy density rate for constituent α supplied by all other constituents. Then, skipping details, the **Clausius-Duhem inequality, assuming existence of a Helmholtz free energy func-**

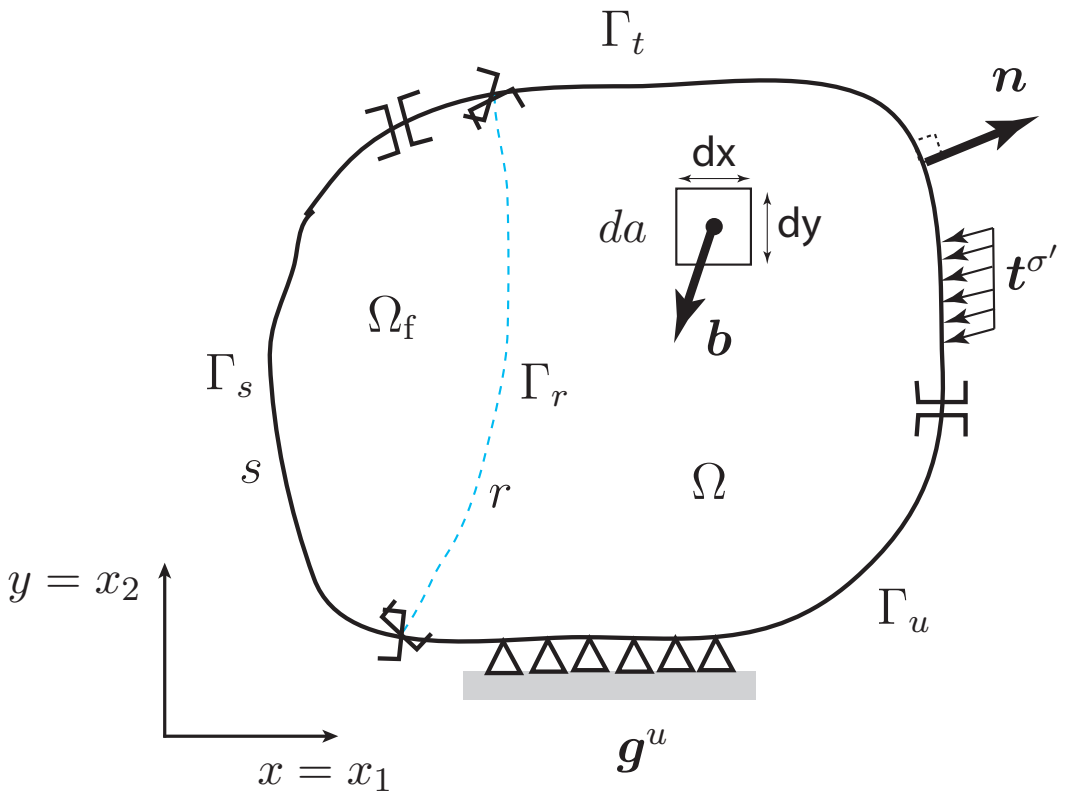

Figure 6.7. A body Ω that can have a saturated region Ω_f, with associated BCs: $\boldsymbol{g}^u$ is the prescribed displacement on Γ_u, $\boldsymbol{t}^{\sigma'}$ is the prescribed traction on Γ_t, r is the prescribed pore fluid pressure on Γ_r, and s is the prescribed fluid flux across Γ_s (positive into the body). We will consider only bodies that are fully saturated, where $\Omega_\mathrm{f} = \Omega$.

tion per unit mass ψ^α for constituent α is written as

$$\hat{e}^\alpha + \gamma^\alpha \left(\theta^\alpha \eta^\alpha + \frac{1}{2} \boldsymbol{v}_\alpha \cdot \boldsymbol{v}_\alpha - e^\alpha \right) - \boldsymbol{v}_\alpha \cdot \boldsymbol{h}^\alpha - \rho^\alpha \frac{D^\alpha \psi^\alpha}{Dt} + \boldsymbol{\sigma}^\alpha : \dot{\boldsymbol{\epsilon}}^\alpha \tag{6.40}$$

$$\geq \rho^\alpha \eta^\alpha \frac{D^\alpha \theta^\alpha}{Dt} + \frac{1}{\theta^\alpha} (\mathrm{grad} \theta^\alpha) \cdot \boldsymbol{q}^\alpha \tag{6.41}$$

Summing over the constituents α =s,f, the **resulting constitutive equations** follow from arguments by Coleman and Noll [1963], Coleman and Gurtin [1967] for independence of rate processes, where we assume inter-constituent mass exchange $\gamma^\alpha = 0$, we use the effective

stress principle, the constituents are incompressible, and we have

$$\eta^{\mathrm{s}} = -\frac{\partial(\rho^{\mathrm{s}}\psi^{\mathrm{s}})}{\partial\theta^{\mathrm{s}}} \ , \ \eta^{\mathrm{f}} = -\frac{\partial(\rho^{\mathrm{f}}\psi^{\mathrm{f}})}{\partial\theta^{\mathrm{f}}} \tag{6.42}$$

$$\boldsymbol{\sigma}' = \frac{\partial(\rho^{\mathrm{s}}\psi^{\mathrm{s}})}{\partial\boldsymbol{\epsilon}^{\mathrm{s}}} \tag{6.43}$$

The **reduced dissipation inequality**, assuming at a local mixture continuum point the temperature $\theta^{\mathrm{s}} = \theta^{\mathrm{f}} = \theta$ and $\boldsymbol{q} = \boldsymbol{q}^{\mathrm{s}} + \boldsymbol{q}^{\mathrm{f}}$, we have,

$$-(\rho^{\mathrm{f}}\psi^{\mathrm{f}})\mathrm{div}\boldsymbol{v}_{\mathrm{f}} - \left[\frac{\partial p_{\mathrm{f}}}{\partial\boldsymbol{x}} + \rho^{\mathrm{fR}}(\boldsymbol{a}_{\mathrm{f}} - \boldsymbol{b}^{\mathrm{f}})\right] \cdot (n^{\mathrm{f}}\tilde{\boldsymbol{v}}_{\mathrm{f}}) - \frac{1}{\theta}\frac{\partial\theta}{\partial\boldsymbol{x}} \cdot \boldsymbol{q} \geq 0 \tag{6.44}$$

For **non-negative dissipation**, we arrive at the generalized Darcy's law for seepage velocity $(n^{\mathrm{f}}\tilde{\boldsymbol{v}}_{\mathrm{f}})$, and the Fourier's law for mixture heat flux $\boldsymbol{q}$, as follows

$$(n^{\mathrm{f}}\tilde{\boldsymbol{v}}_{\mathrm{f}}) \propto -\left[\frac{\partial p_{\mathrm{f}}}{\partial\boldsymbol{x}} + \rho^{\mathrm{fR}}(\boldsymbol{a}_{\mathrm{f}} - \boldsymbol{b}^{\mathrm{f}})\right] \Longrightarrow (n^{\mathrm{f}}\tilde{\boldsymbol{v}}_{\mathrm{f}}) = -\hat{k}\left[\frac{\partial p_{\mathrm{f}}}{\partial\boldsymbol{x}} + \rho^{\mathrm{fR}}(\boldsymbol{a}_{\mathrm{f}} - \boldsymbol{b}^{\mathrm{f}})\right] \tag{6.45}$$

$$\boldsymbol{q} \propto -\frac{1}{\theta}\frac{\partial\theta}{\partial\boldsymbol{x}} \Longrightarrow \boldsymbol{q} = -k^{\theta}\frac{1}{\theta}\frac{\partial\theta}{\partial\boldsymbol{x}} \tag{6.46}$$

where hydraulic conductivity $\hat{k}$ and thermal conductivity $k^{\theta} = n^{\mathrm{f}}k^{\theta^{\mathrm{f}}} + n^{\mathrm{s}}k^{\theta^{\mathrm{s}}}$ are proportionality parameters. Thus, a generalized form of Darcy's law and Fourier's law result from the second law of thermodynamics. We will assume isothermal ($\dot{\theta} = 0$) and homogeneous temperature ($\partial\theta/\partial\boldsymbol{x} = \boldsymbol{0}$) for now. We assume the body force per unit mass on the fluid is a result of gravity, $\boldsymbol{b}^{\mathrm{f}} = \boldsymbol{g}$.

Assuming a quadratic form of the Helmholtz free energy function for the solid skeleton $\rho^{\mathrm{s}}\psi^{\mathrm{s}}$,

we arrive at a linear elasticity model, which we further assume is isotropic, such that

$$\rho^{\mathrm{s}}\psi^{\mathrm{s}}(\boldsymbol{\epsilon}^{\mathrm{s}}) = \frac{1}{2}\boldsymbol{\epsilon}^{\mathrm{s}} : \boldsymbol{c} : \boldsymbol{\epsilon}^{\mathrm{s}} \tag{6.47}$$

$$\boldsymbol{\sigma}' = \frac{\partial(\rho^{\mathrm{s}}\psi^{\mathrm{s}})}{\partial\boldsymbol{\epsilon}^{\mathrm{s}}} = \boldsymbol{c} : \boldsymbol{\epsilon}\ ,\ \boldsymbol{\epsilon} = \boldsymbol{\epsilon}^{\mathrm{s}} \tag{6.48}$$

$$\sigma'_{ij} = c_{ijkl}\epsilon_{kl} \tag{6.49}$$

$$\boldsymbol{c} = \lambda\mathbf{1}\otimes\mathbf{1} + 2\mu\boldsymbol{I} \tag{6.50}$$

$$c_{ijkl} = \lambda\delta_{ij}\delta_{kl} + 2\mu I_{ijkl} \tag{6.51}$$

$$I_{ijkl} = \frac{1}{2}(\delta_{ik}\delta_{jl} + \delta_{il}\delta_{jk}) \tag{6.52}$$

We could generalize the constitutive equation for the effective stress governing the response of the solid skeleton by including plasticity, or viscoelasticity, or viscoplasticity, etc.

Constitutively, based on the thermodynamics resulting in Eq.(6.45), we can assume Darcy's law for the superficial (Darcy) seepage fluid velocity. Refer to Coussy [2004] (pg45) for more details. Recall from undergraduate soil mechanics (if you ever took such a course) the 1D Darcy experiment illustrated in Fig.6.8.

We can generalize Eq.(6.45) further by considering anisotropic hydraulic conductivity, but for now we stick to the isotropic assumption that a hydraulic conductivity tensor $\hat{\boldsymbol{k}} = \hat{k}\mathbf{1}$. If we ignore inertia terms ($\boldsymbol{a}_{\mathrm{f}} \approx \mathbf{0}$), assume the body force on the fluid is that of gravity ($\boldsymbol{b}^{\mathrm{f}} = \boldsymbol{g}$), then we have the simplified version of the generalized Darcy's law as

$$\tilde{\boldsymbol{v}}_{\mathrm{f}}^{\mathrm{Darcy}} = -\hat{k}\left[\boldsymbol{\nabla}p_{\mathrm{f}} - \rho^{\mathrm{fR}}\boldsymbol{g}\right] \tag{6.53}$$

where $\boldsymbol{g}$ is the gravitational vector. From Coussy [2004] (pg46), we find that the hydraulic

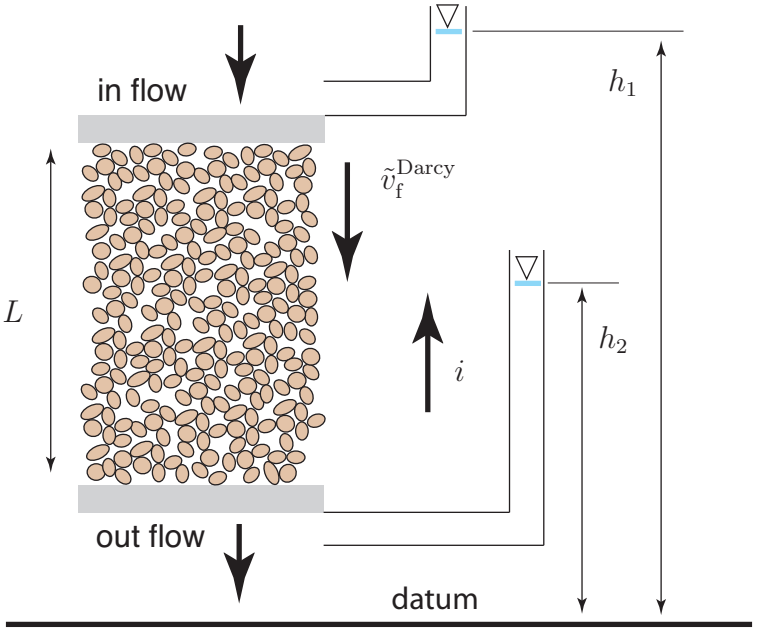

Figure 6.8. An illustration of Darcy's classic seepage experiment to measure hydraulic conductivity k of a porous medium. The 1D equation for the superficial Darcy seepage velocity is $\tilde{v}_{\mathrm{f}}^{\mathrm{Darcy}} = -ki$, and the hydraulic gradient $i = (h_1 - h_2)/L$, ignoring body force and velocity head.

conductivity may be a function of porosity n ($n = n^{\mathrm{f}}$ for fluid-saturated porous medium)

$$\hat{k}(n^{\mathrm{f}}) = \frac{\varkappa}{\eta_{\mathrm{f}}} \frac{\mathcal{F}(n^{\mathrm{f}})}{\mathcal{F}(n_0^{\mathrm{f}})} \tag{6.54}$$

$$\mathcal{F}(n^{\mathrm{f}}) = \frac{(n^{\mathrm{f}})^3}{1 - (n^{\mathrm{f}})^2} \tag{6.55}$$

where for fine sand, the *intrinsic permeability* $\varkappa \approx 1{\times}10^{-12} m^2$ [Coussy, 2004] (Table3.1,pg47), for lung parenchyma $\varkappa \approx 2 \times 10^{-12} m^2$ * [Lande and Mitzner, 2006] and at 20° C, for water the viscosity is $\eta_{\mathrm{f}} = 10^{-3}$Pa.s. Note that $k = \gamma_{\mathrm{f}} \hat{k}$, and the unit weight of fluid is $\gamma_{\mathrm{f}} = \rho^{\mathrm{fR}} g$, $g = 9.81 m/s^2$. Equation (6.55) is the Kozeny-Carman formula [Coussy, 2004]. Assuming small strain kinematics, we can relate the rate of change of the fluid volume fraction (the

*calculated from provided hydraulic conductivity of air through the lung parenchyma, and viscosity of air at 20° C $\eta_{\mathrm{f}} = 1.83 \times 10^{-5}$Pa.s

porosity) to the solid skeleton volumetric strain as,

$$\dot{n}^{\mathrm{f}} = (1-n^{\mathrm{f}})\dot{\epsilon}_v \tag{6.56}$$

$$n^{\mathrm{f}}_{n+1} = \frac{n^{\mathrm{f}}_n + \Delta\epsilon_v}{1+\Delta\epsilon_v} \tag{6.57}$$

$$\Delta\epsilon_v = \mathrm{tr}(\Delta\boldsymbol{\epsilon}) \tag{6.58}$$

This will introduce nonlinearity into the governing equations, requiring a nonlinear Newton-Raphson finite element solution; more details to follow.

6.2 Coupled, Variational, Weak Form (W)

The first step in obtaining the finite element coupled equations to solve for coupled poromechanics (pore fluid flow coupled to solid skeleton deformation), we must formulate the Weak Form (W) starting from the Strong Form (S). We introduce a weighting function $w_i(\boldsymbol{x})$ that is used in formulating the weak form of balance of linear momentum for a 2D porous medium with domain Ω, such that

$$\int_\Omega w_i(\sigma_{ij,j} + \rho g_i)da = 0 \tag{6.59}$$

We introduce a weighting function $\eta(\boldsymbol{x})$ to be used in formulating the weak form of balance of mass as follows (we assume saturated porous medium $\Omega_{\mathrm{f}} = \Omega$),

$$\int_\Omega \eta\left[\dot{u}_{i,i} + \tilde{v}^{\mathrm{Darcy}}_{i(\mathrm{f}),i}\right]da = 0 \tag{6.60}$$

After integration by parts, and assuming a two-dimensional domain Ω, the coupled weak form is written as,

$$
(W)\begin{cases}
\text{Find } u_i(\boldsymbol{x},t)\in\mathscr{S}^u \text{ and } p_{\mathrm{f}}(\boldsymbol{x},t)\in\mathscr{S}^p \text{ such that} \\
\quad \int_\Omega w_{i,j}(\sigma'_{ij}-p_{\mathrm{f}}\delta_{ij})da=\int_\Omega \rho w_i g_i da+\int_{\Gamma_t} w_i t_i^{\sigma'} ds-\int_{\Gamma_t} w_i n_i p_{\mathrm{f}} ds \\
\quad \int_\Omega \eta \dot{u}_{i,i} da-\int_\Omega \eta_{,i}\tilde{v}^{\mathrm{Darcy}}_{i(\mathrm{f})} da=\int_{\Gamma_s}\eta s ds \\
\text{holds } \forall w_i(\boldsymbol{x})\in\mathscr{V}^u \text{ and } \eta(\boldsymbol{x})\in\mathscr{V}^p \\
\mathscr{S}^u=\{u_i:\Omega\times[0,T]\mapsto\mathbb{R}^2, u_i\in H^1, u_i(t)=g_i^u(t)\,\text{on}\,\Gamma_u, u_i(\boldsymbol{x},0)=u_{i0}(\boldsymbol{x})\} \\
\mathscr{S}^p=\{p_{\mathrm{f}}:\Omega\times[0,T]\mapsto\mathbb{R}, p_{\mathrm{f}}\in H^1, p_{\mathrm{f}}(t)=r(t)\,\text{on}\,\Gamma_r,\Gamma_t,\ p_{\mathrm{f}}(\boldsymbol{x},0)=p_{\mathrm{f}0}(\boldsymbol{x})\} \\
\mathscr{V}^u=\{w_i:\Omega\mapsto\mathbb{R}^2, w_i\in H^1, w_i=0\,\text{on}\,\Gamma_u\} \\
\mathscr{V}^p=\{\eta:\Omega\mapsto\mathbb{R}, \eta\in H^1, \eta=0\,\text{on}\,\Gamma_r\}
\end{cases}
\tag{6.61}
$$

where $t_i^{\sigma'}$ is the effective traction vector acting on the solid skeleton, n_i is the unit normal vector to the surface Γ_t, $\mathscr{S}^u$ is the trial solution space for solid skeleton displacement vector u_i, $\mathscr{S}^p$ is the trial solution space for pore fluid pressure p_{f}, $\mathscr{V}^u$ is the variational space for weighting function vector w_i, and $\mathscr{V}^p$ is the variational space for weighting function η.

6.3 Coupled, Discrete, Galerkin Form (G)

Details aside (refer to [Hughes, 1987]), the discrete, Bubnov-Galerkin form is expressed as follows:

$$
\begin{aligned}
(\mathscr{S}^u)^h\subset\mathscr{S}^u \quad &, \quad (\mathscr{S}^p)^h\subset\mathscr{S}^p \\
(\mathscr{V}^u)^h\subset\mathscr{V}^u \quad &, \quad (\mathscr{V}^p)^h\subset\mathscr{V}^p \\
u_i^h(\boldsymbol{x},t)\in(\mathscr{S}^u)^h \quad &, \quad p_{\mathrm{f}}^h(\boldsymbol{x},t)\in(\mathscr{S}^p)^h \\
w_i^h(\boldsymbol{x})\in(\mathscr{V}^u)^h \quad &, \quad \eta^h(\boldsymbol{x})\in(\mathscr{V}^p)^h
\end{aligned}
\tag{6.62}
$$

where h implies a discretization parameter, typically related to the finite element "diameter" (i.e., diameter of circle that circumscribes a 2D element, or diameter of a sphere that

circumscribes a 3D element).

6.4 Coupled, Finite Element (FE), Matrix Form

To illustrate the coupled finite element (FE) implementation of solid-fluid saturated poromechanics at small strain, ignoring inertia terms and chemical reaction of constituents, we start with a mixed quadrilateral finite element shown in Fig.6.9.

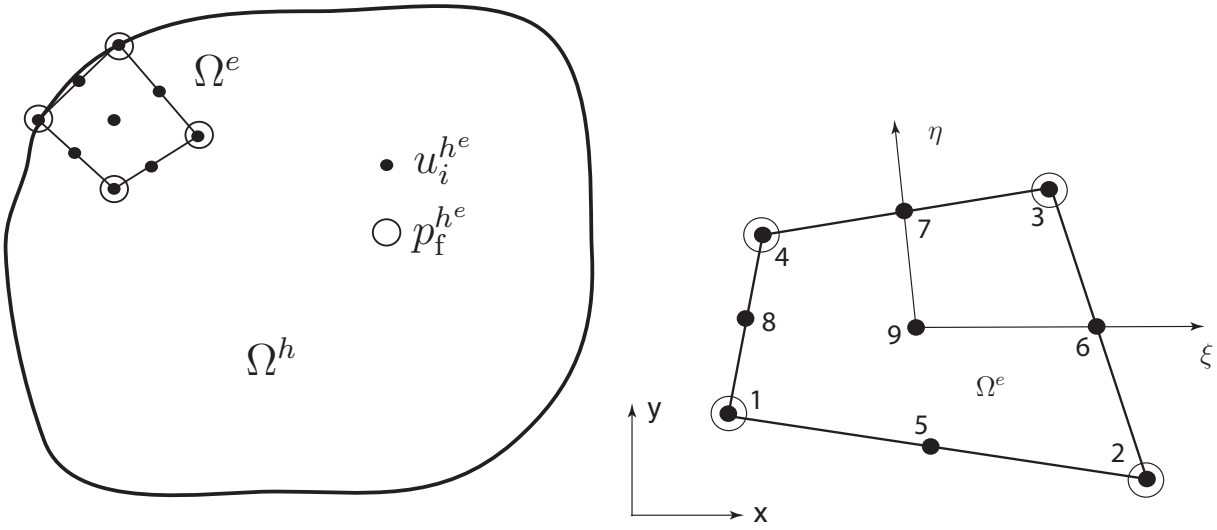

Figure 6.9. A mixed quadrilateral element (Q9P4, 9 nodes for biquadratic interpolation of displacement $u_i^{h^e}$, and 4 nodes for bilinear interpolation of pore fluid pressure $p_{\mathrm{f}}^{h^e}$), that is shown to be convergent with respect to spatial discretization [Hughes, 1987]. Ω^e is the element domain, and the overall discrete domain subdivided into finite element domains from which it is assembled: $\Omega^h = \mathbf{A}_{e=1}^{n_{\mathrm{el}}} \Omega^e$.

We then interpolate as follows:

$$\boldsymbol{u}^{h^e}(\boldsymbol{\xi},t) = \sum_{a=1}^{9} N_a^u(\boldsymbol{\xi})\boldsymbol{d}_a^e(t) = \underbrace{\boldsymbol{N}^{e,u}(\boldsymbol{\xi})}_{2\times(2*9)} \cdot \underbrace{\boldsymbol{d}^e(t)}_{(2*9)\times 1} \tag{6.63}$$

$$= \begin{bmatrix} \boldsymbol{N}_1^u & \dots & \boldsymbol{N}_9^u \end{bmatrix} \cdot \begin{bmatrix} \boldsymbol{d}_1^e \\ \vdots \\ \boldsymbol{d}_9^e \end{bmatrix} \tag{6.64}$$

$$\boldsymbol{N}_a^u = \begin{bmatrix} N_a^u & 0 \\ 0 & N_a^u \end{bmatrix}, \quad \boldsymbol{d}_a^e = \begin{bmatrix} d_{x(a)}^e \\ d_{y(a)}^e \end{bmatrix} \tag{6.65}$$

$$\boldsymbol{w}^{h^e}(\boldsymbol{\xi}) = \boldsymbol{N}^{e,u}(\boldsymbol{\xi}) \cdot \boldsymbol{c}^e \tag{6.66}$$

$$p_{\mathrm{f}}^{h^e}(\boldsymbol{\xi},t) = \sum_{b=1}^{4} N_b^p(\boldsymbol{\xi})\theta_b^e(t) = \underbrace{\boldsymbol{N}^{e,p}}_{1\times(1*4)} \cdot \underbrace{\boldsymbol{\theta}^e}_{(1*4)\times 1} \tag{6.67}$$

$$= \begin{bmatrix} N_1^p & N_2^p & N_3^p & N_4^p \end{bmatrix} \cdot \begin{bmatrix} \theta_1^e \\ \theta_2^e \\ \theta_3^e \\ \theta_4^e \end{bmatrix} \tag{6.68}$$

$$\eta^{h^e} = \boldsymbol{N}^{e,p} \cdot \boldsymbol{\alpha}^e \tag{6.69}$$

where the derivatives are

$$\dot{u}^{h^e}_{i,i}(\boldsymbol{\xi},t) = \sum_{a=1}^{9} \left[\begin{array}{cc} \frac{\partial N^u_a}{\partial x} & \frac{\partial N^u_a}{\partial y} \end{array} \right] \cdot \left[\begin{array}{c} \dot{d}^e_{x(a)} \\ \dot{d}^e_{y(a)} \end{array} \right] \tag{6.70}$$

$$= \left[\begin{array}{ccc} \tilde{\boldsymbol{B}}^u_1 & \dots & \tilde{\boldsymbol{B}}^u_9 \end{array} \right] \cdot \left[\begin{array}{c} \dot{\boldsymbol{d}}^e_1 \\ \vdots \\ \dot{\boldsymbol{d}}^e_9 \end{array} \right] = \tilde{\boldsymbol{B}}^{e,u} \cdot \dot{\boldsymbol{d}}^e \tag{6.71}$$

$$\eta^{h^e}_{,i}(\boldsymbol{\xi}) = \sum_{b=1}^{4} \frac{\partial N^p_b(\boldsymbol{\xi})}{\partial x_i} \alpha^e_b = \sum_{b=1}^{4} \left[\begin{array}{c} \frac{\partial N^p_b(\boldsymbol{\xi})}{\partial x} \\ \frac{\partial N^p_b(\boldsymbol{\xi})}{\partial y} \end{array} \right] \alpha^e_b \tag{6.72}$$

$$= \sum_{b=1}^{4} \boldsymbol{B}^p_b \alpha^e_b = \left[\begin{array}{cccc} \boldsymbol{B}^p_1 & \boldsymbol{B}^p_2 & \boldsymbol{B}^p_3 & \boldsymbol{B}^p_4 \end{array} \right] \cdot \left[\begin{array}{c} \alpha^e_1 \\ \alpha^e_2 \\ \alpha^e_3 \\ \alpha^e_4 \end{array} \right] \tag{6.73}$$

$$\boldsymbol{\nabla} \eta^{h^e} = \boldsymbol{B}^{e,p} \cdot \boldsymbol{\alpha}^e \tag{6.74}$$

$$\boldsymbol{\nabla} p^{h^e}_{\mathrm{f}} = \boldsymbol{B}^{e,p} \cdot \boldsymbol{\theta}^e \tag{6.75}$$

Currently, our equations are nonlinear because the porosity $n^{\mathrm{f}}(\boldsymbol{u})$ is a nonlinear function of displacement $\boldsymbol{u}$. To simplify the formulation initially, we will ignore the change in porosity due to volumetric deformation of the solid skeleton. This assumption may be appropriate for certain rocks and hard biological tissues like bone, but is NOT appropriate for soils and soft biological tissues (a full finite deformation formulation is actually needed, which is beyond the scope of this course; refer to Li et al. [2004], de Boer [2005], Regueiro and Ebrahimi [2010], Regueiro et al. [2014], etc.). Recall that

$$\rho = \rho^{\mathrm{s}} + \rho^{\mathrm{f}} = n^{\mathrm{s}} \rho^{\mathrm{sR}} + n^{\mathrm{f}} \rho^{\mathrm{fR}} \tag{6.76}$$

$$= \rho^{\mathrm{sR}} + n^{\mathrm{f}} (\rho^{\mathrm{fR}} - \rho^{\mathrm{sR}}) \tag{6.77}$$

$$\rho(\boldsymbol{d}) = \rho^{\mathrm{sR}} + n^{\mathrm{f}}(\boldsymbol{d}) (\rho^{\mathrm{fR}} - \rho^{\mathrm{sR}}) \tag{6.78}$$

Thus, since the porosity $n^{\mathrm{f}}(\boldsymbol{d})$ is a nonlinear function of displacement, then so is the mixture mass density $\rho(\boldsymbol{d})$. We will ignore this nonlinearity for now, and revisit later.

The coupled FE equations are written then as:

$$\begin{aligned}
&\mathop{\mathsf{A}}_{e=1}^{n_{\mathrm{el}}}(\boldsymbol{c}^e)^T\cdot\Bigg[\underbrace{\left(\int_{\Omega^e}(\boldsymbol{B}^{e,u})^T\cdot\boldsymbol{D}^{\mathrm{elastic}}\cdot\boldsymbol{B}^{e,u}da\right)}_{\boldsymbol{k}^{e,dd}}\cdot\boldsymbol{d}^e-\underbrace{\left(\int_{\Omega^e}(\tilde{\boldsymbol{B}}^{e,u})^T\cdot\boldsymbol{N}^{e,p}da\right)}_{\boldsymbol{k}^{e,d\theta}}\cdot\boldsymbol{\theta}^e\\
&=\underbrace{\int_{\Omega^e}\rho(\boldsymbol{N}^{e,u})^T\cdot\boldsymbol{b}da}_{\boldsymbol{f}_f^{e,d}}+\underbrace{\int_{\Gamma_t^e}(\boldsymbol{N}^{e,u})^T\cdot\boldsymbol{t}^{\sigma'}ds}_{\boldsymbol{f}_t^{e,d}}-\underbrace{\int_{\Gamma_t^e}(\boldsymbol{N}^{e,u})^T\cdot\boldsymbol{n}p_{\mathrm{f}}^{h^e}ds}_{\boldsymbol{f}_p^{e,d}}\Bigg]
\end{aligned}\tag{6.79}$$

$$\begin{aligned}
&\mathop{\mathsf{A}}_{e=1}^{n_{\mathrm{el}}}(\boldsymbol{\alpha}^e)^T\cdot\Bigg[\underbrace{\left(\int_{\Omega^e}(\boldsymbol{N}^{e,p})^T\cdot\tilde{\boldsymbol{B}}^{e,u}da\right)}_{(\boldsymbol{k}^{e,d\theta})^T}\cdot\dot{\boldsymbol{d}}^e+\underbrace{\left(\int_{\Omega^e}(\boldsymbol{B}^{e,p})^T\cdot\boldsymbol{k}\cdot\boldsymbol{B}^{e,p}da\right)}_{\boldsymbol{k}^{e,\theta\theta}}\cdot\boldsymbol{\theta}^e\\
&=\underbrace{\int_{\Omega^e}\rho^{\mathrm{fR}}(\boldsymbol{B}^{e,p})^T\cdot\boldsymbol{k}\cdot\boldsymbol{g}da+\int_{\Gamma_s^e}(\boldsymbol{N}^{e,p})^Tsds}_{\boldsymbol{f}^{e,\theta}}\Bigg]
\end{aligned}\tag{6.80}$$

and in more compact form

$$\mathop{\mathsf{A}}_{e=1}^{n_{\mathrm{el}}}(\boldsymbol{c}^e)^T\cdot\Big[\boldsymbol{k}^{e,dd}\cdot\boldsymbol{d}^e-\boldsymbol{k}^{e,d\theta}\cdot\boldsymbol{\theta}^e=\boldsymbol{f}_f^{e,d}+\boldsymbol{f}_t^{e,d}-\boldsymbol{f}_p^{e,d}\Big]\tag{6.81}$$

$$\mathop{\mathsf{A}}_{e=1}^{n_{\mathrm{el}}}(\boldsymbol{\alpha}^e)^T\cdot\Big[(\boldsymbol{k}^{e,d\theta})^T\cdot\dot{\boldsymbol{d}}^e+\boldsymbol{k}^{e,\theta\theta}\cdot\boldsymbol{\theta}^e=\boldsymbol{f}^{e,\theta}\Big]\tag{6.82}$$

After element assembly, we have the coupled parabolic PDEs to solve using generalized

trapezoidal integration in time as,

$$\boldsymbol{C}\cdot\dot{\boldsymbol{D}}+\boldsymbol{K}\cdot\boldsymbol{D}=\boldsymbol{F} \tag{6.83}$$

$$\dot{\boldsymbol{D}}=\begin{bmatrix}\dot{\boldsymbol{d}}\\ \dot{\boldsymbol{\theta}}\end{bmatrix},\quad \boldsymbol{D}=\begin{bmatrix}\boldsymbol{d}\\ \boldsymbol{\theta}\end{bmatrix} \tag{6.84}$$

$$\boldsymbol{C}=\begin{bmatrix}\boldsymbol{0} & \boldsymbol{0}\\ (\boldsymbol{K}^{d\theta})^T & \boldsymbol{0}\end{bmatrix},\quad \boldsymbol{K}=\begin{bmatrix}\boldsymbol{K}^{dd} & -\boldsymbol{K}^{d\theta}\\ \boldsymbol{0} & \boldsymbol{K}^{\theta\theta}\end{bmatrix} \tag{6.85}$$

$$\boldsymbol{F}=\begin{bmatrix}\boldsymbol{F}^{d}\\ \boldsymbol{F}^{\theta}\end{bmatrix} \tag{6.86}$$

but we must assemble the global stiffness $\boldsymbol{K}$ and "damping" $\boldsymbol{C}$ matrices. An example will show such assembly process.

But before we do this, we summarize the generalized trapezoidal rule to integrate in time Eq.(6.83).

6.5 Time Integration using Generalized Trapezoidal Rule

Refer to Hughes [1987] for more details. First, evaluate the FE coupled balance of mass and linear momentum equations at time t_{n+1}, and introduce difference formulas for $\boldsymbol{D}_{n+1}$ and $\boldsymbol{V}_{n+1}$, where α is the time integration parameter

$$\boldsymbol{C}\cdot\boldsymbol{V}_{n+1} \;+\; \boldsymbol{K}\cdot\boldsymbol{D}_{n+1}=\boldsymbol{F}_{n+1} \tag{6.87}$$

$$\boldsymbol{D}_{n+1}=\boldsymbol{D}_n+\Delta t\boldsymbol{V}_{n+\alpha} \tag{6.88}$$

$$\boldsymbol{V}_{n+\alpha}=(1-\alpha)\boldsymbol{V}_n+\alpha\boldsymbol{V}_{n+1} \tag{6.89}$$

where the classical choices for α are:

α	method	type
0	forward Euler	explicit (if $\boldsymbol{C}$ is diagonal, which it is not)
1/2	trapezoidal rule	implicit
1	backward Euler	implicit

The code implementation follows this approach:

1. **initialize:** given initial displacement and pore pressure $\boldsymbol{D}_0$, solve for $\boldsymbol{V}_0$

$$\boldsymbol{C} \cdot \boldsymbol{V}_0 = \boldsymbol{F}_0 - \boldsymbol{K} \cdot \boldsymbol{D}_0 \tag{6.90}$$

2. **predictor:**

$$\tilde{\boldsymbol{D}}_{n+1} = \boldsymbol{D}_n + (1-\alpha)\Delta t \boldsymbol{V}_n \tag{6.91}$$

3. **solution:** for $\boldsymbol{V}_{n+1}$

$$(\boldsymbol{C} + \alpha\Delta t \boldsymbol{K}) \cdot \boldsymbol{V}_{n+1} = \boldsymbol{F}_{n+1} - \boldsymbol{K} \cdot \tilde{\boldsymbol{D}}_{n+1} \tag{6.92}$$

4. **corrector:**

$$\boldsymbol{D}_{n+1} = \tilde{\boldsymbol{D}}_{n+1} + \alpha\Delta t \boldsymbol{V}_{n+1} \tag{6.93}$$

5. **stability:** we will choose an unconditionally-stable method: $\alpha = 1$ (Backward Euler)

6.6 Example of Element Assembly to obtain Global Matrix form

We consider as an example of the coupled pore fluid and solid skeleton deformation, a 3 element plane strain consolidation problem, with parameters $\lambda = 29e6$Pa, $\mu = 7e6$Pa, $t^{\sigma'} = 4e4Pa$, k =1e-6(m^{3}s)/kg, $n^{s0} = 0.58$, $n^{f0} = 0.42$, $\rho^{sR} = 2700$kg/m^3, $\rho^{fR} = 1000$kg/m^3, $\rho_0 = n^{s0}\rho^{sR} + n^{f0}\rho^{fR} = 1566 + 420 = 1986$kg/m^3. Refer to Fig.6.10 for geometry of the mesh and the IEN array [Hughes, 1987] that relates the local node numbers per element to the global node numbers.

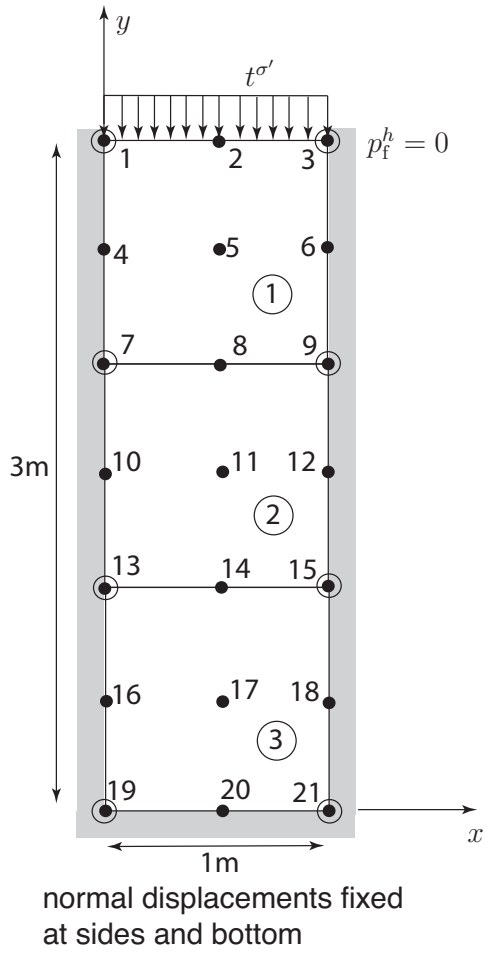

- **analytical small strain solution of settlement at end of consolidation**: $\Delta H = H_0 t^{\sigma'}/(\lambda + 2\mu) = 2.8$mm
- **IEN array**:

a \ e	e1	e2	e3
1	7	13	19
2	9	15	21
3	3	9	15
4	1	7	13
5	8	14	20
6	6	12	18
7	2	8	14
8	4	10	16
9	5	11	17

Figure 6.10. 3 element plane strain mesh example.

We continue with the ID array [Hughes, 1987] that relates the global dof numbers to the global node numbers and local dof, as follows

	global node number											
local nodal dof	1	2	3	4	5	6	7	8	9	10	11	12
1	0	2	0	0	6	0	0	10	0	0	14	0
2	1	3	4	5	7	8	9	11	12	13	15	16
3	0	0	0	0	0	0	26	0	27	0	0	0
	d.o.f.											

13	14	15	16	17	18	19	20	21
0	18	0	0	22	0	0	25	0
17	19	20	21	23	24	0	0	0
28	0	29	0	0	0	30	0	31
d.o.f.								

Combining the ID array with the IEN array [Hughes, 1987], we obtain the Location Matrix (LM) that we will use in our element assembly process:

local node #	nodal dof	e1	e2	e3
1	1	0	0	0
	2	9	17	0
2	1	0	0	0
	2	12	20	0
3	1	0	0	0
	2	4	12	20
4	1	0	0	0
	2	1	9	17
5	1	10	18	25
	2	11	19	0
6	1	0	0	0
	2	8	16	24
7	1	2	10	18
	2	3	11	19
8	1	0	0	0
	2	5	13	21
9	1	6	14	22
	2	7	15	23
1	{3	26	28	30
2	{3	27	29	31
3	{3	0	27	29
4	{3	0	26	28

Continuing with the example, we show the details of calculating the various element matrices and vectors, starting with the element stiffness matrix for displacement dof:

$$\boldsymbol{k}^{e,dd} = \int_{\Omega^e} (\boldsymbol{B}^{e,u})^T \cdot \boldsymbol{D}^{\text{elastic}} \cdot \boldsymbol{B}^{e,u} da \tag{6.94}$$

$$= \int_{-1}^{1}\int_{-1}^{1} (\boldsymbol{B}^{e,u})^T \cdot \boldsymbol{D}^{\text{elastic}} \cdot \boldsymbol{B}^{e,u} \jmath^e d\xi d\eta \tag{6.95}$$

$$\boldsymbol{B}^{e,u} = \begin{bmatrix} \boldsymbol{B}^u_1 & \boldsymbol{B}^u_2 & \dots & \boldsymbol{B}^u_9 \end{bmatrix} \tag{6.96}$$

$$\boldsymbol{B}^u_a = \begin{bmatrix} \frac{\partial N^u_a}{\partial x} & 0 \\ 0 & \frac{\partial N^u_a}{\partial y} \\ \frac{\partial N^u_a}{\partial y} & \frac{\partial N^u_a}{\partial x} \end{bmatrix} \tag{6.97}$$

where for plane strain, linear isotropic elasticity, we have

$$\boldsymbol{D}^{\text{elastic}} = \begin{bmatrix} \lambda + 2\mu & \lambda & 0 \\ \lambda & \lambda + 2\mu & 0 \\ 0 & 0 & \mu \end{bmatrix} \tag{6.98}$$

where recall $\mu = \frac{E}{2(1+\nu)}$, $\lambda = \frac{2\mu\nu}{(1-2\nu}$, and we ignore currently the calculation of the out-of-plane stress (which becomes important for pressure-sensitive materials like geomaterials). Recall that we interpolate the displacement field $\boldsymbol{u}^{h^e}$ using quadratic shape functions, as shown in Fig.6.11.

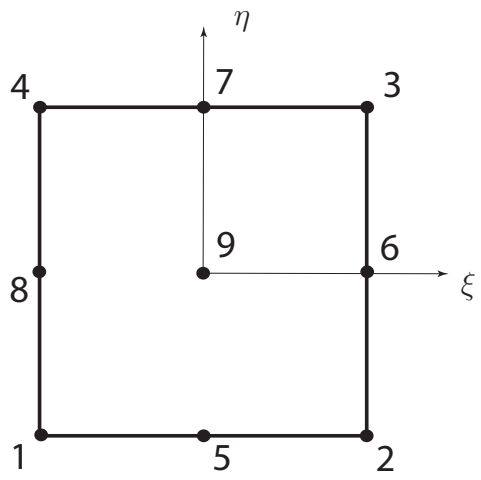

$$
\begin{aligned}
N_1^u(\xi,\eta) &= \frac{1}{4}\xi\eta(\xi-1)(\eta-1)\\
N_2^u(\xi,\eta) &= \frac{1}{4}\xi\eta(\xi+1)(\eta-1)\\
N_3^u(\xi,\eta) &= \frac{1}{4}\xi\eta(\xi+1)(\eta+1)\\
N_4^u(\xi,\eta) &= \frac{1}{4}\xi\eta(\xi-1)(\eta+1)\\
N_5^u(\xi,\eta) &= \frac{1}{2}\eta(1-\xi^2)(\eta-1)\\
N_6^u(\xi,\eta) &= \frac{1}{2}\xi(\xi+1)(1-\eta^2)\\
N_7^u(\xi,\eta) &= \frac{1}{2}\eta(\eta+1)(1-\xi^2)\\
N_8^u(\xi,\eta) &= \frac{1}{2}\xi(\xi-1)(1-\eta^2)\\
N_9^u(\xi,\eta) &= (1-\xi^2)(1-\eta^2)
\end{aligned}
$$

Figure 6.11. Biquadratic shape functions for quadrilateral.

With these shape functions, we need to transform global (x, y) to local coordinates (ξ, η), such that coordinate transformation of the shape function derivatives are:

$$\begin{bmatrix} \frac{\partial N_a^u}{\partial x} \\ \frac{\partial N_a^u}{\partial y} \end{bmatrix} = \frac{1}{j^e} \begin{bmatrix} \frac{\partial y}{\partial \eta} & -\frac{\partial y}{\partial \xi} \\ -\frac{\partial x}{\partial \eta} & \frac{\partial x}{\partial \xi} \end{bmatrix}^{h^e} \begin{bmatrix} \frac{\partial N_a^u}{\partial \xi} \\ \frac{\partial N_a^u}{\partial \eta} \end{bmatrix} \tag{6.99}$$

$$j^e = x_{,\xi}^{h^e} y_{,\eta}^{h^e} - y_{,\xi}^{h^e} x_{,\eta}^{h^e} \tag{6.100}$$

where the coordinate derivatives are (leaving off superscript h^e on x and y)

$$x_{,\xi}^{h^e} = \sum_{a=1}^{9} \frac{\partial N_a^u}{\partial \xi} x_a^e \,, \; x_{,\eta}^{h^e} = \sum_{a=1}^{9} \frac{\partial N_a^u}{\partial \eta} x_a^e \tag{6.101}$$

$$y_{,\xi}^{h^e} = \sum_{a=1}^{9} \frac{\partial N_a^u}{\partial \xi} y_a^e \,, \; y_{,\eta}^{h^e} = \sum_{a=1}^{9} \frac{\partial N_a^u}{\partial \eta} y_a^e \tag{6.102}$$

Once the coordinate transformation is complete, we can take advantage of spatial Gaussian integration [Hughes, 1987], in this case for integrating $\boldsymbol{k}^{e,dd}$, we use 3×3 Gauss integration, as shown in Fig.6.12.

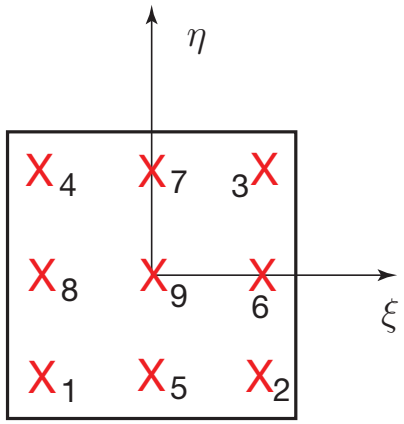

$a = \sqrt{3/5}$, $b = 25/81$, $c = 40/81$, $d = 64/81$

i.p.	$\tilde{\xi}$	$\tilde{\eta}$	W
1	$-a$	$-a$	b
2	a	$-a$	b
3	a	a	b
4	$-a$	a	b
5	0	$-a$	c
6	a	0	c
7	0	a	c
8	$-a$	0	c
9	0	0	d

Figure 6.12. 3×3 Gauss integration.

For the coupling element matrix, we may likewise use 3×3 Gauss integration, such that

$$\boldsymbol{k}^{e,d\theta} = \int_{\Omega^e} (\tilde{\boldsymbol{B}}^{e,u})^T \cdot \boldsymbol{N}^{e,p} da \tag{6.103}$$

$$= \int_{-1}^{1}\int_{-1}^{1} (\tilde{\boldsymbol{B}}^{e,u})^T \cdot \boldsymbol{N}^{e,p} j^e d\xi d\eta \tag{6.104}$$

$$\tilde{\boldsymbol{B}}^{e,u} = \begin{bmatrix} \tilde{\boldsymbol{B}}_1^u & \tilde{\boldsymbol{B}}_2^u & \dots & \tilde{\boldsymbol{B}}_9^u \end{bmatrix} \tag{6.105}$$

$$\tilde{\boldsymbol{B}}_a^u = \begin{bmatrix} \frac{\partial N_a^u}{\partial x} & \frac{\partial N_a^u}{\partial y} \end{bmatrix} \tag{6.106}$$

$$\boldsymbol{N}^{e,p} = \begin{bmatrix} N_1^p & N_2^p & N_3^p & N_4^p \end{bmatrix} \tag{6.107}$$

$$N_1^p = \frac{1}{4}(1-\xi)(1-\eta) \tag{6.108}$$

$$N_2^p = \frac{1}{4}(1+\xi)(1-\eta) \tag{6.109}$$

$$N_3^p = \frac{1}{4}(1+\xi)(1+\eta) \tag{6.110}$$

$$N_4^p = \frac{1}{4}(1-\xi)(1+\eta) \tag{6.111}$$

We may use 3×3 Gauss integration to integrate the element body force vector as

$$\boldsymbol{f}_f^{e,d} = \int_{\Omega^e} \rho (\boldsymbol{N}^{e,u})^T \cdot \boldsymbol{g} da \tag{6.112}$$

$$= \int_{-1}^{1}\int_{-1}^{1} \rho (\boldsymbol{N}^{e,u})^T \cdot \boldsymbol{g} j^e d\xi d\eta \tag{6.113}$$

$$\boldsymbol{g} = \begin{bmatrix} 0 \\ -g \end{bmatrix}, \quad g = 9.8 m/s^2 \tag{6.114}$$

$$\boldsymbol{N}^{e,u} = \begin{bmatrix} \boldsymbol{N}_1^u & \boldsymbol{N}_2^u & \dots & \boldsymbol{N}_9^u \end{bmatrix} \tag{6.115}$$

$$\boldsymbol{N}_a^u = \begin{bmatrix} N_a^u & 0 \\ 0 & N_a^u \end{bmatrix} \tag{6.116}$$

For element 1, $e = 1$, we have a nonzero traction force vector, but for elements $e = 2, 3$,

$\boldsymbol{f}_t^{e,d} = \mathbf{0}$. Thus for element 1, we have,

$$\boldsymbol{f}_t^{e,d} = \int_{\Gamma_t^e} (\boldsymbol{N}^{e,u})^T \cdot \boldsymbol{t}^{\sigma'} ds \tag{6.117}$$

$$= \int_{-1}^{1} [\boldsymbol{N}^{e,u}(\eta = 1)]^T \cdot \boldsymbol{t}^{\sigma'}(0.5) d\xi \tag{6.118}$$

$$\boldsymbol{t}^{\sigma'} = \begin{bmatrix} 0 \\ -t^{\sigma'} \end{bmatrix} \tag{6.119}$$

$$\boldsymbol{N}^{e,u}(\eta = 1) = \begin{bmatrix} \mathbf{0} & \mathbf{0} & \boldsymbol{N}_3^u & \boldsymbol{N}_4^u & \mathbf{0} & \mathbf{0} & \boldsymbol{N}_7^u & \mathbf{0} & \mathbf{0} \end{bmatrix} \tag{6.120}$$

$$= \begin{bmatrix} 0 & 0 & 0 & 0 & \frac{1}{2}\xi(\xi+1) & 0 & \frac{1}{2}\xi(\xi-1) & 0 \\ 0 & 0 & 0 & 0 & 0 & \frac{1}{2}\xi(\xi+1) & 0 & \frac{1}{2}\xi(\xi-1) \end{bmatrix}$$

$$\begin{bmatrix} 0 & 0 & 0 & 0 & 1-\xi^2 & 0 & 0 & 0 & 0 & 0 \\ 0 & 0 & 0 & 0 & 0 & 1-\xi^2 & 0 & 0 & 0 & 0 \end{bmatrix} \tag{6.121}$$

where we will use 3pt Gauss integration along ξ. Recall that $ds = \sqrt{dx^2 + dy^2} = d\xi \sqrt{(\frac{\partial x}{\partial \xi})^2 + (\frac{\partial y}{\partial \xi})^2}$ along an element edge. Given the element node numbering, the top surface of element 1 where the traction $t^{\sigma'}$ is applied in Fig.6.10 is $\eta = 1$, then $x^{h^e}(\xi) = N_3^u(\xi, \eta = 1)(1m) + N_4^u(\xi, \eta = 1)(0m) + N_7^u(\xi, \eta = 1)(0.5m)$, $y^{h^e}(\xi) = N_3^u(\xi, \eta = 1)(3m) + N_4^u(\xi, \eta = 1)(3m) + N_7^u(\xi, \eta = 1)(3m) = 3m$, where $\frac{\partial x^{h^e}}{\partial \xi} = 0.5m$ and $\frac{\partial y^{h^e}}{\partial \xi} = 0.0m$, then $ds = d\xi \sqrt{(0.5m)^2 + (0.0m)^2} = (0.5) d\xi$.

For the boundary force vector due to pore fluid pressure p_{f}^h acting on the boundary where traction is applied, we have

$$\begin{aligned}
\boldsymbol{f}_p^{e,d} &= \int_{\Gamma_t^e} (\boldsymbol{N}^{e,u})^T \cdot \boldsymbol{n}\, p_{\mathrm{f}}^{h^e}\, ds && (6.122)\\
&= \int_{-1}^{1} [\boldsymbol{N}^{e,u}(\eta=1)]^T \cdot \boldsymbol{n}\, p_{\mathrm{f}}^{h^e}(0.5) d\xi && (6.123)\\
&\qquad \boldsymbol{n} = \begin{bmatrix} 0 \\ 1 \end{bmatrix} && (6.124)\\
&\qquad \boldsymbol{N}^{e,u}(\eta=1) = \begin{bmatrix} \mathbf{0} & \mathbf{0} & \boldsymbol{N}_3^u & \boldsymbol{N}_4^u & \mathbf{0} & \mathbf{0} & \boldsymbol{N}_7^u & \mathbf{0} & \mathbf{0} \end{bmatrix} && (6.125)\\
&\qquad = \begin{bmatrix} 0 & 0 & 0 & 0 & \frac{1}{2}\xi(\xi+1) & 0 & \frac{1}{2}\xi(\xi-1) & 0 \\ 0 & 0 & 0 & 0 & 0 & \frac{1}{2}\xi(\xi+1) & 0 & \frac{1}{2}\xi(\xi-1) \end{bmatrix} \\
&\qquad \begin{bmatrix} 0 & 0 & 0 & 0 & 1-\xi^2 & 0 & 0 & 0 & 0 & 0 \\ 0 & 0 & 0 & 0 & 0 & 1-\xi^2 & 0 & 0 & 0 & 0 \end{bmatrix} && (6.126)
\end{aligned}$$

where for element 1, $p_{\mathrm{f}}^{h^e} = 0$ on Γ_t^e. The element matrix for pore pressure dof is

$$\begin{aligned}
\boldsymbol{k}^{e,\theta\theta} &= \int_{\Omega^e} (\boldsymbol{B}^{e,p})^T \cdot \boldsymbol{k} \cdot \boldsymbol{B}^{e,p} da && (6.127)\\
&= \int_{-1}^{1}\int_{-1}^{1} (\boldsymbol{B}^{e,p})^T \cdot \boldsymbol{k} \cdot \boldsymbol{B}^{e,p} j^e d\xi d\eta && (6.128)\\
&\qquad \boldsymbol{B}^{e,p} = \begin{bmatrix} \boldsymbol{B}_1^p & \boldsymbol{B}_2^p & \boldsymbol{B}_3^p & \boldsymbol{B}_4^p \end{bmatrix} && (6.129)\\
&\qquad \boldsymbol{B}_b^p = \begin{bmatrix} \frac{\partial N_b^p}{\partial x} \\ \frac{\partial N_b^p}{\partial y} \end{bmatrix} && (6.130)
\end{aligned}$$

where we may use 2×2 Gauss integration to integrate.

For the fluid forcing vector, we assume the flux $s = 0$ is zero on Γ_s^h, then

$$\boldsymbol{f}^{e,\theta} = \int_{\Omega^e} \rho^{\mathrm{fR}} (\boldsymbol{B}^{e,p})^T \cdot \boldsymbol{k} \cdot \boldsymbol{g} da \tag{6.131}$$

$$= \int_{-1}^{1} \int_{-1}^{1} \rho^{\mathrm{fR}} (\boldsymbol{B}^{e,p})^T \cdot \boldsymbol{k} \cdot \boldsymbol{g} j^e d\xi d\eta \tag{6.132}$$

where we may use 2×2 Gauss integration to integrate.

We then **insert these individual contributions into coupled element matrices and a forcing vector:**

$$\boldsymbol{K}^e = \begin{bmatrix} \boldsymbol{k}^{e,dd} & -\boldsymbol{k}^{e,d\theta} \\ \boldsymbol{0} & \boldsymbol{k}^{e,\theta\theta} \end{bmatrix} \tag{6.133}$$

$$\boldsymbol{C}^e = \begin{bmatrix} \boldsymbol{0} & \boldsymbol{0} \\ (\boldsymbol{k}^{e,d\theta})^T & \boldsymbol{0} \end{bmatrix} \tag{6.134}$$

$$\boldsymbol{F}^e = \begin{bmatrix} \boldsymbol{f}_f^{e,d} + \boldsymbol{f}_t^{e,d} - \boldsymbol{f}_p^{e,d} \\ \boldsymbol{f}^{e,\theta} \end{bmatrix} \tag{6.135}$$

We must then use the LM matrix to assemble the individual 22×22 and 22×1 contributions to the global "coupling" matrix, stiffness matrix, and forcing vector, and then use generalized trapezoidal integration to solve the transient matrix equations.

6.7 Nonlinearity: Porosity Dependence on Solid Skeleton Deformation

Now assume that the solid skeleton effective stress $\boldsymbol{\sigma}'$ can be governed by a nonlinear constitutive model (e.g., elastoplasticity), and that the density and hydraulic conductivity are functions of porosity n^{f}, and porosity is a function of the solid skeleton volumetric strain ϵ_v. The coupled FE equations are written then as:

$$\begin{aligned}
&\mathop{\mathsf{A}}_{e=1}^{n_{\mathrm{el}}} (\boldsymbol{c}^e)^T \cdot \Bigg[\underbrace{\left(\int_{\Omega^e} (\boldsymbol{B}^{e,u})^T \cdot \boldsymbol{\sigma}'(\boldsymbol{d}^e) da \right)}_{\boldsymbol{f}^{e,d,INT}(\boldsymbol{d}^e)} - \underbrace{\left(\int_{\Omega^e} (\tilde{\boldsymbol{B}}^{e,u})^T \cdot \boldsymbol{N}^{e,p} da \right)}_{\boldsymbol{k}^{e,d\theta}} \cdot \boldsymbol{\theta}^e \\
&= \underbrace{\int_{\Omega^e} \rho(\boldsymbol{d}^e)(\boldsymbol{N}^{e,u})^T \cdot \boldsymbol{g} da + \int_{\Gamma_t^e} (\boldsymbol{N}^{e,u})^T \cdot \boldsymbol{t}^{\sigma'} ds - \int_{\Gamma_t^e} (\boldsymbol{N}^{e,u})^T \cdot \boldsymbol{n}\, p_{\mathrm{f}}^{h^e}\, ds}_{\boldsymbol{f}^{e,d,EXT}(\boldsymbol{d}^e)} \Bigg] \qquad (6.136)
\end{aligned}$$

$$\mathop{\mathsf{A}}_{e=1}^{n_{\mathrm{el}}} (\boldsymbol{\alpha}^e)^T \cdot \Bigg[\underbrace{\left(\int_{\Omega^e} (\boldsymbol{N}^{e,p})^T \cdot \tilde{\boldsymbol{B}}^{e,u} da \right)}_{(\boldsymbol{k}^{e,d\theta})^T} \cdot \dot{\boldsymbol{d}}^e - \underbrace{\left(\int_{\Omega^e} (\boldsymbol{B}^{e,p})^T \cdot \tilde{\boldsymbol{v}}_{\mathrm{f}}^{\mathrm{Darcy}}(\boldsymbol{d}^e, \boldsymbol{\theta}^e) da \right)}_{\boldsymbol{f}^{e,\theta,INT}(\boldsymbol{d}^e, \boldsymbol{\theta}^e)} = \underbrace{\int_{\Gamma_s^e} (\boldsymbol{N}^{e,p})^T s ds}_{\boldsymbol{f}^{e,\theta,EXT}} \Bigg]$$

and

$$\mathop{\mathsf{A}}_{e=1}^{n_{\mathrm{el}}} (\boldsymbol{c}^e)^T \cdot \left[\boldsymbol{f}^{e,d,INT}(\boldsymbol{d}^e) - \boldsymbol{k}^{e,d\theta} \cdot \boldsymbol{\theta}^e = \boldsymbol{f}^{e,d,EXT}(\boldsymbol{d}^e) \right] \qquad (6.137)$$

$$\mathop{\mathsf{A}}_{e=1}^{n_{\mathrm{el}}} (\boldsymbol{\alpha}^e)^T \cdot \left[(\boldsymbol{k}^{e,d\theta})^T \cdot \dot{\boldsymbol{d}}^e - \boldsymbol{f}^{e,\theta,INT}(\boldsymbol{d}^e, \boldsymbol{\theta}^e) = \boldsymbol{f}^{e,\theta,EXT} \right] \qquad (6.138)$$

After element assembly, we have the coupled nonlinear parabolic PDEs to solve using generalized trapezoidal integration in time, and the Newton-Raphson method, assuming the time

integration method is implicit. These equations are

$$\boldsymbol{F}^{d,INT}(\boldsymbol{d}) - \boldsymbol{K}^{d\theta} \cdot \boldsymbol{\theta} = \boldsymbol{F}^{d,EXT}(\boldsymbol{d}) \tag{6.139}$$

$$(\boldsymbol{K}^{d\theta})^T \cdot \dot{\boldsymbol{d}} - \boldsymbol{F}^{\theta,INT}(\boldsymbol{d},\boldsymbol{\theta}) = \boldsymbol{F}^{\theta,EXT} \tag{6.140}$$

which we may rewrite as,

$$\boldsymbol{C} \cdot \dot{\boldsymbol{D}} + \boldsymbol{F}^{INT}(\boldsymbol{D}) = \boldsymbol{F}^{EXT}(\boldsymbol{D}) \tag{6.141}$$

$$\dot{\boldsymbol{D}} = \begin{bmatrix} \dot{\boldsymbol{d}} \\ \dot{\boldsymbol{\theta}} \end{bmatrix}, \quad \boldsymbol{D} = \begin{bmatrix} \boldsymbol{d} \\ \boldsymbol{\theta} \end{bmatrix} \tag{6.142}$$

$$\boldsymbol{C} = \begin{bmatrix} \boldsymbol{0} & \boldsymbol{0} \\ (\boldsymbol{K}^{d\theta})^T & \boldsymbol{0} \end{bmatrix}, \quad \boldsymbol{F}^{INT}(\boldsymbol{D}) = \begin{bmatrix} \boldsymbol{F}^{d,INT}(\boldsymbol{d}) - \boldsymbol{K}^{d\theta} \cdot \boldsymbol{\theta} \\ -\boldsymbol{F}^{\theta,INT}(\boldsymbol{d},\boldsymbol{\theta}) \end{bmatrix} \tag{6.143}$$

$$\boldsymbol{F}^{EXT}(\boldsymbol{D}) = \begin{bmatrix} \boldsymbol{F}^{d,EXT}(\boldsymbol{d}) \\ \boldsymbol{F}^{\theta,EXT} \end{bmatrix} \tag{6.144}$$

Recall the generalized trapezoidal integration:

$$\boldsymbol{C} \cdot \boldsymbol{V}_{n+1} + \boldsymbol{F}^{INT}(\boldsymbol{D}_{n+1}) = \boldsymbol{F}^{EXT}(\boldsymbol{D}_{n+1}) \tag{6.145}$$

$$\boldsymbol{D}_{n+1} = \tilde{\boldsymbol{D}}_{n+1} + \alpha \Delta t \boldsymbol{V}_{n+1} \tag{6.146}$$

and express in residual form, solving for $\boldsymbol{V}_{n+1}^{k+1}$ in a Newton-Raphson iteration algorithm:

$$\begin{aligned}
\boldsymbol{R}(\boldsymbol{V}_{n+1}^{k+1}) &= \boldsymbol{C}\cdot\boldsymbol{V}_{n+1}^{k+1} + \boldsymbol{F}^{INT}(\boldsymbol{D}_{n+1}^{k+1}) - \boldsymbol{F}^{EXT}(\boldsymbol{D}_{n+1}^{k+1}) = \boldsymbol{0} && (6.147)\\
&= \boldsymbol{R}^k + \frac{\partial \boldsymbol{R}^k}{\partial \boldsymbol{V}}\cdot\delta\boldsymbol{V} = \boldsymbol{0} && (6.148)\\
\implies \delta\boldsymbol{V} &= -\left(\frac{\partial \boldsymbol{R}^k}{\partial \boldsymbol{V}}\right)^{-1}\cdot\boldsymbol{R}^k && (6.149)\\
&\boldsymbol{V}_{n+1}^{k+1} = \boldsymbol{V}_{n+1}^{k} + \delta\boldsymbol{V} && (6.150)\\
&\boldsymbol{D}_{n+1}^{k+1} = \tilde{\boldsymbol{D}}_{n+1} + \alpha\Delta t\boldsymbol{V}_{n+1}^{k+1} && (6.151)
\end{aligned}$$

We then have the consistent tangent:

$$\begin{aligned}
\frac{\partial \boldsymbol{R}}{\partial \boldsymbol{V}} &= \boldsymbol{C} + \frac{\partial \boldsymbol{F}^{INT}}{\partial \boldsymbol{D}}\cdot\frac{\partial \boldsymbol{D}}{\partial \boldsymbol{V}} - \frac{\partial \boldsymbol{F}^{EXT}}{\partial \boldsymbol{D}}\cdot\frac{\partial \boldsymbol{D}}{\partial \boldsymbol{V}} && (6.152)\\
&\frac{\partial \boldsymbol{D}}{\partial \boldsymbol{V}} = \alpha\Delta t && (6.153)\\
&\frac{\partial \boldsymbol{F}^{INT}}{\partial \boldsymbol{D}} = \begin{bmatrix} \frac{\partial \boldsymbol{F}^{INT}}{\partial \boldsymbol{d}} & \frac{\partial \boldsymbol{F}^{INT}}{\partial \boldsymbol{\theta}} \end{bmatrix} && (6.154)\\
&\frac{\partial \boldsymbol{F}^{INT}}{\partial \boldsymbol{d}} = \begin{bmatrix} \frac{\partial \boldsymbol{F}^{d,INT}}{\partial \boldsymbol{d}} \\ -\frac{\partial \boldsymbol{F}^{\theta,INT}}{\partial \boldsymbol{d}} \end{bmatrix} && (6.155)\\
&\frac{\partial \boldsymbol{F}^{INT}}{\partial \boldsymbol{\theta}} = \begin{bmatrix} -\boldsymbol{K}^{d\theta} \\ -\frac{\partial \boldsymbol{F}^{\theta,INT}}{\partial \boldsymbol{\theta}} \end{bmatrix} && (6.156)\\
&\frac{\partial \boldsymbol{F}^{EXT}}{\partial \boldsymbol{D}} = \begin{bmatrix} \frac{\partial \boldsymbol{F}^{EXT}}{\partial \boldsymbol{d}} & \frac{\partial \boldsymbol{F}^{EXT}}{\partial \boldsymbol{\theta}} \end{bmatrix} && (6.157)\\
&\frac{\partial \boldsymbol{F}^{EXT}}{\partial \boldsymbol{d}} = \begin{bmatrix} \frac{\partial \boldsymbol{F}^{d,EXT}}{\partial \boldsymbol{d}} \\ \boldsymbol{0} \end{bmatrix} && (6.158)\\
&\frac{\partial \boldsymbol{F}^{EXT}}{\partial \boldsymbol{\theta}} = \begin{bmatrix} \boldsymbol{0} \\ \boldsymbol{0} \end{bmatrix} && (6.159)
\end{aligned}$$

where:

$$\frac{\partial \boldsymbol{F}^{d,INT}}{\partial \boldsymbol{d}} = \mathop{\mathsf{A}}_{e=1}^{n_{\rm el}} \frac{\partial \boldsymbol{f}^{e,d,INT}}{\partial \boldsymbol{d}^e} = \mathop{\mathsf{A}}_{e=1}^{n_{\rm el}} \int_{\Omega^e} (\boldsymbol{B}^{e,u})^T \cdot \frac{\partial \boldsymbol{\sigma}'}{\partial \boldsymbol{\epsilon}} \cdot \boldsymbol{B}^{e,u} da \tag{6.160}$$

$$\frac{\partial \boldsymbol{F}^{\theta,INT}}{\partial \boldsymbol{d}} = \mathop{\mathsf{A}}_{e=1}^{n_{\rm el}} \frac{\partial \boldsymbol{f}^{e,\theta,INT}}{\partial \boldsymbol{d}^e} = \mathop{\mathsf{A}}_{e=1}^{n_{\rm el}} \int_{\Omega^e} (\boldsymbol{B}^{e,p})^T \cdot \frac{\partial \tilde{\boldsymbol{v}}_{\rm f}^{\rm Darcy}}{\partial \boldsymbol{d}^e} da \tag{6.161}$$

$$\frac{\partial \tilde{\boldsymbol{v}}_{\rm f}^{\rm Darcy}}{\partial \boldsymbol{d}^e} = -\left[\boldsymbol{\nabla} p_{\rm f}^{h^e} - \rho^{\rm fR} \boldsymbol{g}\right] \otimes \frac{\partial \hat{k}}{\partial n^{\rm f}} \frac{\partial n^{\rm f}}{\partial \boldsymbol{d}^e} \tag{6.162}$$

$$\frac{\partial \hat{k}}{\partial n^{\rm f}} = \hat{k} \left[\frac{3 - (n^{\rm f})^2}{n^{\rm f}(1 - (n^{\rm f})^2)}\right] \tag{6.163}$$

$$\frac{\partial n^{\rm f}}{\partial \boldsymbol{d}^e} = \left(\frac{1 - n^{\rm f}}{1 + \Delta\epsilon_v}\right) \tilde{\boldsymbol{B}}^{e,u} \tag{6.164}$$

$$\frac{\partial \boldsymbol{F}^{\theta,INT}}{\partial \boldsymbol{\theta}} = \mathop{\mathsf{A}}_{e=1}^{n_{\rm el}} \frac{\partial \boldsymbol{f}^{e,\theta,INT}}{\partial \boldsymbol{\theta}^e} = \mathop{\mathsf{A}}_{e=1}^{n_{\rm el}} \int_{\Omega^e} (\boldsymbol{B}^{e,p})^T \cdot \frac{\partial \tilde{\boldsymbol{v}}_{\rm f}^{\rm Darcy}}{\partial \boldsymbol{\theta}^e} da \tag{6.165}$$

$$\frac{\partial \tilde{\boldsymbol{v}}_{\rm f}^{\rm Darcy}}{\partial \boldsymbol{\theta}^e} = -\hat{\boldsymbol{k}} \cdot \boldsymbol{B}^{e,p} \tag{6.166}$$

$$\hat{\boldsymbol{k}} = \hat{k} \begin{bmatrix} 1 & 0 \\ 0 & 1 \end{bmatrix} \tag{6.167}$$

$$\frac{\partial \boldsymbol{F}^{d,EXT}}{\partial \boldsymbol{d}} = \mathop{\mathsf{A}}_{e=1}^{n_{\rm el}} \frac{\partial \boldsymbol{f}^{e,d,EXT}}{\partial \boldsymbol{d}^e} = \mathop{\mathsf{A}}_{e=1}^{n_{\rm el}} \int_{\Omega^e} (\boldsymbol{N}^{e,u})^T \cdot \boldsymbol{g} \otimes \frac{\partial \rho}{\partial \boldsymbol{d}^e} da \tag{6.168}$$

$$\frac{\partial \rho}{\partial \boldsymbol{d}^e} = (\rho^{\rm fR} - \rho^{\rm sR}) \frac{\partial n^{\rm f}}{\partial \boldsymbol{d}^e} = (\rho^{\rm fR} - \rho^{\rm sR}) \left(\frac{1 - n^{\rm f}}{1 + \Delta\epsilon_v}\right) \tilde{\boldsymbol{B}}^{e,u}$$

6.8 Dynamic Mixture Theory and FE Implementation

For 'long' period motions such as earthquakes, or human exercise activity (jumping, running; i.e., NOT high impact such as during a car crash, etc.), to simplify the formulation we assume fluid and solid accelerations are equal: $\boldsymbol{a}_{\mathrm{f}} \approx \boldsymbol{a}$. Then, the coupled balance equations in FE matrix form after assembly, but now with inertia terms (acceleration) are:

$$\boldsymbol{M}^{dd}(\boldsymbol{d}) \cdot \ddot{\boldsymbol{d}} + \boldsymbol{F}^{d,INT}(\boldsymbol{d}) - \boldsymbol{K}^{d\theta} \cdot \boldsymbol{\theta} = \boldsymbol{F}^{d,EXT}(\boldsymbol{d}) \tag{6.169}$$

$$(\boldsymbol{K}^{d\theta})^T \cdot \dot{\boldsymbol{d}} - \boldsymbol{F}^{\theta,INT}(\ddot{\boldsymbol{d}}, \boldsymbol{d}, \boldsymbol{\theta}) = \boldsymbol{F}^{\theta,EXT} \tag{6.170}$$

where the mass matrix for the mixture is

$$\boldsymbol{M}^{dd} = \mathop{\mathsf{A}}_{e=1}^{n_{\mathrm{el}}} \int_{\Omega^e} \rho (\boldsymbol{N}^{e,u})^T \cdot \boldsymbol{N}^{e,u} da \tag{6.171}$$

Also, the generalized Darcy's law including acceleration [Coussy, 2004] (pg.45):

$$\tilde{\boldsymbol{v}}_{\mathrm{f}}^{\mathrm{Darcy}} = -\hat{k} \left[\boldsymbol{\nabla} p_{\mathrm{f}} - \rho^{\mathrm{fR}} (\boldsymbol{g} - \boldsymbol{a}) \right] \tag{6.172}$$

$$\boldsymbol{a}^{h^e}(\boldsymbol{\xi}, t) = \boldsymbol{N}^{e,u}(\boldsymbol{\xi}) \cdot \ddot{\boldsymbol{d}}^e(t) \tag{6.173}$$

Then, we can rewrite as

$$\boldsymbol{M} \cdot \ddot{\boldsymbol{D}} + \boldsymbol{C} \cdot \dot{\boldsymbol{D}} + \boldsymbol{F}^{INT}(\ddot{\boldsymbol{D}}, \boldsymbol{D}) = \boldsymbol{F}^{EXT}(\boldsymbol{D}) \tag{6.174}$$

$$\ddot{\boldsymbol{D}} = \begin{bmatrix} \ddot{\boldsymbol{d}} \\ \ddot{\boldsymbol{\theta}} \end{bmatrix}, \quad \boldsymbol{M} = \begin{bmatrix} \boldsymbol{M}^{dd} & \boldsymbol{0} \\ \boldsymbol{0} & \boldsymbol{0} \end{bmatrix} \tag{6.175}$$

$$\boldsymbol{F}^{INT}(\ddot{\boldsymbol{D}}, \boldsymbol{D}) = \begin{bmatrix} \boldsymbol{F}^{d,INT}(\boldsymbol{d}) - \boldsymbol{K}^{d\theta} \cdot \boldsymbol{\theta} \\ -\boldsymbol{F}^{\theta,INT}(\ddot{\boldsymbol{d}}, \boldsymbol{d}, \boldsymbol{\theta}) \end{bmatrix} \tag{6.176}$$

$$\boldsymbol{F}^{\theta,INT}(\ddot{\boldsymbol{d}}, \boldsymbol{d}, \boldsymbol{\theta}) = \mathop{\mathsf{A}}_{e=1}^{n_{\mathrm{el}}} \boldsymbol{f}^{e,\theta,INT}(\ddot{\boldsymbol{d}}^e, \boldsymbol{d}^e, \boldsymbol{\theta}^e) = \mathop{\mathsf{A}}_{e=1}^{n_{\mathrm{el}}} \int_{\Omega^e} (\boldsymbol{B}^{e,p})^T \cdot \tilde{\boldsymbol{v}}_{\mathrm{f}}^{\mathrm{Darcy}}(\ddot{\boldsymbol{d}}^e, \boldsymbol{d}^e, \boldsymbol{\theta}^e) da$$

These equations are integrated in time using Newmark's method and solved by the Newton-Raphson method. To summarize:

1. given $\boldsymbol{D}_n$, $\boldsymbol{V}_n$, and $\boldsymbol{A}_n$ from the previous time step, solve for $\boldsymbol{D}_{n+1}$, $\boldsymbol{V}_{n+1}$, and $\boldsymbol{A}_{n+1}$ at the current time

$$\boldsymbol{M} \cdot \boldsymbol{A}_{n+1} + \boldsymbol{C} \cdot \boldsymbol{V}_{n+1} + \boldsymbol{F}^{INT}(\boldsymbol{A}_{n+1}, \boldsymbol{D}_{n+1}) = \boldsymbol{F}^{EXT}(\boldsymbol{D}_{n+1}) \tag{6.177}$$

$$\boldsymbol{D}_{n+1} = \boldsymbol{D}_n + \Delta t \boldsymbol{V}_n + \frac{\Delta t^2}{2}\left[(1-2\beta)\boldsymbol{A}_n + 2\beta \boldsymbol{A}_{n+1}\right] \tag{6.178}$$

$$\boldsymbol{V}_{n+1} = \boldsymbol{V}_n + \Delta t\left[(1-\gamma)\boldsymbol{A}_n + \gamma \boldsymbol{A}_{n+1}\right] \tag{6.179}$$

   where γ, β are integration parameters; can substitute to solve for $\boldsymbol{A}_{n+1}^{k+1}$ using Newton-Raphson, and then update $\boldsymbol{D}_{n+1}^{k+1}$ and $\boldsymbol{V}_{n+1}^{k+1}$ during iteration

2. introduce "predictors" from known values

$$\tilde{\boldsymbol{D}}_{n+1} = \boldsymbol{D}_n + \Delta t \boldsymbol{V}_n + \frac{\Delta t^2}{2}(1-2\beta)\boldsymbol{A}_n \tag{6.180}$$

$$\tilde{\boldsymbol{V}}_{n+1} = \boldsymbol{V}_n + \Delta t(1-\gamma)\boldsymbol{A}_n \tag{6.181}$$

   such that

$$\boldsymbol{D}_{n+1}^{k+1} = \tilde{\boldsymbol{D}}_{n+1} + \beta \Delta t^2 \boldsymbol{A}_{n+1}^{k+1} \tag{6.182}$$

$$\boldsymbol{V}_{n+1}^{k+1} = \tilde{\boldsymbol{V}}_{n+1} + \gamma \Delta t \boldsymbol{A}_{n+1}^{k+1} \tag{6.183}$$

3. to initialize time-stepping, we must solve for initial solid skeleton acceleration $\boldsymbol{a}_0$ from the first coupled FE equation

$$\boldsymbol{M}^{dd} \cdot \boldsymbol{a}_0 = \boldsymbol{F}^{d,EXT}(\boldsymbol{d}_0) - \boldsymbol{F}^{d,INT}(\boldsymbol{d}_0) + \boldsymbol{K}^{d\theta} \cdot \boldsymbol{\theta}_0 \tag{6.184}$$

4. assume $\ddot{\boldsymbol{\theta}}_0 = \mathbf{0}$

5. rewrite in residual form, and solve via Newton-Raphson (many of the derivatives for consistent tangent already are given for the nonlinear consolidation problem without inertia terms)

$$\boldsymbol{R}(\boldsymbol{A}_{n+1}^{k+1}) = \boldsymbol{M} \cdot \boldsymbol{A}_{n+1}^{k+1} + \boldsymbol{C} \cdot \boldsymbol{V}_{n+1}^{k+1} + \boldsymbol{F}^{INT}(\boldsymbol{A}_{n+1}^{k+1}, \boldsymbol{D}_{n+1}^{k+1}) - \boldsymbol{F}^{EXT}(\boldsymbol{D}_{n+1}^{k+1}) = \mathbf{0} \quad (6.185)$$

Bibliography

A. Anandarajah. *Computational Methods in Elasticity and Plasticity: Solids and Porous Media*. Springer Science, 2010.

J. Atkinson. *An Introduction to the Mechanics of Soils and Foundations through Critical State Soil Mechanics*. McGraw-Hill, New York, NY, 1993.

I. Babuska and J.T. Oden. Verification and validation in computational engineering and science: basic concepts. *Comp. Meth. App. Mech. Engr.*, 193:4057–66, 2004.

Z.P. Bazant and M. Jirasek. Nonlocal integral formulations of plasticity and damage: Survey of progress. In J.S. Russell, editor, *Perspectives in Civil Engineering: Commemorating the 150th Anniversary of the American Society of Civil Engineers*, pages 21–51. ASCE, Reston, VA, 2003.

T. Belytschko, W. K. Liu, and B. Moran. *Nonlinear Finite Elements for Continua and Structures*. John Wiley & Sons, 2000.

R.I. Borja. Theory of porous media. unpublished course notes, Stanford University, 2004.

R.I. Borja. *Plasticity: Modeling & Computation*. Springer-Verlag, 2013.

R.I. Borja, K.M. Sama, and P.F. Sanz. On the numerical integration of three-invariant elastoplastic constitutive models. *Comp. Meth. App. Mech. Engr.*, 192:1227–58, 2003.

CG-Method. An introduction to the conjugate gradient method without the agonizing pain. `http://www.cs.berkeley.edu/~jrs/`.

B. D. Coleman and M. E. Gurtin. Thermodynamics with internal state variables. *J. Chem. Phys.*, 47:597–613, 1967.

B. D. Coleman and W. Noll. The thermodynamics of elastic materials with heat conduction and viscosity. *Arch. Ration. Mech. Anal.*, 13:167–178, 1963.

O. Coussy. *Poromechanics*. John Wiley & Sons, 2004.

M.A. Crisfield. *Non-linear Finite Element Analysis of Solids and Structures*, volume 1. John Wiley & Sons, 1991.

R. de Boer. *Trends in Continuum Mechanics of Porous Media: Theory and Applications of Transport in Porous Media*. Springer, 2005.

J.E. Dennis and J.J. Moré. Quasi-Newton Methods, Motivation and Theory. *SIAM Review*, 19:46–89, 1977.

C.S. Desai and H.J. Siriwardane. *Constitutive Laws for Engineering Materials: With Emphasis on Geologic Materials*. Prentice-Hall, 1984.

D.C. Drucker and W. Prager. Soil mechanics and plastic analysis or limit design. *Quarterly of Applied Mathematics*, 10(2):157 – 165, 1952.

R.M. Ferencz and T.J.R. Hughes. Iterative Finite Element Solutions in Nonlinear Solid Mechanics. In P.G. Ciarlet and J.L. Lions, editors, *Handbook of Numerical Analysis*, pages 3–178. Elsevier Science, 1998.

R. Hill. *The Mathematical Theory of Plasticity*. Clarendon Press, Oxford, 1950.

G. A. Holzapfel. *Nonlinear Solid Mechanics: A Continuum Approach for Engineering*. John Wiley & Sons, 2000.

T. J. R. Hughes. *The Finite Element Method*. Prentice-Hall: New Jersey, 1987.

T.J.R. Hughes. Numerical implementation of constitutive models: Rate-independent deviatoric plasticity. In S. Nemat-Nasser, R. Asaro, and G. Hegemier, editors, *Theoretical Foundations for Large Scale Computations of Nonlinear Material Behavior*, pages 29–63. Martinus Nijhoff Pub., Netherlands, 1984.

T.J.R. Hughes and R.M Ferencz. Finite Element Methods for Nonlinear Problems. unpublished course notes, Stanford University, 1990.

Jaeger and Cook. *Fundamentals of Rock Mechanics*. Chapman and Hall, London, UK, 1976.

S.W. Key, C.M. Stone, and R.D. Krieg. Dynamic Relaxation Applied to the Quasi-Static, Large Deformation, Inelastic Response of Axisymmetric Solids. In Wunderlich et al., editor, *Nonlinear Finite Element Analysis in Structural Mechanics*, pages 585–620. Springer-Verlag, 1981.

B. Lande and W. Mitzner. Analysis of lung parenchyma as a parametric porous medium. *J. Appl. Physiol.*, 101:926–933, 2006.

C. Li, R.I. Borja, and R.A. Regueiro. Dynamics of porous media at finite strain. *Comp. Meth. App. Mech. Engr.*, 193(36-38):3837 – 70, 2004.

B. Loret and J.H. Prevost. Dynamic strain localization in fluid-saturated porous media. *J. Eng. Mech.*, 117:907–922, 1991.

J. Lubliner. *Plasticity Theory*. Macmillan Pub., NY, 1990.

L.E. Malvern. *Introduction to the Mechanics of a Continuous Medium*. Prentice-Hall: New York, 1969.

H. Matsuoka and T. Nakai. Stress-deformation and strength characteristics of soil under three different principal stresses. *Proc. JSCE*, 232:59–70, 1974.

H. Matthies and G. Strang. The Solution of Nonlinear F.E. Equations. *Int. J. Numer. Methods Eng.*, 14:1613–1626, 1979.

A. Needleman. Material rate dependence and mesh sensitivity in localization problems. *Comp. Meth. App. Mech. Engr.*, 67:69–85, 1988.

W.L. Oberkampf, T.G. Trucano, and C. Hirsch. Verification, validation, and predictive capability in computational engineering and physics. *App. Mech. Rev.*, 57:345–84, 2004.

J.M. Ortega and W.C. Rheinboldt. *Iterative Solution of Nonlinear Equations in Several Variables*. Academic Press, 1970.

M. Ortiz and A. Pandolfi. Finite-deformation irreversible cohesive elements for three-dimensional crack-propagation analysis. *Int. J. Numer. Methods Eng.*, 44:1267–82, 1999.

R. de Borst and H. Mühlhaus. Gradient-dependent plasticity: formulation and algorithmic aspects. *Int. J. Numer. Methods Eng.*, 35:521–539, 1992.

H.E. Read and G.A. Hegemier. Strain softening of rock, soil, and concrete—A review article. *Mech. Mater.*, 3:271–94, 1984.

R.A. Regueiro and D. Ebrahimi. Implicit dynamic three-dimensional finite element analysis of an inelastic biphasic mixture at finite strain. Part 1: application to a simple geomaterial. *Comp. Meth. App. Mech. Engr.*, 199:2024–2049, 2010.

R.A. Regueiro, B. Zhang, and S.L. Wozniak. Large deformation dynamic three-dimensional coupled finite element analysis of soft biological tissues treated as biphasic porous media. *Computer Modeling in Engineering and Sciences*, 96(1):1–39, 2014.

E. Riks. An incremental approach to the solution of snapping and buckling problems. *Int. J. Solids Struct.*, 15:529–551, 1979.

I.S. Sandler and J.P. Wright. Strain-softening. In S. Nemat-Nasser et al., editor, *Theoretical Foundations for Large Scale Computations of Nonlinear Material Behavior*, pages 285–315. Martinus Nijhoff Pub., The Netherlands, 1976.

L.E. Schwer. An overview of the PTC 60/V and V 10: Guide for verification and validation in computational solid mechanics. *Engineering with Computers*, 23(4):245 – 252, 2007.

J. C. Simo and T. J. R. Hughes. *Computational Inelasticity*. Prentice-Hall: New York, 1998.

L.J. Sluys and R. de Borst. Wave propagation and localization in a rate-dependent cracked medium: Model formulation and one-dimensional examples. *Int. J. Solids Struct.*, 29: 2945–58, 1992.

K. Terzaghi. *Theoretical Soil Mechanics*. John Wiley and Sons, 1943.

TMS. Verification & Validation of Computational Models Associated with the Mechanics of Materials. *The Minerals, Metals & Materials Society*, 2019.

P. Underwood. Dynamic relaxation. In T. Belytschko and T.J.R. Hughes, editors, *Computational Methods for Transient Analysis*, pages "245–265". North-Holland, Amsterdam, 1983.

I. Vardoulakis and M. Goldschieder. Biaxial apparatus for testing shear bands in soils. In *Soil Mechanics and Foundation Engineering*, pages 819–824. A.A. Balkema, 1981.

I. Vardoulakis, M. Goldschieder, and G. Gudehus. Formation of shear bands in sand bodies as a bifurcation problem. *Int. J. Numer. Anal. Methods Geomech.*, 2:99–128, 1978.

P. A. Vermeer and R. de Borst. Non-associated plasticity for soils, concrete, and rock. *Heron*, 29(3):3–64, 1984.